2.12.2 Elastomer O-ring Seal Performance Tests

2.12.2.1 Introduction

Elastomer O-ring seal testing was performed in support of the certification of the TRUPACT–III package. The elastomer O-ring seal tests demonstrated the ability of a butyl rubber compound that meets the acceptance requirements of Section 8.1.5.3, *Butyl Rubber O-rings*, to maintain a leaktight[1] containment boundary under a reduced compression for the face-seal configuration. In addition, previous butyl O-ring seal testing performed for the certification of the TRUPACT–II packaging[2] and the Radioisotope Thermoelectric Generator (RTG) Transportation System Packaging[3] has demonstrated the ability of the butyl O-ring seal compound to maintain a leaktight containment boundary under worst-case conditions of compression and temperature duration that are beyond the conditions for the TRUPACT–III package. The results of the previous TRUPACT–II butyl O-ring tests are summarized in Table 2.12.2-1.

2.12.2.2 Test Specimen and Equipment

A production TN-Gemini package, which has an identical closure lid/seal design as the TRUPACT–III, was utilized to perform variable O-ring seal compression tests. An O-ring seal of prototypic cross-section, overall diameter, and butyl material, as delineated on the drawings in Appendix 1.3.1, *Packaging General Arrangement Drawings*, was installed in each dovetail groove on the closure lid.

2.12.2.3 Test Conditions

Since previous TRUPACT-II tests demonstrated the leaktight capability of the butyl O-ring compound at extreme temperatures and extended durations, the O-ring seal compression helium leakage rate tests were only performed at ambient temperature (e.g., 20 °C to 30 °C).

---

[1] Leaktight is defined as leakage of 1×10^{-8} reference Pascals – cubic meter per second (Pa–m^3/s), air, or less, per Section 6.3, *Application of Referenced Air Leakage Rate (L_R)*, of ANSI N14.5–1997 (or later), *American National Standard for Radioactive Materials – Leakage Tests on Packages for Shipment,* American National Standards Institute, Inc. (ANSI).

[2] U. S. Department of Energy (DOE), *Safety Analysis Report for the TRUPACT–II Shipping Package*, USNRC Certificate of Compliance 71–9218, U.S Department of Energy, Carlsbad Field Office, Carlsbad, New Mexico.

[3] DOE Docket No. 94–6–9904, *Radioisotope Thermoelectric Generator Transportation System Safety Analysis Report for Packaging*, WHC-SD-RTG-SARP-001, prepared for the U.S. Department of Energy Office of Nuclear Energy under Contract No. DE-AC06-87RL10930 by Westinghouse Hanford Company, Richland, WA. Per Appendix 2.10.6, elevated temperature tests were performed on Rainier Rubber Company butyl rubber compound No. RR–0405–70 O-ring seals with compressions as low as 10%. The specific time-temperature test parameters evaluated were 193 °C for 24 hours followed by 177 °C for 144 hours, for a total of 168 hours (1 week). At these temperatures, all elastomeric compounds are susceptible to relatively high helium permeability; thus, helium leak testing was not performed. Instead, a hard vacuum of less than 20 Pa was maintained on the test O-ring seals with no measurable pressure loss that would indicate leakage. At the end of the entire test sequence, the test O-ring seals were stabilized at -29 °C and shown, via helium leak testing, to be leaktight (i.e., a leak rate less than 1×10^{-8} reference Pascals – cubic meter per second (Pa–m^3/s), air leakage).

2.12.2.4 Test Procedure

To vary the O-ring face-seal compression, 30-mm diameter metallic shims of varying thickness were installed between each of the forty-four closure lid bolts. By varying the thickness of the shims, the percentage of O-ring seal compression was varied. The process of leakage rate testing an O-ring seal is as follows:

1. Install the inner and outer O-ring seals in the TN–Gemini closure lid.
2. Install shims of a given thickness between each of the closure lid bolt holes on the body.
3. Install the closure lid onto the body. Tighten the closure lid bolts to 20 N-m torque. This is conservatively less than the installation torque used in transport.
4. Perform a helium leakage rate test of the main O-ring containment seal.

2.12.2.5 Example of O–ring Seal Compression Calculation

The minimum and maximum O-ring seal compressions were calculated based on as-measured dimensions for the cross-sectional diameter and inner diameter of the test O-ring seals, and the O-ring seal groove depth of the TN–Gemini package. Stretch was determined using the as-measured length of the O-ring groove in the closure lid.

Four quantities are required for the compression calculation: 1) the cross-sectional diameter, D, of the O-ring seal, 2) stretch, S, of the O-ring seal, 3) groove depth, d, of the O-ring groove, and 4) the thickness of the shim, *e*. The minimum O-ring seal compression for Test No. 2 is determined as follows:

1. Extract the pertinent data from Table 2.12.2-2.

   D_{min} = 12.01 mm, the minimum O-ring seal cross-sectional diameter

   D_{max} = 12.14 mm, the maximum O-ring seal cross-sectional diameter

   d_{min} = 8.31 mm, the minimum groove depth

   d_{max} = 8.40 mm, the maximum groove depth

   e = 1.24 mm, the thickness of the shim

2. Determine the reduction in O-ring seal cross-sectional diameter due to stretch.

   From Table 2.12.2-2, the stretch of the O-ring seal diameter in the groove length was 3.0%. From Figure 3-3 for the calculated curve of the Parker O-ring Handbook[4], the resulting reduction in O-ring seal cross-sectional diameter is 1.5%. The reduced cross-sectional diameter, D_{Rmin} and D_{Rmax}, is therefore 1.5% less than the non-stretched diameters, D_{min} and D_{max}, or:

   $D_{Rmin} = (1 - 0.015)D_{min}$ = 11.83 mm

   $D_{Rmax} = (1 - 0.015)D_{max}$ = 11.96 mm

3. Calculate the O-ring seal compression.

[4] ORD 5700, *Parker O-ring Handbook*, 2007, Parker Hannifin Corporation, Cleveland, OH.

Using the quantities determined in (1) and (2) above, the seal compression, C_{seal}, is calculated as follows:

$$C_{seal} = \left[1 - \left(\frac{e + d}{D_R}\right)\right] \times 100$$

$$C_{seal\text{-}min} = \left[1 - \left(\frac{1.24 + d_{max}}{D_{Rmin}}\right)\right] \times 100 = 18.5\%$$

$$C_{seal\text{-}max} = \left[1 - \left(\frac{1.24 + d_{min}}{D_{Rmax}}\right)\right] \times 100 = 20.2\%$$

Following the procedure used above, the minimum and maximum O-ring seal compressions are calculated for all tests, and summarized in Table 2.12.2-2.

2.12.2.6 Test Results

Test results are summarized in Table 2.12.2-2. As shown in the table, the minimum O-ring seal compression that the butyl rubber material maintained a leaktight seal for the TRUPACT–III face seal configuration was 18.5%. Since the O-ring seal will contract more than the groove depth with temperature change, the minimum tested compression of 18.5% must be adjusted for minimum temperature of -40 °C. From the Parker O-ring Handbook, Table A3-2, an upper bound coefficient of expansion for all elastomer materials listed (butyl is not listed) is 2×10^{-4} mm/mm-°C. The O-ring cross-sectional diameter is 12 mm, and the temperature change between 21 °C and -40 °C is 61 °C. The contraction of the stainless steel is conservatively neglected. Therefore, the cross-sectional diameter contraction, C_{seal}, of the O-ring seal is:

$$C_{seal} = (2 \times 10^{-4})(12)(61) = 0.15 \text{ mm}$$

This contraction represents 1.3% of the cross-sectional diameter. Therefore, the minimum O-ring seal compression at room temperature for a leaktight seal is 18.5 + 1.3 = 19.8%, which ensures that the tested compression of 18.5% is still present at the minimum temperature of -40 °C.

These results, in conjunction with prior TRUPACT–II testing, confirm that the butyl O-ring seals used in the TRUPACT–III package will remain leaktight if subjected to worst-case seal compressions over the range of NCT and HAC cold and hot temperatures. Additionally, following a HAC thermal event, the O-ring seals will remain leaktight when cooled to a temperature of -29 °C, as demonstrated in the TRUPACT–II O-ring seal tests.

An additional test using a maximum elevated temperature of 232 °C was performed (see Test 2 in Table 2.12.2-1). In this case, the O-ring seals were not leaktight during the final, post-heat, -29 °C leak test, a vacuum at the high temperature could not be rapidly achieved, and the seals evidenced loss of elasticity and visible cracking was evident. Such was not the case for tests where the maximum temperature was 204 °C. It is therefore concluded that the upper temperature limit for this butyl compound is somewhere between 204 °C and 232 °C, but an upper temperature limit of 204 °C is conservatively utilized for analysis purposes.

This page intentionally left blank.

Table 2.12.2-1 – TRUPACT–II O-ring Seal Performance Test Results[5]

Test Number	O-ring Seal Cross-Sectional Diameter (inches)①				Stretch (%)		Maximum Gap (inches)		Minimum Compression (%)				Temperature for "Leaktight" Leak Test (Leakage ≤ 2.0×10^{-9} Pa-m³/s, He)				
	O-ring Seal No. 1		O-ring Seal No. 2				Center Disk	Offset Disk	Center Disk		Offset Disk		Center Disk④		Offset Disk④		
	Min	Max	Min	Max	Min	Max			Min	Max	Min	Max	Ambient	-40 °C	-29 °C	8 hrs⑤	-29 °C
1	0.387	0.397	0.387	0.396	2.0	4.1	0.026	③	22.1	25.6	14.9	20.0	Yes	Yes	Yes	177 °C	Yes
2	0.388	0.398	0.387	0.398	2.0	4.1	0.029	0.050	21.3	25.1	15.7	19.7	Yes	Yes	⑥	232 °C	No
3	0.387	0.397	0.387	0.399	2.0	4.1	0.027	0.052	21.9	25.8	15.2	19.4	Yes	Yes	Yes	204 °C	Yes
4	②	②	②	②	2.0	4.1	0.027	0.053	21.9	25.8	14.9	19.1	Yes	Yes	Yes	204 °C	Yes
5	②	②	②	②	2.0	4.1	0.026	0.050	22.1	26.0	15.7	19.9	Yes	Yes	Yes	204 °C	Yes

Notes:

① Material for all O-ring seal test specimens is butyl rubber compound RR-0405-70, Rainier Rubber Co., Seattle, WA.

② Not measured; calculations assume the worst case range as taken from Tests Numbers 1 - 3 (i.e., Ø0.387 minimum to Ø0.399 maximum).

③ Range of values is 0.048 minimum to 0.053 maximum due to an indirect method of gap measurement (used for this test only).

④ A "Yes" response indicates that helium leakage testing demonstrated that the leak rate was ≤ 1.0×10^{-8} Pa-m³/s, air (i.e., "leaktight" per ANSI N14.5). In all cases, measured leak rates were ≤ 2.0×10^{-9} Pa-m³/s, helium, for tests with a "Yes" response.

⑤ No helium leak tests were performed at elevated temperatures due to O-ring seal permeation and saturation by helium gas. The ability of the test fixture to establish a rapid, hard vacuum between the O-ring seals was used as the basis for leak test acceptance at elevated temperatures. All tests rapidly developed a hard vacuum, with the exception of Test Number 2 at an elevated temperature of 232 °C, which slowly developed a vacuum.

⑥ Initial leakage of 1.0×10^{-6} Pa–m³/s, helium; became leaktight (≤ 2.0×10^{-9} Pa–m³/s, He) approximately one minute later.

[5] U. S. Department of Energy (DOE), §2.10.2, *Elastomer O-ring Seal Performance Tests*, *Safety Analysis Report for the TRUPACT-II Shipping Package*, USNRC Certificate of Compliance 71–9218, U.S Department of Energy, Carlsbad Field Office, Carlsbad, New Mexico.

Table 2.12.2-2 – TRUPACT–III Containment O-ring Seal Performance Test Results

Test Number	O-ring Seal Cross-Sectional × Inner Diameter (mm)①		O-ring Groove Depth (mm)		Shim Thickness (mm)	Stretch (%)②	Compression (%)		"Leaktight" Leak Test (Leakage Rate ≤ 1.0 × 10^{-8} Pa-m^3/s, air)
	Min	Max	Min	Max			Min	Max	
1	12.01 × 2393	12.14 × 2393	8.31	8.40	0.00	3.0	29.0	30.5	Yes
2					1.24		18.5	20.2	Yes
3					1.56		15.8	17.4	No
4					2.27		9.8	11.5	No
5					2.29		9.6	11.3	No
6					2.32		9.4	11.1	No

Notes:

① Material for all O-ring seal test specimens is butyl rubber compound RR–0405–70, Rainier Rubber Co., Seattle, WA.

② Stretch, S, computed based on as-measured O-ring groove length (1,887.2 mm × 2,048.0 mm × R50 mm) with actual diameter measurements of O-ring seals per the following formula:

$$S = \frac{(\text{Groove Length}) - (\text{O-ring Length})}{(\text{O-ring Length})} \times 100$$

2.12.3 Certification Tests on CTU-1

This appendix presents the results of normal conditions of transport (NCT) and hypothetical accident condition (HAC) tests that address the free drop and puncture test performance requirements of 10 CFR 71[1]. This appendix summarizes the information presented in the test report[2] for the first TRUPACT–III certification test unit (CTU-1). Wherever the acronym "CTU" is used in this section, it is to be understood as meaning CTU-1.

2.12.3.1 Introduction

Demonstration of the compliance of the design of the TRUPACT–III transportation package with the requirements of 10 CFR §71.73 was primarily achieved using formal certification testing. Analysis was used for all NCT events except the free drop, and for HAC thermal and immersion cases. Performance of the debris shield, which was not present in the testing, was also evaluated by analysis. The NCT and HAC free drop events and HAC puncture event were demonstrated by testing. This appendix describes the results of the free drop and puncture testing, including post-test measurements and evaluations. One NCT free drop, four HAC free drops, and four HAC puncture tests were performed. The primary success criterion was that, subsequent to all free drop and puncture testing, the CTU containment boundary, including the closure lid and vent port seals, be leaktight per ANSI N14.5[3]. Other supporting data, including accelerations and physical measurements, was collected as described herein.

The TRUPACT–III CTU was fabricated in prototypic full-scale, which was in full compliance with the drawings given in Section 1.3.1, *Packaging General Arrangement Drawings* (except for differences noted and justified below). The results of extensive engineering tests on a half-scale engineering test unit (ETU) are provided in Section 2.12.1, *Engineering Tests*.

2.12.3.2 Test Facilities

Free drop and puncture testing of the TRUPACT–III package test unit was performed at Sandia National Laboratories' Coyote Canyon Aerial Cable Facility in Albuquerque, New Mexico. The drop pad is designed to accommodate test packages weighing up to 90,000 kg. The embedded steel plate target has a varying thickness of approximately 100 to 200 mm. The pad therefore constituted an essentially unyielding surface for the CTU, which weighed approximately 25,052 kg.

In accordance with the requirements of 10 CFR §71.73(c)(3), puncture bars were fabricated from a solid, 150 mm diameter mild steel. The length of each bar was designed to allow the puncture event to proceed to completion before the CTU gained any support from the unyielding surface, but without excessive length. Each puncture bar was welded with gussets perpendicularly to a thick

---

[1] Title 10, Code of Federal Regulations, Part 71 (10 CFR 71), *Packaging and Transportation of Radioactive Material*, 01–01–09 Edition.

[2] *TRUPACT–III Full–Scale Certification Test Report*, TR-024, Packaging Technology, Inc.

[3] "Leaktight" is a leakage rate not exceeding 1×10^{-8} Pascals – cubic meters per second ($Pa–m^3/s$), air, as defined in ANSI N14.5–1997 (or later), *American National Standard for Radioactive Materials – Leakage Tests on Packages for Shipment,* American National Standards Institute, Inc. (ANSI).

mild steel square plate. The top edge of each puncture bar was finished to a 6-mm radius maximum. Each puncture bar assembly was securely welded to the impact surface.

2.12.3.3 Test Unit Configuration

The CTU was an essentially prototypic, full-scale model of the TRUPACT–III package. The CTU was fabricated according to the drawings given in Section 1.3.1, *Packaging General Arrangement Drawings*. Prior to testing, the CTU data package was examined and a certificate of conformance was issued. Any differences between the CTU and a regular production TRUPACT–III unit are discussed and justified below.

1. The CTU utilized no thread inserts. The production unit inserts are stronger than threads made directly in the parent material. However, the production unit thread inserts are optional, therefore the CTU conservatively represented the minimum pull-out strength possible in a production unit.
2. The CTU utilized washers for closure bolts and overpack cover attachment bolts made from ASTM Type 304L material. The production unit washers are made from ASTM A564, Grade 630, Condition H1025 (17-4 PH) material. The production unit washers are significantly stronger than the CTU washers, thus, this substitution is conservative.
3. To reduce the effect of polyurethane crush strength tolerance on free drop impact and deformation results, the allowable range of properties in certain critical regions was reduced. In regions where the crush strength of the foam would affect maximum impact (the same drop tests for which cold temperature was used), the foam was fabricated using only the upper (stronger) half of the normally acceptable tolerance range. This helped ensure that the resulting impact magnitudes were not significantly affected by lower strength foam. In production units, expanding the crush strength tolerance to include the lower half of the range is conservative, since impacts could only be reduced. Likewise, in regions where the crush strength of the foam would affect maximum deflection (the same drop tests for which ambient temperature was used), the foam was fabricated using only the lower (weaker) half of the normally acceptable tolerance range. This helped ensure that the resulting deformations were not significantly affected by higher strength foam. In production units, expanding the crush strength tolerance to include the upper half of the range is conservative, since deformation could only be reduced. Of note, this use of biased strength tolerances was possible because the free drop tests were performed on different areas of the package, and interference of test results was not significant. Foam crush strength tolerances were biased according to the following table. Note that the 0.10 kg/dm^3 foam, located behind the puncture-resistant plates only, played a negligible role in free drops and was fabricated using the full production unit tolerance range.

CTU Reduced Foam Tolerance		
Density, kg/dm^3	**Tolerance Bias**	**Test Purpose**
0.16 (all locations)	Upper half-range	Primarily affects the end (LD1 & LD2) and side (LD3) orientations, for maximum impact.
0.29 (all locations)	Lower half-range	Primarily affects the CG-over-side-edge (LD5) orientation, for maximum deformation.
0.48 (left side only)	Upper half-range	Primarily affects the side (LD3) orientation, for maximum impact.
0.48 (all other locations)	Lower half-range	Primarily affects the CG-over-side-edge (LD5) and CG-over-corner (LD4) orientations, for maximum deformation.

4. To ensure conservative leakage rate measurement of the CTU containment O-ring seal, care was taken to ensure that the compression of the seal was near the minimum compression of the production unit seal. The as-built depth of the containment seal O-ring groove was d_G = 8.72 mm, and the cross-sectional diameter of the containment O-ring was D_R = 11.99 mm. From Section 4.1.3.1, *Seals*, the cross sectional diameter reduction due to O-ring stretch is 1.5%. The effective O-ring diameter is therefore:

$$D_{Re} = (1 - 0.015)D_R = 11.81\,\text{mm}$$

The compression of the CTU containment seal was therefore:

$$C_{CTU} = \left[1 - \left(\frac{d_G}{D_{Re}}\right)\right] \times 100 = 26.2\%$$

This is conservatively less than the minimum standard production unit containment seal compression of 27.8% calculated in Section 4.1.3.1, *Seals*.

5. Special vent and test ports were added to the side of the CTU that do not occur on the production unit. These were provided to allow leakage rate testing of the CTU without the need to remove the overpack cover or disturb the prototypic vent and test ports. They were located away from structural damage areas, and did not affect the behavior of the CTU.

6. The roller floor guide rails, the roller floor, and the pallet were not included in the test unit. Absence of these structures was conservative, since their beneficial capacity to absorb impact energy was not present. Their gross weight was included as part of the simulated payload.

7. The debris shield, including the receptacle, holder, foam rubber seal, and associated payload guide bars were not included. Absence of these components allowed debris contamination of the containment seal, as discussed in Section 2.12.3.8.1, *Leakage Rate Tests*. Their absence was also structurally conservative, since they would have a tendency to strengthen the containment boundary.

8. Several minor package features were omitted from the CTU: Package nameplate, tamper-indicating device, pressure relief valve on the overpack cover, paint, and the optional rubber bumper strips in the payload cavity. Lack of these items did not affect the outcome of the certification tests.
9. Small steel accelerometer mounting blocks and threaded steel lifting bosses were welded to the outside surface of the CTU. Since they were not directly involved in test damage, their presence did not affect results.
10. Several nonconformances were encountered during fabrication of the CTU. All are recorded in the data package for the CTU, and were dispositioned according to the Quality Assurance program and approved by Packaging Technology. The nonconformances were very minor in nature and did not have a significant effect on the performance of the CTU during testing. The most significant nonconformances are noted in the following list.

    - Twelve V-stiffeners having a design for the closed end of the CSA were placed on the top and bottom sides (six each). Since the V-stiffeners for the end and sides are of a very similar design, this had no effect.
    - The body flange face thickness should be 20 - 30 mm. The thickness of the CTU flange face ranges from 16 to 22 mm. The regions of under-thickness were not extensive. In any case, the resulting strength of the flange was less than a production unit, and was therefore conservative.
    - The internal length of the CTU was 2,783 – 2,785 mm [109.57 – 109.65 inches] versus the specified dimension of 2,790 +20/-5 mm [109.84 +0.79/-0.20 inches]. This had no effect on test results.
    - The thickness of the calcium silicate insulation was 1-inch and 1½ inches thick instead of 30 mm and 42 mm thick. This had no effect on test results.
    - The M120 threads for the vent port retaining ring were mis-cut for a depth of 86 mm. This would tend to reduce slightly the strength of the vent port closure, and is conservative.
    - The weld connecting the front edge of the right side outer skin sheet to the CTU had poor penetration. This caused an excessively long weld tear during a free drop. This is further discussed in Section 2.12.3.7.4, *Free Drop, Side-Edge, HAC (Test LD5)*.
    - The washers used with the overpack cover attachment bolts had an outer diameter of 54 mm instead of the 64 mm required by the drawings. In addition, the 44-mm diameter mounting holes on the top of the overpack cover were elongated similar to the mounting holes on the bottom of the cover. Since both of these conditions would increase the likelihood of the bolt head being pulled through the hole, they conservatively reduce attachment integrity.
    - The width to the outside of the front cheeks was 2,155 mm versus the specified dimension of 2,120 ±25 mm due to weld distortion. This condition would tend to apply lateral forces to the cheeks during end impacts, and is conservative for testing.

Except for these differences, the CTU was in full compliance with the SAR drawings of the TRUPACT–III package. Prior to any certification testing, the CTU was subject to acceptance testing, including a lifting load test, an internal pressure (1.5 times MNOP) test, and leakage rate tests of the containment boundary.

The test payload consisted primarily of a large quantity of square-ended, two-inch and four-inch diameter aluminum bars, with additions of other items made from brass and aluminum. The total weight of the test payload was 6,747 kg, which is 30.4% more than the maximum TRUPACT–III payload of 5,175 kg. This condition is particularly conservative for impact loads on the closure lid. The gross weight of the CTU was 25,052 kg, slightly more than the maximum gross weight of the TRUPACT–III package of 25,000 kg.

2.12.3.4 Instrumentation

2.12.3.4.1 Accelerometers

Accelerometers were utilized to record each free drop impact. No accelerometers were used for puncture drop tests. At least four single axis accelerometers were used to record each free drop event. The accelerometers were attached to solid stainless steel blocks that were fillet welded to the outer sheet on the body at the locations shown in Figure 2.12.3-1. The accelerometer type used in the tests was piezoresistive. Data was recorded, conditioned, and reduced by the Sandia Mobile Instrumentation Data Acquisition System (MIDAS). A Fast Fourier Transform (FFT) of the raw data was performed to determine the appropriate cutoff, or filtering frequency. The accelerometer data was filtered using a six-pole Butterworth filter with the cutoff set no lower than 250 Hz.

2.12.3.4.2 Thermocouples

As discussed in Section 2.12.3.5.2, *Temperature*, maximum impact will occur at the minimum initial temperature condition of -29 °C, as defined in 10 CFR §71.73(b). Type K thermocouples were installed and numbered in each end of the package to measure the temperatures of the polyurethane foam in the critical regions. The thermocouple locations that were utilized for the free drop tests are shown in Figure 2.12.3-2. Temperatures were monitored only in critical areas, i.e., those experiencing deformation in the free drop event. The data was monitored by Sandia's MIDAS data acquisition system during the chilling period, and continued until impact.

2.12.3.5 Initial Test Conditions

2.12.3.5.1 Internal Pressure

Since internal pressure has the effect of increasing the stress on the containment boundary, the CTU was pressurized (at ambient temperature) to an internal pressure of 172 kPa, equal to the design pressure. Since resistance to puncture is not significantly affected by internal pressure, the CTU was not pressurized for the puncture tests. Since the pressure is only an initial condition, monitoring the pressure was not performed.

2.12.3.5.2 Temperature

The free drop tests evaluated the integrity of the containment boundary under maximum impact, as well as the maximum deformation of the overpack for analysis of the HAC fire event. The greatest impact corresponds to the minimum regulatory temperature condition of -29 °C, due to

the increase in crush strength of the impact limiting materials with decreasing temperature. Consequently, in free drops LD1, LD2, and LD3, the CTU was tested at a material temperature below -29 °C. Ambient temperature was used for all puncture drop tests. For those free drop orientations where maximum deformation was of concern (free drops LD4 and LD5), the test was performed at a temperature of at least 7 °C and extrapolated using analysis to the deformation corresponding to maximum NCT temperature.

2.12.3.6 Certification Tests Performed

The evaluation and selection of tests to be performed for certification testing is discussed in Section 2.7.1, *Free Drop*, and Section 2.7.3, *Puncture Drop*. A total of four HAC free drops and one NCT free drop were performed, as summarized in Table 2.12.3-1. A total of four puncture drops were performed, as summarized in Table 2.12.3-2. The free drops (except for tests LD1 and LD2, which are flat on the closure lid end, and LD3, which is flat on the side) are shown schematically in Figure 2.12.3-3 and Figure 2.12.3-4, and the punctures in Figure 2.12.3-5 through Figure 2.12.3-8.

2.12.3.7 Test Results

Five free drop tests were performed: one from a height of 0.3 m and four from a height of 9 m. After certain key drop tests, a vacuum was placed between the closure lid seals as an approximate confirmation of the sealing integrity of the seals, using the special test port on the CTU side. An adequate vacuum could not be obtained after the last free drop had been performed, likely as a consequence of the debris contamination of the containment seal as discussed in Section 2.12.3.8.1, *Leakage Rate Tests*. The tests were performed in the sequence: LD1, LD2, LD3, LD5, and LD4.

Four puncture drop tests were performed, all from a height of one meter. The internal pressure was bled off to approximately 2 psig. Accelerations were not recorded. All puncture tests occurred at prevailing CTU temperatures, which, based on ambient temperatures and the temperature of the last free drop, were between approximately 13 °C and 18 °C. The puncture bars typically did not survive the tests without damage. Two became bent, and one completely broke off subsequent to impact. However, the baseplate joints and attachment to the impact pad remained intact in all cases. For rigging convenience, the puncture tests were performed in the order: LP3, LP4, LP1, and LP2.

Prior to performing any free or puncture drop tests, helium leakage rate tests were performed on the containment metallic boundary, the main O-ring seal, and the sampling/vent port plug O-ring seal. All free drop and puncture drop measurements and testing were performed in accordance with a written test plan prepared for the TRUPACT–III certification testing program. Photos of certification testing are provided in Figure 2.12.3-9 to Figure 2.12.3-34.

2.12.3.7.1 Free Drop, Vertical, Overpack Cover Down, NCT (Test LD1)

Test LD1 was a free drop from a height of 0.3 m, oriented with the CTU axis vertical, striking the overpack cover flat on the surface. In order to preclude the necessity of re-chilling the CTU before the following test, the CTU was over-chilled for test LD1. The average temperature of thermocouples T1 and T3 was -42 °C. The average temperature of the deeper thermocouples T2 and T4 was -40 °C. The ambient temperature was 23 °C. Accelerations were obtained from gages A1A, A3A, and A4A. The raw signals were filtered at 250 Hz, and the resulting acceleration plots are shown in Section 2.12.3.9, *Acceleration Time History Plots*. The peak accelerations and overall average maximum acceleration

are shown in the table below. After the drop, there was little visible damage to the CTU. However, the overpack cover, which had projected an average of 22 mm beyond the end faces of the cheeks, was uniformly crushed by an average of 7 mm. Photos of the post-test condition are not provided since no damage was visible.

A1A	A3A	A4A	Avg.
36.8g	49.1g	26.1g	**37.3g**

2.12.3.7.2 Free Drop, Vertical, Overpack Cover Down, HAC (Test LD2)

Test LD2 was a free drop from a height of 9 m, oriented with the CTU axis vertical (same as LD1), striking the overpack cover flat on the surface. The average temperature of thermocouples T1 and T3 was -34 °C. The average temperature of the deeper thermocouples T2 and T4 was also -34 °C. The ambient temperature was 12 °C. Accelerations were obtained from gages A1A and A3A. (Note: velocity integrations of gages A2A and A4A showed velocities which are not physically possible, thus these gages were ignored.) The raw signals were filtered at 250 Hz, and the resulting acceleration plots are shown in Section 2.12.3.9, *Acceleration Time History Plots*. The peak accelerations and overall average maximum acceleration are shown in the table below.

A1A	A3A	Avg.
208.9g	199.8g	**204.4g**

In this case, both the overpack cover and the cheeks came into contact with the ground. There was very little rebound after impact. The additional crush was an average of 29 mm for a total end crush of 36 mm. There were a number of small weld cracks around the impacted end, but they were not significant relative to exposure of foam. The gaps between the cheeks and the overpack cover on the left and right sides were essentially closed by the buckling deformation of the 14-ga [0.0751-inch] thick sheets located on the cheeks and overpack cover. A hard vacuum was obtained between the closure lid O-ring seals after the test. Photos of the damage are shown in Figure 2.12.3-9 through Figure 2.12.3-12.

2.12.3.7.3 Free Drop, Flat Side, HAC (Test LD3)

Test LD3 was a free drop from a height of 9 m, oriented with the CTU axis horizontal, striking flat on the left side of the package. The average temperature of thermocouples T5 through T8 was -39 °C. The ambient temperature was 12 °C. Accelerations were obtained from gages A1L, A4L, A5L, A8L, A9L, and A10L. The raw signals were filtered at 300 Hz, and the resulting acceleration plots are shown in Section 2.12.3.9, *Acceleration Time History Plots*. The peak accelerations and overall average maximum acceleration are shown in the table below.

A1L	A4L	A5L	A8L	A9L	A10L	Avg.
529.2g	378.5g	438.2g	455.4g	352.2g	288.3g	**407.0g**

Some slight additional damage was noted in the areas around the ISO fittings, but little other external damage could be found. Measurements were taken at the four corners of the package between the outside surface and the surface of the internal containment structural assembly (CSA) using small drilled holes in the outer skin. These holes, designated S1 – S4, are located as shown in Figure 2.12.3-2. The depth of the holes was measured before any testing and

compared to measurements after test LD3, and show the magnitude of any "inside-out" deformations of the CSA relative to the outside of the CTU. The average decrease in the four measurements (i.e., the amount that the CSA approached the impact surface from inside of the body overpack) was 7 mm. A hard vacuum was obtained between the closure lid seals after the test. Photos of the damage are shown in Figure 2.12.3-13 through Figure 2.12.3-15.

2.12.3.7.4 Free Drop, Side-Edge, HAC (Test LD5)

Test LD5 was performed prior to Test LD4 for expediency in rigging. Test LD5 was a free drop from a height of 9 m, oriented with the CTU axis horizontal, and rotated about that axis so that it impacted with the center of gravity (CG) over one long edge (the upper right edge), as shown in Figure 2.12.3-3. The average temperature of thermocouples T6 and T8 was 7 °C. The temperature of the body overpack skin was between 17 and 24 °C. The ambient temperature was 18 °C. Accelerations were obtained from gages A1L, A3L, A5L, and A7L. The raw signals were filtered at 250 Hz, and the resulting acceleration plots are shown in Section 2.12.3.9, *Acceleration Time History Plots*. The peak accelerations and overall average maximum acceleration lateral to the CTU are shown in the table below. A resolution of the average acceleration to the vertical direction is performed using the following equation:

$$A_{\perp} = \frac{A_L}{\cos(47)} = 142.2\text{g}$$

where A_L is the overall average lateral acceleration and the lateral direction is oriented at an angle of 47° to the vertical as defined in Figure 2.12.3-3.

A1L	A3L	A5L	A7L	A_L	Resolved Average
118.4g	90.2g	94.3g	85.2g	**97.0g**	**142.2g**

The impact caused a flat region along the central side-edge approximately 305 mm wide. This tapered down to approximately 178 mm toward each end. During post-test disassembly, it was noted that the minimum perpendicular distance between the inside surface of the outer skin and the corner of the relatively rigid weldment which protects the calcium silicate insulation was 95 mm. A gap opened up between the front cheek and the steel plate encasing the 0.29 kg/dm^3 foam equal to approximately 16 mm across the crush width. Additionally, the weld between the side outer skin and the front cheek unzipped for a distance of approximately 914 mm, and was a maximum of 51 mm wide, exposing the balsa wood in the side panel. It was subsequently determined that this weld was substandard. A vacuum test on the closure lid seals was not performed. Photos of the damage are shown in Figure 2.12.3-16 through Figure 2.12.3-18.

2.12.3.7.5 CG-Over-Corner, Overpack Cover Down, HAC (Test LD4)

Test LD4 was a free drop from a height of 9 m, oriented with the CTU axis oriented approximately 50° to the ground, striking the lower right corner of the package as shown in Figure 2.12.3-4. The center of gravity of the package was over the point of initial impact. The average temperature of thermocouples T1 and T2 was 12 °C. These two temperatures were the shallow and deep readings on the opposite corner of the package, and were representative of the temperature of the impacted corner. The ambient temperature was 14 °C. Accelerations were obtained from gages A1A, A2A,

A3A, and A4A. The raw signals were filtered at 250 Hz, and the resulting acceleration plots are shown in Section 2.12.3.9, *Acceleration Time History Plots*. The peak accelerations and overall average maximum acceleration axial to the CTU are shown in the table below. A resolution of the average acceleration to the vertical direction is performed using the following equation:

$$A_{\perp} = \frac{A_A}{\cos(40)} = 52.7g$$

where A_A is the overall average axial acceleration and the axial direction is oriented at an angle of 40° to the vertical as defined in Figure 2.12.3-4.

A1A	A2A	A3A	A4A	A_A	Resolved Average
35.4g	44.1g	39.8g	42.3g	**40.4g**	**52.7g**

The impact caused a triangular flat region having dimensions of 1,054 mm along the overpack cover, 838 mm along the bottom, and 800 mm along the right side of the CTU. The combined damage from all of the free drops caused a slight bowing of the right cheek, and a gap of up to 76 mm at the center between the cheek and the overpack cover right edge. The gap was however blocked with buckled material starting about 89 mm deep into the gap, and the gap reduced to zero width at the top and bottom of the cheek-to-cover joint. No significant weld seam failures were noted from this test. A hard vacuum could not be obtained between the closure lid seals, but the leak was not significant enough to have a measureable effect on the internal cavity pressure. Photos of the damage are shown in Figure 2.12.3-19 and Figure 2.12.3-20.

2.12.3.7.6 Puncture Drop On CG-over-Corner Damage (Test LP3)

The ambient temperature for this test was 17 °C. The puncture bar struck at essentially the center of the prior c.g.-over-corner free drop (LD4) damage and created a further deformation of approximately 178 mm in diameter and 102 mm deep. The effect of the impact was to further locally compress the deformed materials in the damaged zone. Small amounts of foam were visible from the free drop test damage, and the puncture test did not significantly alter this. After cutting away the damaged material, a minimum distance of 51 mm was measured between the deformed steel resulting from the puncture drop and the nearest part of the calcium silicate protection box. This distance was filled with compressed, 0.48 kg/dm^3 foam. A photograph of the damage is shown in Figure 2.12.3-21.

2.12.3.7.7 Puncture Drop On Side-Edge Damage (Test LP4)

The ambient temperature for this test was 16 °C. The puncture bar struck on the prior damage from free drop test LD5, with the center of the bar placed approximately 584 mm from the cover end of the package, with the package inclined 30° from the horizontal. The bar penetrated the outer skin (creating an approx. 178 mm diameter disk), and struck the top corner of the heavy structural box which protects the calcium silicate insulation in the cheek. This box is only 52 mm across, and is made from 16 mm thick material, and is therefore very rigid. Later disassembly showed relatively minor weld cracks in this region and only approximately 3 mm of deformation of the protective box. There was no damage to the calcium silicate insulating board, which maintained full integrity without crumbling or breaking. Note: the puncture bar fractured completely at a plane just above the reinforcement gussets as the package tipped off of the bar

following impact. However, all puncture bar welds, including those to the drop pad, remained intact. Photos of the damage are shown in Figure 2.12.3-22 and Figure 2.12.3-23.

2.12.3.7.8 Puncture Drop On Side Damage (Test LP1)

The ambient temperature for this test was 22 °C. The puncture bar penetrated both the outer skin and the puncture-resistant plate, and left a dent of approximately 51 mm deep in the CSA outer structural sheet. There was no cutting or cracking of the CSA outer sheet, demonstrated by placing the CSA annular region under a vacuum. There was no deformation of the inner CSA containment sheet. The opening in the overpack was 254 mm long and 178 mm wide. Photos of the damage are shown in Figure 2.12.3-24 through Figure 2.12.3-26.

2.12.3.7.9 Puncture Drop On Overpack Cover (Test LP2)

The ambient temperature for this test was 17 °C. The puncture bar struck the overpack cover approximately 292 mm from the left edge of the octagonal recess. The depth of penetration of the bar, measured from the outside surface, was 210 mm. From this value, the calculated depth of the dent in the puncture-resistant plate is approximately 145 mm deep. However, the puncture-resistant plate was not penetrated nor cracked. Removal of the overpack cover showed the impact to have been aligned between two V-stiffeners in the closure lid. A dent of approximately 5 mm deep was noted in the outer sheet of the closure lid at the puncture location. There was no deformation of the inner closure lid containment sheet. Photos of the damage are shown in Figure 2.12.3-27 and Figure 2.12.3-28.

2.12.3.8 Leakage Rate Tests and Post-Test Measurements

2.12.3.8.1 Leakage Rate Tests

Post-test leakage rate testing of the containment boundary was performed using helium test gas and a mass spectrometry leak detector (MSLD). The testing consisted of three elements:

- Metallic portion of the containment boundary
- Closure lid containment O-ring seal
- Vent port containment O-ring seal

The metallic portion of the containment boundary was tested by evacuating the payload (interior) cavity and then replacing the air in the annulus between the containment and structural sheets of the CSA with helium. The closure lid and vent/test port containment seals were both tested by evacuating the space between the containment seal and the test seal and then filling the payload cavity with helium. The metallic containment boundary leakage rate test was successful, with an adjusted leakage rate of 8.00×10^{-10} Pa-m^3/s, He, against a criterion of 2.2×10^{-8} Pa-m^3/s, He. The vent port containment O-ring seal leakage rate test was also successful, with an adjusted leakage rate of 4.07×10^{-9} Pa-m^3/s, He, against the same criterion.

The leakage rate test of the closure lid containment O-ring seal was, however, not initially successful. After removal of the closure lid, an amount of small debris was found to be present on both the containment and test O-ring seals, as shown in Figure 2.12.3-32 through Figure

2.12.3-34. Examination of the debris proved it to be made from thin shards or chips of aluminum that had been generated from the dummy payload bars in the testing. Some grain-like material may have come from some broken aluminum castings in the payload. Since the cavity was pressurized to 172 kPa, it is concluded that a transient opening of the closure joint during the impact event allowed debris to be blown outward by escaping air pressure over the sealing surfaces. Note: this does not mean that the gap size was larger than the amount by which the O-ring seal was initially compressed. Rather, the elastomer containment seal could not elastically respond in the very brief gap opening duration (on the order of milliseconds).

After cleaning the exposed surface of the O-rings (without removing them) and the body flange, the closure lid was reinstalled and all of the closure bolts were retightened to the smallest recorded residual tightening torque (that of bolt no. 16) of 149 N-m. See Section 2.12.3.8.2.2, *Closure Lid Bolt Removal Torque and Related Observations*, for a definition of residual torque. The leakage rate test of the closure lid containment seal was repeated and was successful, with an adjusted leakage rate of 1.76×10^{-9} Pa-m^3/s, He. As a further demonstration that the lack of leaktight condition was wholly attributable to the presence of debris, and not to low residual closure bolt torques, a third leak test was performed with only the four bolts in the corners of the closure lid installed (bolt nos. 1, 11, 23, and 33), again tightened to only 149 N-m. This test was also successful, with an adjusted leakage rate of zero. Note that since the internal pressure during the tests was atmospheric, there was no assistance from atmospheric pressure in holding the closure lid against the body. Furthermore, as the package was oriented horizontally, there was no assistance from the lid deadweight. These two supplemental leakage rate tests of the closure lid containment O-ring seal were performed for information only. They do not replace the initial, failed leakage rate test, but rather demonstrate leaktight capability in the absence of debris. The leakage rate test results are recorded in Table 2.12.3-3.

2.12.3.8.2 CTU Measurements

Besides measurement of the damage reported above, various measurements were taken of the CTU during disassembly as discussed below. A view of the payload cavity showing the state of the simulated payload after testing is shown in Figure 2.12.3-29.

The interior dimensions of the payload cavity were measured both prior to and subsequent to testing, and comparison of the measurements indicated only one negligible change. The diagonal of the open end which was in line with the impact from the Side-edge free drop impact LD5, having a nominal measurement of 2,718 mm, decreased by approximately 2 mm. Of note, this deformation was in the plane of the closure flange, and did not affect the closure seal. Careful measurements of the containment surface undulations indicated no evidence of actual or incipient local or global buckling. The inner walls of the CSA featured numerous dents as a result of impact with the simulated payload bars. The dents were of modest depth and there was no indication of failure of the containment sheet material.

2.12.3.8.2.1 Body Flange and Closure Lid Observations

The closure lid shear lip contacted the top right corner of the body (on both the top and right side flanges) corresponding to the side-edge free drop impact. The maximum indent was approximately 1.3 mm deep (See Figure 2.12.3-30). There was a local waviness of the body flange face of approximately 0.61 mm, possibly the result of bulged metal which was associated

with the shear lip impacts. There were no other indications of contact with the shear lips. In addition, the body flange exhibited a consistent slope on all four sides. Looking into the cavity, the inner flange edge of the CSA was nearest the observer, and the outer flange edge was farthest from the observer, on all four sides. The taper amounts varied between 0.25 to 0.50 mm, over the distance between the inner surface edge and the bolt line. This effect is probably due to the distortion caused by welding the body overpack parts in place after final flange machining. The small magnitude of this slope makes it of negligible importance. In addition, the direction of the taper is such that greater lid deformation would be necessary to open the containment seal.

To determine the lateral clearance which existed between the lid shear lip and the body flange, measurements of the lip and body flange were taken at three points along each side. Taking into account the shape and orientation of the interfacing edges, the maximum clearance (i.e., maximum possible movement) between the lid and the body in the lateral (side-to-side) direction was 3.37 mm, and in the vertical (top-bottom) direction, 4.49 mm.

2.12.3.8.2.2 Closure Lid Bolt Removal Torque and Related Observations

The residual torque of the closure bolts was checked by turning them counter-clockwise until impending motion of the bolt was sensed, and recording the torque achieved (the 'loosening' value). The bolt was subsequently turned clockwise, and the torque for impending motion was again recorded (the 'tightening' value). Both readings are given in Table 2.12.3-4. It was found that bolts on the right side, and some on the right ends of the top and bottom sides, featured relatively low residual torques compared to the other bolts. Upon removal of all bolts, it was also discovered that many bolts were bent. There was very good correlation between lower-than-expected residual torque and the degree of bending. The worst bolts (lowest torque, greatest bending) were located near the center of the right flange. Each bolt was bent in two opposite directions, with the axes of the threaded portion and of the bolt head nearly parallel, but with the axes offset. All bolts were chucked in a lathe to measure the runout between the head and the threads. The indicator was placed approximately 6 mm from the lower bearing surface of the head. The results as total indicator reading (TIR) are given in Table 2.12.3-5. The worst bolt was no. 17, having a TIR of 10.7 mm. A plot showing the correlation between runout and tightening torque is given in Figure 2.12.3-35. The direction of bolt bending relative to the package was toward the 11:00 o'clock direction, viewed from the open end, and was essentially uniform for all bent bolts. Each of the bent bolts also showed evidence of a side impact on the head. A smaller number of washers showed a similar side impact. As shown in Figure 2.12.3-31, the impact occurred near the lower bearing surface of the bolt head. The impact on the head aligned with the direction of bending and with evidence of contact in the overpack cover bolt head clearance cups. The location of the contact between the closure bolts and the overpack cover cups indicates that the overpack cover, most likely in the CG-over-corner free drop, moved into contact with the bolt heads and bent them.

Most of the clearance cups also showed some axial collapse due, presumably, to the lid down free drop. In some cases, the flat top of the bolt head contacted the inside bottom of the cups. This contact was most likely to occur near the center of each side of the lid. However, as noted, only the bolts on the right side had below-average residual torque.

The lid guide pin on the right side was sheared by approximately 4.3 mm towards the 11:00 o'clock direction. The guide pin on the left was sheared approximately 1.0 mm towards the 3:00 o'clock

direction. All closure bolt washers showed evidence of a thickness reduction, due to initial preload torque, applied impact loads, or both.

Table 2.12.3-1 – Free Drop Test Summary

Test	Description[1]	Orientation	Temperature[2]	Accelerometers & Direction[3]	Temperature Monitors
LD1	Vertical, overpack cover down, NCT	CTU axis vertical, impacting flat on cover end. (No figure)	Cold	A1A thru A4A	T1 & T3
LD2	Vertical, overpack cover down, HAC	CTU axis vertical, impacting flat on cover end. (No figure)	Cold	A1A thru A4A	T1 & T3
LD3	Flat side, HAC	CTU axis horizontal, impacting flat on left side. (No figure)	Cold	A1L, A4L, A5L, A8L, A9L, A10L	T5 thru T8
LD4	CG-over-corner, overpack cover down, HAC	CTU axis inclined 50° from horizontal, impacting on lower right corner. See Figure 2.12.3-4.	Prevailing, >7 °C	A1A thru A4A	T1 & T2
LD5 [4]	Side-edge, HAC	CTU axis horizontal, rotated 47° from horiz., impacting on upper right edge. See Figure 2.12.3-3.	Prevailing, >7 °C	A1L, A3L, A5L, A7L	T6 & T8

Notes:
1. NCT drop height 0.3 m; HAC drop height 9 m.
2. Recorded temperatures of the energy absorbing material are reported in Section 2.12.3.7.
3. Accelerometer designations are as follows: A1A is location no. 1, axial direction; A5L is location no. 5, lateral direction, etc. (lateral is defined as perpendicular to the package side as normally transported).
4. Test LD5 was performed before test LD4.

Table 2.12.3-2 – Puncture Drop Test Summary

Test No.	Description	Orientation
LP1*	On side damage	Impact on left side, inclined at 20° from horizontal, through CG. See Figure 2.12.3-5.
LP2	On overpack cover	Impact overpack cover in the octagonal recess, inclined at 25° to horizontal, through CG. See Figure 2.12.3-6.
LP3	On c.g.-over-corner damage	Impact on crushed corner at same orientation as test LD4, through CG. See Figure 2.12.3-7.
LP4	On side-edge damage	Impact on crushed edge from test LD5, inclined 30° from horizontal. See Figure 2.12.3-8.

*Sequence of test performance was LP3, LP4, LP1, LP2.

Table 2.12.3-3 – Leakage Rate Test Results

Test Date	Test Performed	Adjusted Leak Rate (Pa-m^3/s, He)	Pass/Fail[1]
12/12/06	Metallic containment boundary	8.00×10^{-10}	Pass
12/14/06	Closure lid containment seal	Test terminated	Fail
12/14/06	Vent port containment seal	4.07×10^{-9}	Pass
12/20/06	Closure lid containment seal, after debris removal (all 44 bolts × 149 N-m)	1.76×10^{-9}	Pass
3/2/07	Closure lid containment seal, after debris removal (4 corner bolts only × 149 N-m)	Zero[2]	Pass

Notes:
1. Pass criterion equals 2.2×10^{-8} Pa–m^3/s, He.
2. Zero leakage rate means that the final MSLD test reading was lower than the initial reading.

Table 2.12.3-4 – Closure Lid Bolt Residual Torques, N-m

Bolt No.	Residual Torque, Top Flange	Bolt No.	Residual Torque, Right Flange	Bolt No.	Residual Torque, Bot. Flange	Bolt No.	Residual Torque, Left Flange
1	759/1,248	12	475/658	23	542/664	34	814/1,112
2	868/1,166	13	522/583	24	678/868	35	976/1,220
3	1,003/>1,356	14	400/549	25	732/732	36	814/814
4	759/1,275	15	346/434	26	814/814	37	895/895
5	1,085/1,356	16	149/149	27	841/841	38	841/949
6	732/1,085	17	393/393	28	841/841	39	841/1,166
7	868/1,112	18	136/190	29	678/678	40	163/271
8	814/1,112	19	353/420	30	976/1,329	41	841/1,139
9	949/1,275	20	441/542	31	1,003/1,003	42	732/1,112
10	922/1,139	21	447/542	32	1,112/1,356	43	949/1,166
11	651/997	22	590/664	33	922/949	44	922/>1,356

Note: The value to the left of the slash character is the residual loosening torque, and the value to the right is the residual tightening torque, in N–m. See Section 2.12.3.8.2.2, *Closure Lid Bolt Removal Torque and Related Observations* for a definition of these quantities.

Table 2.12.3-5 – Closure Bolt Runout, TIR, mm

Bolt No.	Bolt Runout, Top Flange	Bolt No.	Bolt Runout, Right Flange	Bolt No.	Bolt Runout, Bot. Flange	Bolt No.	Bolt Runout, Left Flange
1	1.17	12	3.18	23	6.07	34	0.64
2	0.71	13	4.37	24	5.05	35	0.89
3	0.81	14	5.82	25	2.44	36	0.61
4	0.74	15	7.11	26	0.74	37	0.91
5	0.81	16	7.75	27	0.41	38	1.35
6	1.37	17	10.67	28	1.19	39	1.35
7	1.32	18	7.49	29	0.86	40	0.91
8	0.51	19	7.67	30	0.61	41	1.42
9	0.94	20	10.19	31	0.79	42	0.79
10	0.97	21	8.03	32	1.07	43	1.07
11	0.58	22	4.57	33	0.51	44	1.22

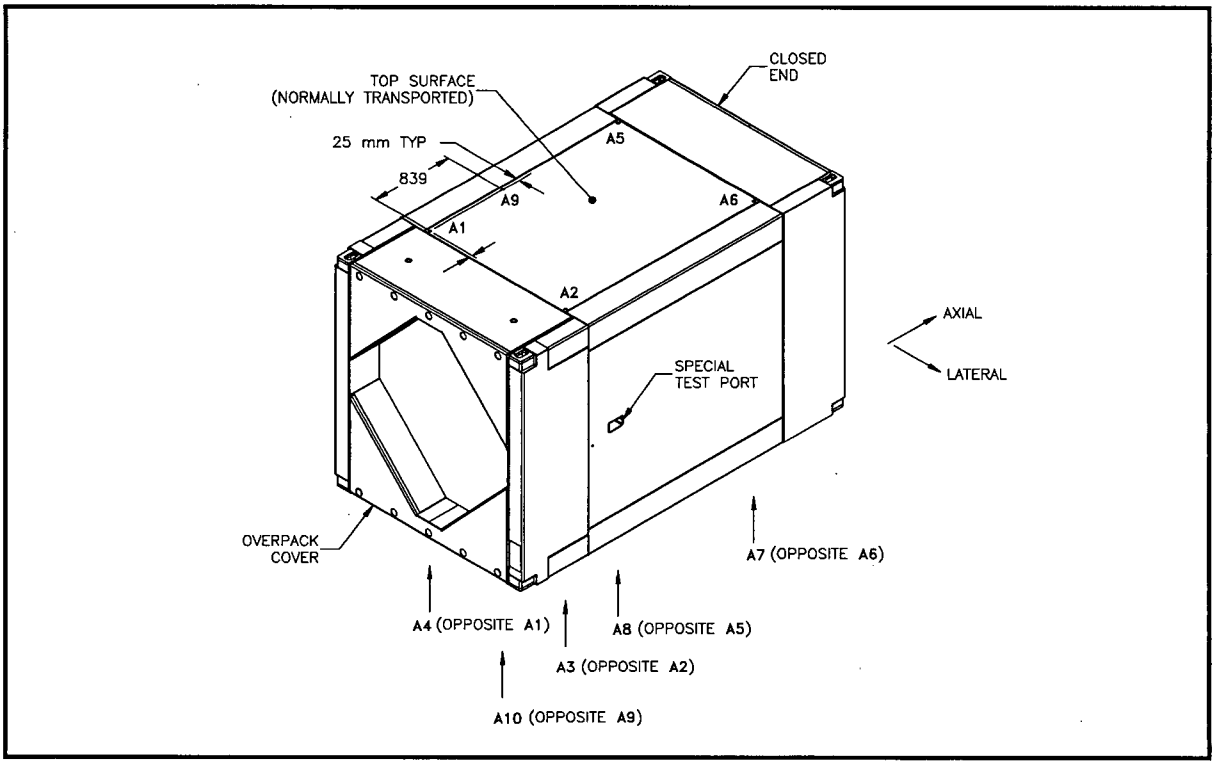

Figure 2.12.3-1 – Accelerometer Locations

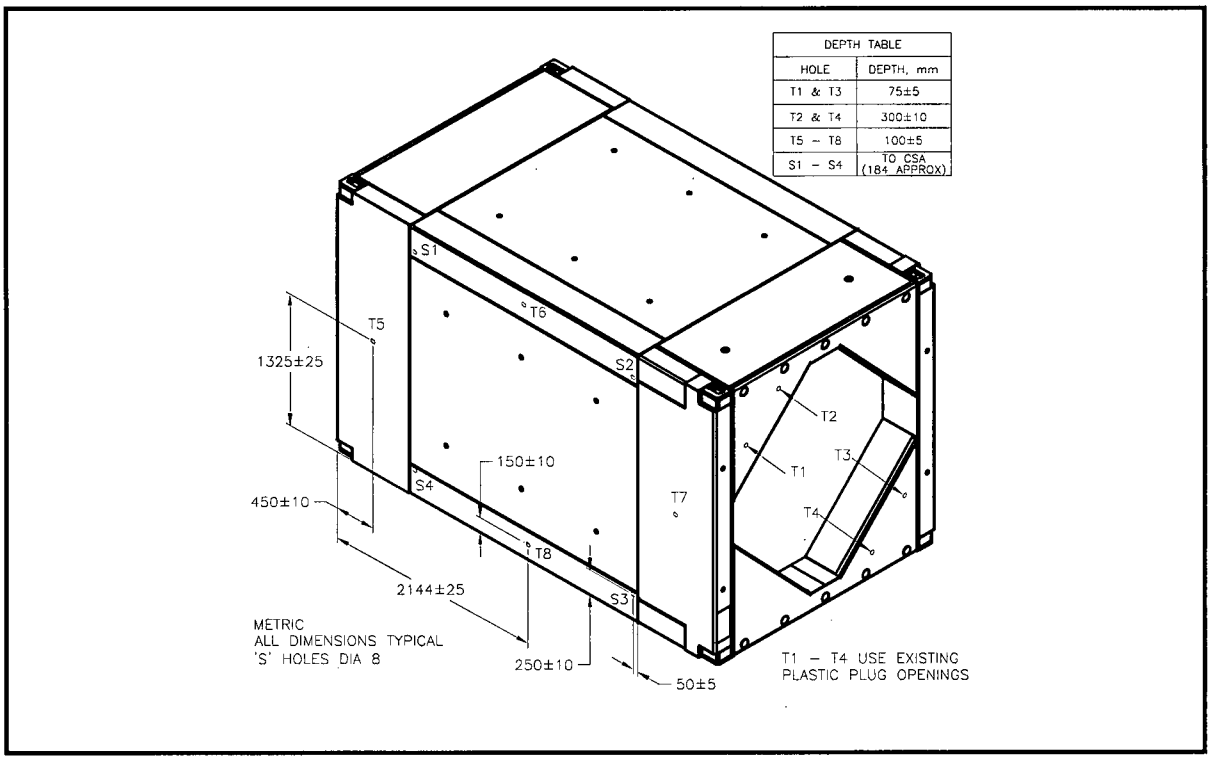

Figure 2.12.3-2 – Thermocouples (Tx) and Depth Measurement Holes (Sx)

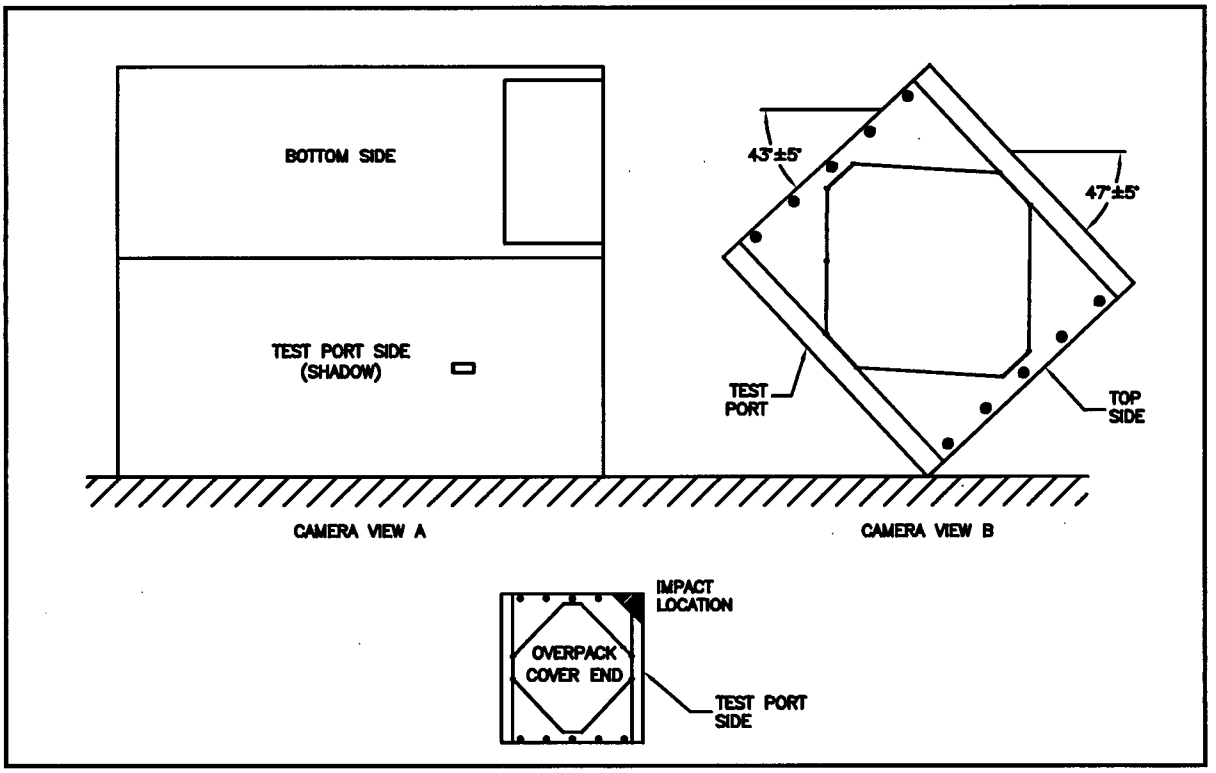

Figure 2.12.3-3 – Side – Edge Free Drop Orientation, Test LD5

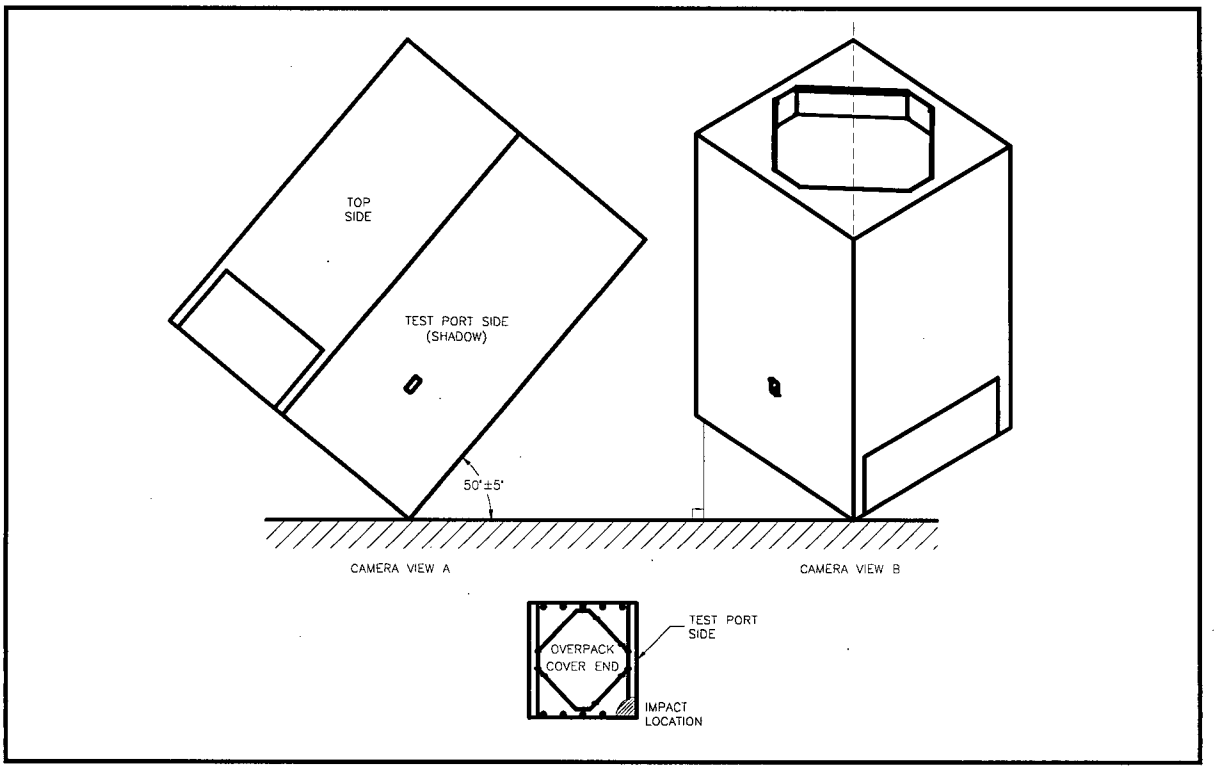

Figure 2.12.3-4 – CG-Over-Corner Free Drop Orientation, Test LD4

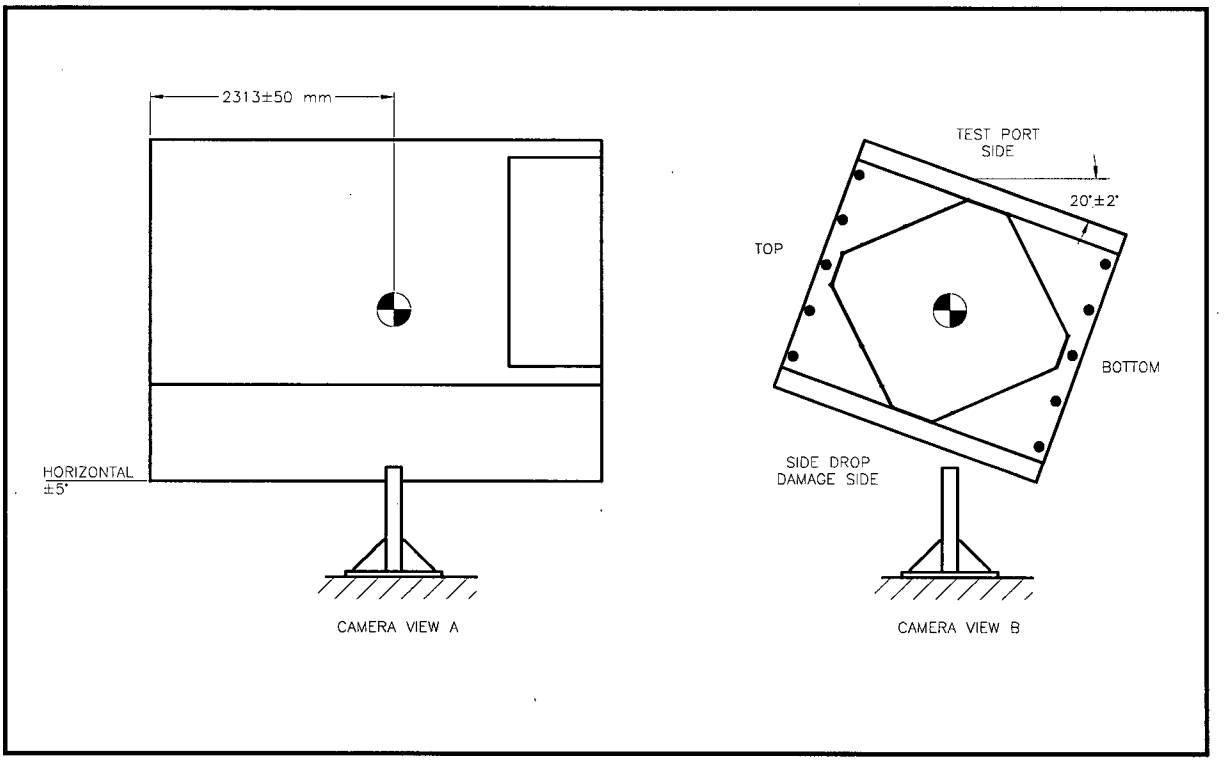

Figure 2.12.3-5 – Puncture on Side Damage Orientation, Test LP1

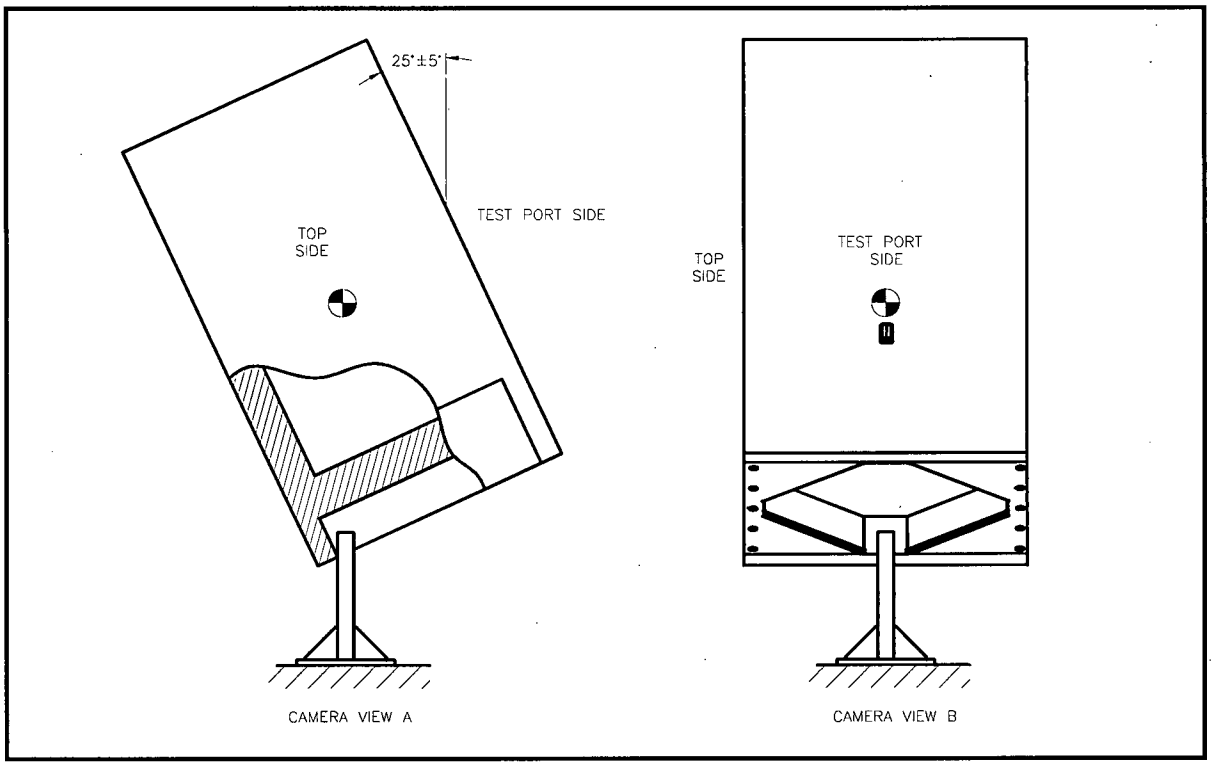

Figure 2.12.3-6 – Puncture on Overpack Cover Orientation, Test LP2

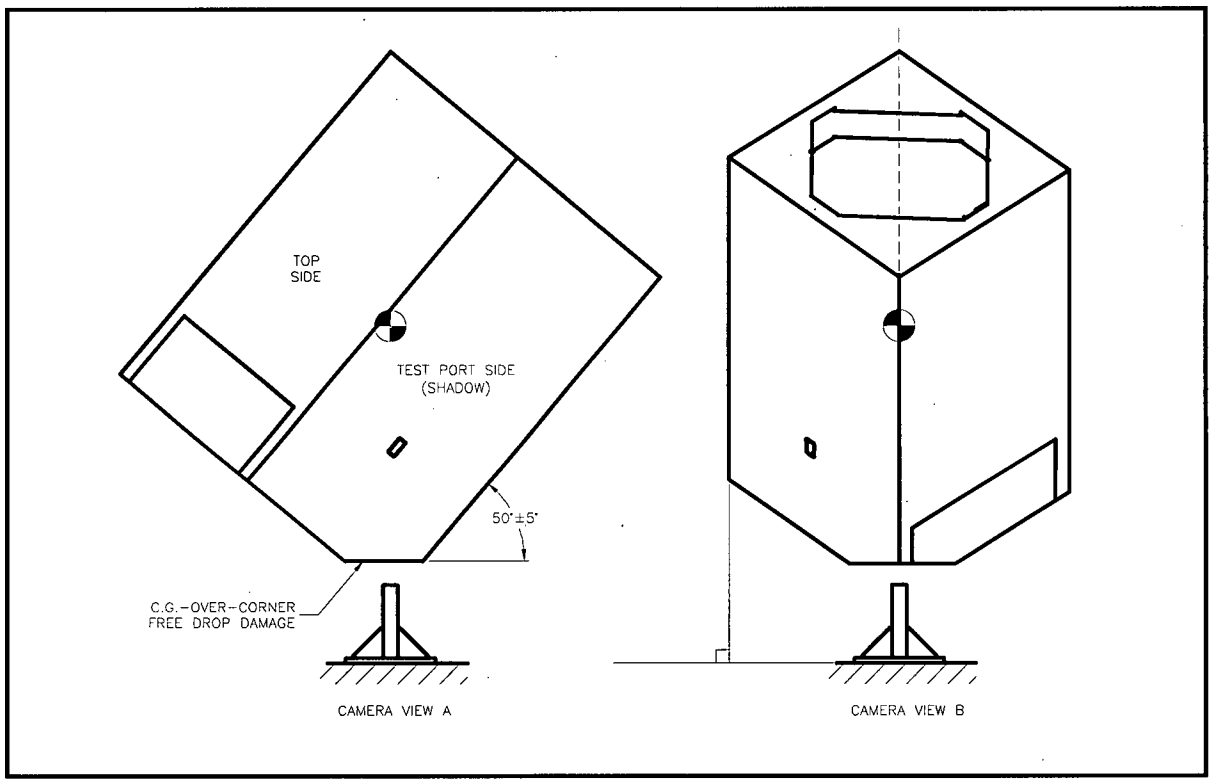

Figure 2.12.3-7 – Puncture on Prior CG-Over-Corner Damage, Test LP3

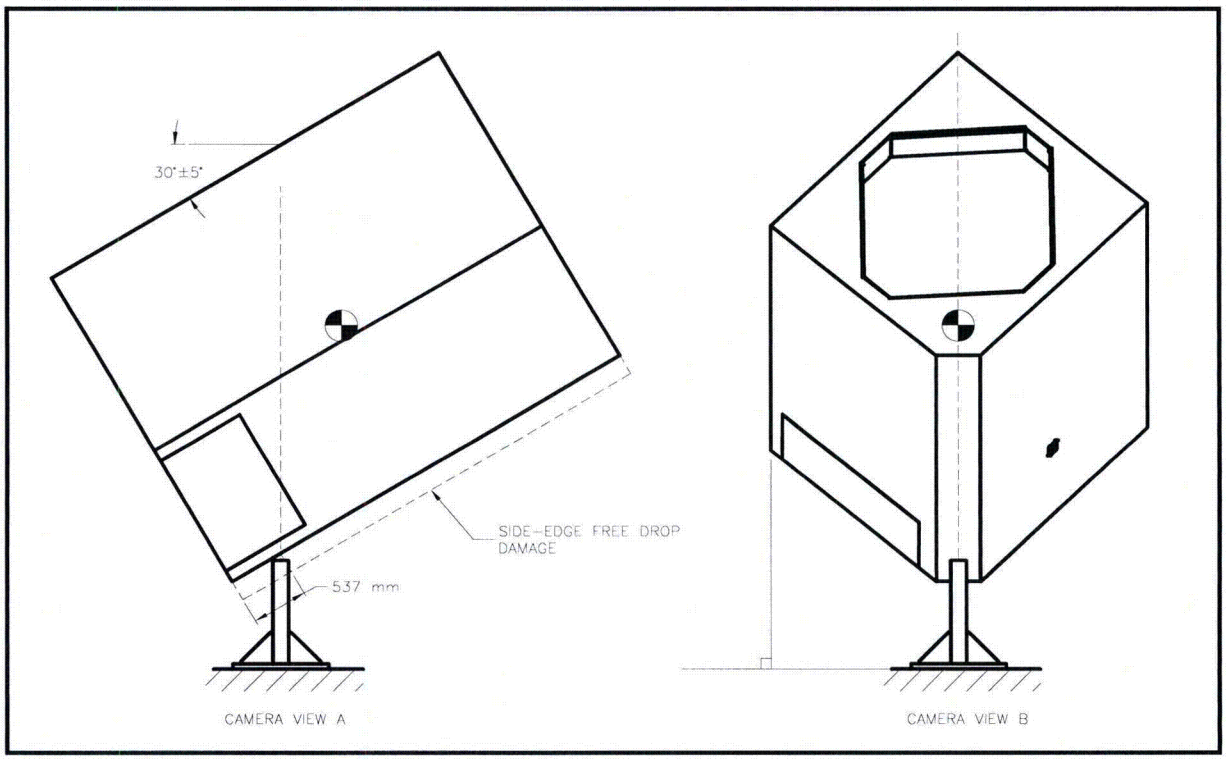

Figure 2.12.3-8 – Puncture on Prior Side – Edge Damage, Test LP4

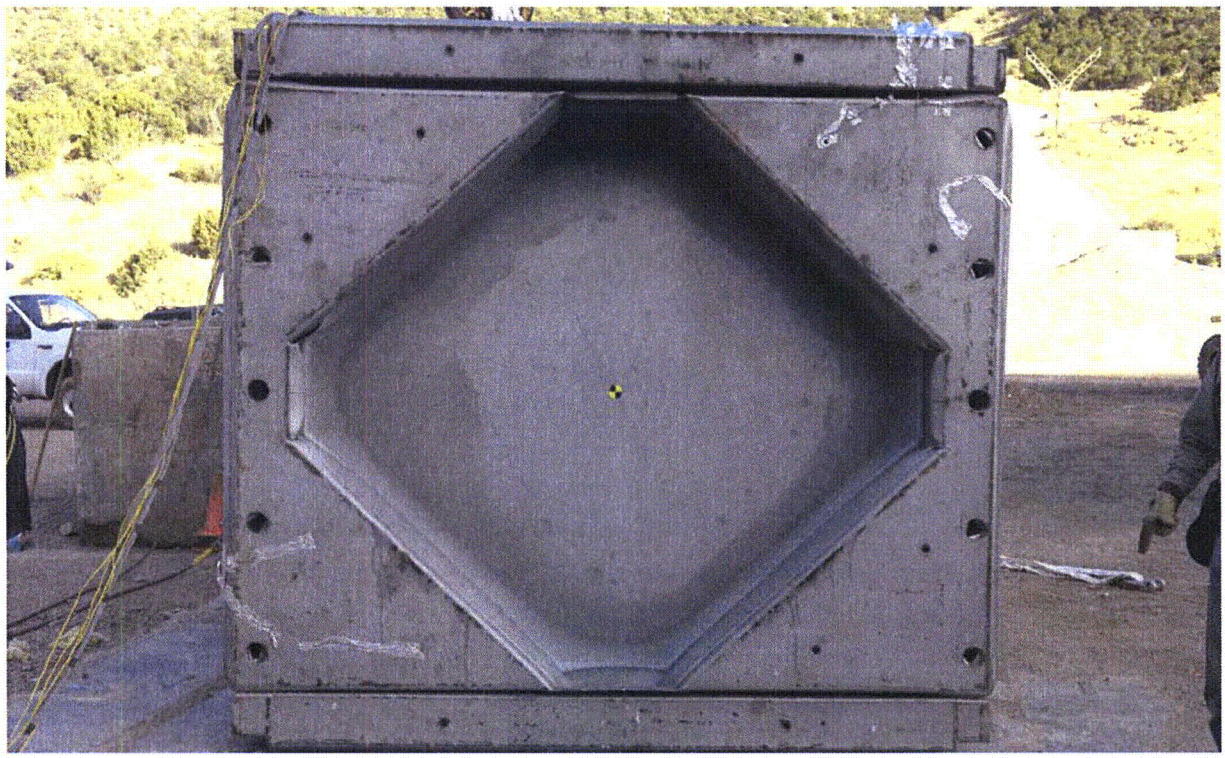

Figure 2.12.3-9 – Test LD2, Overall View of Impact Surface

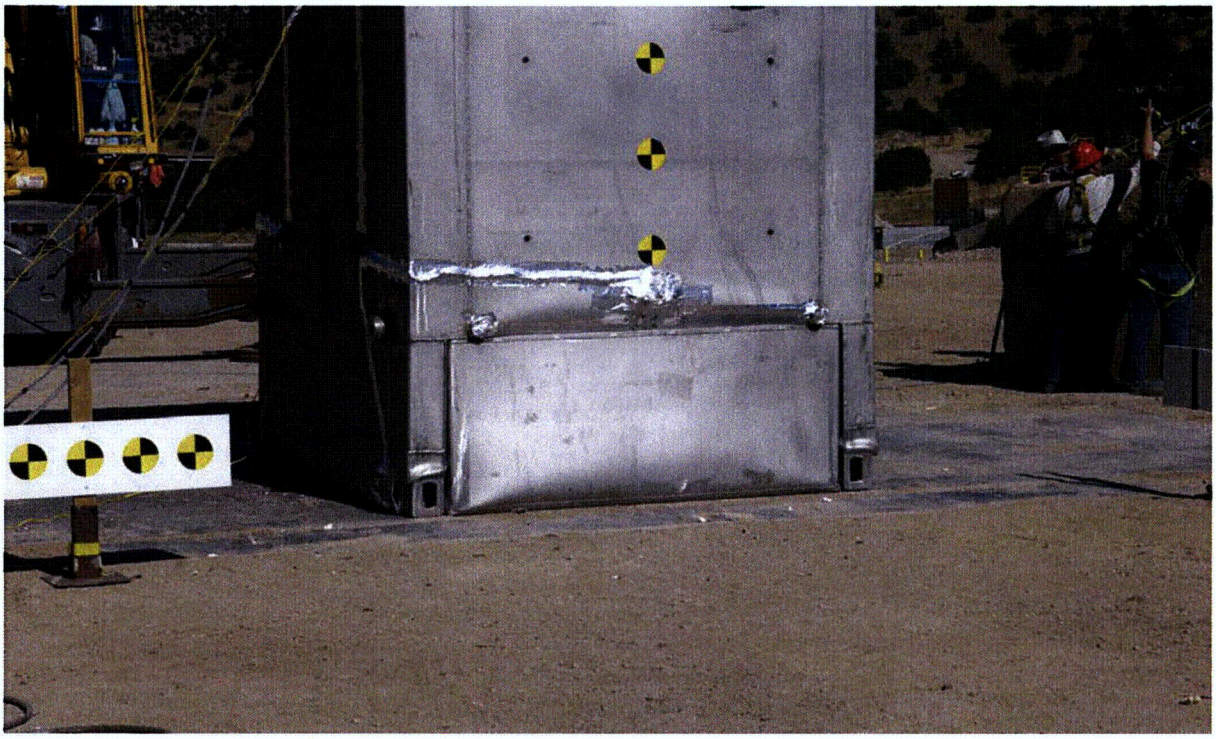

Figure 2.12.3-10 – Test LD2, Typical Deformations at Closure End

Figure 2.12.3-11 – Test LD2, Typical Torn Welds on Overpack Cover

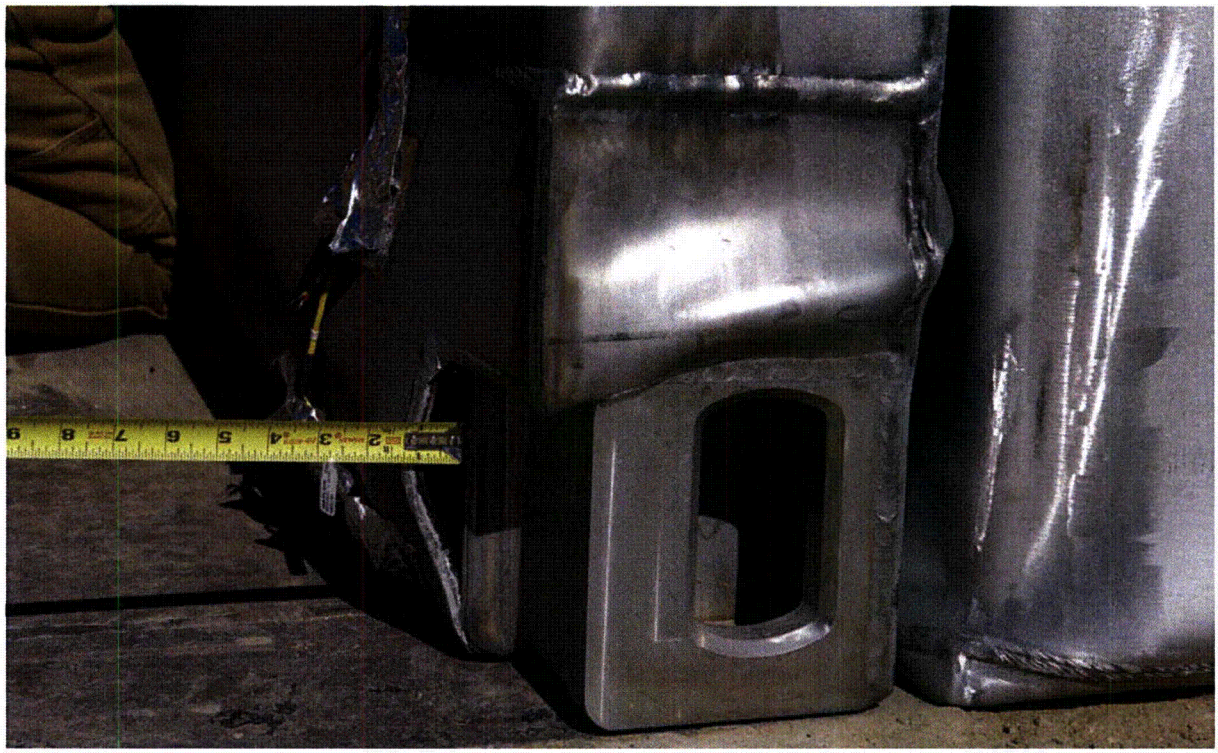

Figure 2.12.3-12 – Test LD2, Close-up of Deformation and Torn Welds Around ISO Fitting

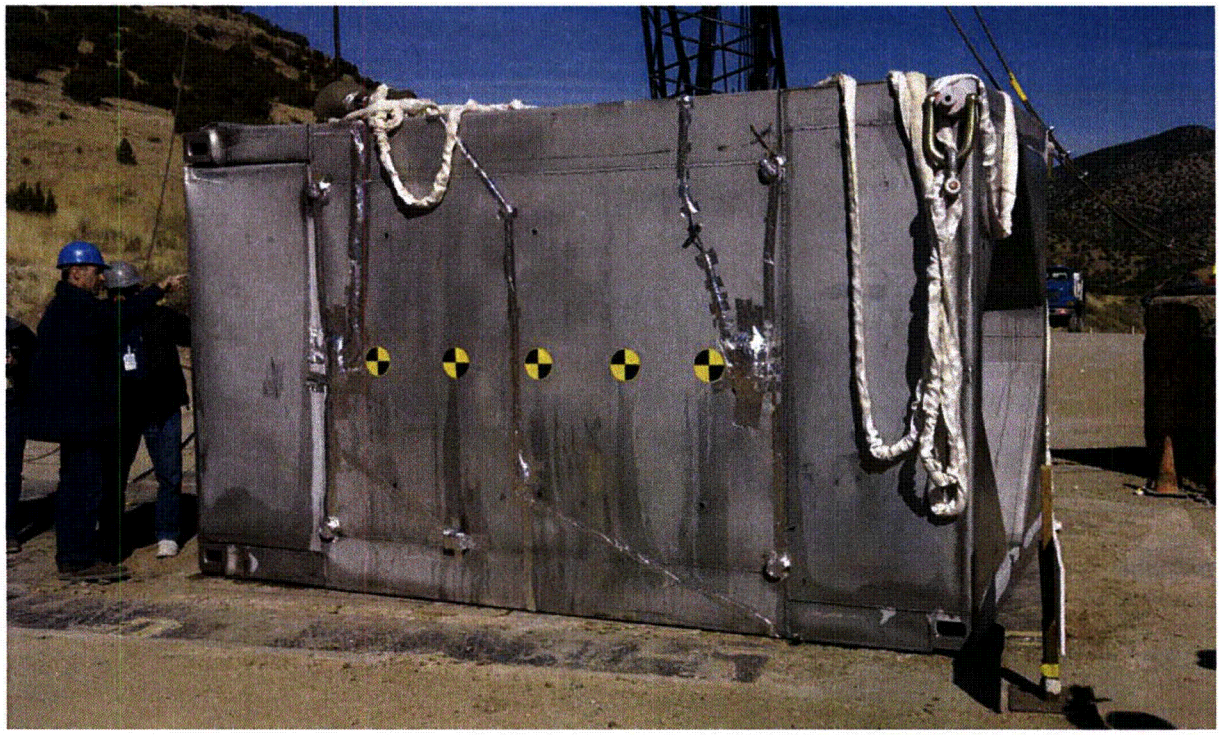

Figure 2.12.3-13 – Test LD3, Typical Side Deformations (Impact Side Down)

Figure 2.12.3-14 – Test LD3, Impact Side

Figure 2.12.3-15 – Test LD3, Weld Tear Near Bottom of Left Cheek

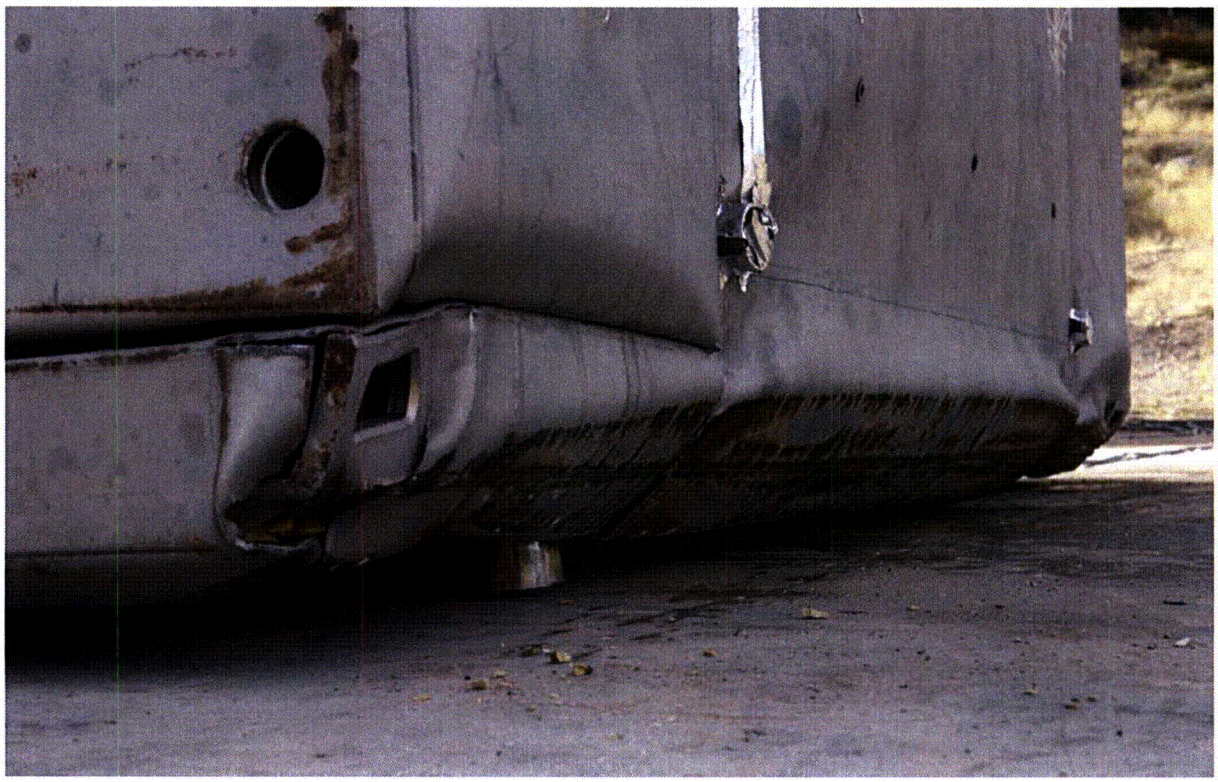

Figure 2.12.3-16 – Test LD5, Typical Deformation

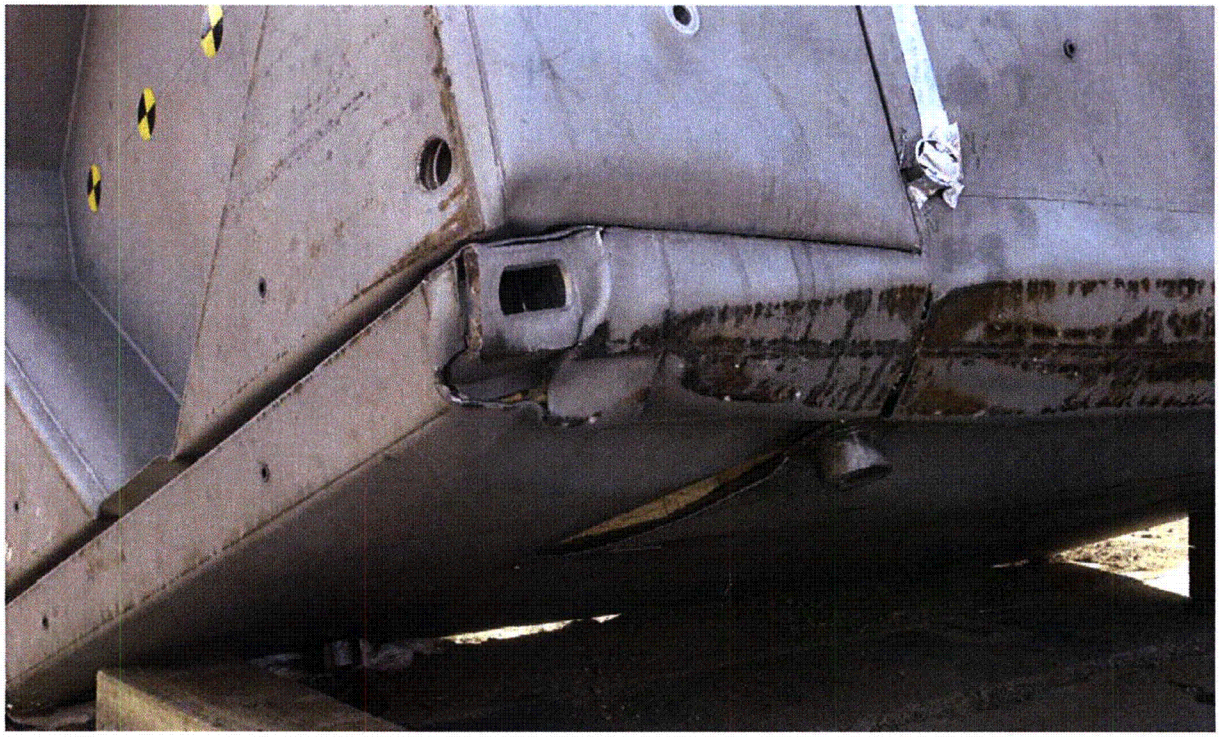

Figure 2.12.3-17 – Test LD5, Weld Tear Along Forward Edge of Side Outer Sheet (2-inch gap)

Figure 2.12.3-18 – Test LD5, Weld Tear Between Cheek (left half) and Body Edge (right half)

Figure 2.12.3-19 – Test LD4, Typical Deformations

Figure 2.12.3-20 – Test LD4, Close-up of Deformations

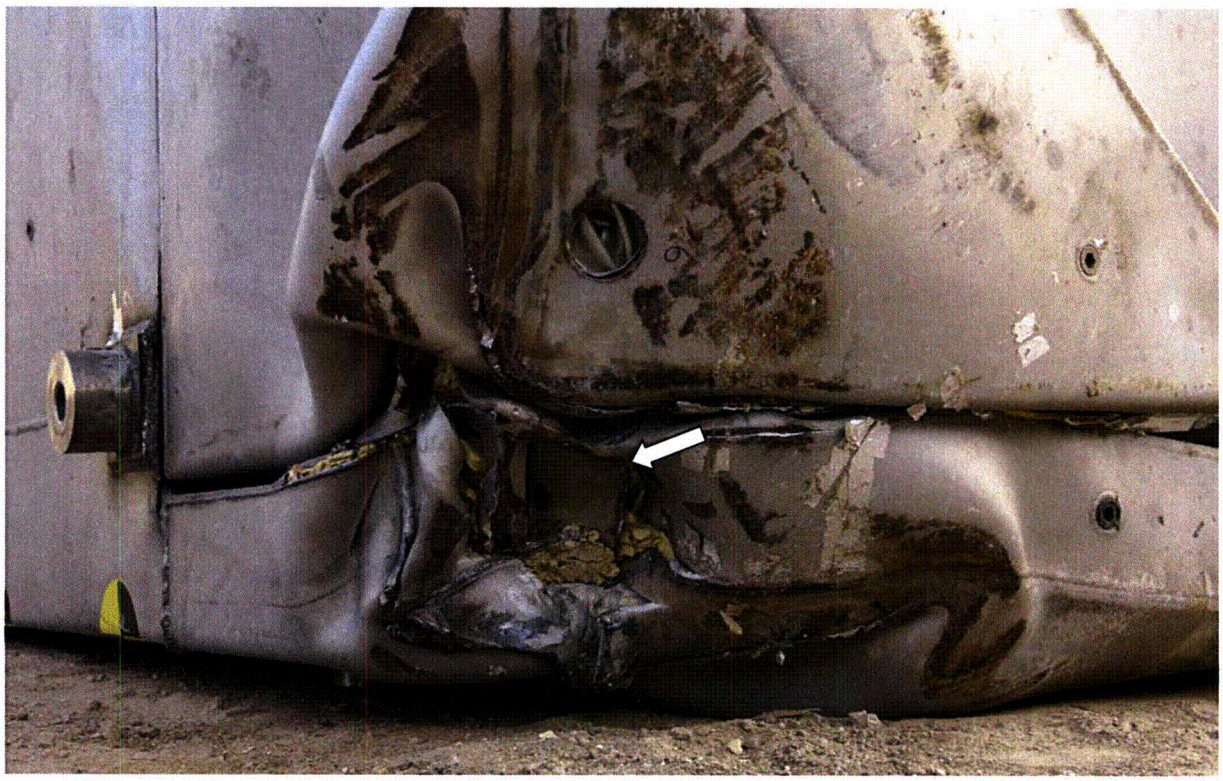

Figure 2.12.3-21 – Test LP3. Puncture Bar Damage Indicated by Arrow

Figure 2.12.3-22 – Test LP4 Puncture Damage. Note Broken Puncture Bar

Figure 2.12.3-23 – Test LP4, Close-up of Damage. Note Corner of 16-mm Thick Insulation Protection Box Inside Hole

Figure 2.12.3-24 – Test LP1, Before Removal of CTU From Bar

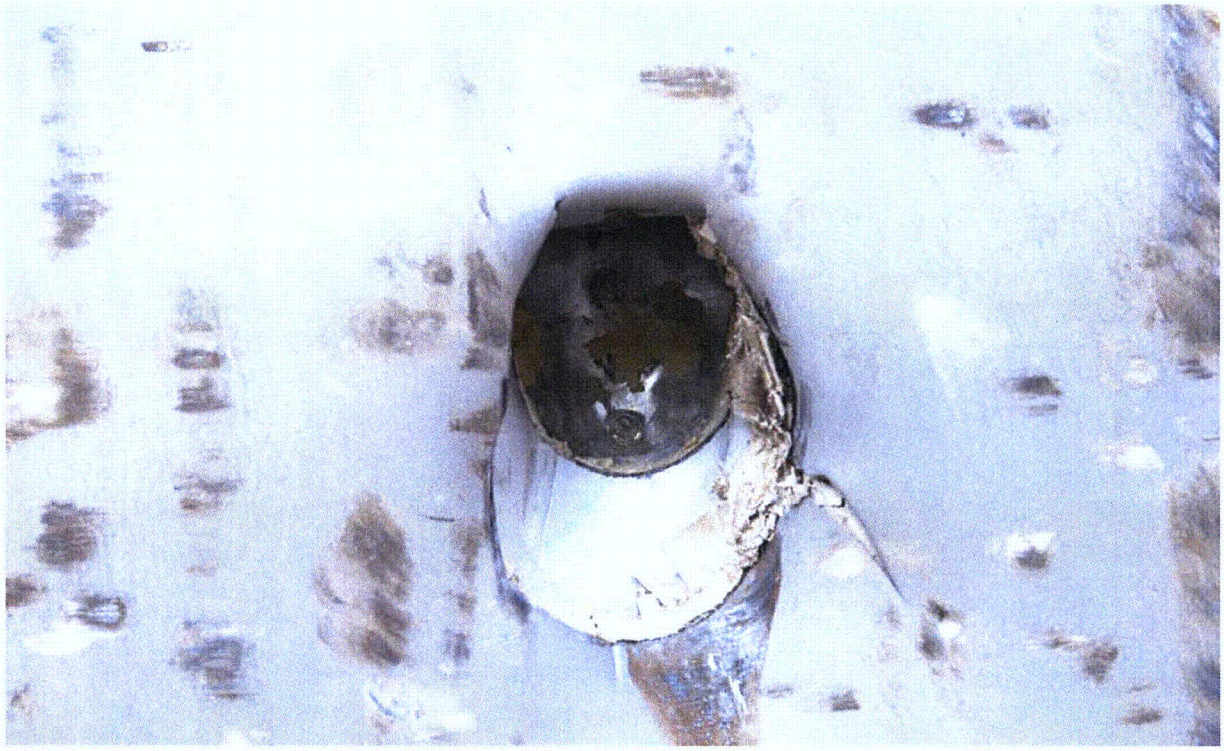

Figure 2.12.3-25 – Test LP1, After Removal of Bar

Figure 2.12.3-26 – Test LP1, Close-up of Damage. Bottom of Hole is CSA Outer Structural Sheet

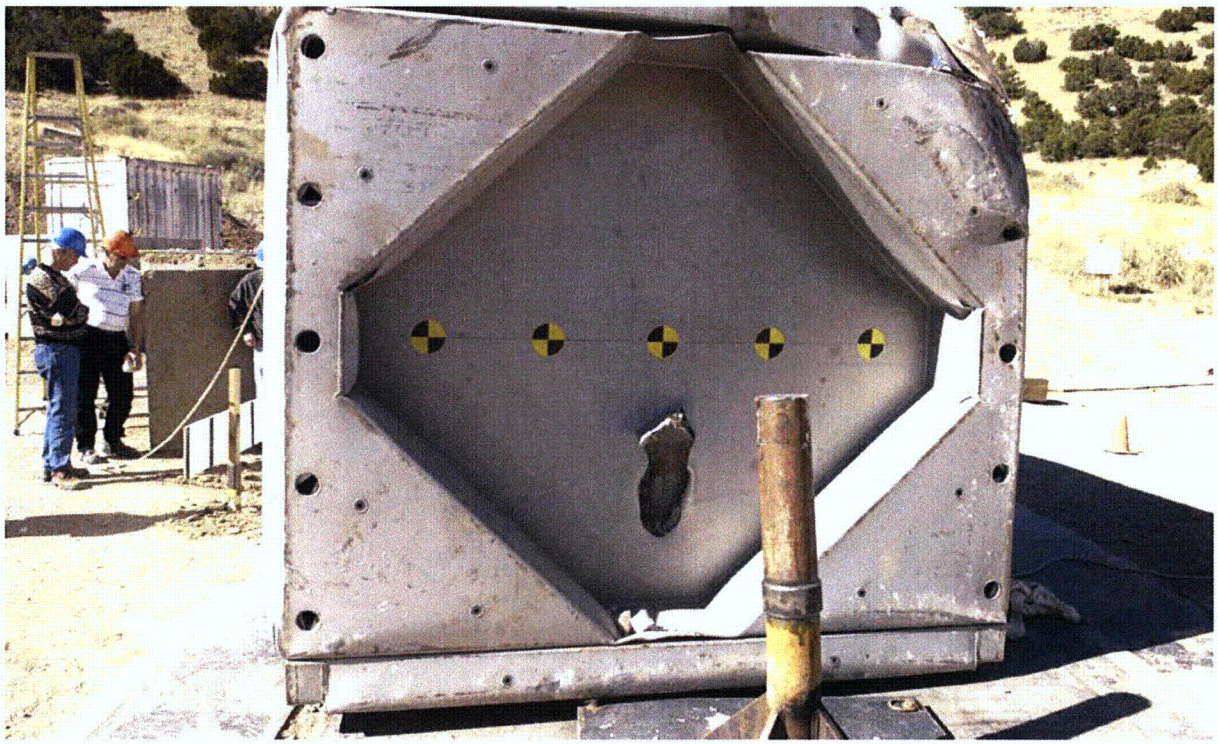

Figure 2.12.3-27 – Test LP2 Puncture Damage

Figure 2.12.3-28 – Test LP2, Close-up of Damage. Bottom of Hole is Puncture-Resistant Plate

Figure 2.12.3-29 – View of Simulated Payload After Testing

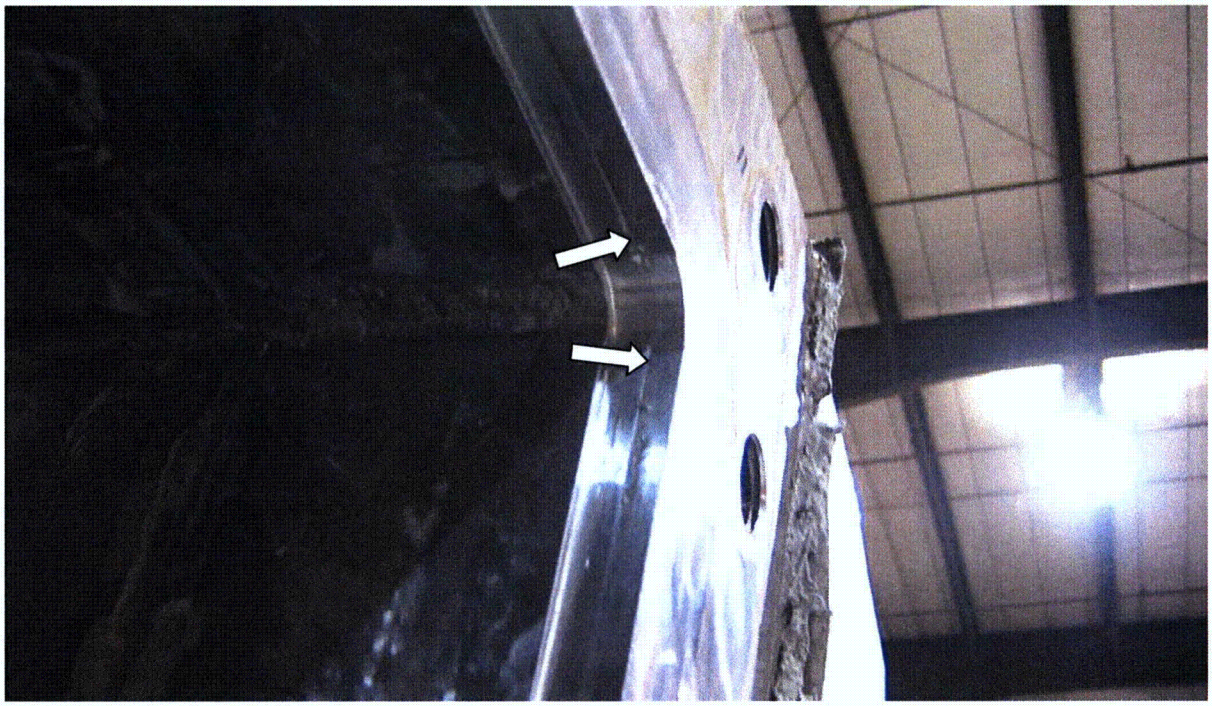

Figure 2.12.3-30 – View of Contact Between Lid Shear Lips and Body Upper Right Corner

Figure 2.12.3-31 – View of Contact on Closure Bolt Head and Washer (Typical)

[redacted]

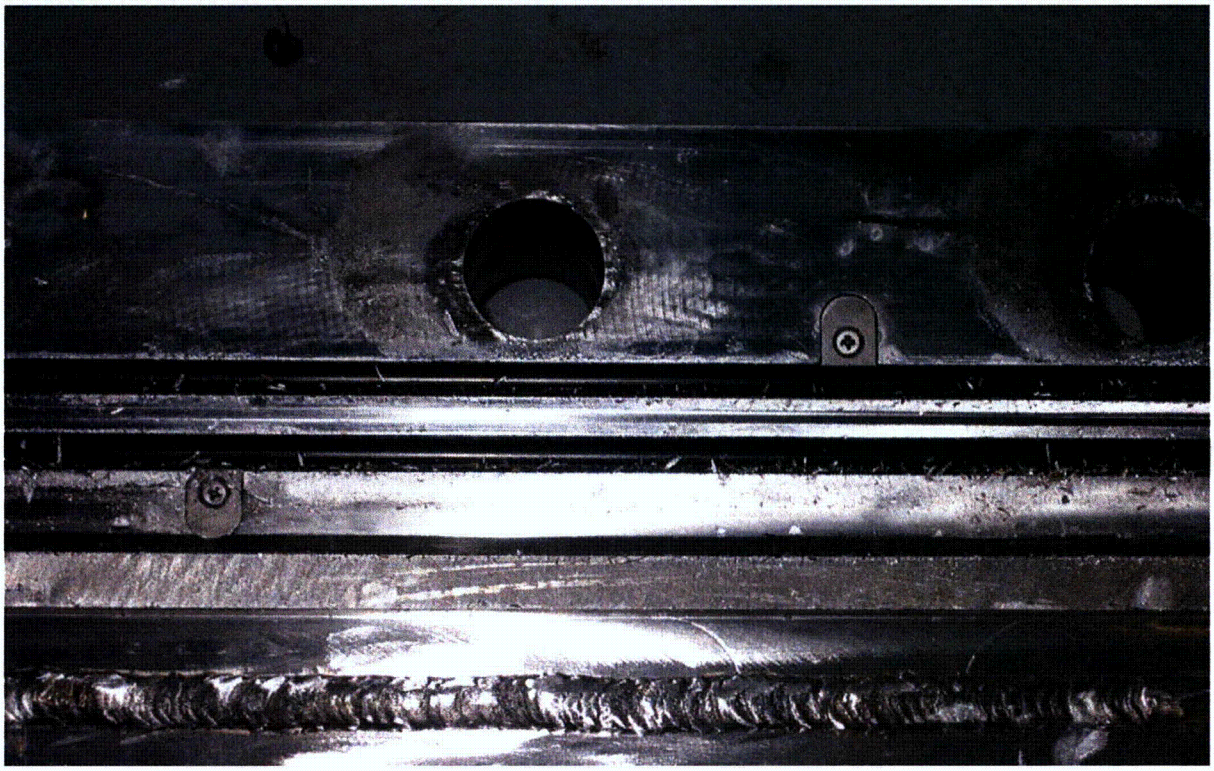

Figure 2.12.3-32 – Debris on Closure Lid Seals (Right Side, Bolt Hole #15 in Center)

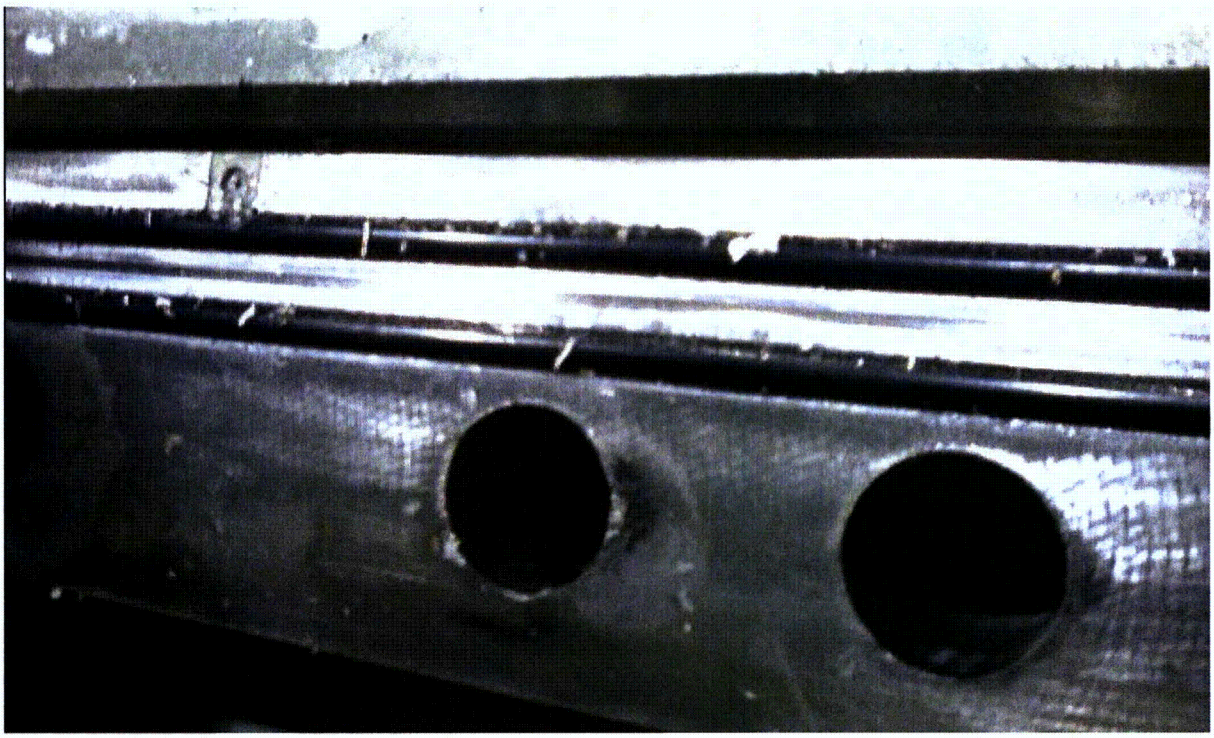

Figure 2.12.3-33 – Debris on Closure Lid Seals (Showing Large Chips)

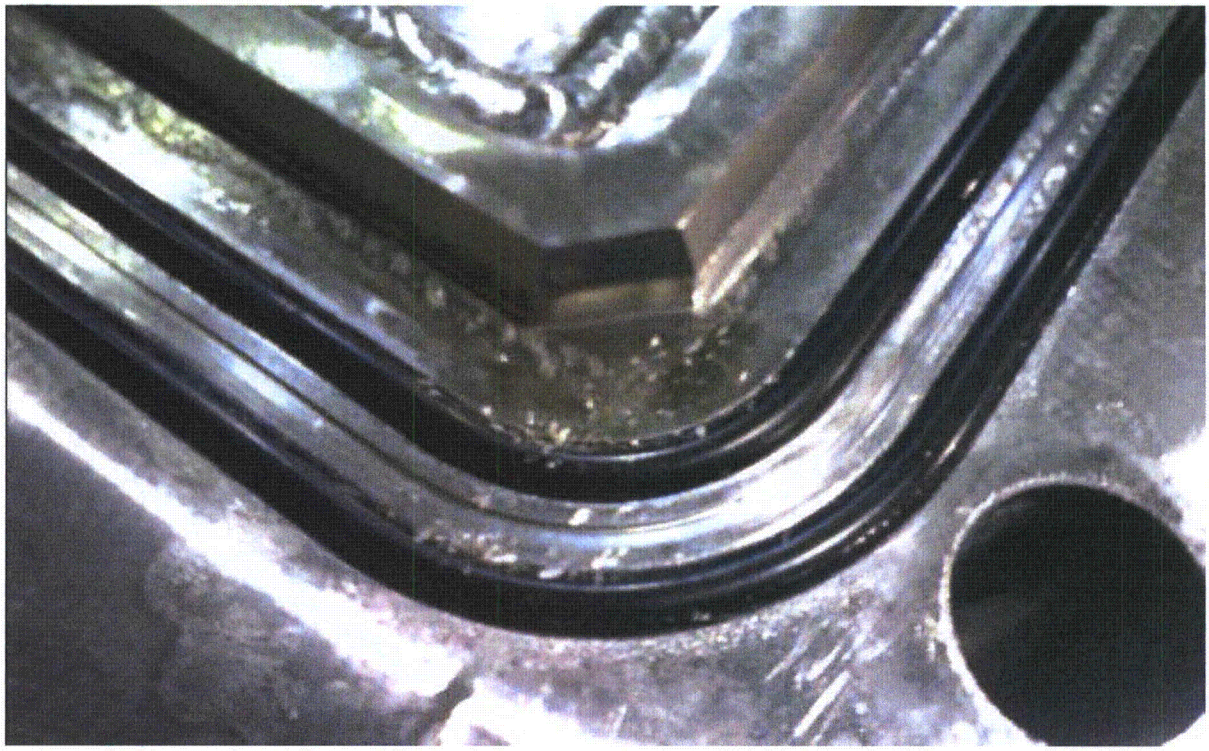

Figure 2.12.3-34 – Debris on Closure Lid Seals (Lower Left Corner of Lid)

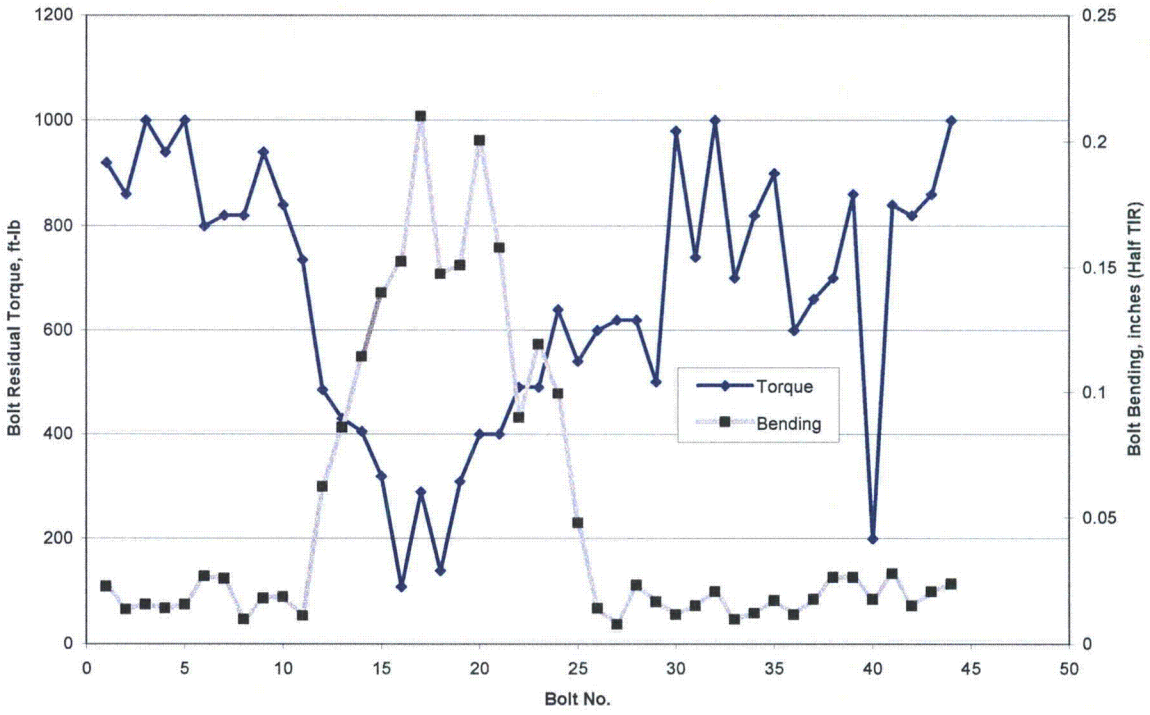

Figure 2.12.3-35 – Correlation of Residual Torque (Tightening) with Bolt Bending

2.12.3.9 Acceleration Time History Plots

Individual accelerometer time history output plots are given in this section in the following order. The designator is the test number followed by the accelerometer location number and direction. For example, 'LD2 – A2A' is test LD2, accelerometer location 2, axial direction; 'LD5 – A5L' is test LD5, accelerometer location 5, lateral direction.

No.	Designator	No.	Designator	No.	Designator
1	LD1 – A1A	8	LD3 – A1L	15	LD4 – A2A
2	LD1 – A3A	9	LD3 – A4L	16	LD4 – A3A
3	LD1 – A4A	10	LD3 – A5L	17	LD4 – A4A
4	LD2 – A1A	11	LD3 – A8L	18	LD5 – A1L
5	LD2 – A2A	12	LD3 – A9L	19	LD5 – A3L
6	LD2 – A3A	13	LD3 – A10L	20	LD5 – A5L
7	LD2 – A4A	14	LD4 – A1A	21	LD5 – A7L

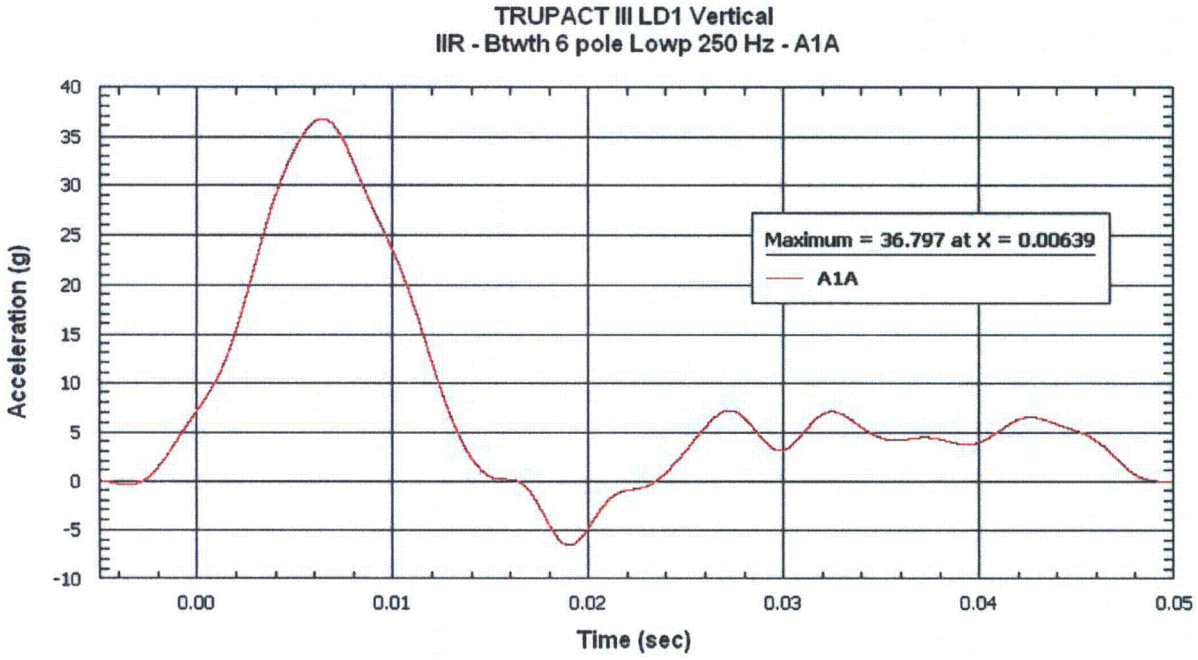

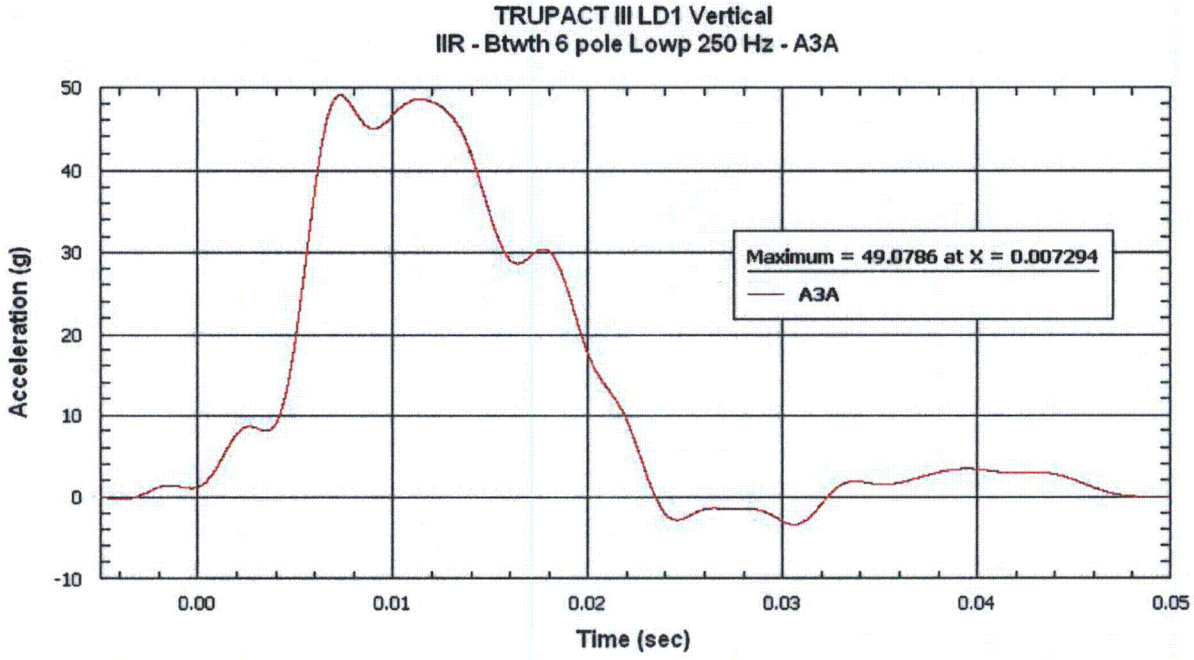
TRUPACT III LD1 Vertical
IIR - Btwth 6 pole Lowp 250 Hz - A3A
Maximum = 49.0786 at X = 0.007294
A3A
Acceleration (g)
Time (sec)
50
40
30
20
10
0
-10
0.00
0.01
0.02
0.03
0.04
0.05

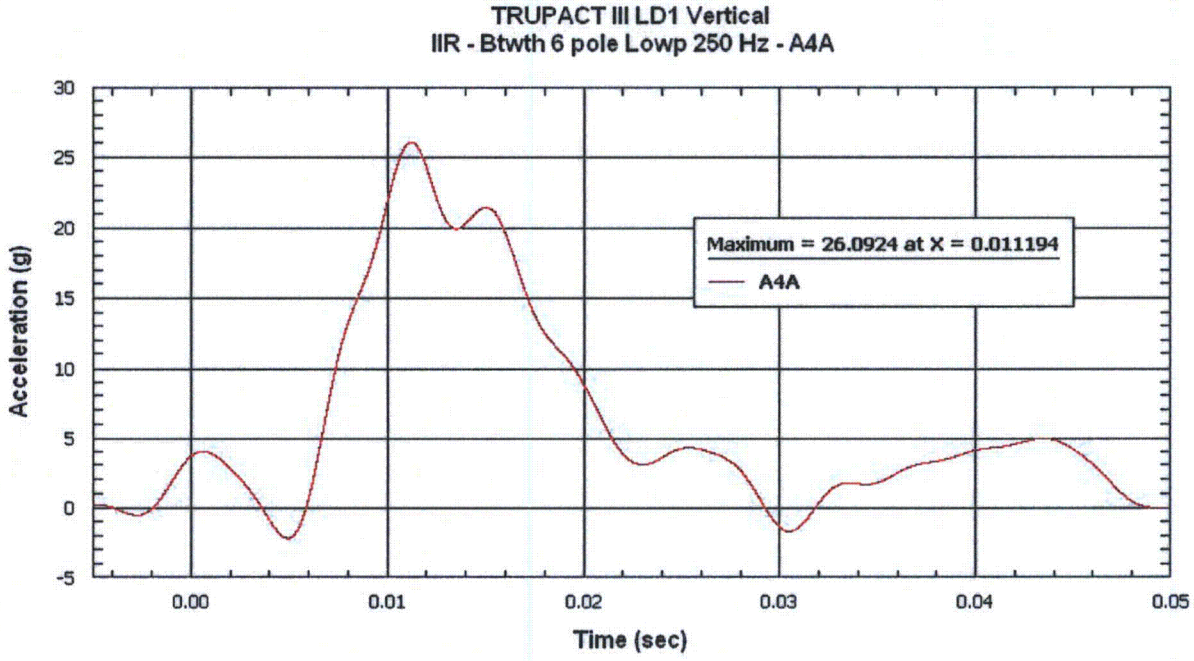
TRUPACT III LD1 Vertical
IIR - Btwth 6 pole Lowp 250 Hz - A4A
Maximum = 26.0924 at X = 0.011194
A4A
Acceleration (g)
Time (sec)
30
25
20
15
10
5
0
-5
0.00
0.01
0.02
0.03
0.04
0.05

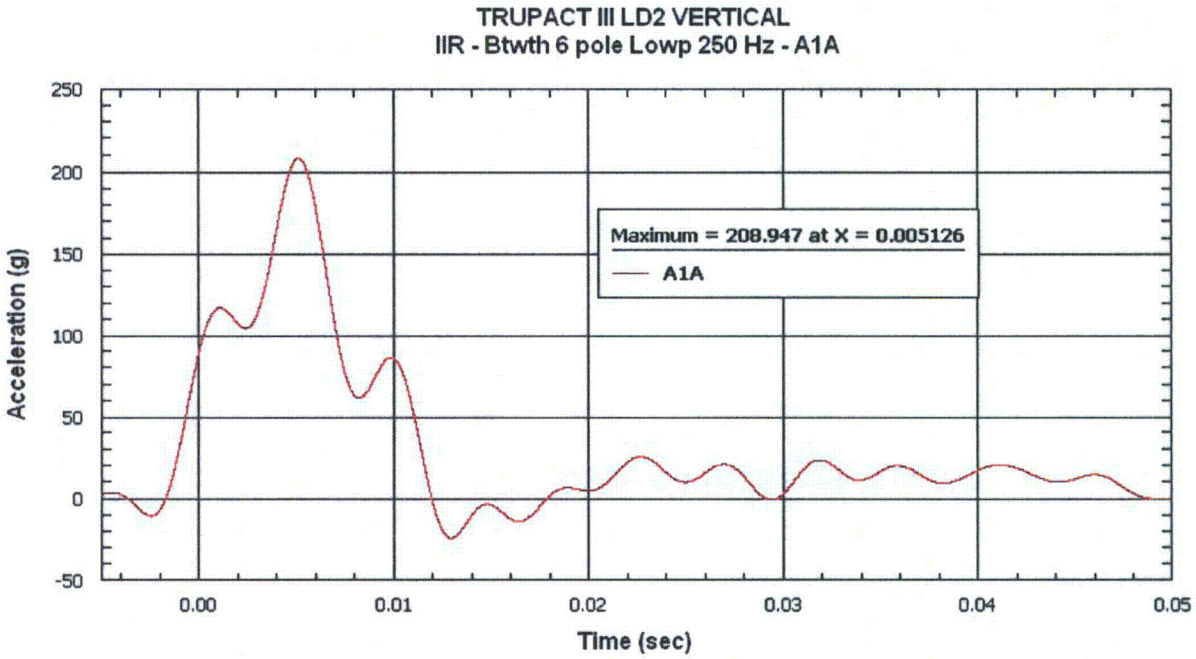
TRUPACT III LD2 VERTICAL
IIR - Btwth 6 pole Lowp 250 Hz - A1A
Maximum = 208.947 at X = 0.005126
A1A
Acceleration (g)
Time (sec)
250
200
150
100
50
0
-50
0.00
0.01
0.02
0.03
0.04
0.05

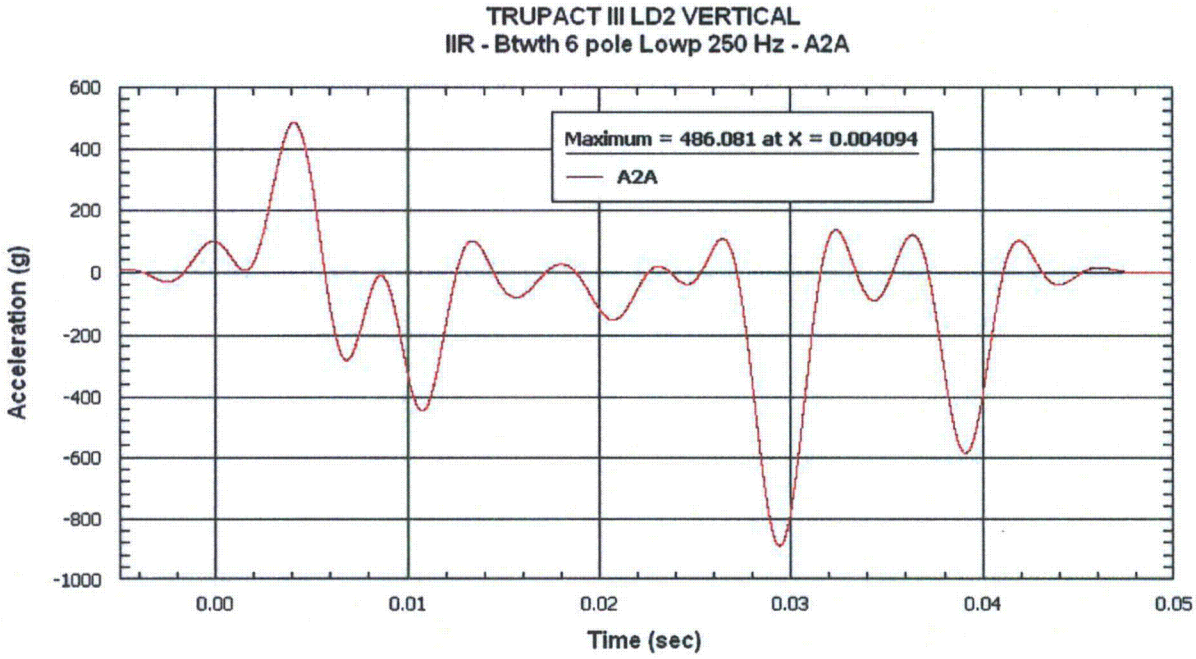
TRUPACT III LD2 VERTICAL
IIR - Btwth 6 pole Lowp 250 Hz - A2A
Maximum = 486.081 at X = 0.004094
A2A
Acceleration (g)
Time (sec)
600
400
200
0
-200
-400
-600
-800
-1000
0.00
0.01
0.02
0.03
0.04
0.05

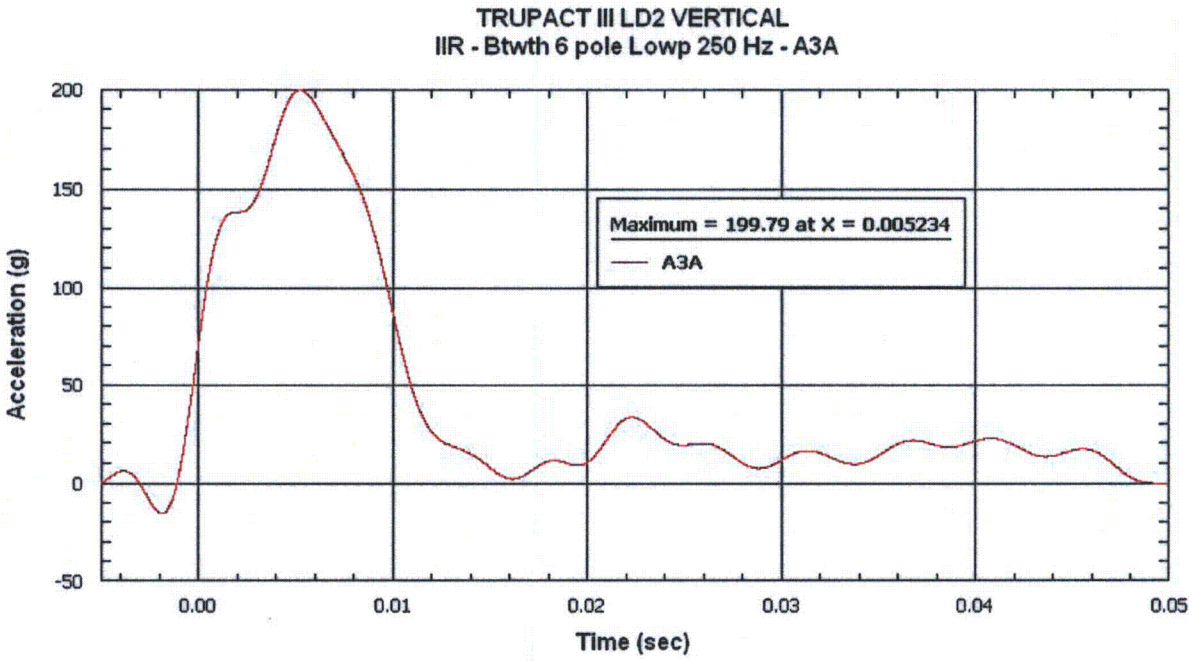
TRUPACT III LD2 VERTICAL
IIR - Btwth 6 pole Lowp 250 Hz - A3A
Maximum = 199.79 at X = 0.005234
A3A
Acceleration (g)
Time (sec)
200
150
100
50
0
-50
0.00
0.01
0.02
0.03
0.04
0.05

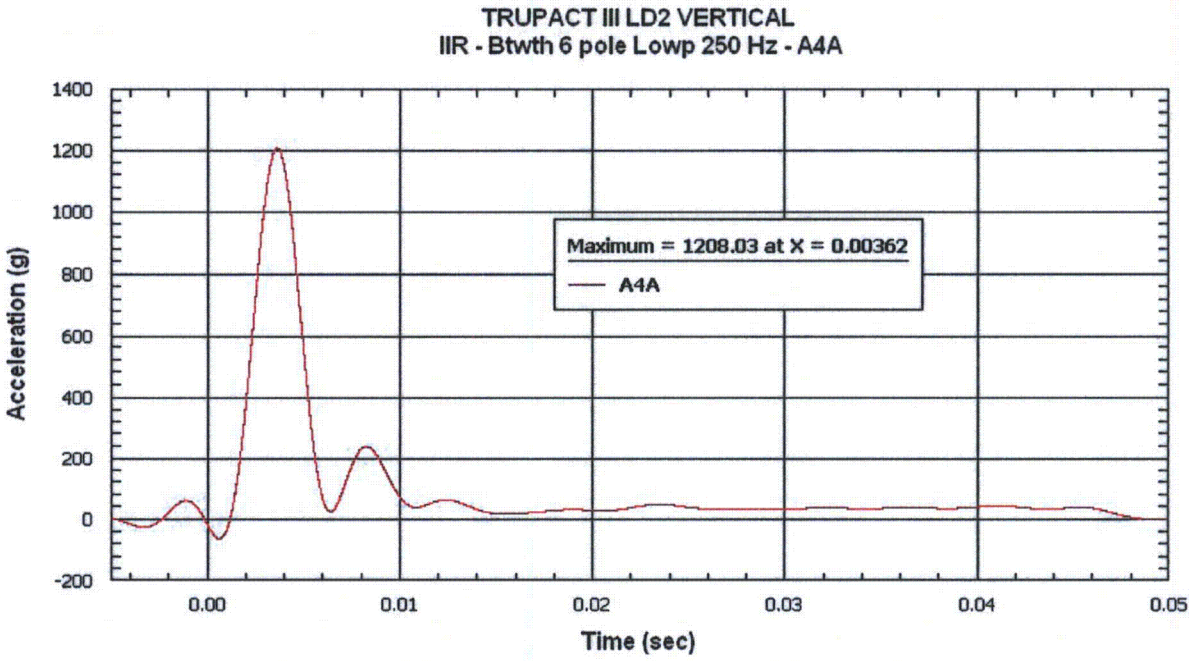
TRUPACT III LD2 VERTICAL
IIR - Btwth 6 pole Lowp 250 Hz - A4A
Maximum = 1208.03 at X = 0.00362
A4A
Acceleration (g)
Time (sec)
1400
1200
1000
800
600
400
200
0
-200
0.00
0.01
0.02
0.03
0.04
0.05

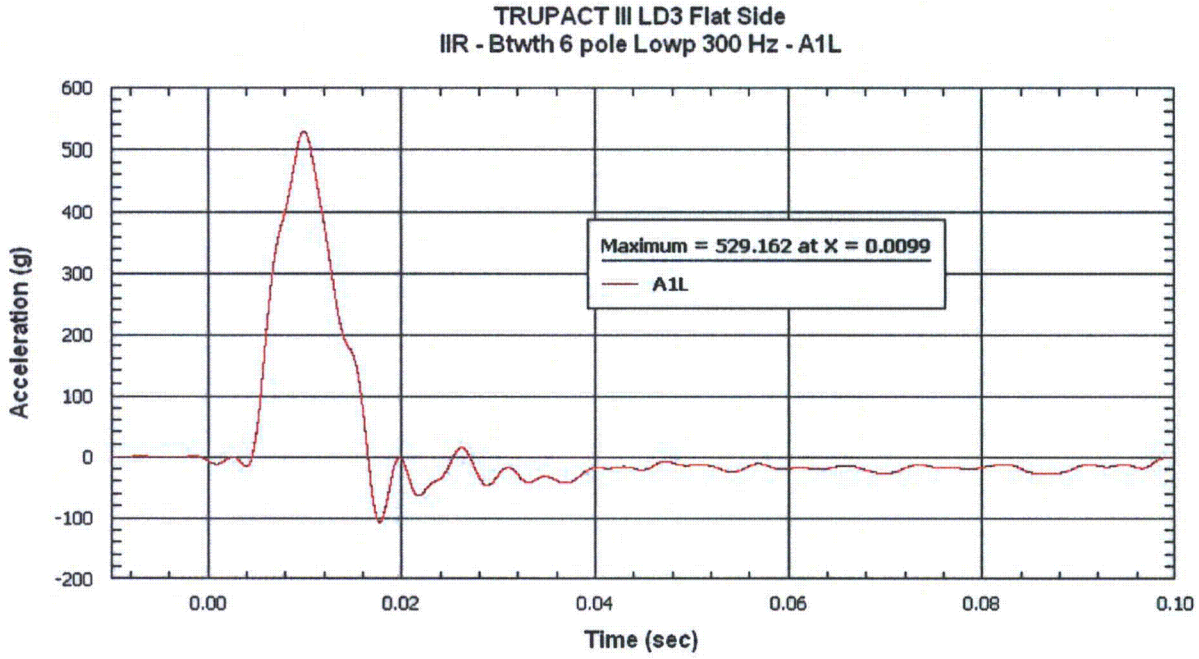
TRUPACT III LD3 Flat Side
IIR - Btwth 6 pole Lowp 300 Hz - A1L
Maximum = 529.162 at X = 0.0099
A1L
Acceleration (g)
Time (sec)
600
500
400
300
200
100
0
-100
-200
0.00
0.02
0.04
0.06
0.08
0.10

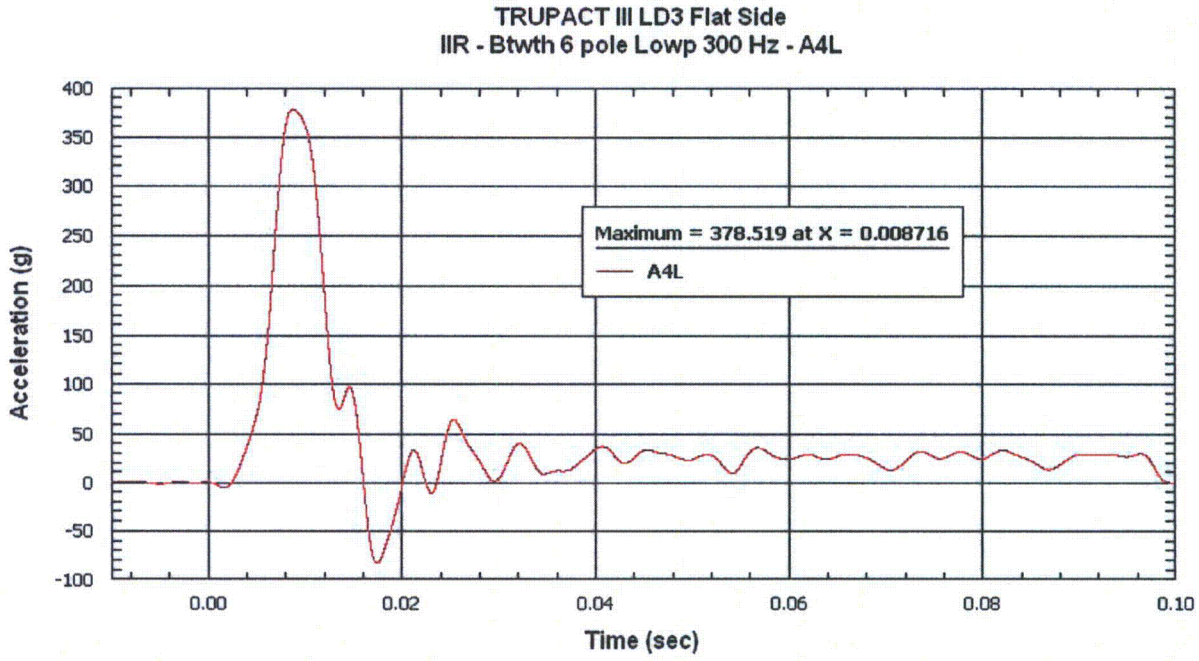
TRUPACT III LD3 Flat Side
IIR - Btwth 6 pole Lowp 300 Hz - A4L
Maximum = 378.519 at X = 0.008716
A4L
Acceleration (g)
Time (sec)
400
350
300
250
200
150
100
50
0
-50
-100
0.00
0.02
0.04
0.06
0.08
0.10

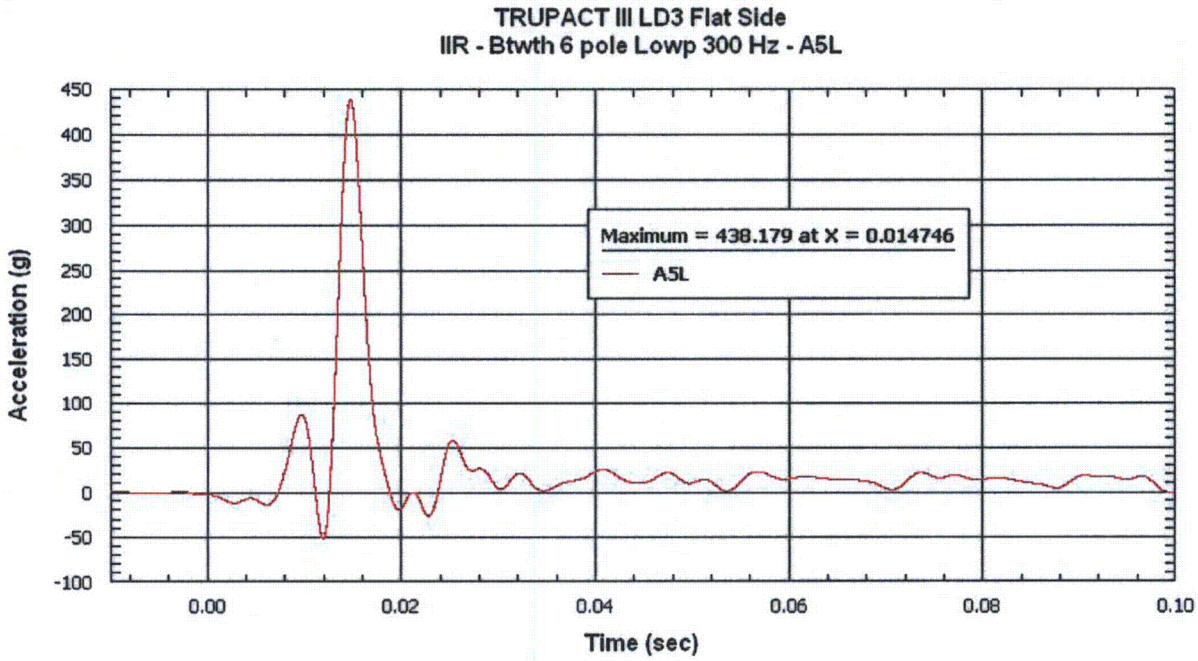
TRUPACT III LD3 Flat Side
IIR - Btwth 6 pole Lowp 300 Hz - A5L
Maximum = 438.179 at X = 0.014746
A5L
Acceleration (g)
Time (sec)
450
400
350
300
250
200
150
100
50
0
-50
-100
0.00
0.02
0.04
0.06
0.08
0.10

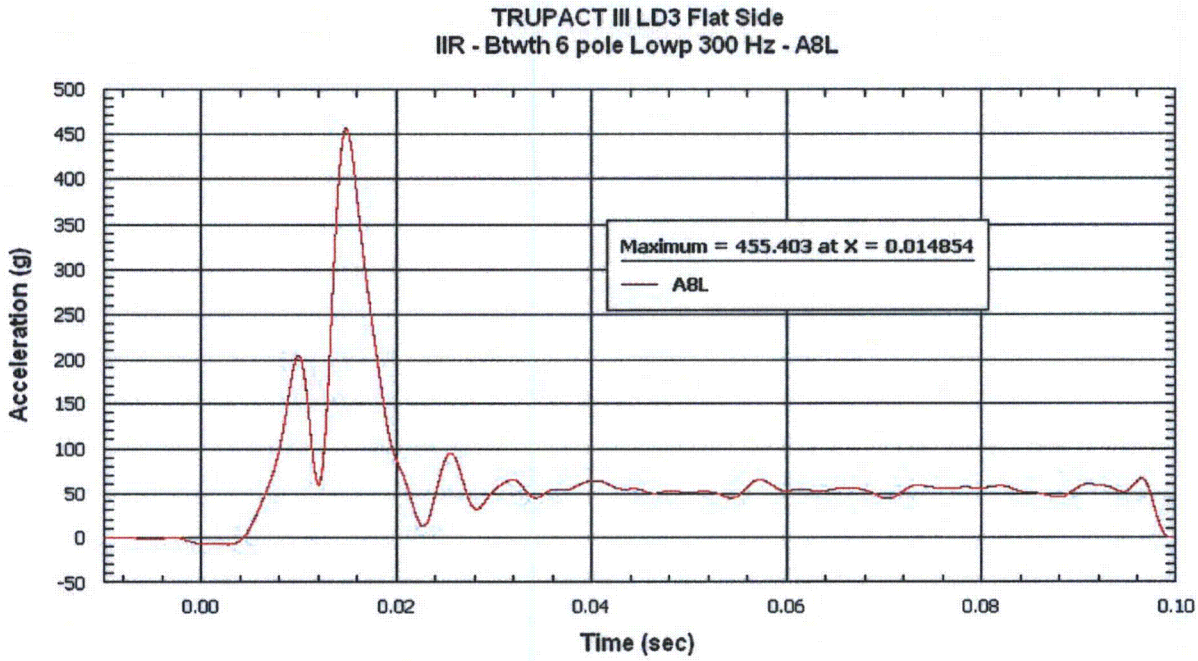
TRUPACT III LD3 Flat Side
IIR - Btwth 6 pole Lowp 300 Hz - A8L
Maximum = 455.403 at X = 0.014854
A8L
Acceleration (g)
Time (sec)
500
450
400
350
300
250
200
150
100
50
0
-50
0.00
0.02
0.04
0.06
0.08
0.10

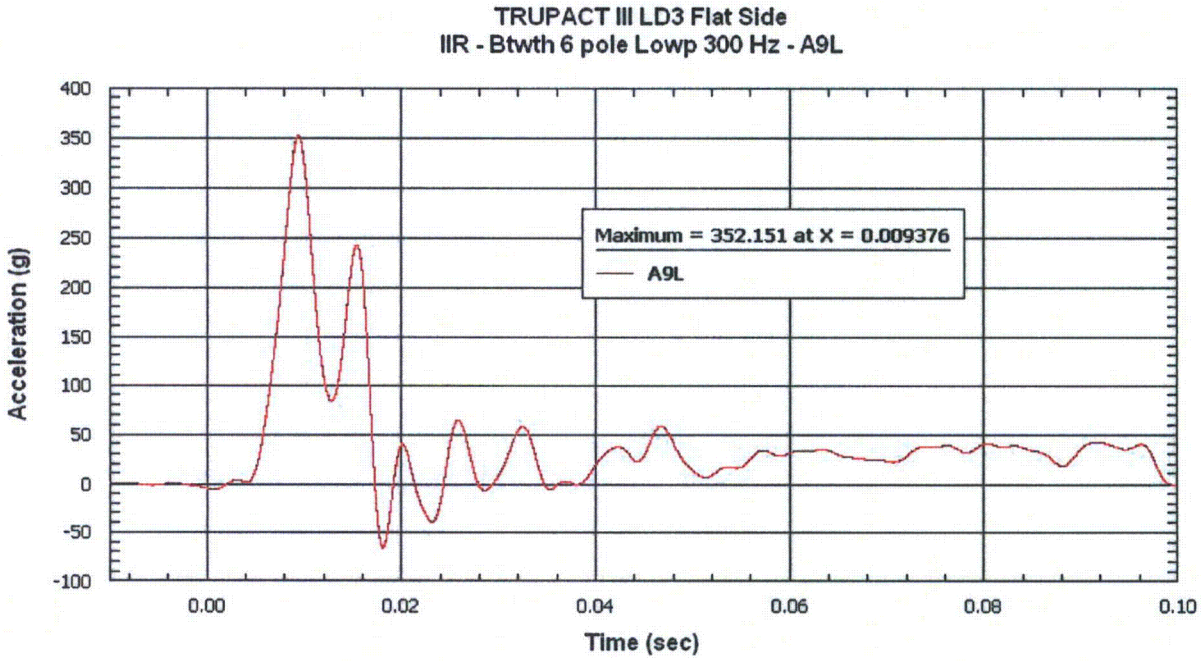
TRUPACT III LD3 Flat Side
IIR - Btwth 6 pole Lowp 300 Hz - A9L
Maximum = 352.151 at X = 0.009376
A9L
Acceleration (g)
Time (sec)
400
350
300
250
200
150
100
50
0
-50
-100
0.00
0.02
0.04
0.06
0.08
0.10

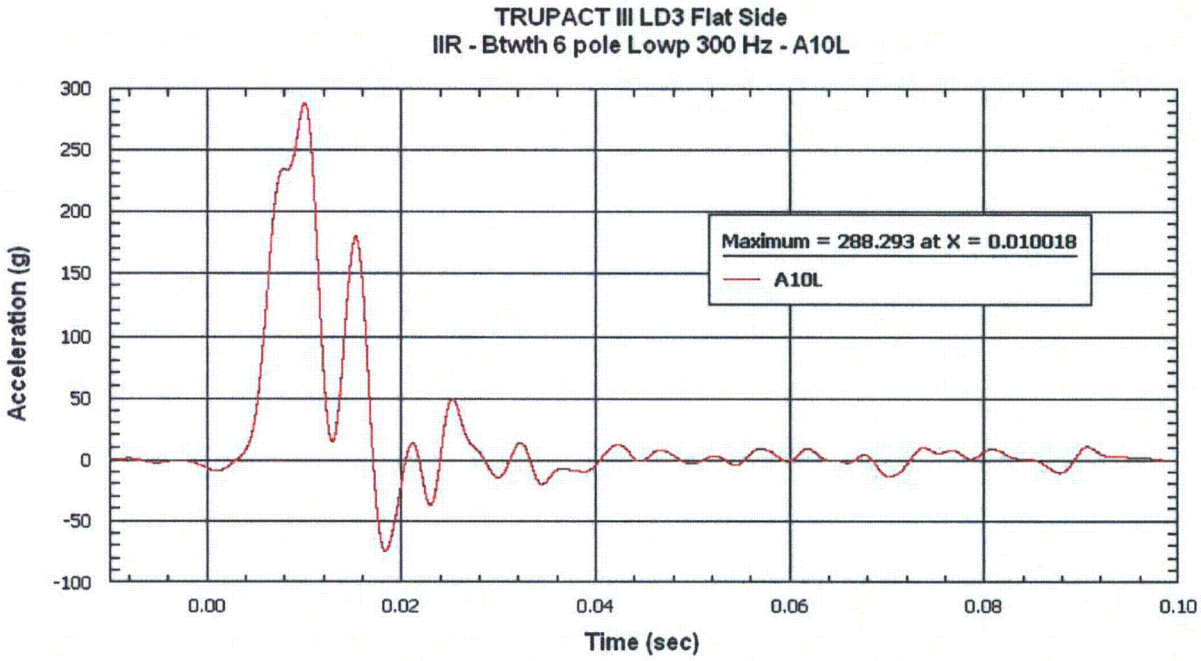
TRUPACT III LD3 Flat Side
IIR - Btwth 6 pole Lowp 300 Hz - A10L
Maximum = 288.293 at X = 0.010018
A10L
Acceleration (g)
Time (sec)
300
250
200
150
100
50
0
-50
-100
0.00
0.02
0.04
0.06
0.08
0.10

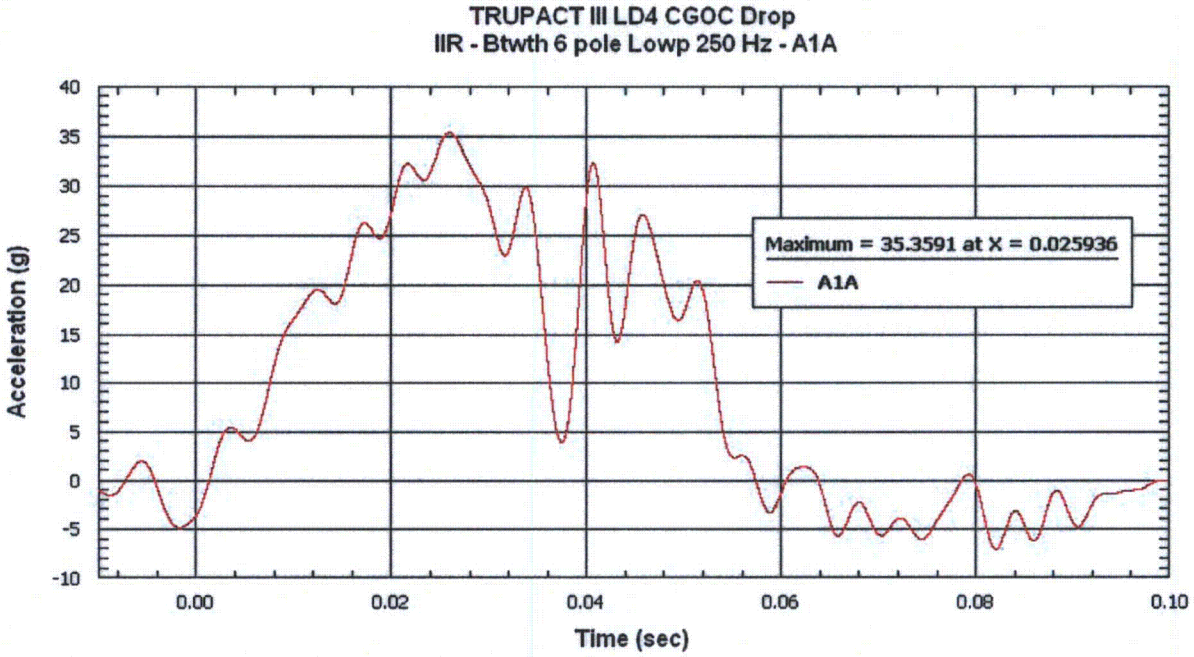
TRUPACT III LD4 CGOC Drop
IIR - Btwth 6 pole Lowp 250 Hz - A1A
Acceleration (g)
Time (sec)
Maximum = 35.3591 at X = 0.025936
A1A
40
35
30
25
20
15
10
5
0
-5
-10
0.00
0.02
0.04
0.06
0.08
0.10

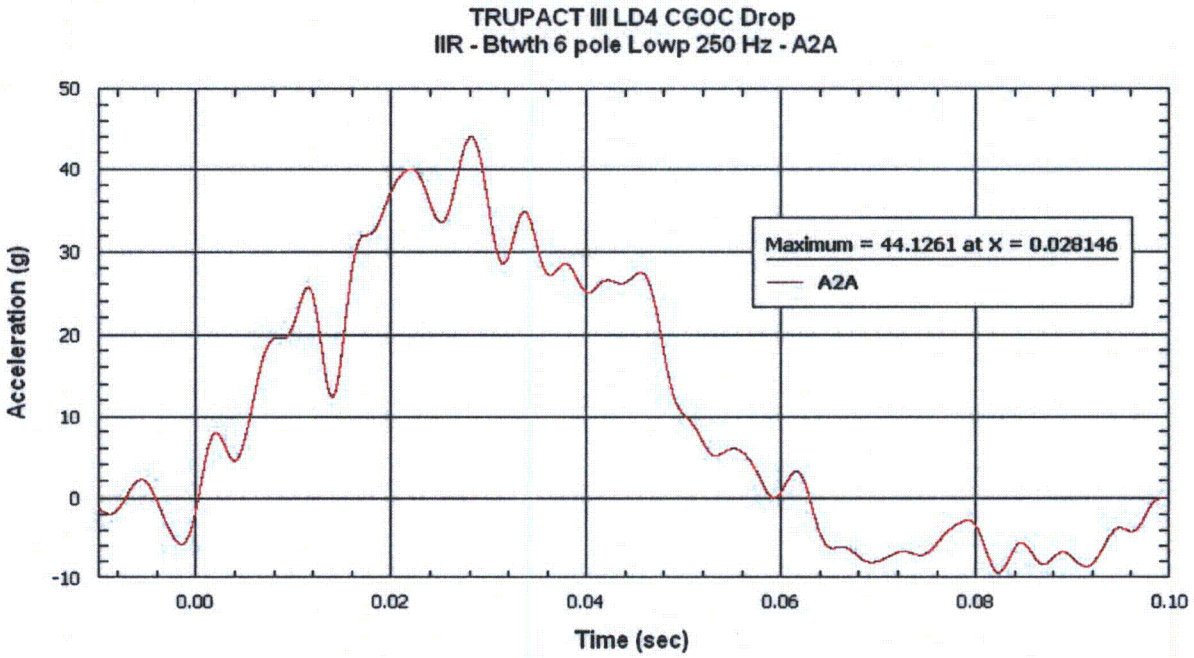
TRUPACT III LD4 CGOC Drop
IIR - Btwth 6 pole Lowp 250 Hz - A2A
Acceleration (g)
Time (sec)
Maximum = 44.1261 at X = 0.028146
A2A
50
40
30
20
10
0
-10
0.00
0.02
0.04
0.06
0.08
0.10

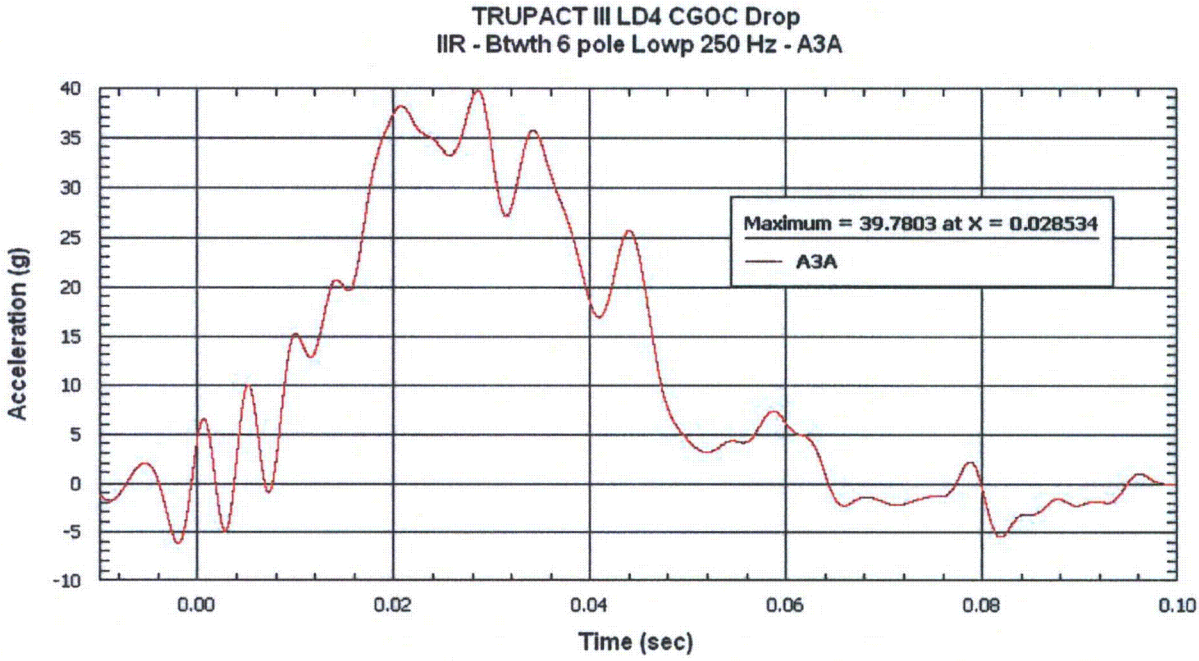
TRUPACT III LD4 CGOC Drop
IIR - Btwth 6 pole Lowp 250 Hz - A3A
Maximum = 39.7803 at X = 0.028534
A3A
Acceleration (g)
Time (sec)
40
35
30
25
20
15
10
5
0
-5
-10
0.00
0.02
0.04
0.06
0.08
0.10

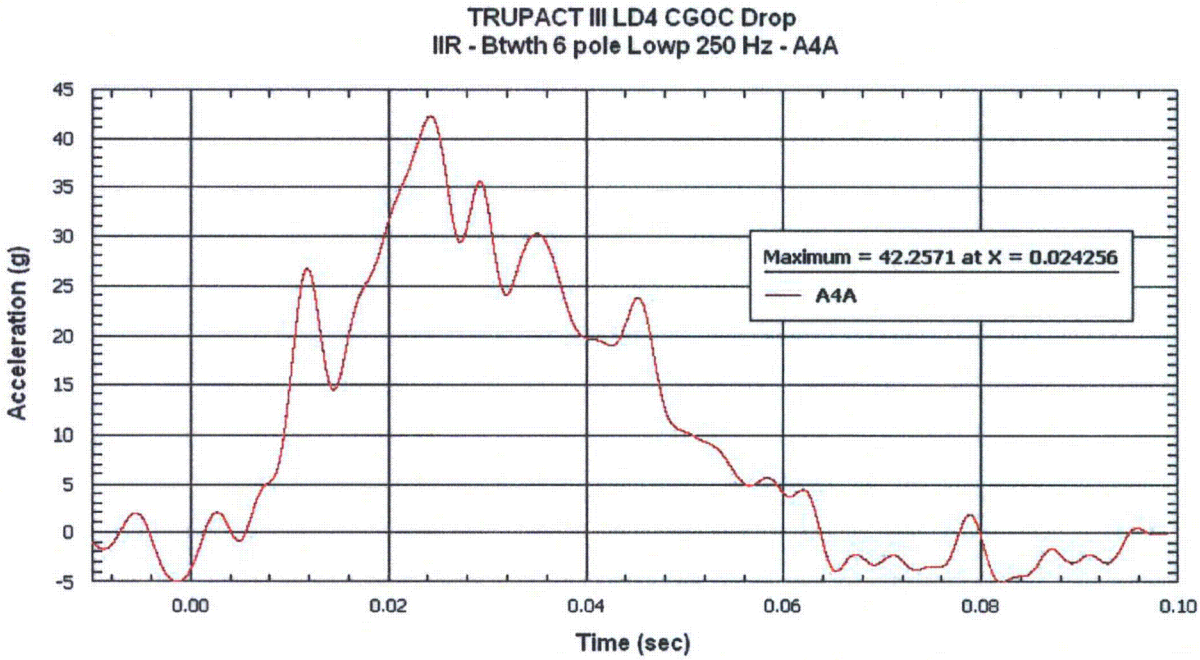
TRUPACT III LD4 CGOC Drop
IIR - Btwth 6 pole Lowp 250 Hz - A4A
Maximum = 42.2571 at X = 0.024256
A4A
Acceleration (g)
Time (sec)
45
40
35
30
25
20
15
10
5
0
-5
0.00
0.02
0.04
0.06
0.08
0.10

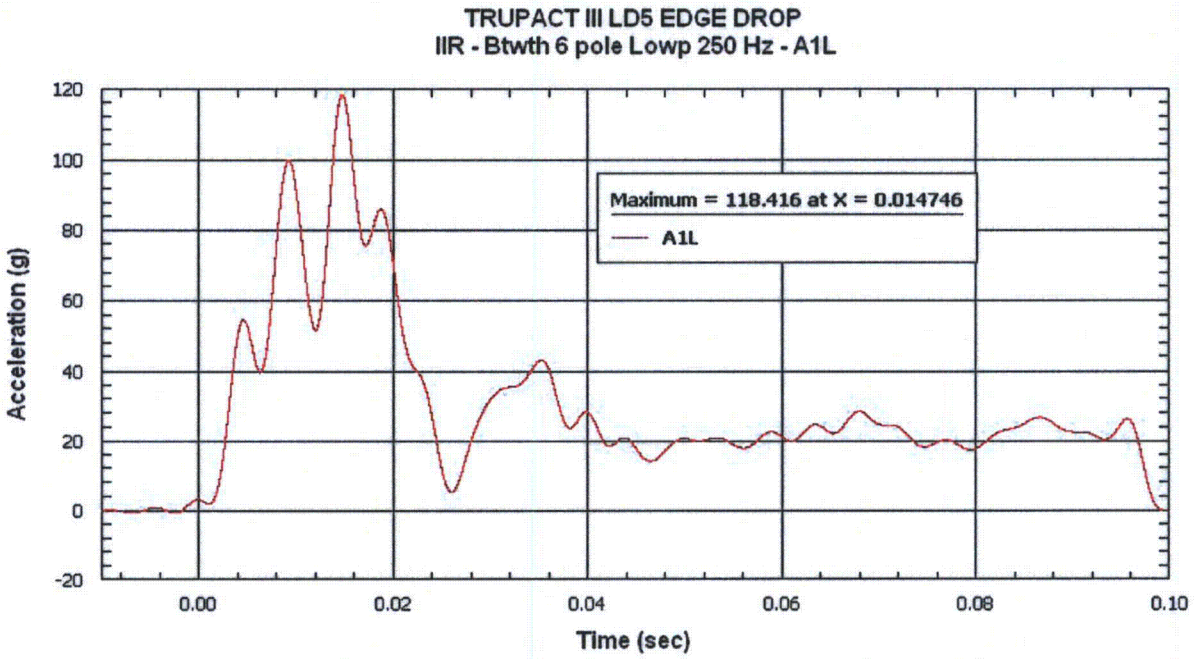
TRUPACT III LD5 EDGE DROP
IIR - Btwth 6 pole Lowp 250 Hz - A1L
Maximum = 118.416 at X = 0.014746
A1L
Acceleration (g)
Time (sec)
120
100
80
60
40
20
0
-20
0.00
0.02
0.04
0.06
0.08
0.10

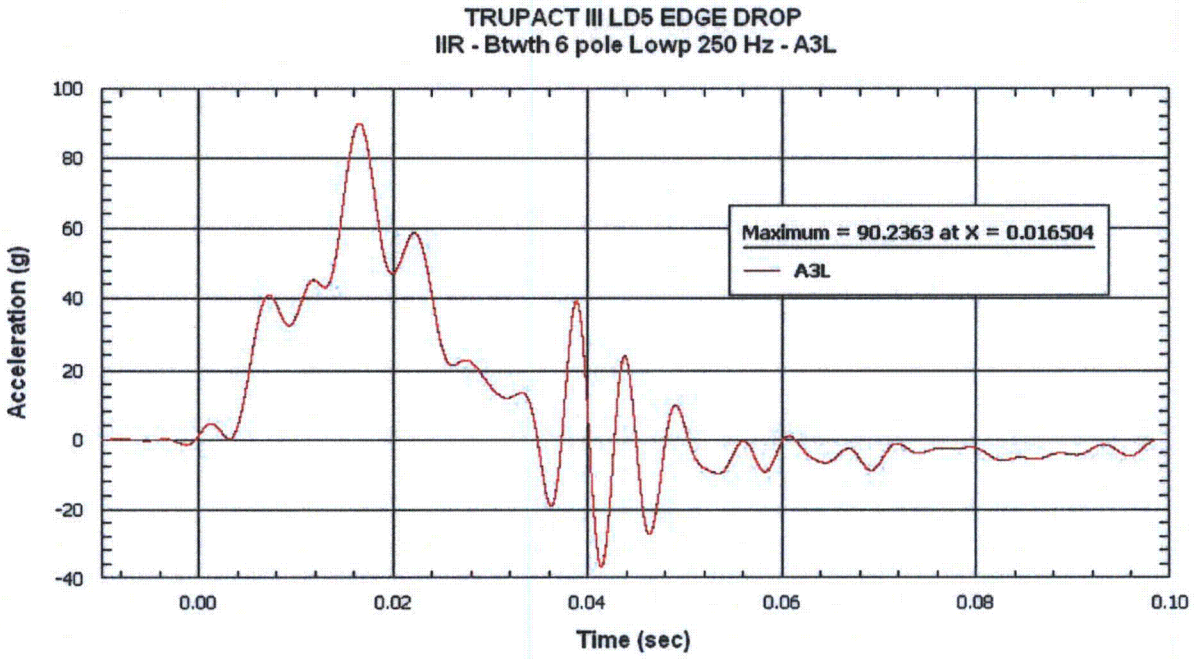
TRUPACT III LD5 EDGE DROP
IIR - Btwth 6 pole Lowp 250 Hz - A3L
Maximum = 90.2363 at X = 0.016504
A3L
Acceleration (g)
Time (sec)
100
80
60
40
20
0
-20
-40
0.00
0.02
0.04
0.06
0.08
0.10

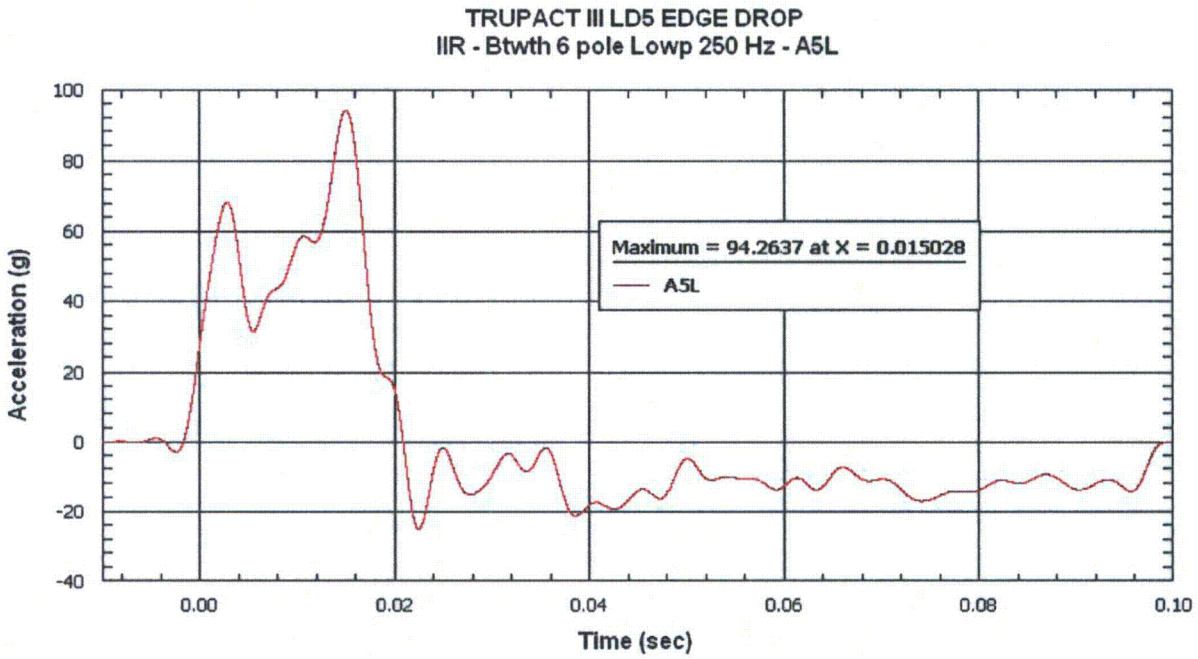
TRUPACT III LD5 EDGE DROP
IIR - Btwth 6 pole Lowp 250 Hz - A5L
Maximum = 94.2637 at X = 0.015028
A5L
Acceleration (g)
Time (sec)
100
80
60
40
20
0
-20
-40
0.00
0.02
0.04
0.06
0.08
0.10

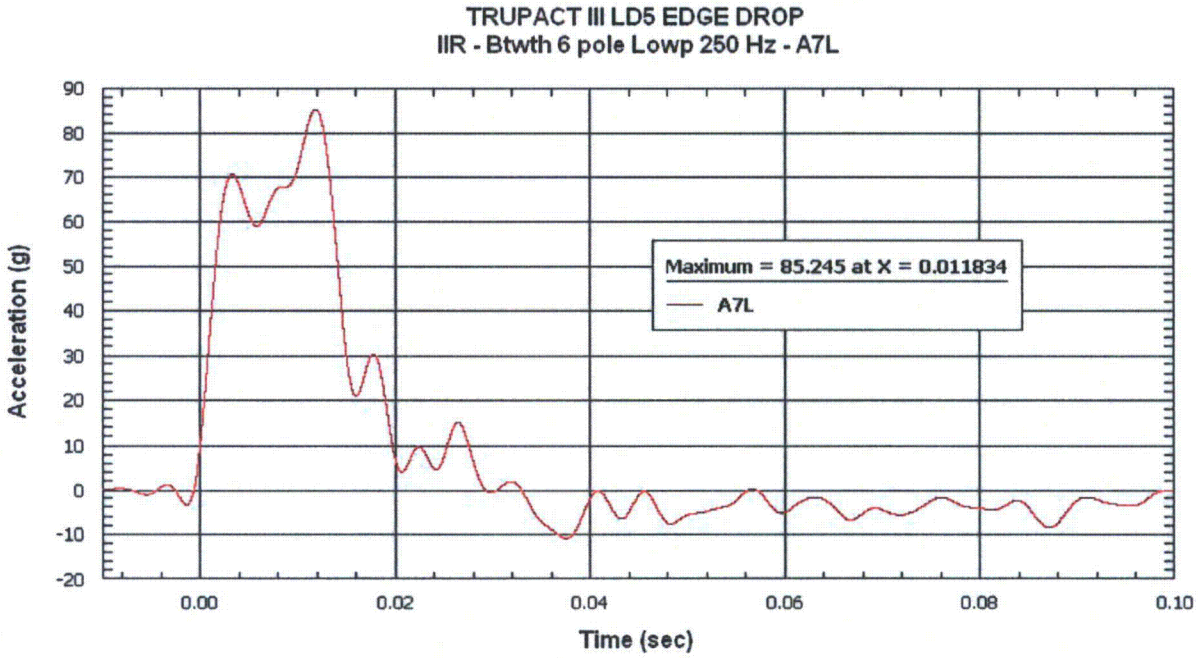
TRUPACT III LD5 EDGE DROP
IIR - Btwth 6 pole Lowp 250 Hz - A7L
Maximum = 85.245 at X = 0.011834
A7L
Acceleration (g)
Time (sec)
90
80
70
60
50
40
30
20
10
0
-10
-20
0.00
0.02
0.04
0.06
0.08
0.10

This page intentionally left blank.

2.12.4 HAC Immersion Buckling Evaluation

2.12.4.1 Introduction

The purpose of this evaluation is to determine the buckling characteristics of the containment structural assembly (CSA) walls due to the immersion requirement for hypothetical accident conditions (HAC) of 150 kPa, gauge, per 10 CFR §71.73(c)(6)[1]. This condition conservatively envelops the increased external pressure condition for normal conditions of transport (NCT) of 140 kPa, absolute, per 10 CFR §71.71(c)(4). The geometry design input is extracted from the general arrangement drawings in Appendix 1.3.1, *Packaging General Arrangement Drawings*. NOTE: All technical references are to be found in Section 2.12.4.5, *References*.

2.12.4.2 Mechanical Properties

The CSA walls are fabricated entirely from Alloy UNS S31803 stainless steel. Material properties utilized in this appendix are extracted from Table 2.2-1 and Table 2.2-2 of Section 2.2, *Mechanical Properties of Materials*.

2.12.4.3 Conditions Analyzed

The CSA structure will be evaluated in this calculation for the following conditions:

1. Buckling analysis of CSA containment sheets.
2. Buckling analysis of sidewall.
3. Stress due to pressure load.
4. Transverse shear stiffness of core.
5. Effect of initial deflections.

2.12.4.4 Calculations

2.12.4.4.1 Buckling Analysis of CSA Containment Sheets

The critical buckling condition is the hypothetical accident condition of immersion of at least 15 m head of water as defined in 10 CFR §71.73(c)(6). The equivalent external pressure and temperature is 150 kPa and 71 °C, respectively.

The sidewall is the largest sheet and as such, will be the bounding case for buckling under the action of edge loads and the design pressure load. The edge loads result from the pressure loads on the adjacent end, top, and bottom sheets.

For conservatism, assume that the height of the sidewall extends from the center of the bottom sheet to the center of the top sheet. Additionally, assume that the length extends from the center of the end sheet to the bolted O-ring seal flange. For purposes of calculating edge loads, the width of

[1] Title 10, Code of Federal Regulations, Part 71 (10 CFR 71), *Packaging and Transportation of Radioactive Material*, 01–01–09 Edition.

the top/bottom sheet is assumed to extend from the center of one sidewall to the center of the other sidewall. These dimensions are as follows:

H = height of sidewall = 2,140 mm

L = length of sidewall = 2,860 mm

W = width of top/bottom sheet = 1,980 mm

Referring to Figure 2.12.4-1, assume that the pressure load acting on Area 1 of the end sheet loads the end edges of the sidewall. Assume that the pressure load on Area 2 of the top sheet loads the top and bottom edges.

The areas, edge loads per unit length, and stresses acting on the end edges are calculated as follows:

A_1 = Area 1 (See Figure 2.12.4-2) = area of two triangles plus one rectangle

$= 2(1/2)(990)^2 + 160(990) = 1.139 \times 10^6$ mm^2

P = external pressure = 150 kPa = 0.150 MPa = 0.150 N/mm^2

N_y = edge load per unit length in y-direction (perpendicular to core longitudinal axis)

$$= \frac{PA_1}{H} = \frac{0.150(1.139\times10^6)}{2140} = 79.8 \text{ N/mm}$$

σ_y = edge stress in y-direction (perpendicular to core longitudinal axis)

$$= \frac{N_y}{2t_1} = \frac{79.8}{2(8)} = 5.0 \text{ MPa}$$

The areas, edge loads per unit length, and stresses acting on the top/bottom edges are calculated as follows:

A_2 = Area 2 (See Figure 2.12.4-3) = 2 $(1/2)(990)^2 + 880(990) = 1.851 \times 10^6$ mm^2

N_x = edge load per unit length in the x-direction (parallel to core longitudinal axis)

$$= \frac{PA_2}{L} = \frac{0.150(1.851\times10^6)}{2{,}860} = 97.1 \text{ N/mm}$$

σ_x = edge stress in x-direction (parallel to core longitudinal axis)

$$= \frac{N_x}{2t_1} = \frac{97.1}{2(8)} = 6.1 \text{ MPa}$$

2.12.4.4.2 Buckling Analysis of Sidewall

The buckling analysis of the sidewall will be performed as follows:

1) Calculate the buckling stress for biaxial compression using the method presented in Reference 2.
2) Calculate the face sheet stress due to the pressure load acting normal to the surface.
3) Calculate the amplification effect of edge loads upon the stress calculated in Step 2 using the combined load formula from Reference 3.
4) Add the amplified stress due to normal pressure to the stress due to edge loads.

5) Calculate a factor of safety using the applied stress from Step 4 and an allowable stress equal to the buckling stress from Step 1.

2.12.4.4.3 Buckling Stress for Biaxial Compression

The following quantities per the notation of Reference 2 will be needed:

a = sheet dimension in x-direction = 2,140 mm

b = sheet dimension in y-direction = 2,860 mm

a/b = 0.75

t = face sheet thickness = 8 mm

c = core height measured between face sheets (See Fig. 2.12.4-7) = 124 mm

E = modulus of elasticity of face sheet material = 19.2×10^4 MPa

μ = Poisson's ratio of face sheet material = 0.3 (Poisson's ratio was taken to be 0.3 since Figure 2.12.4-4 used later is based on this value. This value is slightly higher than the 0.29 value given in Table 1. Per Table 2 of Reference 2, the buckling coefficient decreases with increasing Poisson's ratio, so it is conservative to use the higher value.)

D = bending rigidity of facing sheets about sandwich centroidal axis

$$= \frac{E(t)(c+t)^2}{2(1-\mu^2)} = \frac{19.2\times10^4(8)(124+8)^2}{2(1-0.3^2)} = 1.471\times10^{10}\ \text{N-mm}$$

U = transverse shear stiffness of core

$= D_{Qy} = 2.050 \times 10^4$ N/mm (See Section 2.12.4.4.5, *Transverse Shear Stiffness of Core*)

J = sandwich stiffness parameter

$$= \frac{U(b)^2}{\pi^2(D)} = \frac{2.050\times10^4(2{,}860)^2}{\pi^2(1.471\times10^{10})} = 1.15$$

Buckling coefficients can be obtained from Figure 8(b) of Reference 2 (Figure 2.12.4-4 herein). This figure applies for a/b = 1.0 which is conservative for the aspect ratio of 0.75 for this analysis.[2] The equations for the buckling coefficients are:

$$K_x = \frac{N_x(b)^2}{\pi^2(D)} \qquad K_y = \frac{N_y(b)^2}{\pi^2(D)}$$

From the equations above, the ratio of the buckling coefficients is

$$\frac{K_y}{K_x} = \frac{N_y}{N_x} = \frac{79.8}{97.1} = 0.822$$

Construct a line with this slope on Figure 2.12.4-4 and read the values for K_x and K_y at the intersection of this line and the curve for J = 1.15, as illustrated in Figure 2.12.4-4. The buckling coefficients are:

[2] The conservatism is evident by comparison with Figure 8(a) of Reference 2, for which the aspect ratio is 0.5 and which yields larger critical buckling loads.

$$K_x = 1.35 \qquad K_y = 1.11$$

The critical buckling loads can be obtained from the equations above for K_x and K_y.

$$(N_x)_{cr} = \frac{\pi^2 (D)(K_x)}{(b)^2} = \frac{\pi^2 (1.471\times10^{10})(1.35)}{(2{,}860)^2} = 2.40\times10^4 \text{ N/mm}$$

$$(N_y)_{cr} = \frac{\pi^2 (D)(K_y)}{(b)^2} = \frac{\pi^2 (1.471\times10^{10})(1.11)}{(2{,}860)^2} = 1.97\times10^4 \text{ N/mm}$$

The critical buckling stress, $(\sigma_{cr})_x$, will be calculated based on the assumption that only the face sheets react the edge loads. This is conservative since the loads shared by the core are neglected.

$$(\sigma_{cr})_x = \frac{(N_x)_{cr}}{2(t)} = \frac{2.40\times10^4}{2(8)} = 1{,}500 \text{ MPa}$$

This stress exceeds the yield stress of 419 MPa at 71 °C indicating that the buckling is inelastic. The critical inelastic buckling stress can be calculated by using the tangent modulus instead of the elastic modulus. The tangent modulus is calculated by an iterative process from the true stress-strain curve for Alloy UNS S31803 material taken from Table 2.2-2 of Section 2.2, *Mechanical Properties of Materials*. True stress-strain and engineering stress-strain are essentially equivalent in the region of low strain under consideration. The data in the region of interest is:

True Strain	True Stress, MPa
0.0008	152
0.0016	276
0.0023	345
0.0042	421

These points are fit to the equation $\sigma = 164.02 ln(\varepsilon) + 1328.4$, with a correlation coefficient of 0.992. The derivative of this equation gives the tangent modulus for a given strain level. At a strain level of 0.00328, the stress is 390 MPa and the tangent modulus is $E_t = 5.0\times10^4$ MPa. Multiplying the elastically calculated buckling stress by the ratio of the tangent modulus to the elastic modulus gives the critical inelastic buckling stress, $(\sigma_{cri})_x$:

$$(\sigma_{cri})_x = (E_t/E)\,(\sigma_{cr})_x = (5.0\times10^4/19.2\times10^4)(1{,}500) = 391 \text{ MPa}$$

Note that the critical inelastic buckling stress value of 391 MPa is essentially equal to the stress value of 390 MPa from the stress-strain curve indicating that no further iterations are necessary.

The critical buckling load is:

$$(N_x)_{cr} = (\sigma_{cri})_x(2)(t) = 391(2)(8) = 6{,}256 \text{ N/mm}$$

2.12.4.4.4 Stress Due to Pressure Load

Consider a strip of unit width taken from the middle of the sidewall, as shown in Figure 2.12.4-5. The strip will be analyzed as a simply supported beam with uniform load, which is conservative since the end support of the sidewall is neglected. The uniform load is:

$$\omega = \text{P (unit width)} = 0.150\ (1) = 0.150\ \text{N/mm}$$

The maximum moment, which occurs at midspan, is:

$$M_{max} = \frac{\omega(H)^2}{8} = \frac{0.150(2{,}140)^2}{8} = 8.587 \times 10^4\ \text{N-mm}$$

The bending cross-section is shown in Figure 2.12.4-6. It is conservatively assumed that the face sheets resist all the bending. No structural credit is assumed for the core. Also, the moment of inertia of the face sheets about their individual centroidal axes is conservatively neglected.

The area of one face sheet per unit width is:

$$A = 1.0\ (8) = 8.0\ \text{mm}^2$$

The distance between the centroids of the face sheets is d = 132 mm. The moment of inertia of the cross-section is:

$$I = 2(A)\left(\frac{d}{2}\right)^2 = \frac{A(d)^2}{2} = \frac{8.0(132)^2}{2} = 69{,}700\ \text{mm}^4$$

The distance from the neutral axis to the centroid of a face sheet is:

$$c = \frac{d}{2} = \frac{132}{2} = 66\ \text{mm}$$

The stress in the face sheet is then:

$$\sigma_b = \frac{M(c)}{I} = \frac{8.587 \times 10^4 (66)}{69{,}700} = 81.3\ \text{MPa}$$

This stress is amplified by the presence of edge loads. Formula 8:5 from Reference 3 is used to calculate the amplified stress, σ_{ba}:

$$\sigma_{ba} = \frac{\sigma_b}{1 - \dfrac{N_x}{(N_x)_{cr}}} = \frac{81.3}{1 - \dfrac{97.1}{6{,}256}} = 82.6\ \text{MPa}$$

The combined stress resulting from normal plus edge loads is:

$$\sigma = \sigma_{ba} + \sigma_x = 82.6 + 6.1 = 88.7\ \text{MPa}$$

The factor of safety against buckling is

$$FS = \frac{(\sigma_{cr})_x}{\sigma} = \frac{391}{88.7} = 4.41$$

This is considerably in excess of the minimum factor of safety of 2.00 for NCT and 1.34 for HAC per Section -1400 of Reference 6. Note that the result for NCT is quite conservative, since it assumes an external pressure of 150 kPa gauge, whereas the required pressure per 10 CFR §71.71(c)(4) is only 140 kPa absolute.

2.12.4.4.5 Transverse Shear Stiffness of Core

The transverse shear stiffness will be calculated using the method presented in Reference 1. A symmetric core is assumed even though there is no crest flat in this case. This assumption is judged to be conservative for the following reasons:

1) Unequal crests and troughs have very little effect on the value of the transverse shear stiffness factor "S" for the geometry of this case (See Figure 4(c) of Reference 1).
2) The method of Reference 1 assumes that the core is attached to the face sheets at the mid-lengths of the trough and crest flats. This configuration is a more flexible geometry than the present case because the core length is longer and the face sheet span between attachment points is greater. The additional flexibility results in a lower value of transverse shear stiffness, which is conservative.
3) In the analysis that follows, a very conservative value of 20 was extracted from Figure 2.12.4-8 for the factor "S". If the curve is extrapolated, a value greater than 30 is obtained.

Dimensions

t_c = core thickness = 4 mm

h_c = vertical core height from crest centerline to centerline at trough (See Fig. 2.12.4-7) = 120 mm

h = distance between middle surfaces of face sheets = 132 mm

t_1 = thickness of face 1 = 8 mm

t_2 = thickness of face 2 = 8 mm

2p = corrugation pitch = 164 mm

p = 164/2 = 82 mm

R_{c1} = radius of corrugation at face 1 = 4 mm

R_{c2} = radius of corrugation at face 2 = 4 mm

θ = angle between corrugation side & face sheet = $\tan^{-1}$ (124/55) = 66.1° (See Figure 2.12.4-7)

f_1 = face width of corrugation at face 1

f_2 = face width of corrugation at face 2 (assume $f_1 = f_2$)

Dimensional Ratios

$h_c/t_c = 120/4 = 30$

$t_c/t_1 = 4/8 = 0.5$

$p/h_c = 82/120 = 0.683$

$R_{c1}/h_c = R_{c2}/h_c = 4/120 = 0.0333$

As previously noted, the modulus of elasticity for the core material (E_c) at 71 °C is 19.2×10^4 MPa.

The formula for transverse shear stiffness contains a factor "S" that can be obtained from charts in the reference above. The Figure 3 charts of Reference 1 are for $R_{c1} = R_{c2} = 0.18\ h_c$. For this analysis, $R_{c1} = R_{c2} = 0.0333\ h_c$. Results for $R_{c1} = R_{c2} \neq 0.18\ h_c$ are presented in the reference where the effect on "S" is seen to be small. Thus, it will be sufficiently accurate to use the Figure 3 charts.

Figure 3(c) of Reference 1 for $t_c/t_1 = 0.50$ and $h_c/t_c = 30$, included as Figure 2.12.4-8, applies for this case. For $p/h_c = 0.683$ and $\theta = 66.1°$, the value of "S" is off the upper end of the chart. The upper chart value of $S = 20$ will be conservatively used.

The transverse shear stiffness, D_{Qy}, is calculated from the following formula:

$$D_{Qy} = S(h)\frac{E_c}{(1-\mu_c^2)}\left(\frac{t_c}{h_c}\right)^3 = 20(132)\frac{19.2 \times 10^4}{(1 - 0.29^2)}\left(\frac{4}{120}\right)^3 = 2.050 \times 10^4 \text{ N/mm}$$

2.12.4.4.6 Effect of Initial Deflections

The effect of initial deflections of the sidewall on the critical buckling load will be evaluated. Initial deflections can occur during the manufacturing process and are controlled by flatness tolerances on the fabrication drawings. The total deflection of a sheet with an initial deflection under the action of edge loads can be calculated from Equation 6.3.7 of Reference 5. The equation is:

$$W + W_o = \frac{W_o}{1 - \frac{N_x}{(N_x)_{cr}}}$$

where: $W + W_o$ = total deflection

W_o = initial deflection

W = additional deflection due to edge loads acting on a sheet with initial deflection W_o

$\frac{N_x}{(N_x)_{cr}}$ = ratio of applied edge load to critical edge load

Note that this equation is similar to the one used in Section 2.12.4.4.4, *Stress Due to Pressure Load,* to calculate the effect of the pressure load acting on the surface of the sidewall.

The stress due to the combined effect of edge loads and initial deflection W_o results from the additional deflection W only. In order to calculate this stress, the equation above will be solved for W. The result is:

$$W = \left[\frac{\frac{N_x}{(N_x)_{cr}}}{1 - \frac{N_x}{(N_x)_{cr}}}\right] W_o$$

The edge load values are:

$N_x = 97.1$ N/mm (See Section 2.12.4.4.1, *Buckling Analysis of CSA Containment Sheets*)

$(N_x)_{cr} = 6{,}256$ N/mm (See Section 2.12.4.4.3, *Buckling Stress for Biaxial Compression*)

The ratio of edge loads is:

$$\frac{N_x}{(N_x)_{cr}} = \frac{97.1}{6{,}256} = 0.0155$$

Substituting this value into the above equation yields:

$$W = \left[\frac{0.0155}{1 - 0.0155}\right] W_o = 0.0157\, W_o$$

The stress associated with the deflection W will be calculated by multiplying W by the ratio of stress to deflection for the uniformly loaded strip analyzed in Section 2.12.4.4.4, *Stress Due to Pressure Load.* The stress for the strip was determined to be:

$$\sigma_b = 81.3 \text{ MPa}$$

The deflection for a uniformly loaded strip is:

$$\delta = \frac{5(\omega)(H)^4}{384(E)(I)}$$

where: $\omega = 0.150$ N/mm

$H = 2{,}140$ mm

$E = 19.2 \times 10^4$ MPa

$I = 69{,}700$ mm^4

Substituting values into the above equation yields:

$$\delta = \frac{5(0.150)(2140)^4}{384(19.2\times10^4)(69{,}700)} = 3.06 \text{ mm}$$

The ratio of stress to deflection is:

$$\frac{\sigma_b}{\delta} = \frac{81.3}{3.06} = 26.6 \text{ MPa/mm}$$

The stress due to deflection W is:

$$\sigma_w = 26.6\ W = 26.6\ (0.0157)W_o = 0.418W_o$$

This stress will be added to the combined stress $\sigma = 88.7$ MPa from Section 2.12.4.4.4, *Stress Due to Pressure Load,* for a total stress of:

$$\sigma_{tot} = 88.7 + 0.418W_o$$

An allowable initial deflection can be calculated by equating the total stress above to the allowable stress. The allowable stress is 391 MPa from Section 2.12.4.4.3, *Buckling Stress for Biaxial Compression.*

$$\sigma_{tot} = \sigma_{all} \Rightarrow 88.7 + 0.418(W_o)_{all} = 391$$

Solving for $(W_o)_{all}$ yields the following:

$$(W_o)_{all} = \frac{391 - 88.7}{0.418} = 723 \text{ mm}$$

The allowable initial deflection is large because the applied edge loads are very small compared to the critical edge loads for buckling. For this case, the ratio $N_x/(N_x)_{cr}$ is 0.0155.

Since the manufacturing tolerance on sheet flatness is much smaller than the allowable initial deflection calculated above, it is concluded that initial deflections due to the manufacturing process will have an insignificant effect on the critical buckling load.

2.12.4.5 References

1. Libove, C. and Hubka, R.E., *Elastic Constants for Corrugated-Core Sandwich Plates*, NACA TN 2289, 1951.
2. Harris, L.A. and Auelmann, R.R., *Stability of Flat, Simply Supported Corrugated-Core Sandwich Plates Under Combined Loads*, Journal of the Aero/Space Sciences, Vol. 27, No. 7, pp. 525-534, July, 1960.
3. MIL-HDBK-23A, *Structural Sandwich Composites*, U.S. Dept. of Defense, 1968.
4. American Society of Mechanical Engineers (ASME) Boiler and Pressure Vessel Code, Section II, *Materials*, Part D, *Properties*, 2004 Edition, 2005 and 2006 Addenda.
5. Plantema, F. J., *Sandwich Construction*, John Wiley and Sons, Inc, New York, 1966.
6. Code Case N–284–1, Metal Containment Shell Buckling Design Methods, Class MC, Section III, Division 1, ASME Boiler & Pressure Vessel Code.

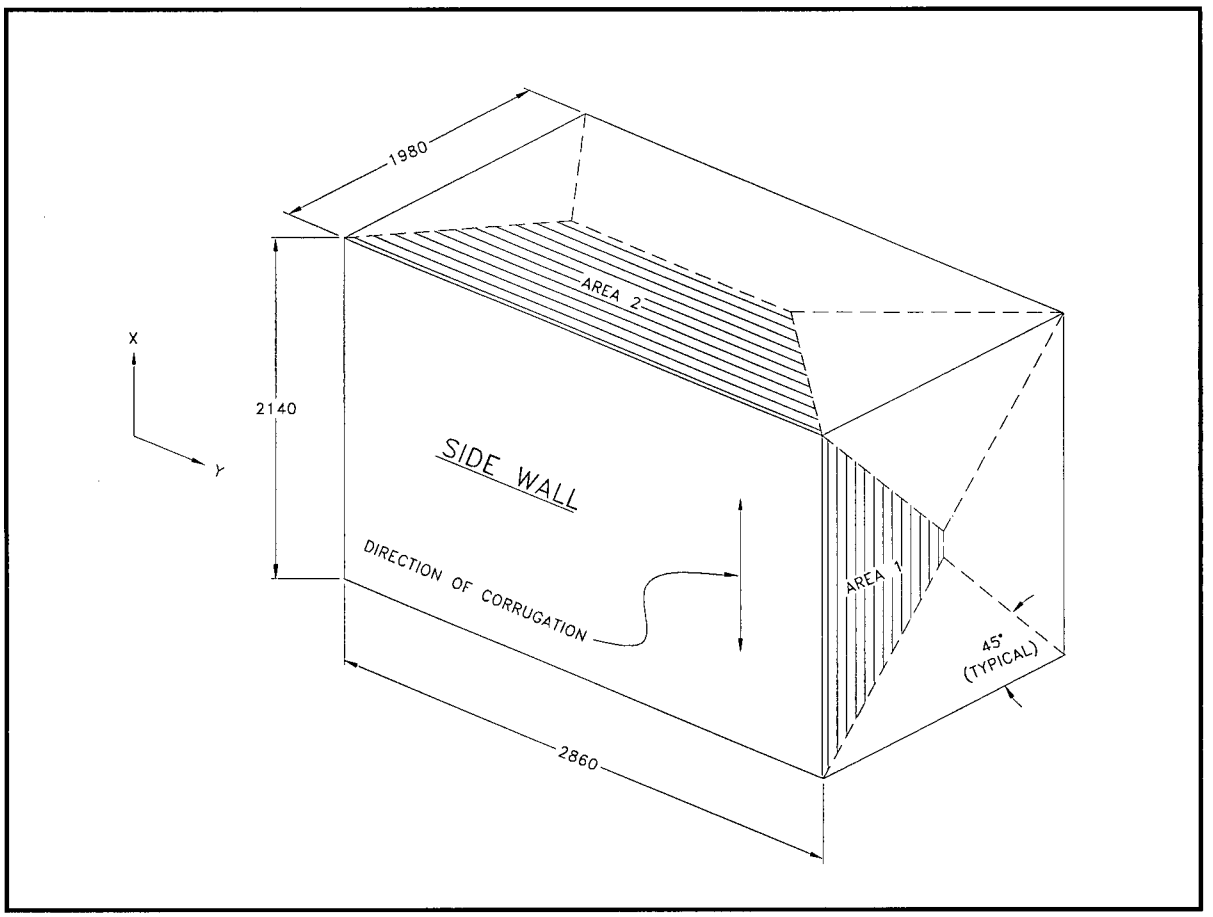

Figure 2.12.4-1 – View of Sidewalls and Adjacent Panels Showing Areas Used to Calculate Edge Loads

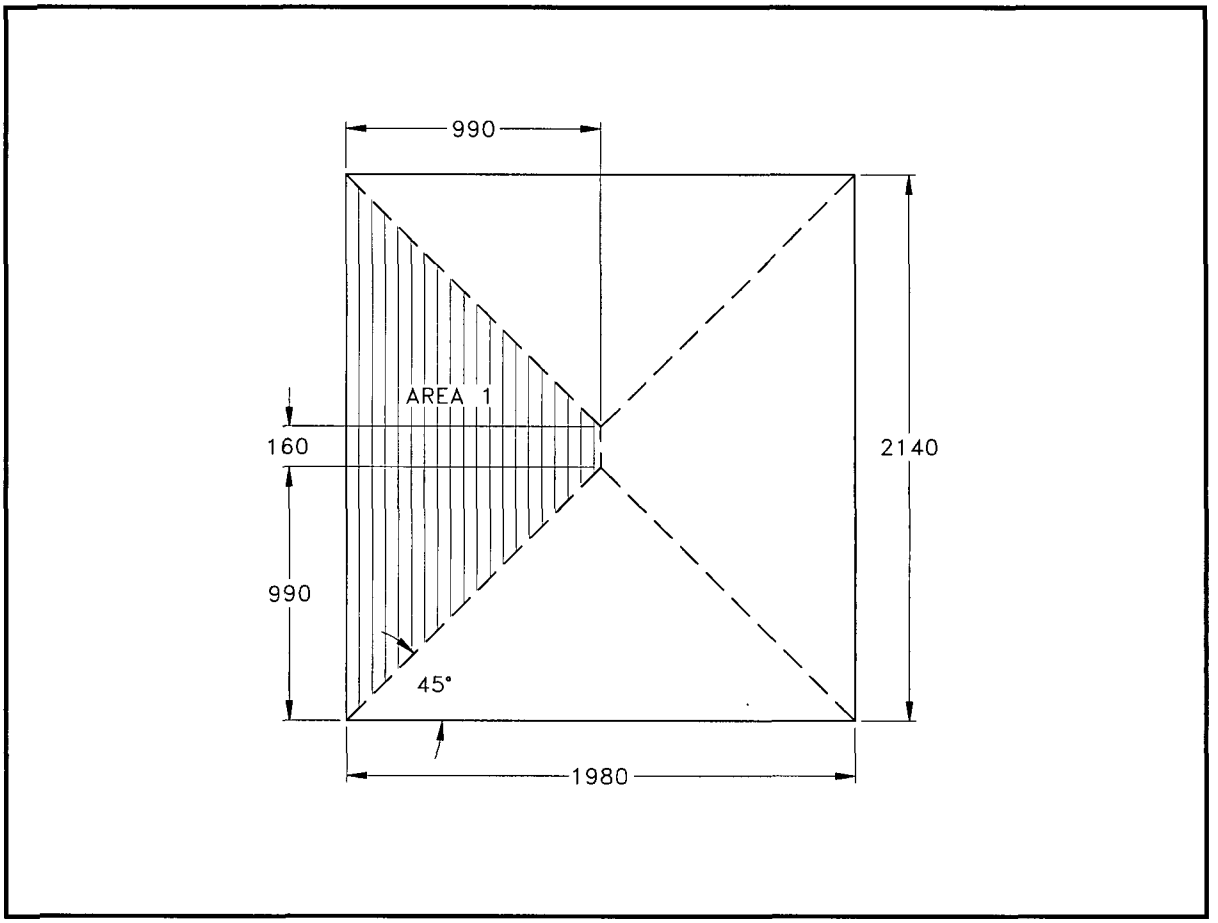

Figure 2.12.4-2 – View of Area 1 on End Sheet Used to Calculate End Edge Load on Sidewall

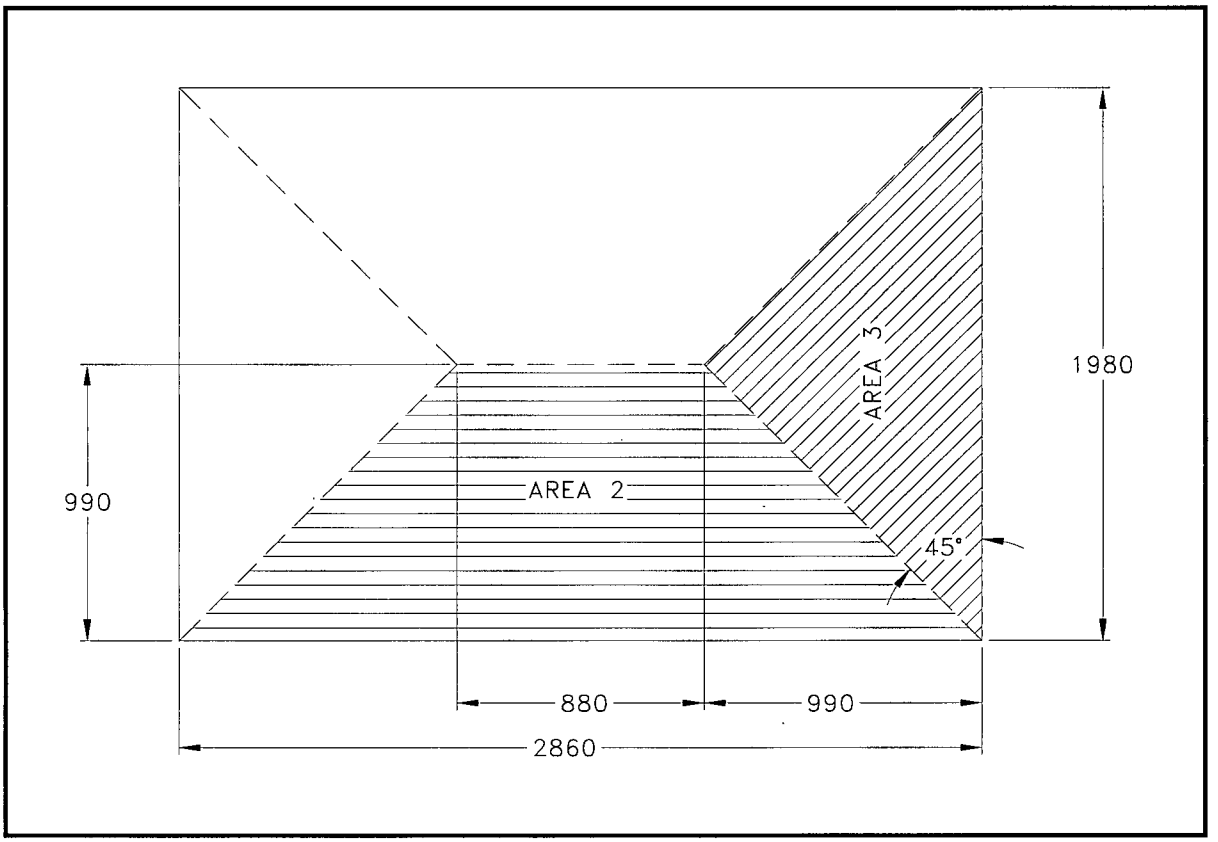

Figure 2.12.4-3 – View of Area 2 on Top Sheet Used to Calculate Top/Bottom Edge Loads on Sidewall

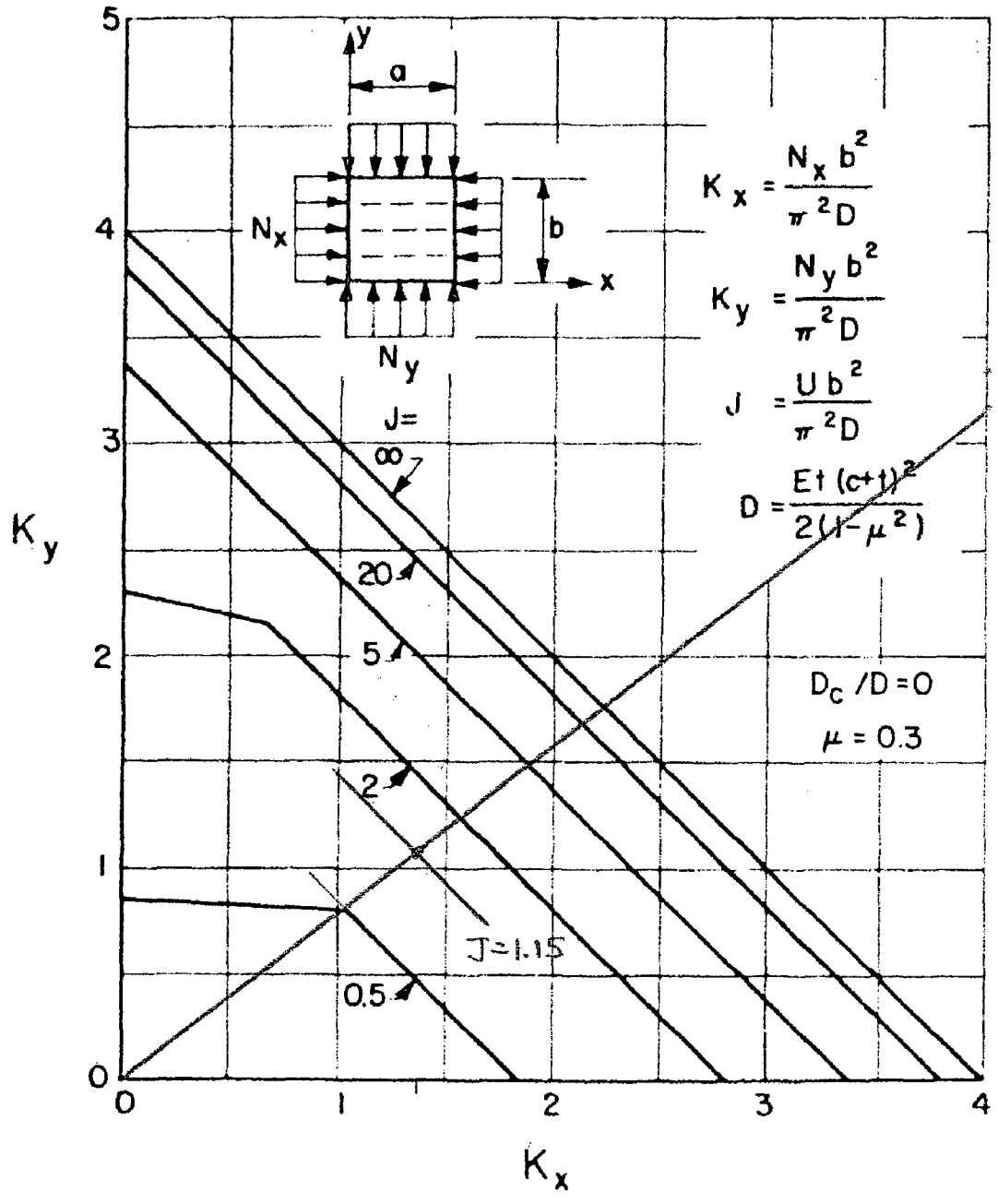

Figure 2.12.4-4 – Buckling Coefficients for Biaxial Compression (a/b = 1) [Figure 8(b) from Reference 2]

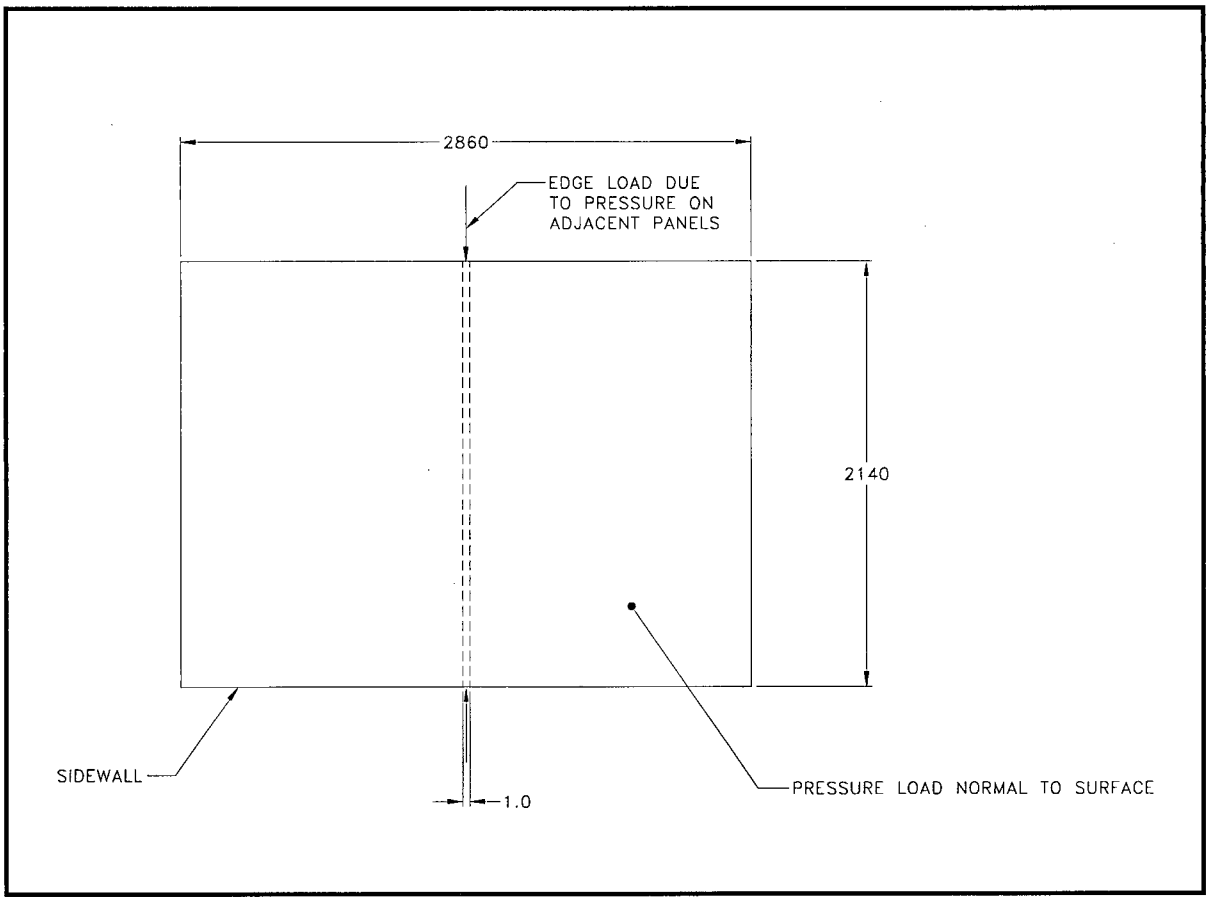

Figure 2.12.4-5 – View of Sidewall Showing Strip of Unit Width

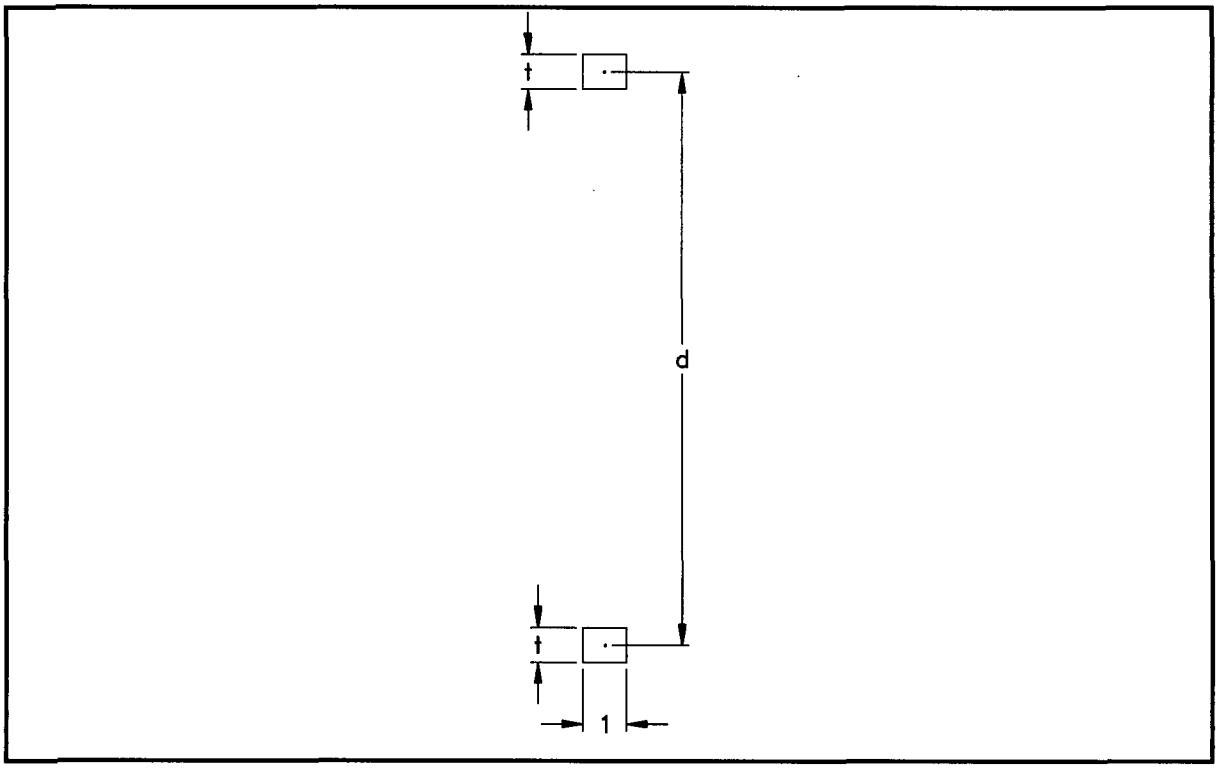

Figure 2.12.4-6 – Bending Cross-Section

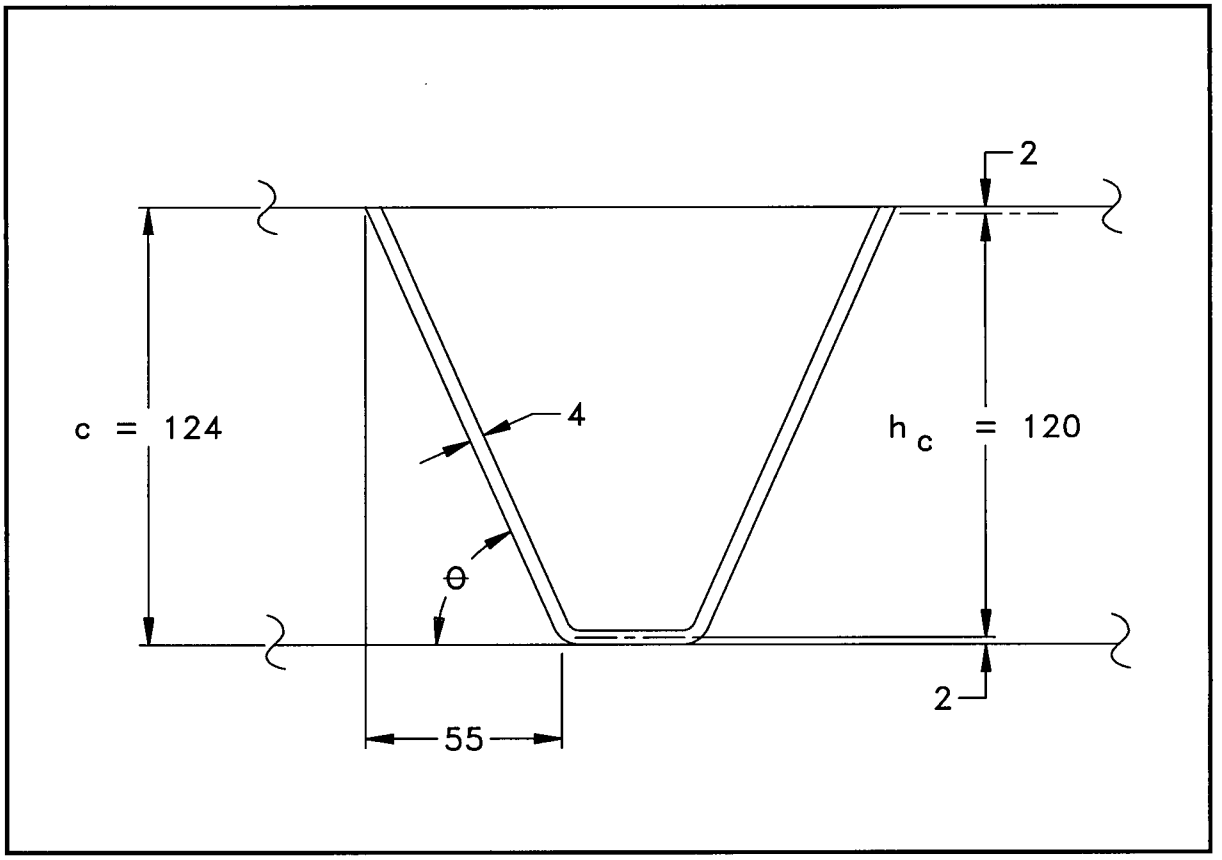

Figure 2.12.4-7 – V-Stiffener Core Geometry

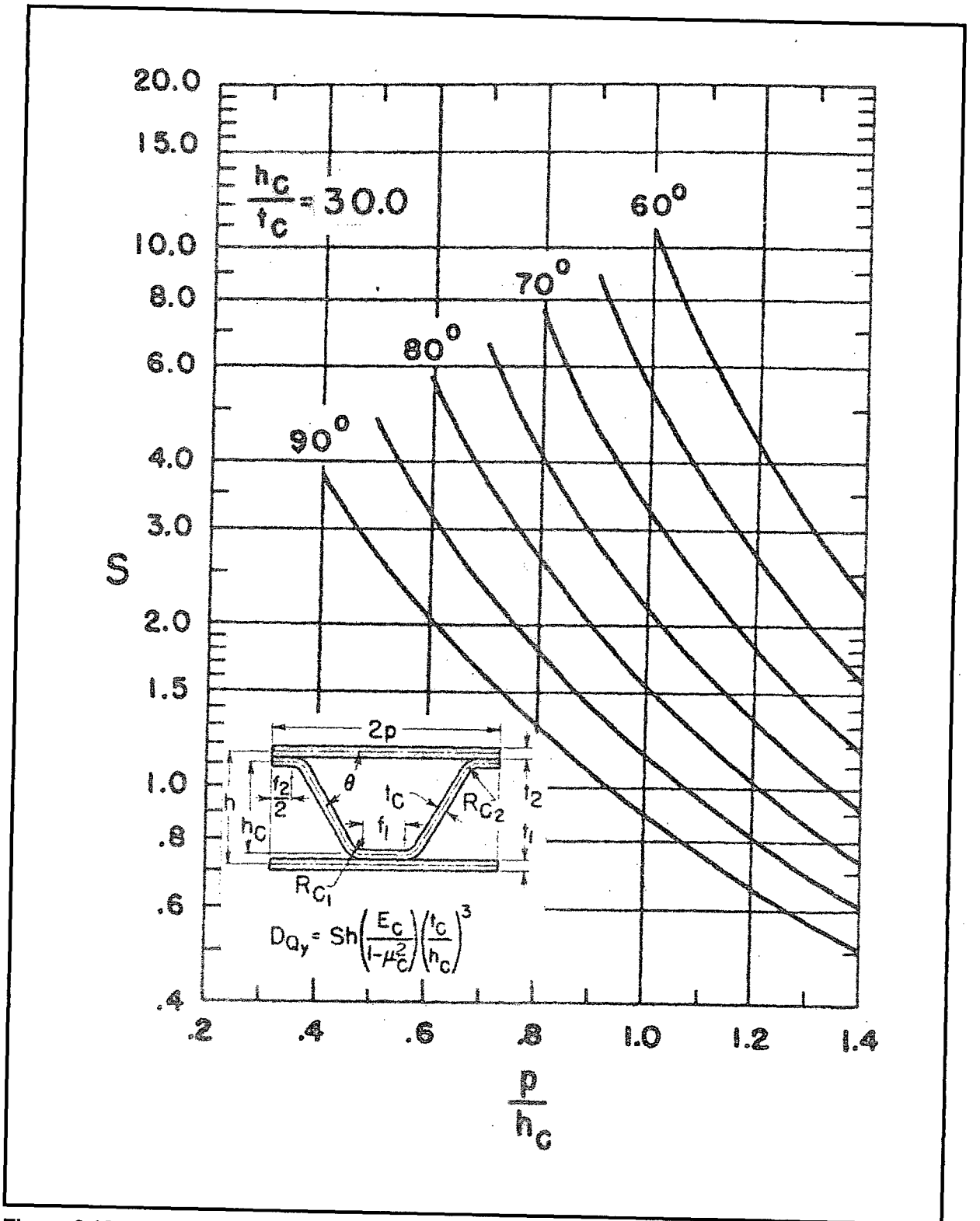

Figure 2.12.4-8 – Chart for Evaluation Coefficient S in Formula for D_{Qy} ($t_c/t_1 = 0.5$) [Figure 3(c) of Ref. 1]

This page intentionally left blank.

2.12.5 Closure Lid Debris Shield

2.12.5.1 Introduction

This section presents a demonstration of the effectiveness of the debris shield design by analysis. The debris shield performance was demonstrated by test using CTU-2 as discussed in Appendix 2.12.6, *Certification Tests on CTU-2*. Note, all references to certification testing in this appendix indicate the first certification test series using CTU-1.

The purpose of the debris shield is to prevent the contamination of the containment O-ring seal with any particulate matter (i.e., debris) which might be present within the payload cavity. As a result of certain HAC free drop impacts, a transient opening of the closure joint could occur, allowing the debris to be deposited on the containment O-ring seal, potentially preventing a leaktight condition. The debris shield utilized in the TRUPACT–III blocks the access of any debris to the vicinity of the closure joint, thus preventing contamination of the seal.

2.12.5.2 Contamination of the Containment O-ring Seal During Certification Testing

The tests performed on the first certification test unit (CTU-1) are fully discussed in Appendix 2.12.3, *Certification Tests on CTU-1*. As detailed therein, the post-test helium leakage rate testing of the closure lid containment O-ring seal was not successful due to the presence of small debris particles lodged between the elastomer seal surface and the mating body flange. The source of the particles was the aluminum bars which were used for the simulated payload. Upon inspection, the particles were found to be spread over the entire closure joint, including both the containment and test O-ring seals.

During disassembly of the closure lid, it was discovered that a number of the closure bolts, particularly on the right side, had become bent. However, the presence of the debris was the only reason for the inability of the CTU to pass the leakage rate test. After inspection of the closure joint was complete, the exposed sealing surfaces were wiped clean (O-rings were not removed for cleaning), and the lid re-attached with reduced bolt preload. Two reduced-preload tests were performed:

1. All 44 closure bolts were tightened to 149 N-m, or approximately one-sixth of the average measured residual torque of all 44 bolts of 898 N-m. This torque was chosen because it was equal to the lowest residual preload of any bolt. The helium leakage rate test was repeated, and the containment O-ring seal was found to be leaktight.
2. Only the bolts in the four corners of the lid were installed, again tightened to 149 N-m. In this case, the total closure force was only 1.5% of the force that would be applied by all 44 bolts tightened to the average measured residual torque of 898 N-m. The helium leakage rate test was repeated, and the containment O-ring seal was again found to be leaktight.

The helium leakage rate test results are presented in Section 2.12.3.8.1, *Leakage Rate Tests*. Note that, since the pressure within the payload cavity was atmospheric during these tests, there was no assistance from atmospheric pressure in obtaining a leaktight seal, nor was there any assistance from gravity, since the package was horizontal. Note further that the only leakage rate test failure occurred with debris on the seal; both tests performed after removal of the debris were successful. From these two supplemental leakage rate tests, it can be concluded that only a

very small clamping force is needed to ensure a leaktight closure joint, as long as the seals are free of contamination. Therefore, to ensure a leaktight condition of the TRUPACT–III, it will be sufficient to prevent debris contamination of the containment O-ring seal.

Before developing the design criteria for the debris seal, a thorough investigation of the debris phenomena was performed. The intrusion of debris into the closure joint was found to depend on several factors:

- *Generation of debris.* Because several free drops were performed, a large number of collisions among the simulated payload aluminum bars and between the bars and the payload cavity walls occurred, generating a quantity of small aluminum shards and flakes. Numerous re-orientations of the CTU allowed some debris to accumulate next to the closure joint, in the crevice between the closure lid shear lip and the body wall.
- *Transient separation of the closure joint.* In certain free drop impacts, a small transient opening of the closure joint can occur, large enough to allow the passage of debris particles, and lasting on the order of 10 – 15 milliseconds. See Section 2.12.5.5, *Finite Element End Drop Analysis*, and Section 2.12.5.6, *Finite Element Side Drop Analysis*, for an investigation of this phenomenon.
- *Elastomer non-response.* The elastomer material from which the O-ring seals are made cannot elastically respond in a 10 millisecond timeframe. The O-rings remained in a compressed configuration, thus briefly opening a gap across the seals. Because the opening was largest at the inside, the gap at the test seal was somewhat smaller than the gap at the containment seal.
- *Internal design pressure.* The internal design pressure, which was present in the CTU, is 172 kPa. Since the containment seal is a pressure boundary, the differential pressure across the containment seal would be equal to the design pressure. In the transient separation event, escaping air flushed the debris into the closure joint, and onto the O-ring seals.
- *Sliding motions.* Lateral motions of the lid in subsequent free drops or puncture drops could have transported more debris into the sealing nip.

Identification of a specific drop test as the primary driver for debris contamination cannot readily be made. Note is made of the fact that a hard vacuum (160 millitorr or less) was successfully applied to the annulus between the containment and test O-ring seals after the first two 9-m free drops (the lid-down and the side-down drops, LD2 and LD3), but the vacuum could not be achieved after completion of the remaining two 9-m free drops (the side-edge and CG-over-corner drops, LD5 and LD4). If the vacuum test can be taken as a surrogate for the complete helium leakage rate test (experience demonstrates that it can), then the loss of leaktight condition occurred sometime during the last two 9-m free drops.

The certification test program was somewhat unique in that several free drops were performed, allowing debris to be generated over time, and possibly intruding more than once. The packaging regulations require only a single free drop and a single puncture drop. However, the presence of some kind of debris in normal use cannot be ruled out, and if present in the right place and in the right quantity, a single free drop could allow debris contamination of the seals and a possible loss of the leaktight condition. Therefore a debris shield is needed.

2.12.5.3 Debris Shield Design Criteria

The purpose of the TRUPACT–III debris shield is to prevent any debris which may be present in the packaging from contaminating the containment seal in the event of a transient separation of the closure joint, such as could occur in the HAC free drop. To accomplish this task, the following safety-related design criteria have been identified (Table 2.12.5-1).

Table 2.12.5-1 – Debris Shield Design Criteria

Environment	*Temperature:* Per Regulatory Guide 7.8, the temperature range is between a minimum temperature of -29 °C (-40 °C for the normal cold condition) and a maximum ambient temperature of 38 °C with full solar. According to Section 3.1.3, *Summary Tables of Temperatures*, the maximum NCT hot temperature of the containment seal, which may be assumed valid for the debris shield, is 52.6 °C. *Pressure:* The design pressure of the TRUPACT–III is 172 kPa, gage. However, as discussed below, the debris shield should be designed to not retain this pressure.
Material	The material used must be capable of instantaneous response, or else not depend upon elastic response for its function. The material must be strong and durable.
Relative Position/Motion	The debris shield must accommodate the possible range of position of the closure lid relative to the body, and must also accommodate any relative motions arising from transient impact events which lead to closure joint separation. This requirement is discussed in more detail below.
Physical Constraints	The debris shield must not reduce the shear area or bearing area of the closure lid shear lip. It must be compatible with the size of the payload container and the installation of the lid. It must not prevent helium from approaching the containment O-ring seal during helium leakage rate testing. It should be vented so that pressure is nominally equal on both sides (to reduce the mechanical forces on the shield and to eliminate a significant driving force for debris to pass the shield).
Reliability	The debris shield must be reliable and easy to use. It must be protected from damage under normal use and under normal and accident conditions of transport. It must not be damaged by motions of the roller floor, pallet, or payload container during NCT and HAC events. Damage to the shield must be readily detectable and repairable.

As shown in Table 2.12.5-1, the debris shield must accommodate the relative motions which could occur between the closure lid and body. These include the lateral position of the lid within the limits established by the lid shear lip, as well as the axial motions resulting from the transient elastic motions of the lid during HAC free drop events.

As shown in the drawings in Section 1.3.1, *Packaging General Arrangement Drawings*, the clearance between the outer dimension of the lid shear lips and the body flange opening (equivalent to the total range of lateral motion of the lid) is 6 mm in both the side-to-side and up-and-down directions.

The bounding axial motions are defined by the two free drop orientations having the maximum cold impact: one, the lid end down, and two, the flat side down orientation. These orientations represent the largest possible deformations at the closure joint because they combine the largest free drop impacts with a direction of impact force oriented normal to the largest panels of the containment structural assembly (CSA).

The lid end down case is equivalent to CTU free drop orientation LD2. A dynamic finite element model of this case is described in Section 2.12.5.5, *Finite Element End Drop Analysis*. In this orientation, the lid deflects outward, resulting in a rotation of the lid flange away from the body flange. The maximum transient dynamic relative motion at the debris shield is calculated to be 0.78 mm.

The flat side down case is equivalent to CTU free drop orientation LD3. A quasi-dynamic finite element model of this case is described in Section 2.12.5.6, *Finite Element Side Drop Analysis*. In this orientation, the large flat side impacts the ground and deflects downward, resulting in a rotation of the body flange away from the lid flange. The maximum transient dynamic relative motion at the debris shield is calculated to be 3.0 mm. This value will therefore be used as a bounding design criterion for axial debris shield function.

2.12.5.4 Debris Shield Design

The debris shield is shown in a section view in Figure 2.12.5-1, and consists of a receptacle, a holder, and an insert. The receptacle is attached to each side of the body opening, and the holder is integral with the closure lid shear lip. The insert is made from silicone rubber foam having a U-shaped cross-section which is attached to the holder using adhesive double-sided tape on each leg. The insert is therefore carried with the lid. The insert interfaces with a 15-mm wide groove in the receptacle. When the lid is installed, the insert component is inserted into the receptacle. The debris shield incorporates two functional principles: a foam rubber-to-steel seal, and a labyrinth configuration.

The total free-state thickness of the foam insert plus the holder is equal to 18 mm (two 7-mm thicknesses of foam plus the 4 mm center holder). Since the receptacle opening width is 15 mm, the nominal compression of the foam when assembled is 1.5 mm per side, or 1.5/7 = 21%. Note that, since the debris shield has two equivalent sides, a seal is maintained regardless of the lateral location[1] of the holder: any compression lost on one side because of a lateral shift of the holder is gained on the opposite side of the holder. The maximum shift from nominal position is 3 mm, based on the total possible lateral clearance between the lid shear lips and the body opening, equal to 6 mm. If the lid shifted laterally by 3 mm in either direction, a 1.5 mm gap would open up on one side, but a compression of (1.5 + 3) = 4.5 mm (equivalent to 4.5/7 = 64%) would occur on the opposite side. See Figure 2.12.5-2. Of note, during normal operation, the lid lateral position is controlled to within ±1 mm by the two closure lid guide pins. Therefore, the maximum lateral lid displacement of ±3 mm is to be expected only in a HAC free drop event.

The receptacle has an approximately 11.5-mm long straight section, ensuring that the shielding function will occur even if the insert is withdrawn somewhat from the receptacle, also depicted

[1] As used here, 'lateral' means any direction which is parallel to the closure flange sealing surface.

in the figure. Note that the bounding axial movement of the holder relative to the receptacle under HAC free drop conditions of 3 mm is equal to only one-fourth of the straight section. A lead-in on the receptacle opening ensures that the insert will move smoothly into and out of the receptacle without binding or damage. Both the holder and the receptacle are made from the same material as the CSA, i.e., UNS S31803 duplex stainless steel (the receptacle may optionally be made from Type 304/304L material). The receptacle is connected to the body inner flange side using groove and fillet welds, and the holder is integral with the closure lid lip.

The labyrinth configuration alluded to above is achieved by requiring any debris to make at least four right angle turns in order to pass by the shield, as illustrated in Figure 2.12.5-3. This feature provides extra assurance that any debris cannot reach the containment O-ring seal.

Also shown in Figure 2.12.5-1 is a cross section of the lid shear lip. To accommodate the holder design, the tapered lead-in portion of the shear lip, which was present in the CTU, was removed. However, the width of the straight portion of the shear lip (10 mm), representing the bearing area between the lip and the mating body flange under lateral HAC loading, is unchanged. The same thing is true for the shear lip shear width (measured in the plane of the lid) of 20 mm. Therefore, the lid shear lip will have the same bearing area and shear strength as the CTU. Also note the presence of a filtered vent passage across the shear lip shown in Figure 2.12.5-1. There are two vent passages per side for a total of eight. Each hole is fitted with a 5/16-inch (7.94-mm) diameter porous polyethylene filter, and used to maintain equal pressure on both sides of the debris shield.

To protect the debris shield from damage from the payload in normal operation or in a hypothetical accident, nominally 1-inch by 3-inch wide (25.4 mm by 76.2 mm) ASTM Type 304L steel guide bars are welded longitudinally to the sides of the CSA containment sheets. There are three bars on each side, and two on the top. No bars are needed on the bottom, since the roller floor and pallet fully protect the debris shield components from contact with the payload. The bars run the full length of the payload cavity, and are located to align with the 1.5-inch (38.1-mm) wide, hollow tube bumpers which are integral parts of the SLB2 payload container. They are connected to the inner CSA wall using fillet welds. The function of the guide bars is to prevent excessive local loading of the debris shield in a HAC free drop which could affect the body flange/sealing surface geometry. They also keep the SLB2 from getting trapped behind the rear edge of the debris shield, which could lead to damage to the shield in a free drop having a vertical impact force component. Since this is the case, no evaluation of loading of the debris shield in a direction parallel to the package axis needs to be performed. However, the SLB2 can apply lateral impact loads to the debris shield and guide bars, and a finite element analysis of this loading condition is given in Section 2.12.5.7, *Finite Element Payload Interaction Analysis*. As shown in that section, under cold side impact loading, the flange remains elastic, and there is no permanent reduction in containment O-ring seal compression. Therefore, interaction between the payload and the CSA, the debris shield, and the guide bars is of no concern.

The design of the debris shield is evaluated in Table 2.12.5-2. As shown, the design meets all of the design requirements listed in Table 2.12.5-1.

Table 2.12.5-2 – Debris Shield Design Evaluation

Environment	*Temperature:* Silicone foam rubber can easily function at the environmental extremes of -40 °C to 52.6 °C. *Pressure:* The presence of the filtered passages in the shear lip prevents any differential pressure across the debris shield.
Material	Since any lateral movement of the closure lid will cause an increase in the debris shield compression on one side or the other, and since any axial movement of the lid can be accommodated without a change in compression due to the receptacle's straight sides, function of the seal does not depend on elastic unloading response of the insert foam material.
Relative Position/Motion	Since there is no differential pressure driving force across the debris shield, only a very small region of contact between the receptacle and the insert is needed to block transport of debris. The conservatively calculated maximum axial motion is 3 mm (see Section 2.12.5.3, *Debris Shield Design Criteria*), which is significantly smaller than the length of the straight sides of the receptacle of 11.5 mm. The full lateral motion of ±3 mm can be accommodated resulting in seal contact and compression on at least one side of the insert. Therefore, debris will be blocked assuming worst-case relative motion in any direction between the closure lid and the body.
Physical Constraints	The bearing area and shear area of the closure lid shear lip are unchanged from the CTU. The design allows access for the SLB2 payload container and easy installation of the closure lid. The vent passages in the shear lip prevent a differential pressure across the debris shield, and allow passage of helium tracer gas to the containment seal during leakage rate testing.
Reliability	The debris shield is protected from payload interactions by means of the guide bars attached to the walls of the payload cavity as described above and in Section 2.12.5.7, *Finite Element Payload Interaction Analysis*. In normal operation, the debris shield insert may be readily inspected for any damage prior to use and replaced if necessary.

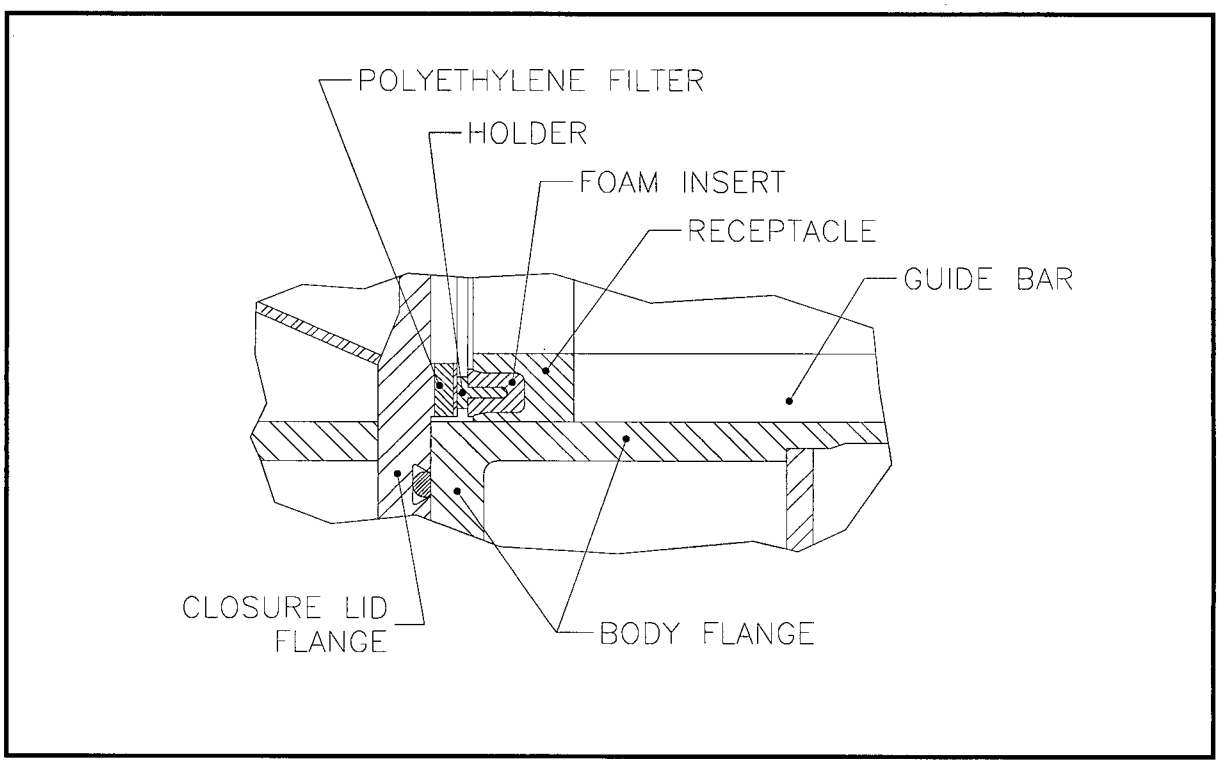

Figure 2.12.5-1 – Debris Shield Cross Sectional View

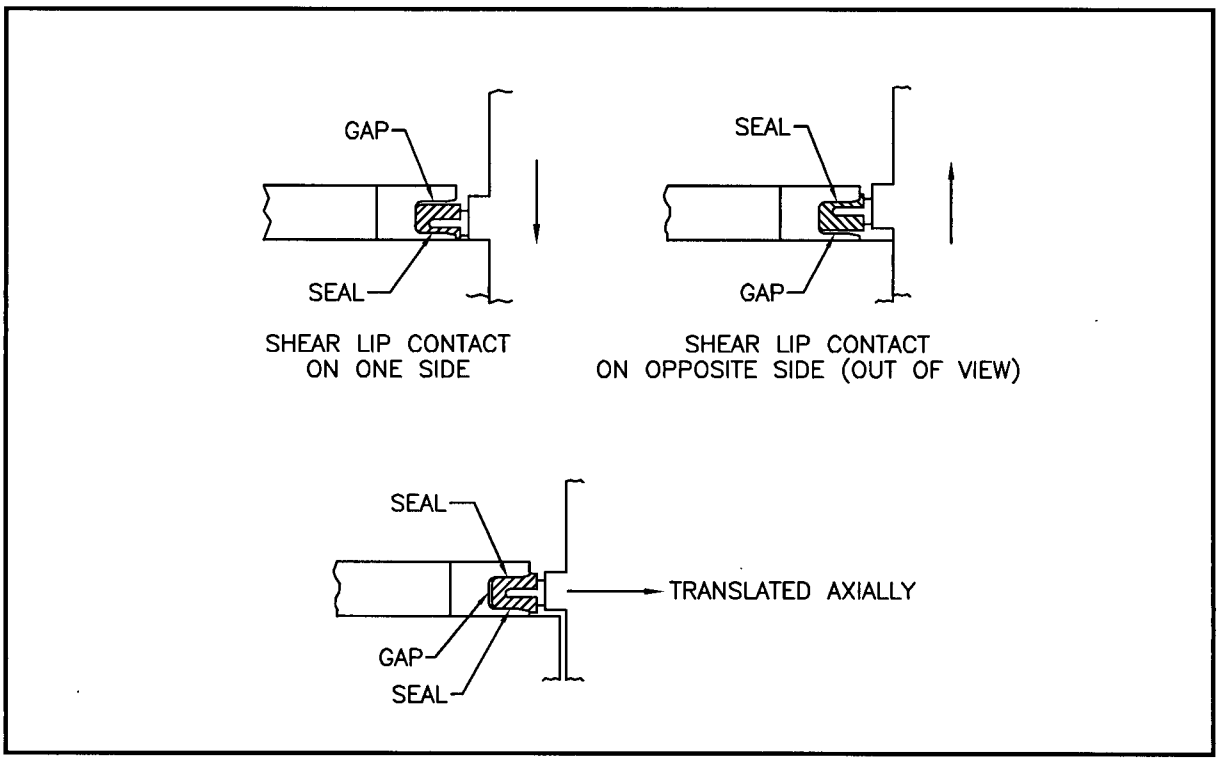

Figure 2.12.5-2 – Debris Shield with Bounding Displacements

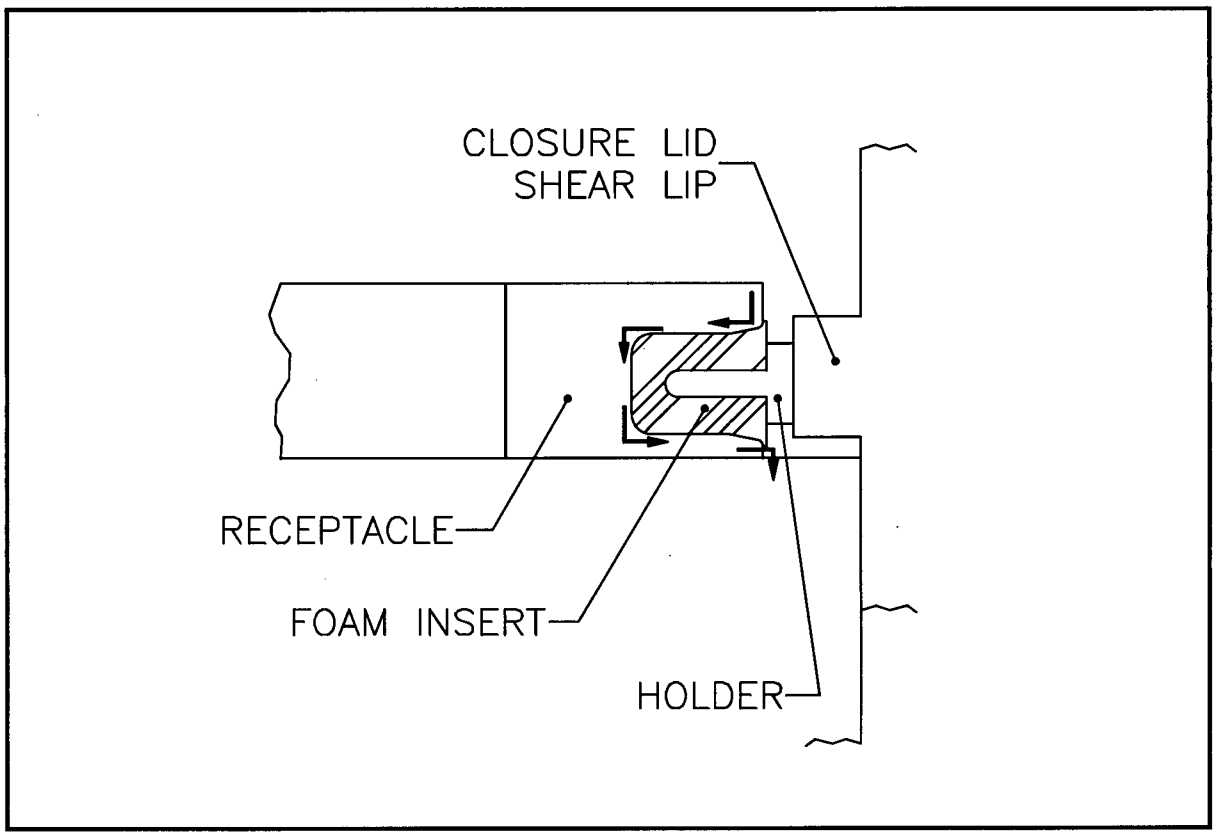

Figure 2.12.5-3 – Debris Shield Showing Labyrinth Configuration

2.12.5.5 Finite Element End Drop Analysis

In the vertical, lid-down HAC free drop orientation, the closure lid is loaded as a membrane by its own weight and the weight of the payload. As the lid deflects under load, a small rotation of the lid flange occurs, resisted by the closure bolts and pivoting about the outside edge of the flange. The containment O-ring seal, located near the inner edge of the flange, briefly separates from the body flange (which remains essentially undeformed). A finite element model using LS-DYNA version LS970s was used to investigate the behavior of the lid and associated parts. The purpose of the investigation was to establish the maximum relative motion which will occur at the debris shield under the cold end drop impact. This data point serves as input to the design of the debris shield. Note, however, that the relative motion calculated in this section is bounded by the larger value calculated in Section 2.12.5.6, *Finite Element Side Drop Analysis*.

The LS-DYNA model was a fully dynamic, explicit formulation of the package vertical, lid-down impact event. The model was constructed in quarter-symmetry. The two planes of symmetry were the longitudinal vertical and horizontal center planes of the package. To simplify modeling and analysis, the length was limited to a total of 614 mm measured from the flange joint. This length included three complete sidewall V-stiffeners. Neglecting the structure above this point (i.e., towards the closed end of the CSA) was not significant since the only result taken from the output is the behavior at the closure, including deformation of the lid flange which might lead to a gap at the containment O-ring and motion at the debris shield. All of the necessary weight was included or otherwise accounted for as described below. Geometry plots of the model are shown in Figure 2.12.5-4 and Figure 2.12.5-5. Model dimensions conform to the drawings given in Appendix 1.3.1, *Packaging General Arrangement Drawings*, and are shown on Figure 2.12.5-6 and Figure 2.12.5-7. Modeled part thicknesses are included in Table 2.12.5-3. The shell elements were defined at the mid-thickness of the structural elements. This may result in small differences between modeled dimensions and actual dimensions. However, such differences are negligible and will not affect results.

The inner and outer sheets, the flange plates, and the V-stiffeners were modeled using four-node Belytschko-Tsay shell elements, with five integration points through the thickness. The tube located in the lid bolting flange which carries the bolt load between the outer and inner surfaces of the lid flange was modeled using the same elements. The bolts were modeled using 8-noded constant stress solid elements with Flanagan-Belytschko hourglass control. The outer end of the bolt was joined to the outer surface of the closure lid flange (the bolt head) and the inner end joined to the body flange at the bolting boss. The 70-mm diameter bolting boss connected the front and rear faces of the body flange, and was constructed using the same solid elements as the bolts. The annular region between the bolt outer diameter and the bolt tube in the closure lid was modeled as rigid, to avoid the creation of a relatively weak diaphragm that does not exist in the prototype. The resulting FEA model correctly models the CSA stiffness and permits a determination of the deformation of the lid flange under the applied impact loading. Stresses are not evaluated since this orientation was physically tested in the certification test program as discussed in Section 2.12.3, *Certification Test Results*, and since only a design input value for the debris shield is required.

The standard nominal preload of 222,000 N was modeled with a target bolt prestress of 314 MPa, whereas 307 MPa (2.2% lower) was actually obtained in the analysis. For the desired output of maximum lid flange deflection, the slightly lower bolt preload is conservative. An internal pressure

of 172 kPa was applied to the lid and sides of the CSA. To balance the pressure on the lid, equivalent forces were applied to the top edge of the CSA inner sheet.

With the exception of the energy-absorbing triangular prism on the bottom of the model, the overpack structures were not explicitly modeled. The weight of the closed end overpack is, however, included in the model. The weight of the overpack sides, cheeks, and overpack cover weight are not included since these items will be self-supporting against the impact surface. The weight of the closed end overpack was 2,860 kg. The weight of the CSA structure (not including the lid) was bounded by 6,390 kg. The weight of the lid was 1,900 kg. Material densities were adjusted to match these weights, as shown in Table 2.12.5-3. The weight of the maximum payload was 5,175 kg. The payload was applied to the lid using discrete mass elements, uniformly distributed over the inside of the lid surface.

The material property of all components except the bolts and bolt sleeves was a bilinear kinematic stress-strain curve which utilizes a tangent modulus obtained from:

$$E_{TAN} = \frac{(S_u - S_y)}{\left(\varepsilon_u - \frac{S_y}{E}\right)}$$

where S_u is the ultimate true stress, S_y is the yield true stress (obtained at a true strain of 0.0047), and ε_u is the ultimate true strain, found for -29 °C in Table 2.2-2 as 888.8 MPa, 528.8 MPa, and 0.2231, respectively. E is found from Table 2.2-1 as $19.8(10^4)$ MPa. Using this data, the tangent modulus E_{TAN} = 1,633 MPa. Bolts and bolt sleeves were assumed elastic, as confirmed by model output.

Vibration damping in the TRUPACT–III is significant, since a) the payload will typically consist of loose objects, b) the impact energy will be absorbed by the crush of polyurethane foam and the deformation of steel, and c) the closure lid is a bolted flange joint. In the model, an effective damping value of 9.3% was used, which is considered relatively low for conditions existing within the packaging.

The model was decelerated by the crush of material in the triangular prism shown in part (c) of Figure 2.12.5-5. The material was constructed of 8-noded solid *MAT_CRUSHABLE_FOAM elements that were undamped. This region simulated the triangular regions of 0.16 kg/dm^3 foam in the four corners of the overpack cover (adjacent to the octagonal recess). The foam material stress-strain curve consisted of a single plateau value which was adjusted until the target acceleration of 204g (equal to the impact measured in the identical full-scale free drop test LD2) was approximately achieved. The rigid body acceleration was measured using the body side walls (since they would have little vibrational response), and equaled 211.3g, thus slightly in excess of the target. The impact velocity was 13.29 m/s, consistent with a 9-m free drop.

The TRUPACT–III package is designed such that under end drop loading, the impact forces tend to support the closure lid, restricting its deformation. This is shown schematically in Figure 2.12.5-8(a), where contact would occur between (1) the impact limiter and the container lid, and (2) between the container lid and the container body. In this analysis, the impact absorbing triangular prism was connected directly to the CSA body flange, thus conservatively leaving the closure lid unsupported and maximizing lid deformation (and relative motion at the debris shield) under impact loads. This is shown schematically in Figure 2.12.5-8(b).

The transient maximum relative displacement at the containment O-ring was extracted in three locations: the center of the long side of the lid (maximum magnitude), the center of the short side, and at the corner. These and additional results are given in Table 2.12.5-4. A plot of the relative motion between the body flange and closure lid flange at the containment O-ring at the center of the long lid side is given in Figure 2.12.5-9.

As can be seen from the table, the transient dynamic motion at the containment O-ring was very small. Since the lid flange pivots about its outer edge, the motion at the debris shield is:

$$Z_{DS-End} = \frac{X_{P-DS}}{X_{P-CO}} Z_{CO} = 0.78 \text{ mm}$$

where the distance between the outer edge of the lid and the debris shield, $X_{P\text{-}DS} = 145$ mm, the distance between the outer edge of the lid and the containment O-ring, $X_{P\text{-}CO} = 110$ mm, and the maximum transient motion at the containment O-ring, $Z_{CO} = 0.59$ mm from Table 2.12.5-4. The value of 0.78 mm is the relative motion which must be accommodated by the debris shield during the vertical, lid-down, maximum-impact free drop. Note also that the maximum transient bolt stress, 465 MPa, is considerably less than the yield strength of ASTM A320, L43 bolting material from Table 2.2-4, justifying the elastic treatment of the bolts in the model.

Input and output files for all LS-DYNA analysis computer runs are included on a DVD attached to this appendix.

Table 2.12.5-3 – LS-DYNA Model Part Identification and Mass Listing

As Modeled Container Mass / Weight						[W_Trupact3_Results-0.xls]Model_Mass		
Part ID	Description / Structural Component		Modeled Thickness	Wt. / Load (1/4 Sym.) Mass	Pounds	Model Color	(x4) Full Structure	Actual
1	Ribs (Lid)	Lid	4 mm	61.58 kg	135.8 lb	Red	--	--
2	Inner Plate	Lid	12 mm	92.47 kg	203.9 lb	Blue	--	--
3	Outer Plate	Lid	12 mm	108.32 kg	238.9 lb	Green	--	--
4	Flange	Lid Flange	16 mm	113.39 kg	250.1 lb	Yellow	--	--
5	Flange (Inner Plate)	Lid Flange	20 mm	46.75 kg	103.1 lb	Brown	--	--
6	Impact Limiter (Lower)	--	n/a (1)	9.95 kg	21.9 lb	Red	--	--
7	Impact Limiter (Upper)	--	n/a (1)	28.98 kg	63.9 lb	Blue	--	--
8	Pipe	Lid Flange	10 mm	19.39 kg	42.8 lb	Green	--	--
9	Bolts	--	n/a (1)	9.09 kg	20.0 lb	Yellow	--	--
10	Container Flange (Face)	Container Flange	20 mm	39.17 kg	86.4 lb	Lt. Brown	--	--
11	Container Flange (Backside)	Container Flange	10 mm	19.59 kg	43.2 lb	Red	--	--
12	Side Walls	Container	8 mm	2,071 kg	4,568.0 lb	Light Blue	--	--
13	Side Wall Ribs	Container	4 mm	66.23 kg	146.1 lb	Green	--	--
14	Rigid (Bolt Heads)	Lid Flange	n/a (2)	5.06 kg	11.2 lb	Yellow	--	--
15	Bar (Threaded Inserts)	--	n/a (1)	47.32 kg	104.4 lb	Tan	--	--
16	Container Flange (Sides)	Container Flange	15 mm	68.45 kg	151.0 lb	Purple	--	--
17	Ground	--	n/a	n/a	n/a	Orange	--	--
Subtotals								
A.	Lid (complete), Parts 1, 2, 3, 4, 5, 8, 9, & 14			456 kg	1,006 lb	--	1,824 kg	1,900 kg
B.	Container (w/o Lid), Parts 10, 11, 12, 13, 15, & 16			2,312 kg	5,099 lb	--	9,248 kg	9,250 kg
C.	Total Container (Parts 1 - 5 & 8 - 17)			2,768 kg	6,105 lb	--	11,072 kg	11,150 kg
Contents (Lumped/Discrete Masses)								
D.	SAR Payload			1293.9 kg	2,853 lb	--	5,176 kg	5,175 kg
E.	CTU Payload			1686.7 kg	3,720 lb	--	6,747 kg	6,745 kg
Package + Payload (1/4 Symmetry Model)								
F.	Standard (STD) Payload: (C + D)			4,062 kg	8,958 lb	--	16,248 kg	--
G.	CTU Payload (C + E)			4,455 kg	9,824 lb	--	17,819 kg	--
Notes:								
1.	Thickness not applicable, modeled with solid elements.							
2.	Modeled as rigid.							
3.	Masses in this table are from the summaries included in the LS-DYNA output files (NLS_CTU_314MPa_1.out)							

Table 2.12.5-4 – End Drop Transient Maximum Results

Location	Value
At containment O-ring:	
Center of long lid side[1]	0.59 mm
Center of short lid side[1]	0.35 mm
Corner of lid[1]	0.06 mm
Center of lid[2]	4.83 mm
Maximum closure bolt stress	465 MPa

Notes:

1. Relative displacement between CSA body flange and closure lid flange.
2. Relative displacement between CSA body flange and geometric center of lid.

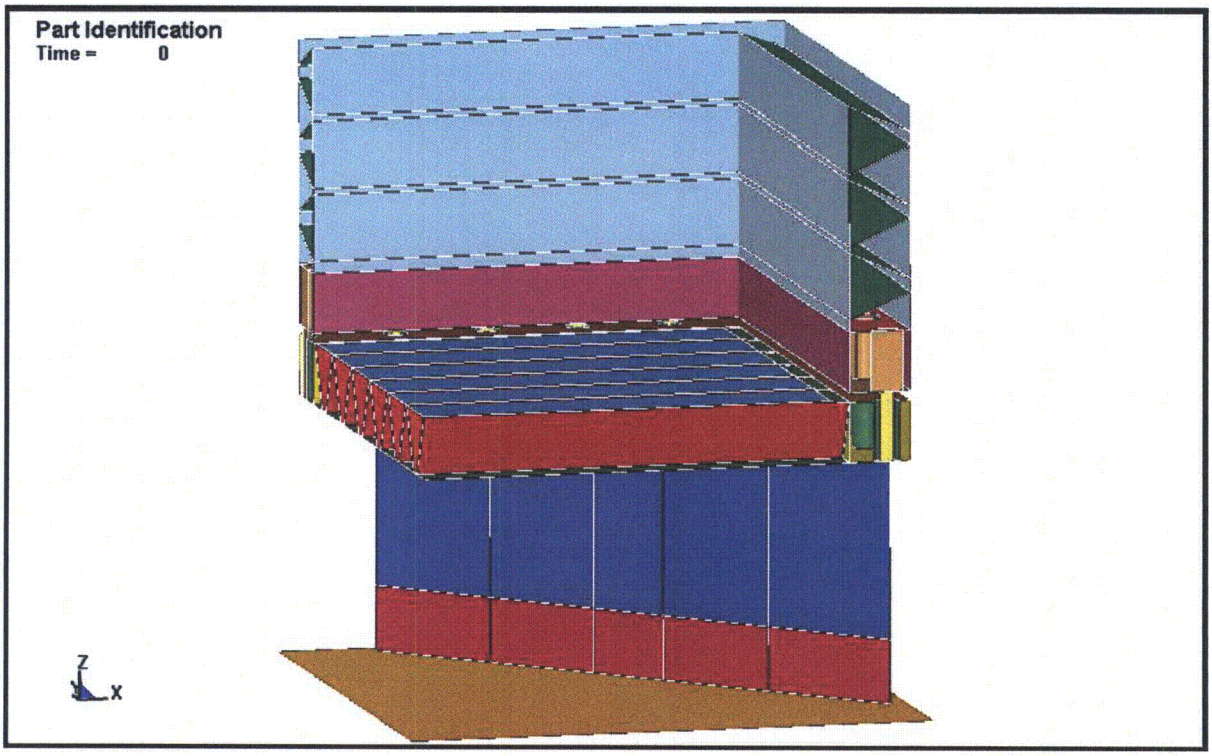

Figure 2.12.5-4 – LS-DYNA End Drop Model

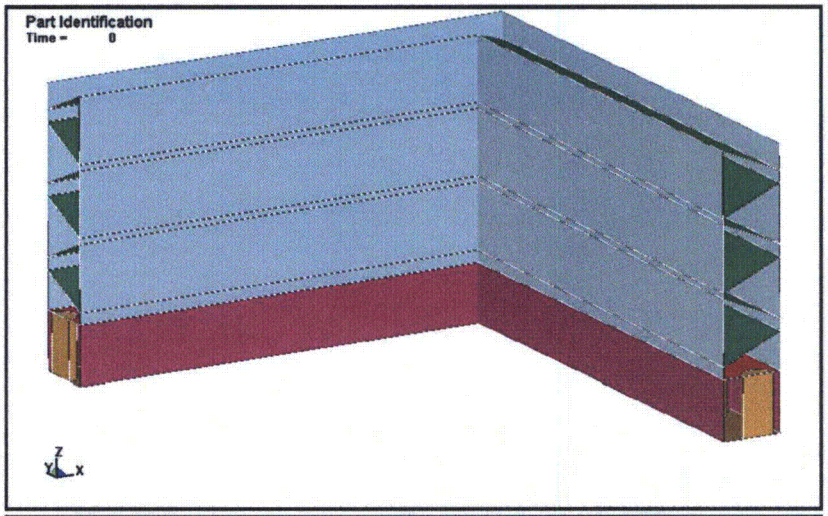

(A) Container Side Wall
(Parts 10, 11, 12, 13, 15, & 16)

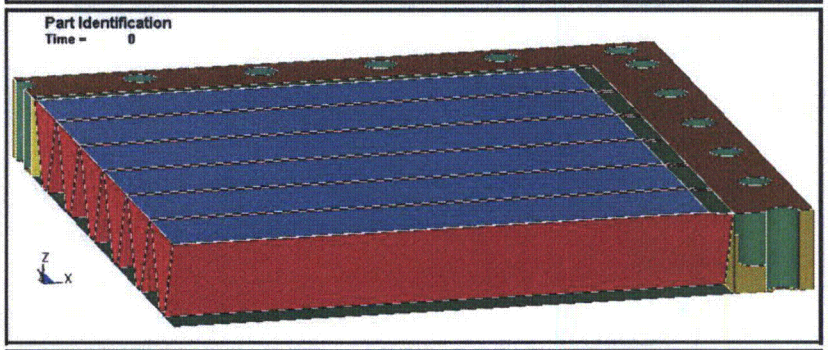

(B) Container Lid
(Parts 1,2,3,4,5,8, & 14)
(Bolts (part 9) not shown)

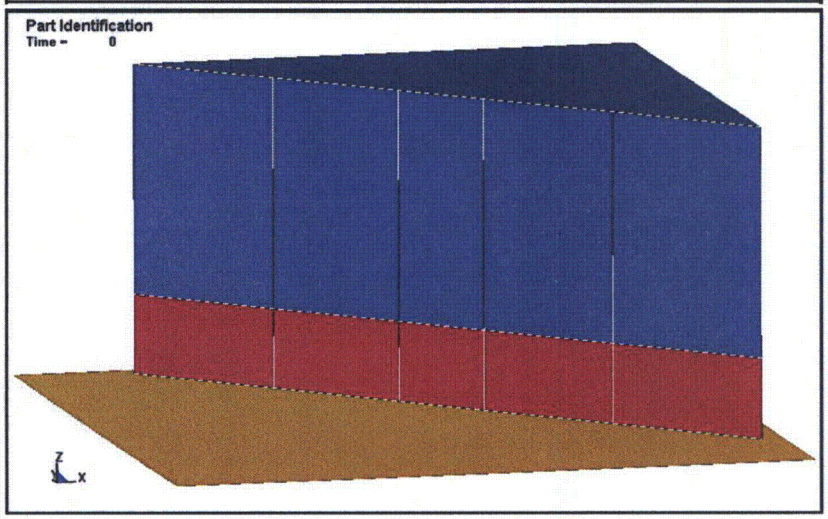

(C) Impact Limiters & Ground
(Parts 6, 7, & 17)

Figure 2.12.5-5 – LS-DYNA Model Components

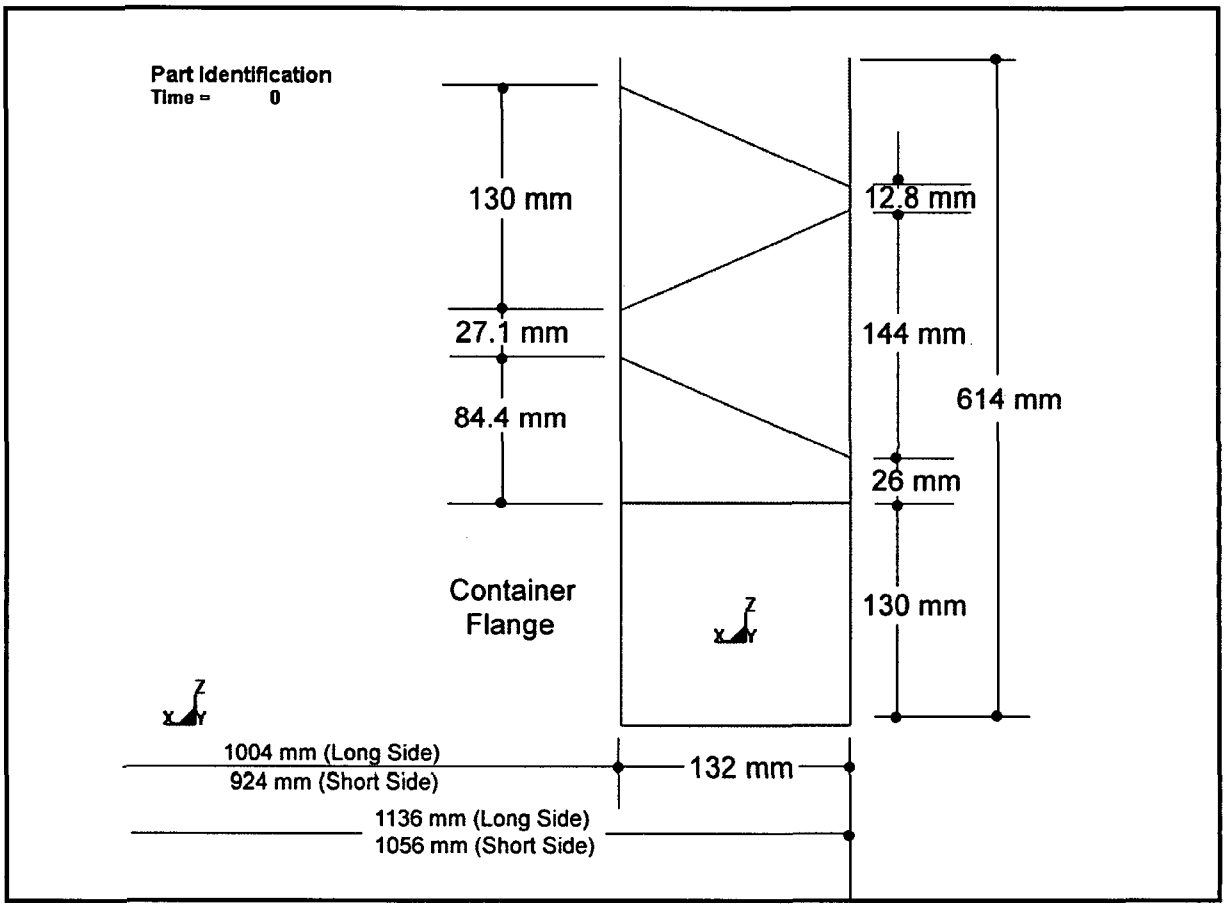

Figure 2.12.5-6 – LS-DYNA Model - Side View of Container with Modeled Dimensions

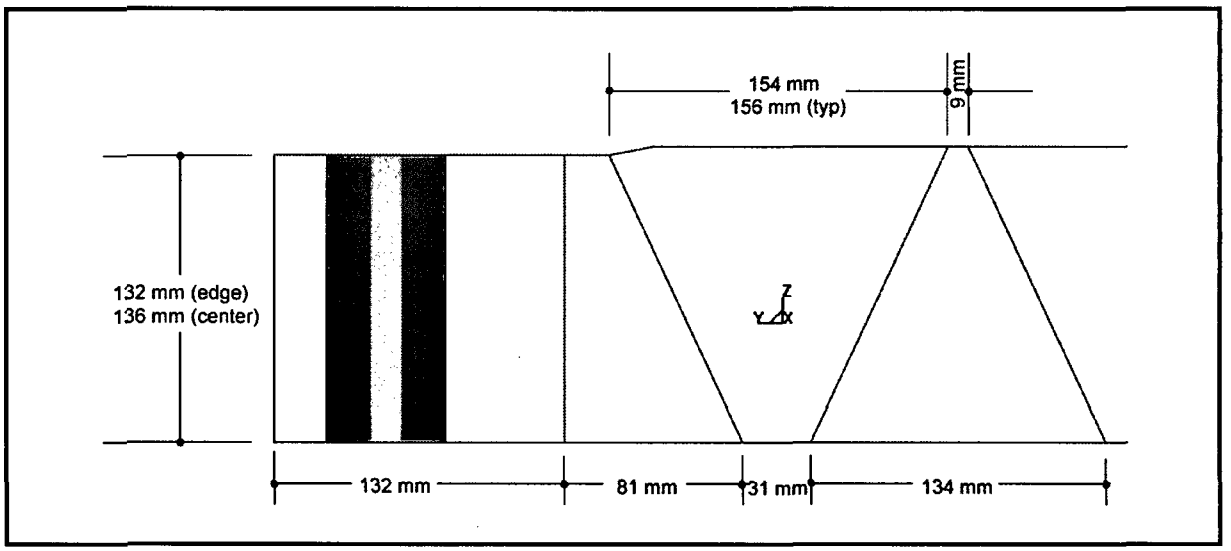

Figure 2.12.5-7 – LS-DYNA Model – Section Through Lid With Modeled Dimensions

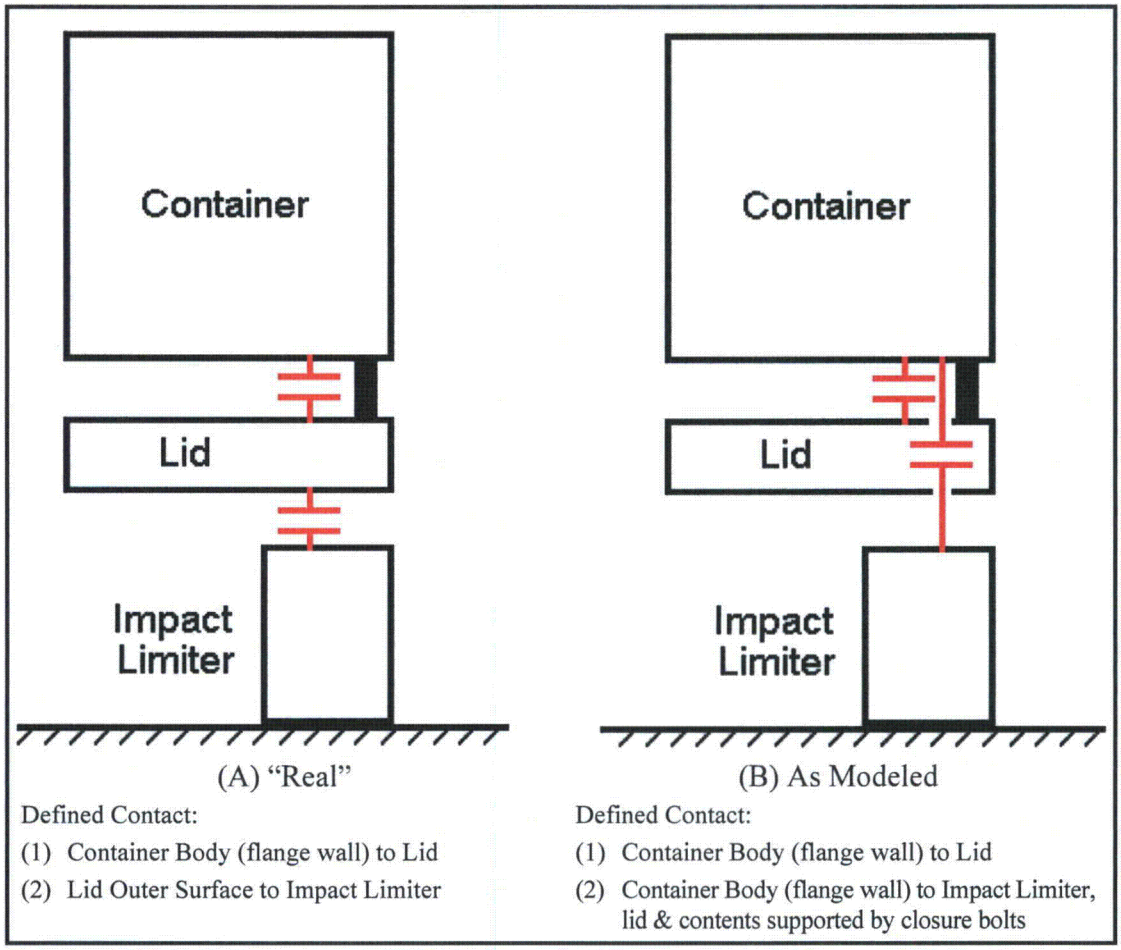

Figure 2.12.5-8 – Contact Definitions

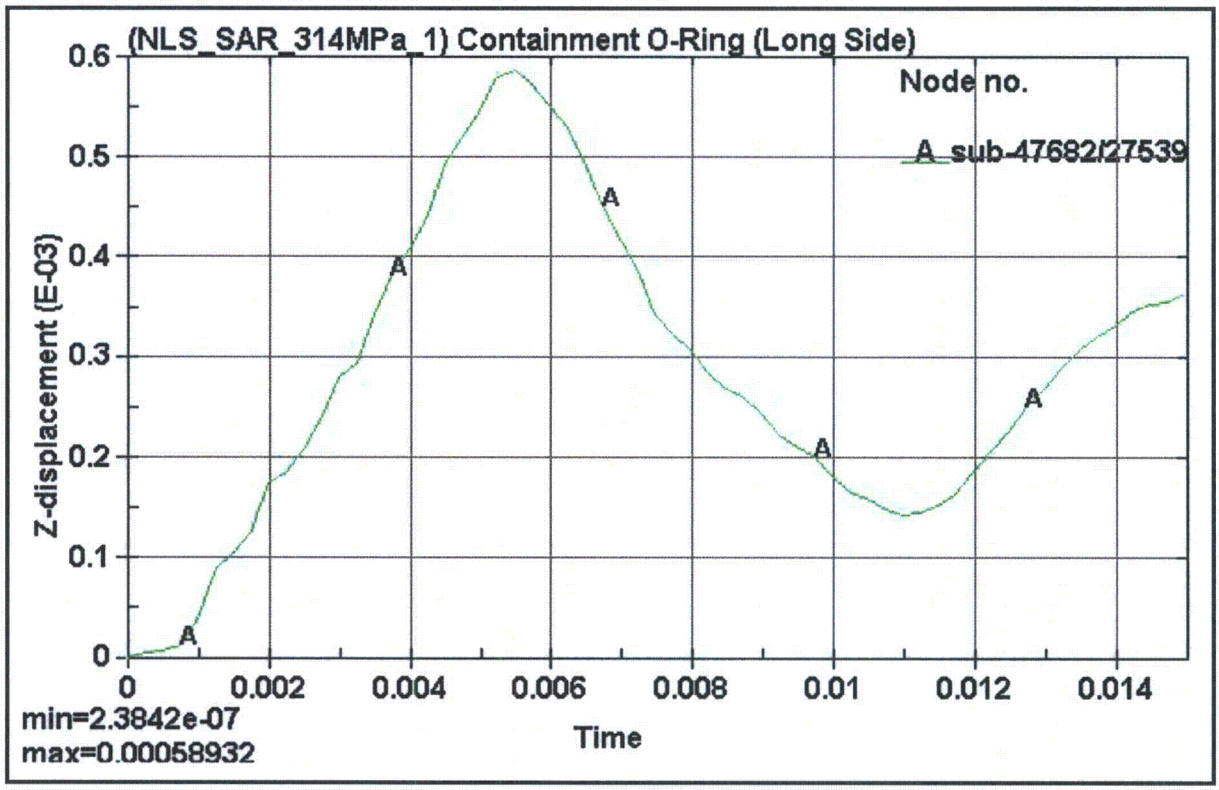

Figure 2.12.5-9 – Transient Maximum Relative Displacement at the Containment O-ring

2.12.5.6 Finite Element Side Drop Analysis

In the horizontal, side-down HAC free drop orientation, the CSA sidewall is loaded as a membrane by its own weight and the weight of the payload. As the sidewall deflects under load, a small rotation of the body flange occurs relative to the closure lid. Note that this side orientation is the inverse of the vertical, lid-down case, in which the closure lid flange rotated relative to an essentially undeformed body flange (see Section 2.12.5.5, *Finite Element End Drop Analysis*). Here, the body flange rotates relative to an essentially undeformed closure lid flange. In both cases, the pivot point of contact between the two flanges is at the outside edge of the flanges. Similar to the end drop case, the containment O-ring seal, located in the lid near the inner edge of the flange, briefly separates from the body flange. A fully elastic, quasi-static finite element model using ANSYS® Version 8.0 was used to evaluate the body flange rotation. The purpose of the analysis was to establish the maximum relative motion which will occur at the debris shield under the cold side drop impact. This data point serves as input to the design of the debris shield.

The body flange rotation was determined using a half symmetry model of the CSA as shown in Figure 2.12.5-9 and Figure 2.12.5-10. The closure lid was not modeled. Since the presence of the lid, attached by the closure bolts, would have the effect of reducing body flange rotation, its absence was conservative. The model used a combination of shell and beam elements to approximate the CSA wall stiffness. The walls of the model used shell elements having a thickness which gave the same bending stiffness as the CSA inner and outer sheets. The model walls were placed on the CSA wall centerplane locations. The stiffness of the V-stiffeners was added to the model by means of beam elements having the bending stiffness of a V-stiffener, placed at the stiffener locations in the walls. The body flange was also modeled as shell elements based on the calculated bending stiffness of the actual body flange. The resulting FEA model correctly models the CSA stiffness and permits a determination of the deformation of the body flange under the applied impact loading. Stresses are not evaluated since this orientation was physically tested in the certification test program as discussed in Section 2.12.3, *Certification Test Results*, and since only a design input value for the debris shield is required. The use of an elastic model is justified based on the results of the testing, which showed no inelastic behavior of the side wall (see Section 2.12.3.8.2, *CTU Measurements*.) The stiffness of the debris shield and guide bars was conservatively neglected in the model, but their weight was included.

The CSA wall, flange, and V-stiffener stiffness and equivalent element properties were calculated as follows. First, the wall bending moment of inertia was calculated for one V-stiffener span including the V-stiffener. A second calculation of the moment of inertia was made, excluding the V-stiffener. The difference between the two results was the moment of inertia of the V-stiffener itself. A set of calculations was performed for both the side and back walls, since the V-stiffener design and pitch of the stiffeners is slightly different. The equivalent thickness of the model wall shell elements is found by equating the moment of inertia of a solid plate over the V-stiffener pitch width to the moment of inertia of the wall excluding the V-stiffener, or:

$$\frac{b \times t_{eq}^3}{12} = I_{ev}$$

where b is the V-stiffener pitch, I_{ev} is the moment of inertia excluding the V-stiffener, and t_{eq} is the shell element thickness. Solving for t_{eq}:

$$t_{eq} = \sqrt[3]{\frac{I_{ev} \times 12}{b}}$$

The calculations for the side wall, back wall, and flange are summarized in Table 2.12.5-5, using information in Figure 2.12.5-11, Figure 2.12.5-12, and Figure 2.12.5-13.

The model has symmetry boundary conditions in the y-z plane. The three edges nearest the ground (back, side, and flange) are restrained in the vertical y-direction. Full support of the front flange at the open end is conservative for the purposes of determining flange rotation, since any motion of the flange perpendicular to the ground would reduce the amount of rotation. The back lower edge is also restrained in the axial z-direction for model stability. The model impact surface (CSA large external side) is supported by a 1.0 MPa pressure to simulate the partial support of the 0.10 kg/dm^3 polyurethane foam underneath. From Table 2.2-5, the 0.10 kg/dm^3 foam has an initial crush strength of approximately 1.0 MPa.

The weight of the CSA of 6,786 kg (3,393 kg in half symmetry) is evenly distributed over the model elements[2]. A pseudo-density is calculated based on the weight and the model volume, and which is then acted on by the impact acceleration. The weight of the payload of 5,175 kg (2,588 kg in half symmetry) is evenly distributed over the elements on the lower side wall, and is additive to the self-weight of the lower side wall. The weight of the overpack skin and puncture-resistant plate which are supported by the upper side wall is added to the model upper side wall elements. (The weight of the 0.10 kg/dm^3 polyurethane foam and of the balsa wood on the top wall is negligible.) The specific weight added to the elements (386 kg) is based on the model wall length and width dimensions, the steel plate thicknesses of 10mm and 6mm, and a density of 7.89 kg/dm^3.

The model is loaded with a 172 kPa internal pressure and an acceleration of 407g, as measured in the HAC cold flat side drop (LD3). The model is elastic, using a modulus of elasticity at -29 °C of 19.8(10^4) MPa from Table 2.2-1 and a Poisson's ratio of 0.3.

The resulting maximum rotation of the body flange was equal to 0.02003 radians, located at the center of the lower body flange as shown in Figure 2.12.5-14. The maximum deflection of the side wall was 16.4 mm (shown in Figure 2.12.5-15 as 0.647 inches). Since the width of the body flange is 140 mm, and the distance from the inner surface of the CSA and the center of the debris shield is 13 mm, the transient motion which must be accommodated by the debris shield in a maximum-impact side drop is:

$$Z_{DS-Side} = 0.02003 \times (140 + 13) = 3 \text{ mm}$$

For establishment of the debris shield design criteria, $Z_{DS\text{-}Side}$ governs over the value $Z_{DS\text{-}End}$ = 0.78 mm calculated above in Section 2.12.5.5, *Finite Element End Drop Analysis*.

Input and output files for this computer run are included on a DVD attached to this appendix.

[2] The CSA weight used in this analysis is 396 kg greater than the weight of 6,390 kg used in the end drop analysis (see Section 2.12.5.5, *Finite Element End Drop Analysis*). This difference is equal to the weight of the debris shield and guide bars. That weight was not included in the end drop analysis because it would not affect the closure lid behavior, but was included here because it would affect side wall behavior.

Table 2.12.5-5 – Shell Element Calculation Results

	Side Wall	Back Wall	Body Flange
V- stiffener pitch or width, b, mm	164	165	145
I_{wv}, mm^4	$13.186(10^6)$	$13.290(10^6)$	
I_{ev}, mm^4	$11.451(10^6)$	$11.521(10^6)$	
I_{vr}, mm^4	$1.735(10^6)$	$1.769(10^6)$	
I_{Flange}, mm^4			$20.412(10^6)$
t_{eq}, mm	94.3	94.3	119.1

Note: The smaller side wall V- stiffener moment of inertia, $I_{vr} = 1.735(10^6)$ mm^4, is conservatively used for all V- stiffeners.

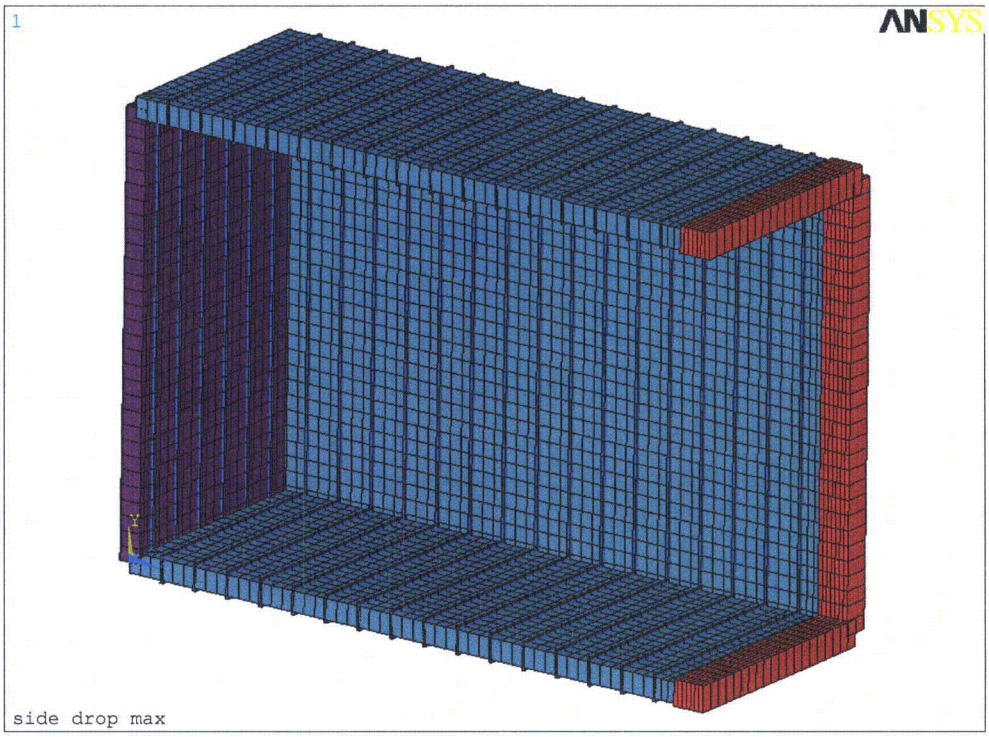

Figure 2.12.5-9 – Half Symmetry Model of the CSA Body Showing Thickness

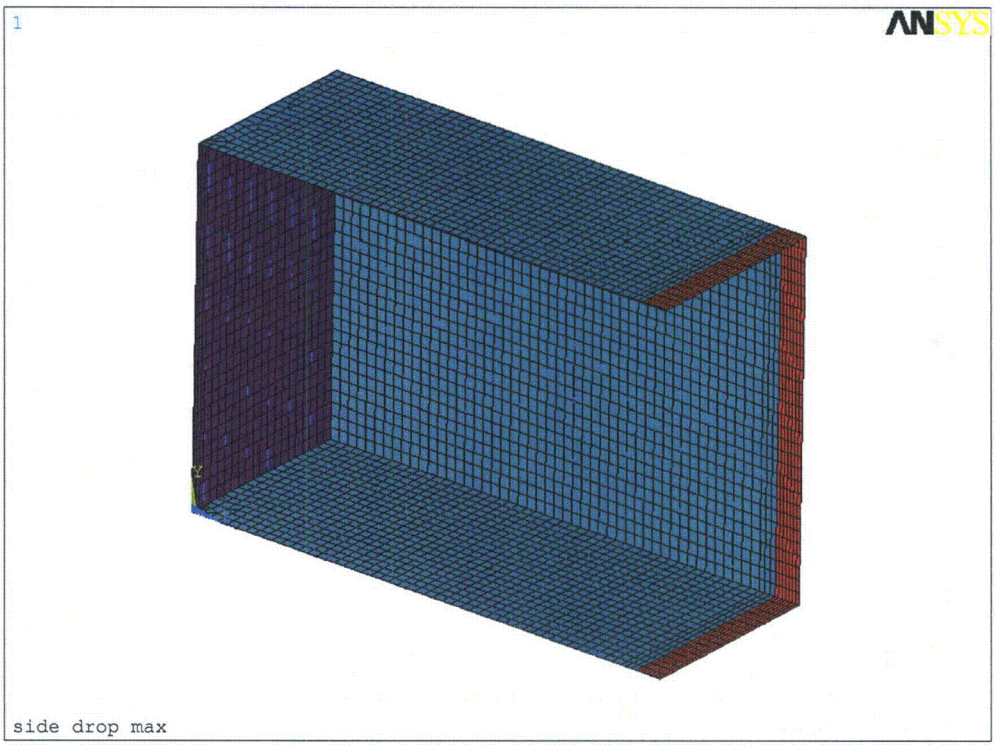

Figure 2.12.5-10 – Model of the CSA Body, Element Plot

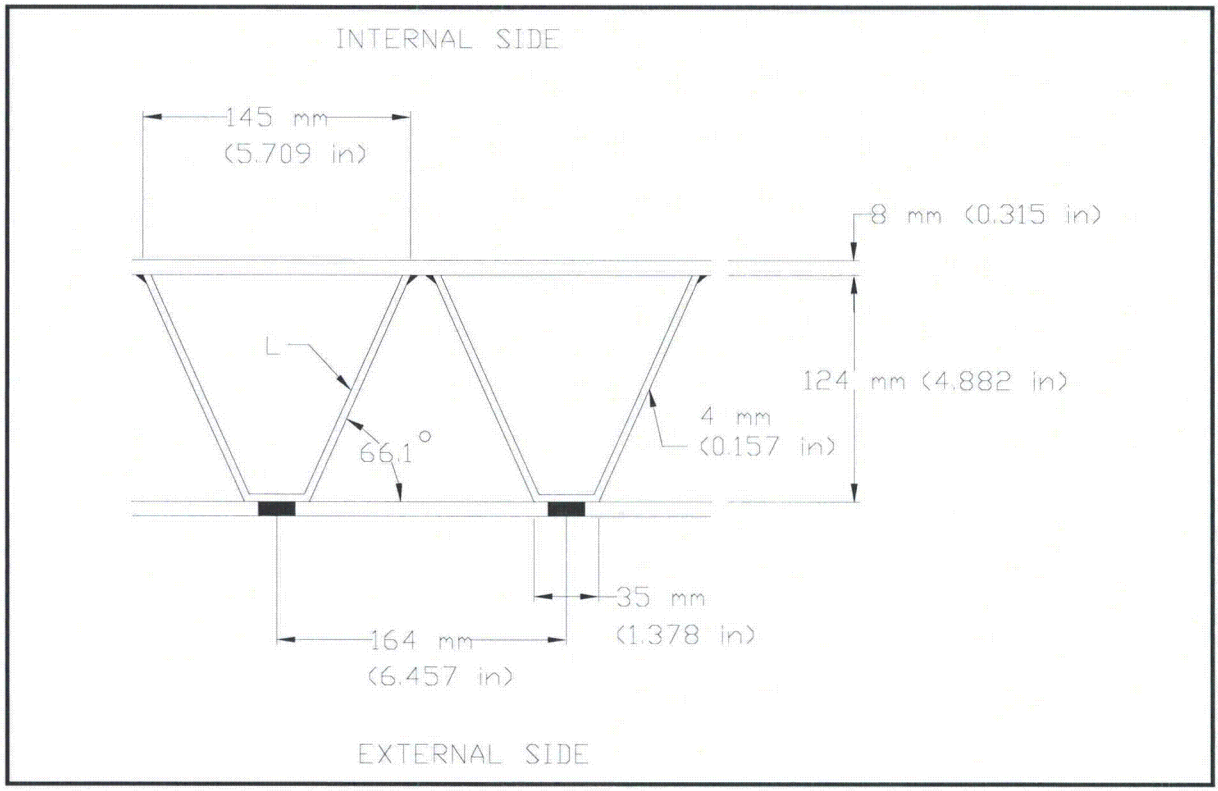

Figure 2.12.5-11 – Side Wall Cross-section Details

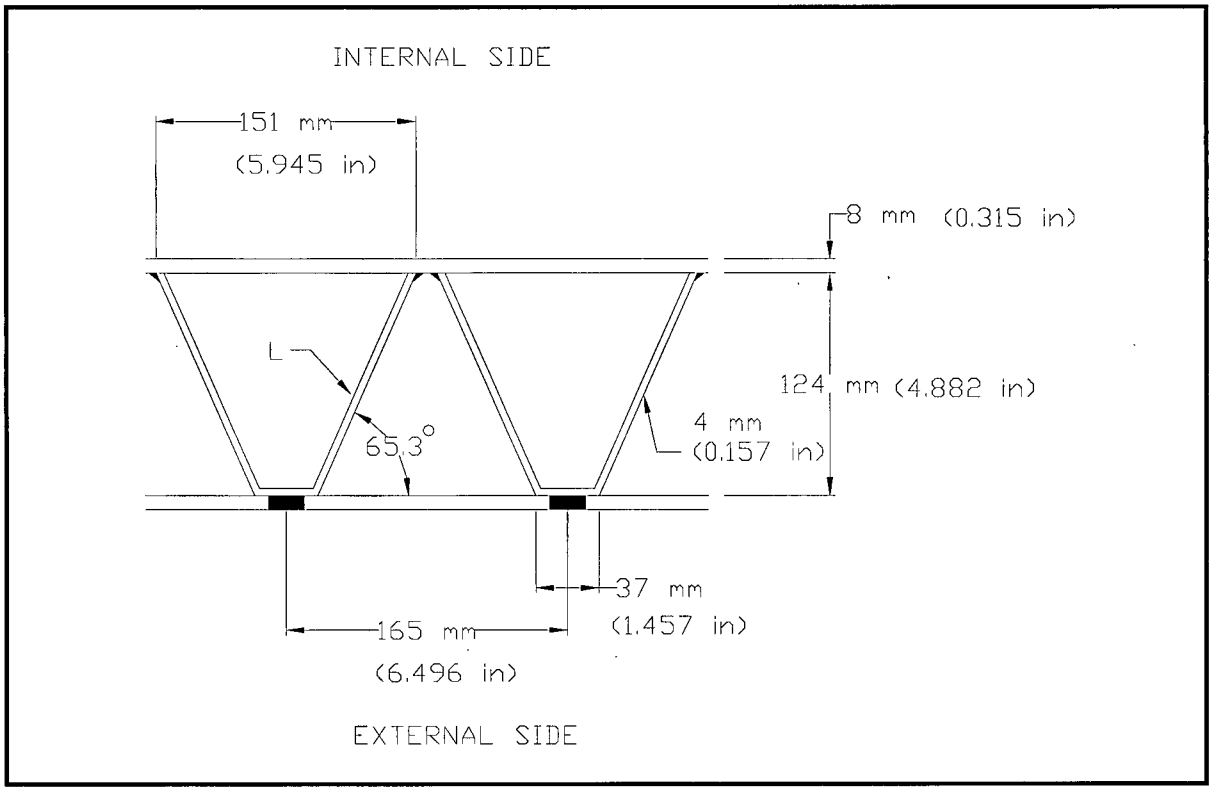

Figure 2.12.5-12 – Back Wall Cross-section Details

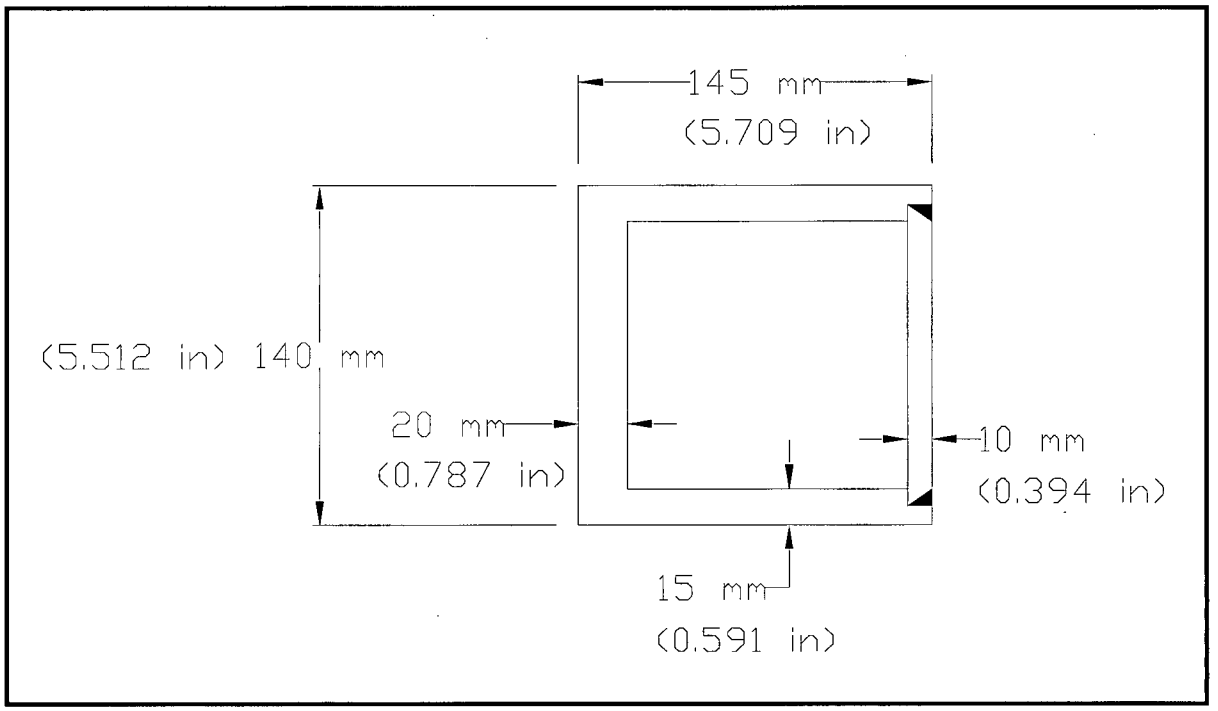

Figure 2.12.5-13 – Flange Cross-section Details

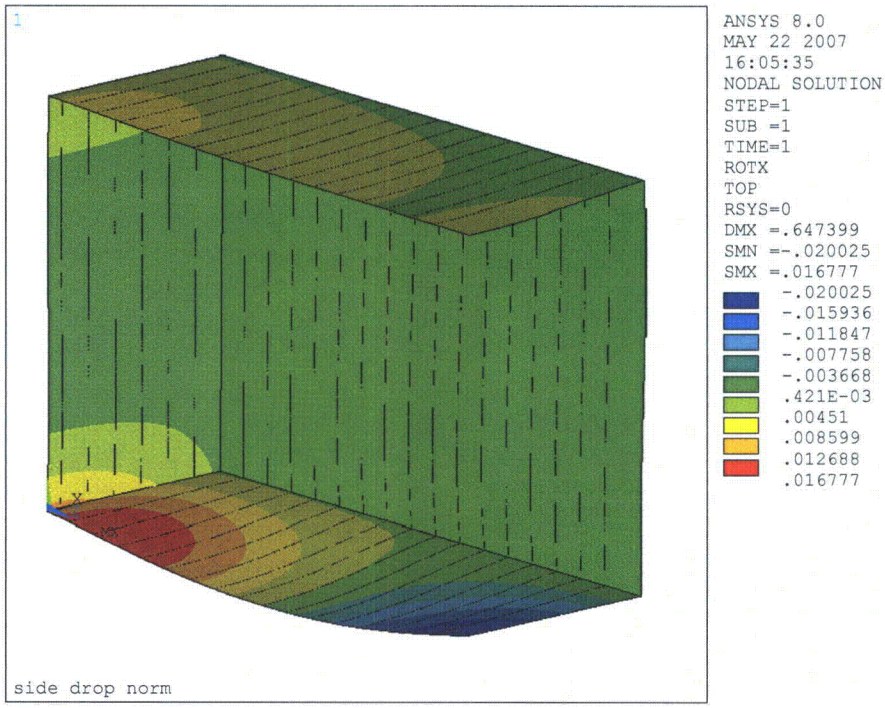

Figure 2.12.5-14 –Flange Rotation (ROTX, Radians)

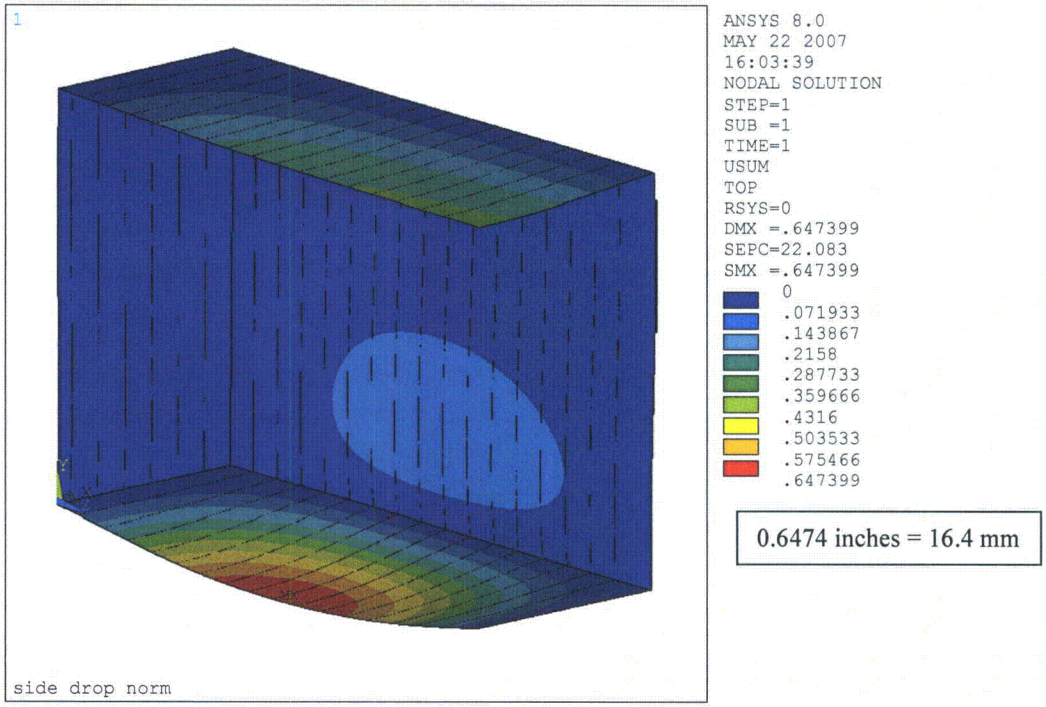

Figure 2.12.5-15 – Maximum Side Wall Displacement, Inches/mm

2.12.5.7 Finite Element Payload Interaction Analysis

The presence of the debris shield on the inside surface of the CSA body flange creates the potential for permanent deformation of the flange sealing surface due to locally high loads being applied by the payload in the HAC free drop. The analysis presented in this section demonstrates that any permanent deformations of the sealing surfaces are negligible in the worst-case interaction between the payload and the CSA.

Due to the design and placement of the guide bars, the SLB2 payload container cannot become trapped behind the debris shield, and consequently, cannot apply any axial impact loads to the debris shield. The only direction from which significant loads are applied to the debris shield and guide bars is from the side (i.e., perpendicular to the plane of the CSA wall). This analysis evaluates the response of the debris shield, guide bars, and body flange when impacted by a maximum-weight SLB2 in the cold side drop impact. Note that this analysis is focused on the potential for containment O-ring compression reduction as a result of the concentrated forces on the guide bars and debris shield. By inspection of Figure 2.12.5-1, a compressive load on the debris shield could, at most, deform the receptacle 'c-section' toward a closed position. This would tend to compress the debris shield foam rubber insert, which would not inhibit the function of the debris shield. Therefore, the function of the debris shield cannot be affected by payload interactions.

There are three guide bars on each TRUPACT–III side wall, located to coincide with the bumpers on the SLB2 container. In a side drop, the bumpers will contact the guide bars. Since the SLB2 wall section is relatively thin, it will deform under impact, and some load could be carried by the containment wall in between the guide bars. In this analysis, however, it is assumed that all of the SLB2 inertia load is carried only by the bars, thus conservatively concentrating the load. The maximum weight of a SLB2 is 4,763 kg. Since the measured impact in the cold, flat side impact in the certification test LD3 was 407g, the maximum impact load is:

$$F = 4{,}763 \times 407 \times 9.81 = 19.017\left(10^6\right)\text{N}$$

Since each bumper is 2,743.2 mm long and 38.1 mm wide (108 inches by 1.5 inches), the uniform pressure on the guide bars is:

$$P = \frac{F}{2{,}743.2 \times 38.1 \times 3} = 60.651\ \text{MPa}$$

Since the bumpers are tubes made of mild carbon steel having a wall thickness of only 1.5 mm (0.06 inches), they will deform under loading, and the uniform load distribution is justified. Conservatively, the analysis assumed a pressure loading of 68.95 MPa (10,000 psi).

The finite element model was built using ANSYS® Version 8.0 and is shown in Figure 2.12.5-16 and Figure 2.12.5-17. The model is built with symmetry: one longitudinal edge is at the center of a guide bar, and the opposite longitudinal edge coincides with the center of the span between two adjacent guide bars. Since the guide bars are separated by 17 inches, the model is 8.5 inches wide. The flange face is included at one end of the model, and the other end extends towards the rear of the package by the distance of one full V-stiffener beyond the rear edge of the flange. Note that the minimum flange face thickness of 20 mm was conservatively used (other dimensions are nominal). Conservatively, the stiff bolting boss located in the flange is omitted from the model. Since the closure lid does not affect the loading of the flange by the payload,

the closure lid is also omitted. However, a rigid lid closure flange is assumed in calculating the maximum reduction in containment O-ring compression as described below.

The model uses solid 3-D elements in conjunction with 3-D point to surface contact elements. The guide bar is fully separate from the flange, and conservatively not attached to the flange, inner sheet, or debris shield. It is held in place only by the symmetry constraints and the applied load. In practice, the guide bar is attached by fillet welds to the CSA side wall, but the successful omission of these welds in the model demonstrates that they are not structural in nature and do not need to be subject to stress limits. In a similar manner, the debris shield receptacle is not attached to the flange, except for two coupled nodes at the center span symmetry edge. These couples help the model solve while not interfering with the action of the debris shield at the loaded area of interest. Therefore, the debris shield welds are also non-structural. The V-stiffener is coupled to the inner sheet at both sides of the "v" to account for the fillet welds, while the base of the stiffener is coupled at the center of the flat to the outer sheet to account for the plug welds.

Both symmetry edges of the model have symmetry boundary conditions. The side of the model furthest from the flange face has constraints in the x-direction, which models the connection of the guide bar, inner, and outer sheets to the rest of the CSA walls. The flange face is free. The model is supported vertically in the y-direction. Two versions of support are used with different types of vertical support. Version A supports the model across the entire bottom surface including the flange and entire CSA outer sheet. Version B supports the model across the CSA outer sheet and flange back wall, but the bottom surface of the flange, including the bottom edge of the flange face, is free. The purpose of the two runs is to examine the difference between the two extreme cases of full flange support and no flange support. Free drop testing indicates that the flange is reasonably well supported in a side drop, but both extremes are conservatively investigated.

The 68.95 MPa pressure calculated above was applied to the top of the debris shield and guide bar. The pressure begins at the solid part of the debris shield and runs the entire length of the guide bar. Pressure is not applied above the open C-section of the debris shield since an insignificant load could be transferred down into the flange from this area due to plastic deformation of the C-section upper leg. (As discussed above, any such deformation would be in the direction to close the C-section, and would therefore not inhibit the function of the debris shield.) The width of the pressure application is 19 mm, which is equal to one half-symmetry width of the bumper of the SLB2. The loading is concentrated on the guide bars and on the debris shield in order to determine whether deleterious permanent plastic deformations of the CSA body flange could result.

Nonlinear true stress-strain properties for ASTM Type 304L (guide bars) and UNS S31803 stainless steel (debris shield and all other CSA components) is taken from Table 2.2-2 for a temperature of -29 °C. The cold temperature corresponds to the maximum impact loading. That is the most critical condition, since with increasing temperature, the impact loading would fall faster than would the steel properties due to the stronger temperature dependence of polyurethane foam.

Allowable stress limits are developed using Table 2.1-1. Since the output stresses are in the form of true stress, the allowables must also have the same basis. For UNS S31803 steel, the last data point in Table 2.2-2 for -29 °C corresponds to the minimum elongation (minimum ultimate strain) of 25%. Therefore, the true ultimate stress for UNS S31803 is 888.8 MPa. For ASTM Type 304L stainless steel, the linearly extrapolated engineering ultimate strength is 515.9 MPa, using values at 38 °C and 93 °C from Table 2.2-3. The minimum elongation (minimum ultimate strain) for Type 304L is 40%. The engineering ultimate strength was converted to true ultimate strength using:

$$S_{u-true} = S_{u-eng}(1 + e_{eng}) = 722.3 \text{ MPa}$$

where S_{u-eng} = 515.9 MPa and e_{eng} = 0.40. From Table 2.1-1, the maximum primary stress intensity is limited to $0.9S_u$. (The membrane allowable stress is applicable primarily to pressure vessels and is not used here.) The allowable stresses therefore are:

	Stress Criteria	Allowable Stress
UNS S31803	0.9 × 888.8	799.9 MPa
ASTM Type 304L	0.9 × 722.3	650.1 MPa

The analysis was performed in two steps. First, the full quasi-static impact load was applied. From this run, maximum stresses and deflections were extracted, representing the transient maximum values during the impact event. A second load step was made with the load reduced to nearly zero (an approximately 1% load is required to maintain model stability since some parts are unconnected), representing the permanent deformation state of the components. These results were examined to find the maximum permanent variation in flatness of the body flange, measured between the most outwardly-deformed point anywhere on the flange (which serves to locate the flat closure lid flange surface) and the least outwardly-deformed point on a line which corresponds to the mating surface of the containment O-ring. This total difference is equal to the reduction in containment O-ring compression which would be expected to result from the worst-case interaction between the payload and the debris shield and guide bars. Note that this analysis does not purport to show the minimum state of O-ring compression under accident conditions. The leaktightness of the containment seal, in the absence of debris, was demonstrated by full-scale testing (see Section 2.12.3.8.1, *Leakage Rate Tests*). Instead, this analysis evaluates only the differential effect on O-ring compression of the interaction with the payload under HAC impact. It demonstrates that the presence of the debris shield and guide bars does not affect the leaktight capability of the TRUPACT–III.

Since the width across the lid from center-to-center of the containment O-ring groove is 1,888 mm, and the width of the CSA opening is 1,840 mm, the location of the containment O-ring mating line on the body flange, measured from the inner edge of the body flange, is:

$$(1{,}888 - 1{,}840)/2 = 24 \text{ mm}$$

Deformations perpendicular to the body flange face are in the model x-direction; outward-bulging deformations are negative. The maximum reduction in compression of the containment O-ring is therefore found using:

[Greatest (–x) deformation of the body flange surface] *minus*

[Least (–x) deformation on a line 24 mm from flange top edge]

Results are shown in Table 2.12.5-6 for Version A (fully supported flange) and in Table 2.12.5-7 for Version B (unsupported flange). Plots of stress intensity for each component for Version A are provided in Figure 2.12.5-18 to Figure 2.12.5-22, and for Version B in Figure 2.12.5-25 to Figure 2.12.5-29. Plots of the body flange face deformation for Version A are provided in Figure 2.12.5-23 (under full transient load) and Figure 2.12.5-24 (unloaded, post-impact), and for Version B in Figure 2.12.5-30 (under full transient load) and Figure 2.12.5-31 (unloaded, post-impact).

As shown in Table 2.12.5-6 and Table 2.12.5-7, a positive margin of safety on maximum stress exists in both cases, having a minimum value of +0.23. It is also noteworthy that the stresses in the debris shield and the body flange are elastic in nature, based on the engineering yield strength of UNS S31803 stainless steel, given in Table 2.2-1 as 448 MPa at a conservative temperature of 38 °C. The flange components are here specified as the 20-mm thick flange front wall and the inner and outer, 15-mm thick flange plates. Only the guide bar and the inner CSA sheet behind the flange structure have stresses above the yield point (but below the nonlinear allowable stress), and the regions above yield are relatively small. This statement applies to both Version A and Version B.

Also shown in the tables is the maximum reduction of containment O-ring compression (column 4, lower half of table, labeled 'Net displacement, mm'). From Table 2.12.5-7 (Version B, unsupported flange), the reduction in the fully loaded transient condition was 0.07 mm, or only 0.58% in terms of the compression of the 12 mm diameter O-ring. In the unloaded, post-impact condition, the reduction was 0.0017 mm, which is equivalent to essentially no reduction in compression. These values are trivial with regard to the leaktight compression criteria determined in Section 2.12.2, *Elastomer O-ring Seal Performance Tests*.

Therefore, since the body flange stresses are elastic, and other nonlinear maximum stresses meet allowable stress criteria, and the maximum effect on O-ring compression is trivial, the interaction between the payload and the CSA is of no concern.

Input and output files for this computer run are included on a DVD attached to this appendix.

Table 2.12.5-6 – Version A (Fully Supported Flange)

Component	Maximum Stress Intensity, MPa	Allowable Stress, MPa	Margin of Safety
Debris Shield	311.2 *(elastic)*①	799.9	+1.57
Guide Bar	262.7	650.1	+1.47
Flange components	330.1 *(elastic)*①	799.9	+1.42
Inner and outer CSA sheets behind flange	471.2	799.9	+0.70
V-stiffener	650.2	799.9	+0.23
Loading Case	**Max overall displacement of flange face, mm**	**Min displacement of flange face at O-ring, mm**	**Net displacement, mm**
Full Transient Load	-0.06764	-0.00902	0.05862
Unloaded	-0.00115	-0.00061	0.00054

Notes:

1. Although the stress is elastic in this case, the inelastic stress criterion is applied for consistency with the rest of the model.

Table 2.12.5-7 – Version B (Unsupported Flange)

Component	Maximum Stress Intensity, MPa	Allowable Stress, MPa	Margin of Safety
Debris Shield	342.3① *(elastic)*②	799.9	+1.34
Guide Bar	261.2	650.1	+1.49
Flange components	381.3 *(elastic)*②	799.9	+1.10
Inner and outer CSA sheets behind flange	557.1	799.9	+0.44
V-stiffener	650.2	799.9	+0.23
Loading Case	**Max overall displacement of flange face, mm**	**Min displacement of flange face at O-ring, mm**	**Net displacement, mm**
Full Transient Load	-0.07206	-0.00153	0.07053
Unloaded	-0.00223	-0.00053	0.00170

Notes:

1. Coupled nodes for debris shield furthest from applied load are removed from the stress plot, since the local stresses at the coupled nodes are artificial.
2. Although the stress is elastic in this case, the inelastic stress criterion is applied for consistency with the rest of the model.

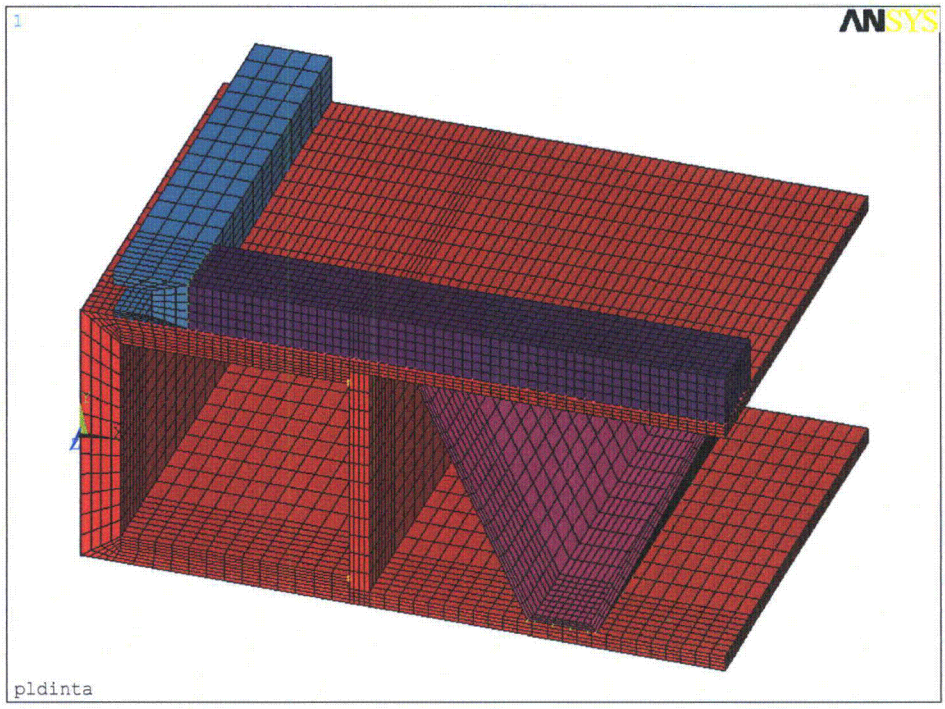

Figure 2.12.5-16 – Payload Interaction Model, Isometric Plot

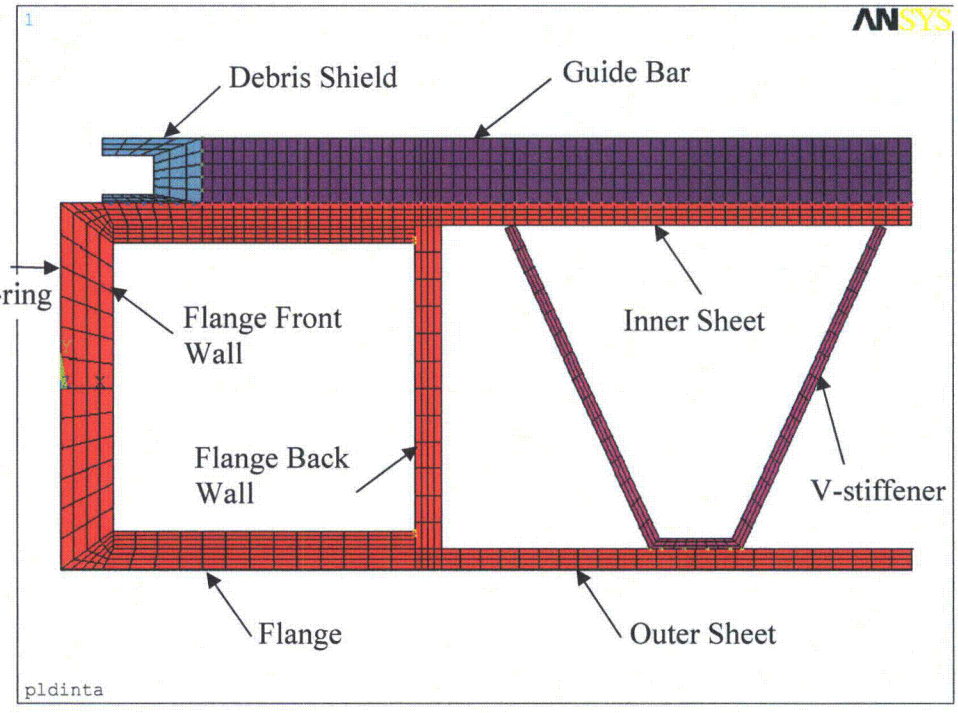

Figure 2.12.5-17 – Element Plot – Cross-section of Body Side Flange

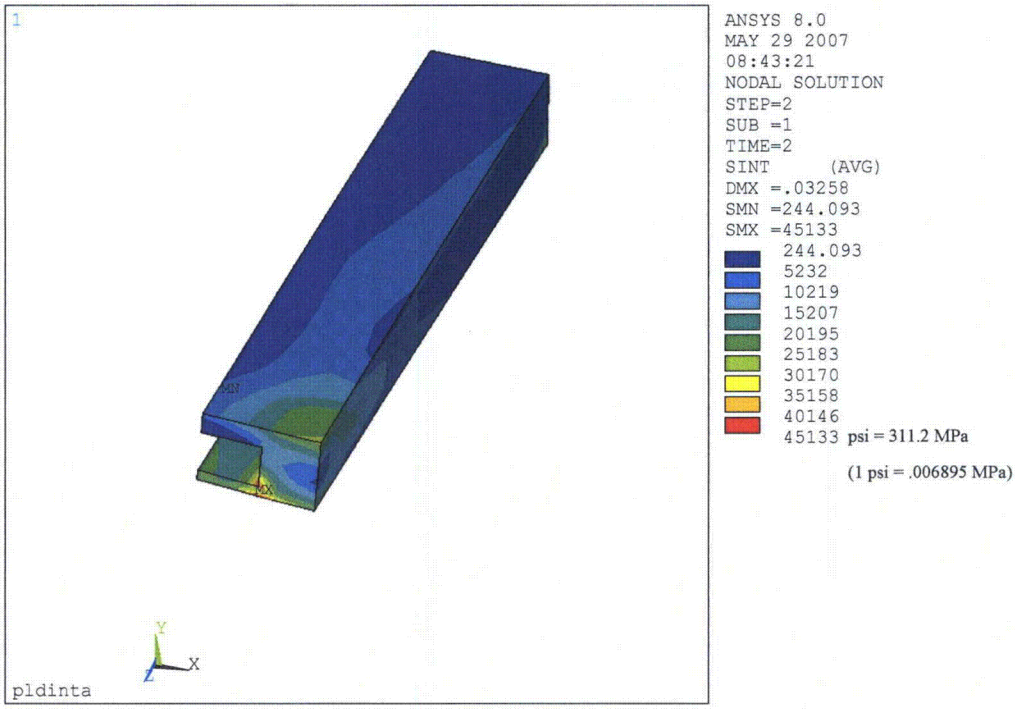

Figure 2.12.5-18 – Debris Shield Receptacle Stress Intensity, Version A

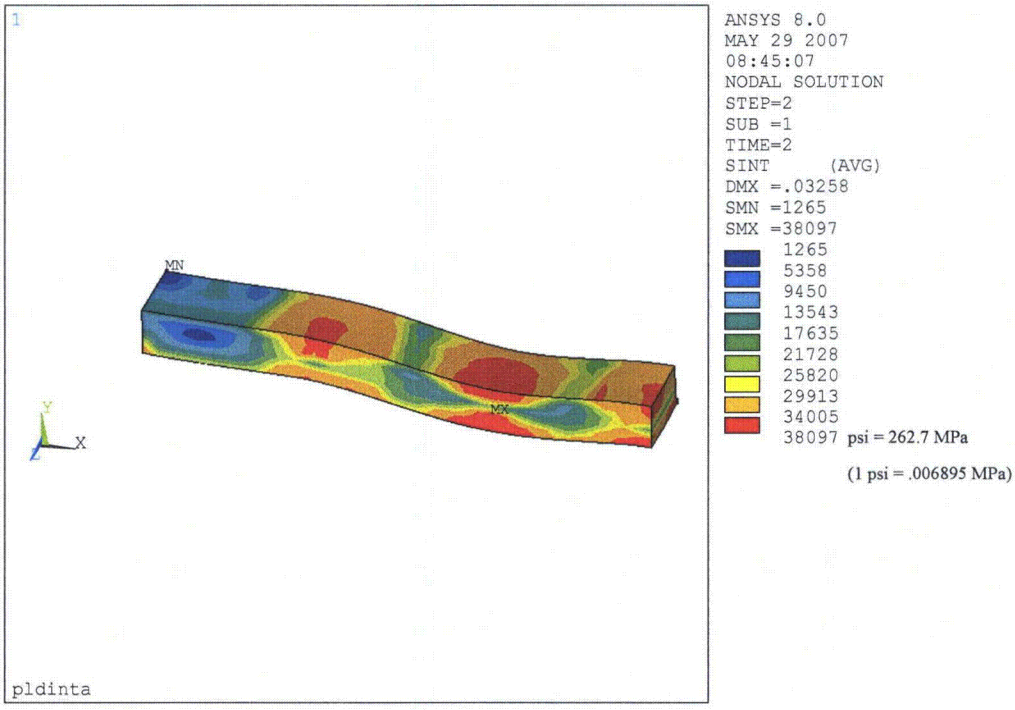

Figure 2.12.5-19 – Guide Bar Stress Intensity, Version A

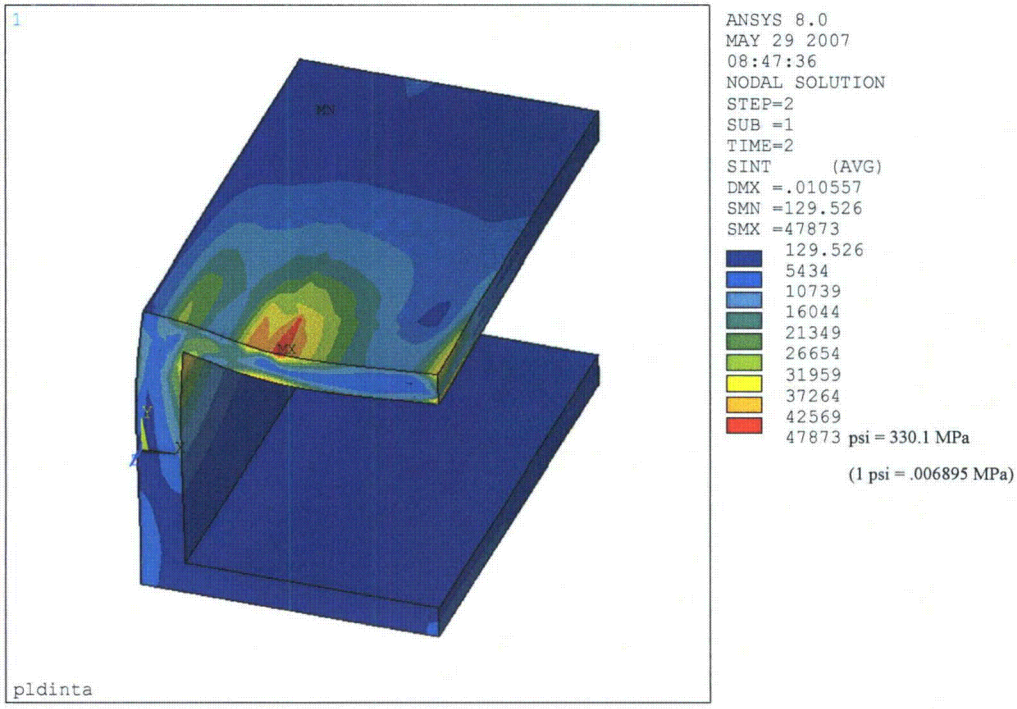

Figure 2.12.5-20 – Flange Component Stress Intensity, Version A

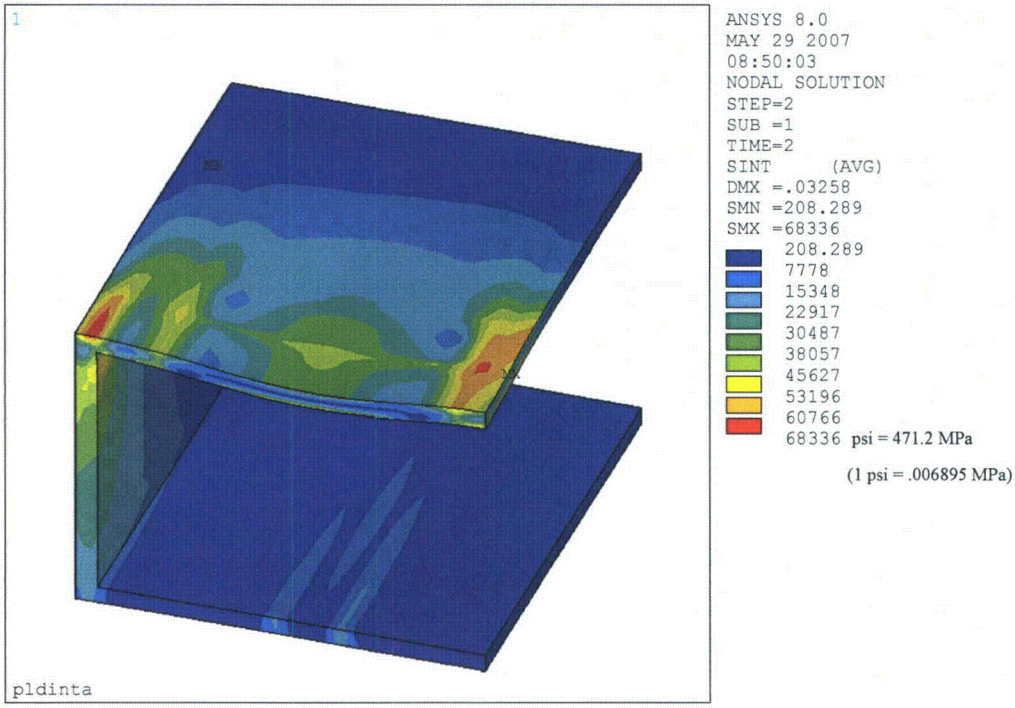

Figure 2.12.5-21 – Flange Rear Wall, Inner, and Outer Sheet Stress Intensity, Version A

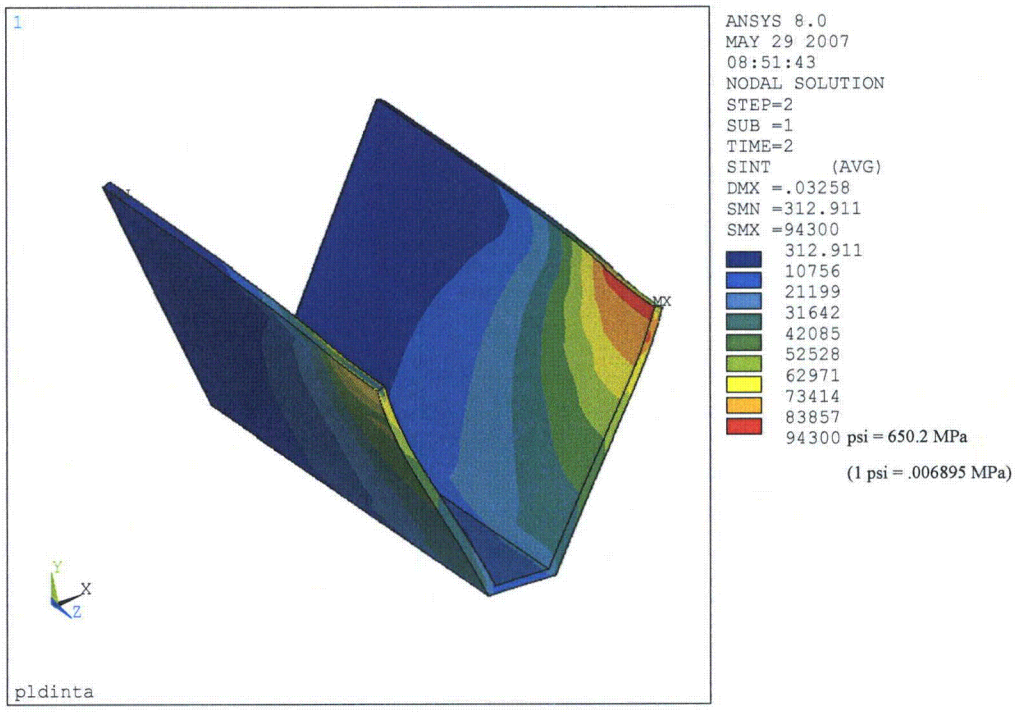

Figure 2.12.5-22 – V-stiffener Stress Intensity, Version A

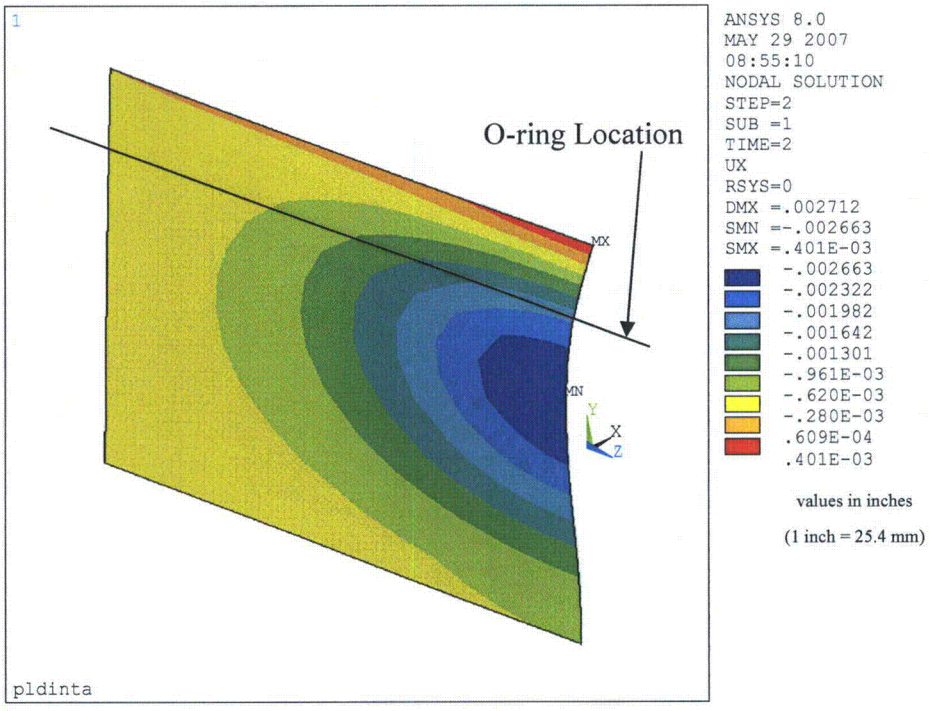

Figure 2.12.5-23 – Flange Face Deformation (Full Load), Version A

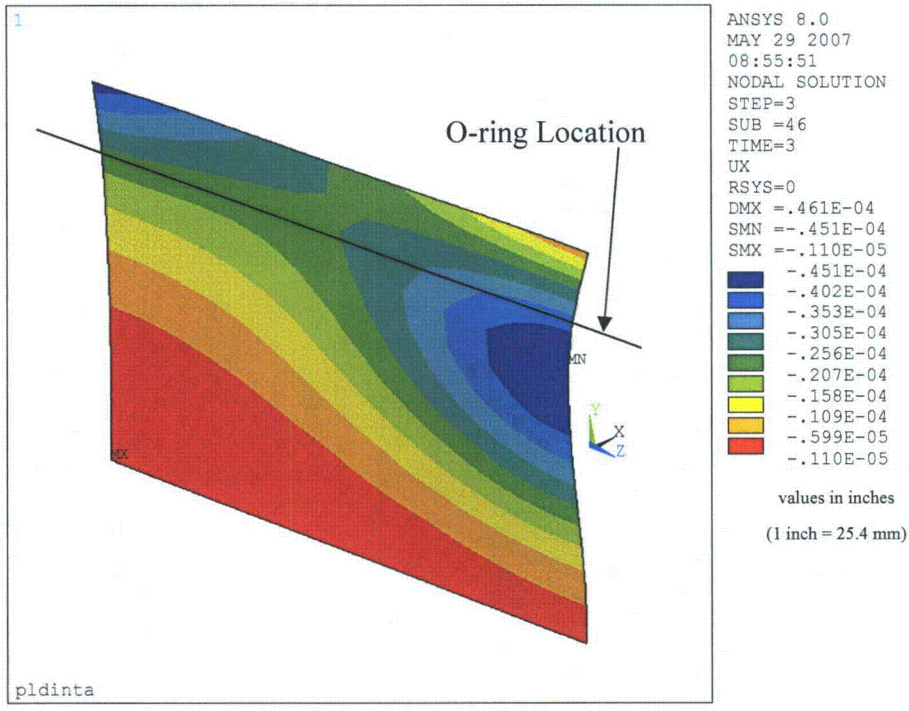

Figure 2.12.5-24 – Flange Face Deformation (Unloaded), Version A

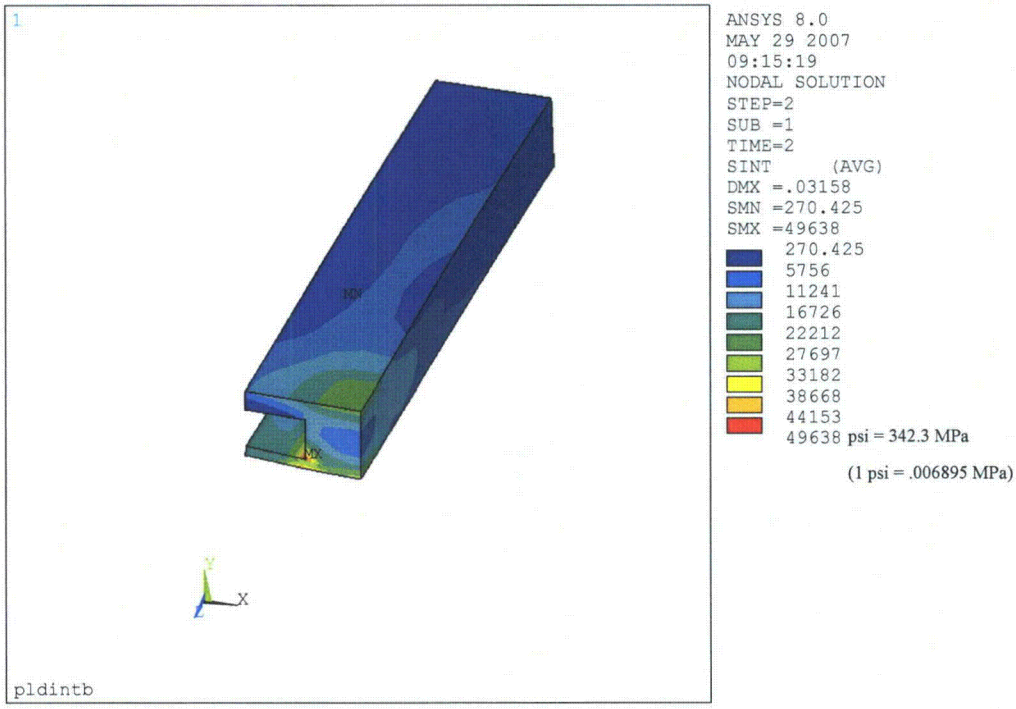

Figure 2.12.5-25 – Debris Shield Receptacle Stress Intensity, Version B

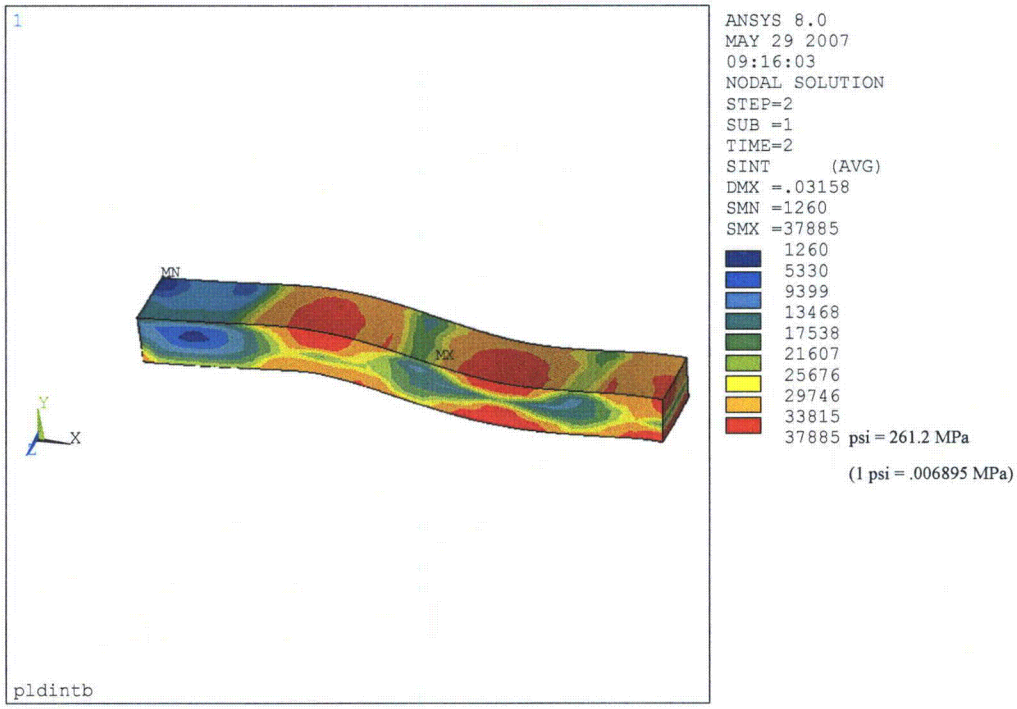

Figure 2.12.5-26 – Guide Bar Stress Intensity, Version B

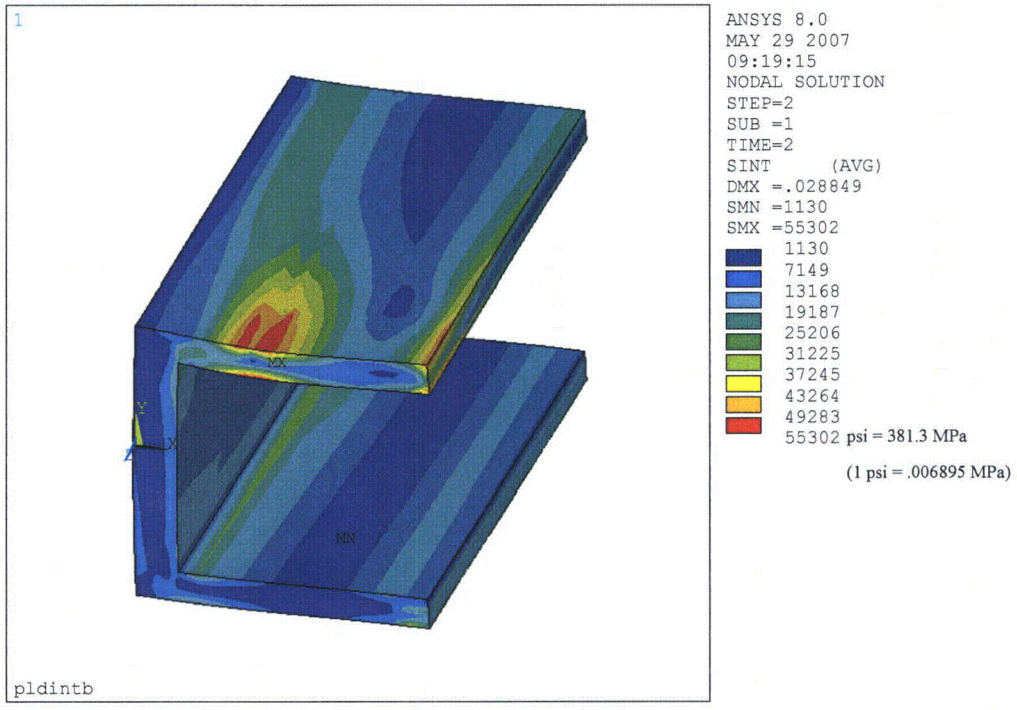

Figure 2.12.5-27 – Flange Component Stress Intensity, Version B

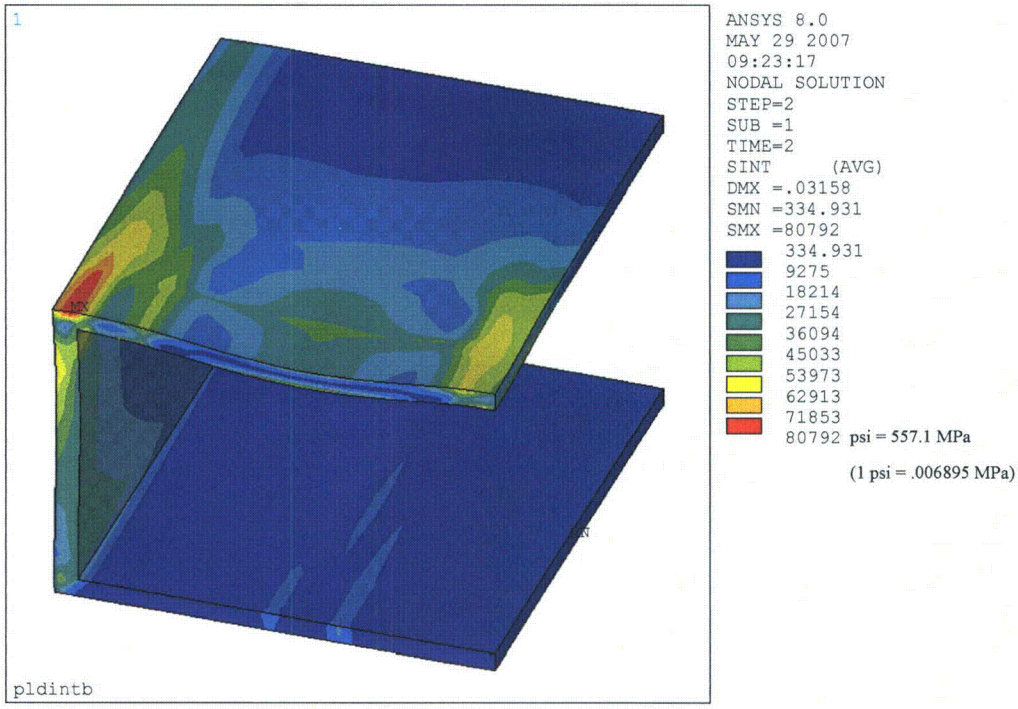

Figure 2.12.5-28 – Flange Rear Wall, Inner, and Outer Sheet Stress Intensity, Version B

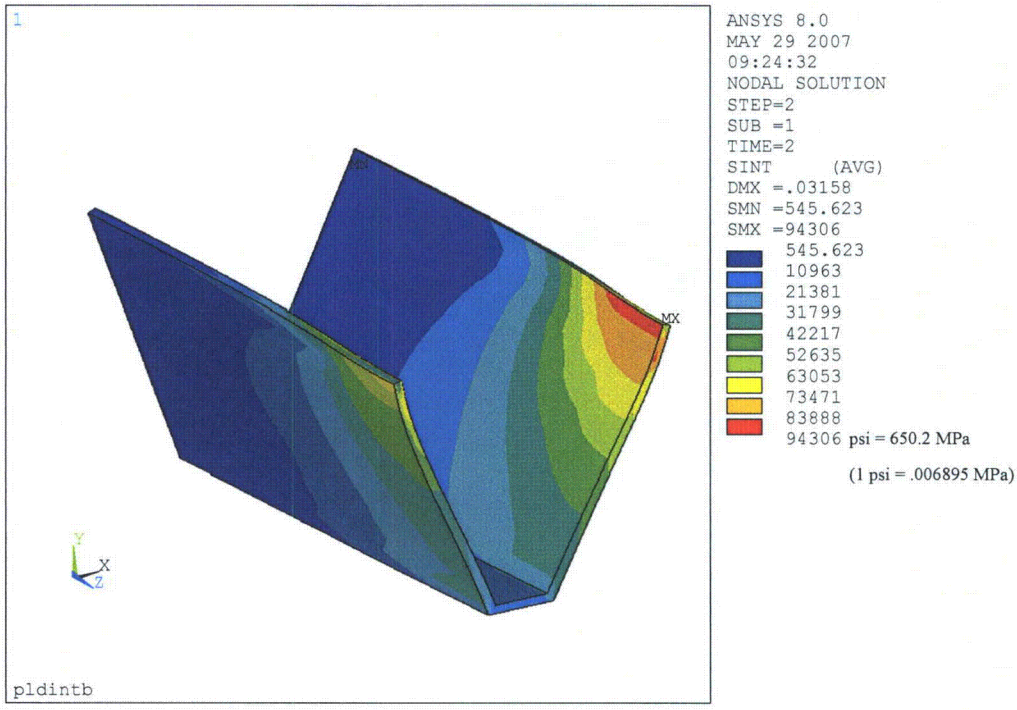

Figure 2.12.5-29 – V-stiffener Stress Intensity, Version B

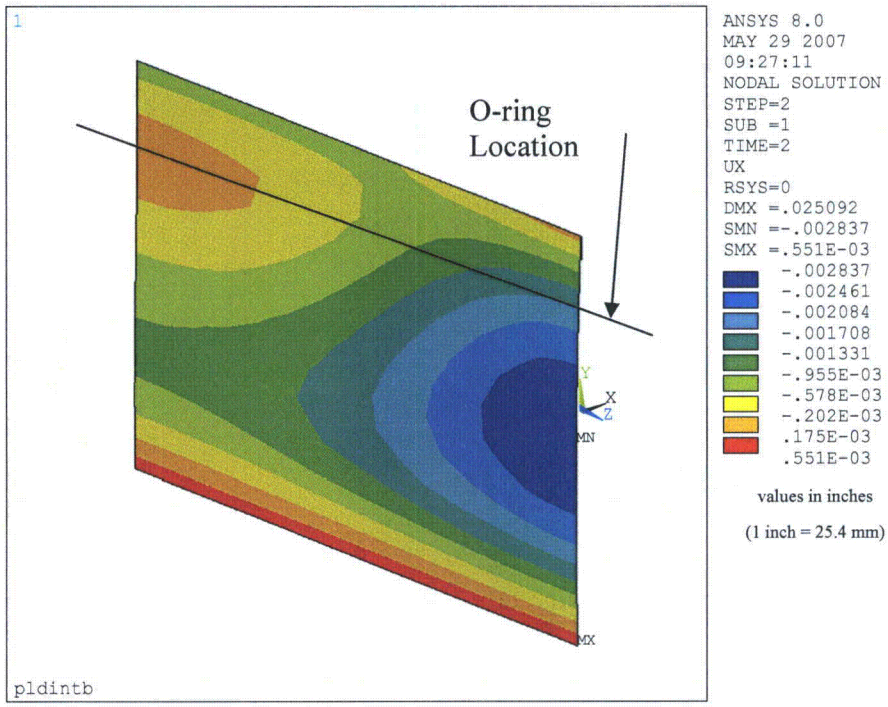

Figure 2.12.5-30 – Flange Face Deformation (Full Load), Version B

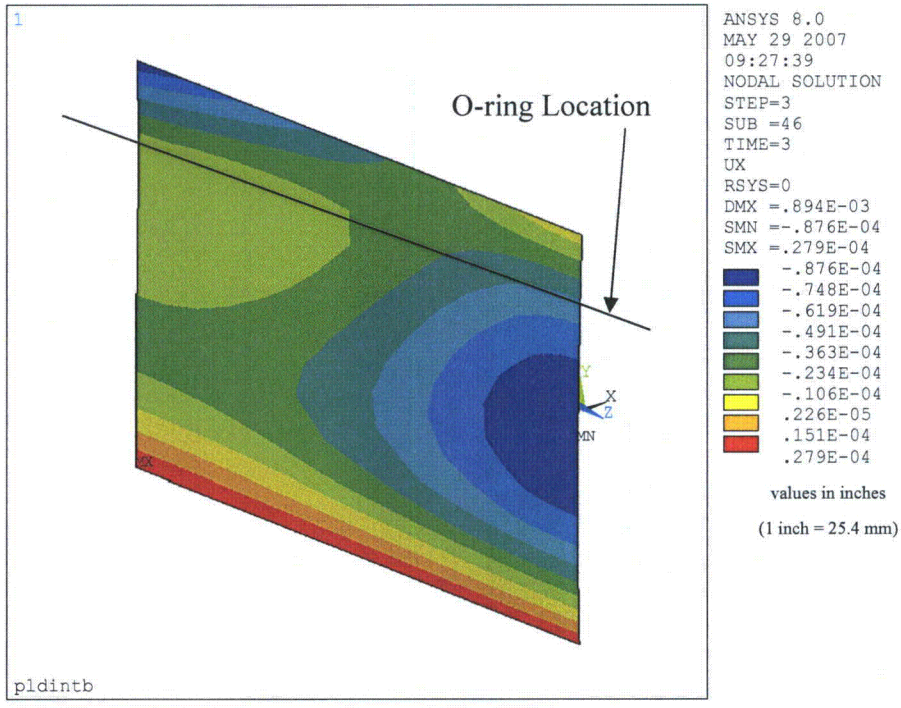

Figure 2.12.5-31 – Flange Face Deformation (Unloaded), Version B

2.12.6 Certification Tests on CTU-2

This appendix presents the results of supplementary tests that address the free drop and puncture test performance requirements of 10 CFR 71[1]. The test was performed using a written test plan[2] and procedure[3]. This appendix summarizes the information presented in the test report[4] for the second TRUPACT–III certification test unit (serial number CTU-2).

2.12.6.1 Introduction

Demonstration of the compliance of the design of the TRUPACT–III transportation package with the requirements of 10 CFR §71.73 was primarily achieved using formal certification testing on two test units, CTU-1 and CTU-2. Results of testing on CTU-1 are documented in Appendix 2.12.3, *Certification Tests on CTU-1*. The testing on CTU-2 consisted of one 9-m free drop and two 1-m puncture drops, in order to ensure a leaktight condition after the worst-case series of HAC events. CTU-2 differed from CTU-1 primarily by including the debris shield that was designed after CTU-1 was tested, and by using a roller floor, pallet, and loaded SLB2 container instead of loose metal bars as contents. This appendix describes the results of the testing, including post-test measurements and evaluations. The primary success criterion was that, subsequent to all free drop and puncture testing, the containment boundary, including the closure lid and vent port seals, be leaktight per ANSI N14.5[5]. Other supporting data, including accelerations and physical measurements, was collected as described herein.

CTU-2, like CTU-1, was fabricated in prototypic full-scale, which was in full compliance with the drawings given in Section 1.3.1, *Packaging General Arrangement Drawings,* except for differences noted and justified below.

2.12.6.2 Test Facilities

Test facilities used for the supplemental testing on CTU-2 are the same as described in Section 2.12.3.2, *Test Facilities*.

---

[1] Title 10, Code of Federal Regulations, Part 71 (10 CFR 71), *Packaging and Transportation of Radioactive Material*, 01–01–09 Edition.

[2] *TRUPACT–III Transportation Package Certification Test Plan for Supplementary Tests in 2009*, PKG–TP–SPC–005, Rev. 1, AREVA Federal Services LLC.

[3] *TRUPACT–III Transportation Package Certification Test Procedure for Supplementary Tests in 2009*, PKG–TP–SPC–006, Rev. 2, AREVA Federal Services LLC.

[4] *TRUPACT–III Transportation Package Certification Test Report for Supplementary Tests in 2009*, PKG–TR–SPC–004, AREVA Federal Services LLC.

[5] "Leaktight" is a leakage rate not exceeding 1×10^{-8} Pascals – cubic meters per second ($Pa–m^3/s$), air, as defined in ANSI N14.5–1997 (or later), *American National Standard for Radioactive Materials – Leakage Tests on Packages for Shipment,* American National Standards Institute, Inc. (ANSI).

2.12.6.3 Test Unit Configuration

CTU-2 was an essentially prototypic, full-scale model of the TRUPACT–III package, fabricated according to the drawings given in Section 1.3.1, *Packaging General Arrangement Drawings*. Prior to testing, a certificate of conformance was issued. Any differences between CTU-2 and a regular production TRUPACT–III unit are discussed and justified below.

1. The CTU utilized no thread inserts. The production unit inserts are stronger than threads made directly in the parent material. However, the production unit thread inserts are optional, therefore the CTU conservatively represented the minimum pull-out strength possible in a production unit.
2. To ensure conservative leakage rate measurement of the CTU containment O-ring seal, care was taken to ensure that the compression of the seal was below the minimum compression of the production unit seal of 27.8%. Therefore, the containment O-ring groove in the closure lid was fabricated with a depth greater than shown on the production unit drawings. The as-built depth of the containment seal O-ring groove varied between 8.76 and 8.84 mm, for an average of 8.80 mm. The average cross-sectional diameter of the containment O-ring was 12.04 mm. The diameter reduction due to the circumferential stretch, as shown in Section 4.1.3.1, *Seals*, is 1.5%. Therefore the installed cross-sectional diameter of the O-ring was:

   $$D_R = (1 - 0.015)D = 11.86 \text{ mm}$$

   where D = 12.04 mm. The compression of the test O-ring was:

   $$C = \left[1 - \left(\frac{d}{D_R}\right)\right] \times 100 = 25.8\%$$

   where d = 8.80 mm. This is conservatively less than the minimum standard production unit containment seal compression of 27.8%, as shown in Section 4.1.3.1, *Seals*.
3. Special vent and test ports were added to the side of the CTU that do not occur on the production unit. These were provided to allow leakage rate testing of the CTU without the need to remove the overpack cover or disturb the prototypic vent and test ports. They were located away from structural damage areas, and did not affect the behavior of the CTU.
4. The CTU did not have guide bars or plastic plates across the rear wall of the payload cavity. The guide bars do not play a significant role in package resistance to damage, and their only purpose is to limit the axial free play of the payload container in the cavity. Based on the length of the payload cavity of the CTU and the length of the SLB2 test unit, the average axial space present was 57 mm. The maximum space allowed in a production unit is 28 mm, as discussed in Section 1.2.1.1, *Body*. Since the axial free play of the payload container was approximately twice the maximum amount allowed in a production model, this difference is conservative.
5. Several minor package features were omitted from the CTU: Package nameplate, tamper-indicating device, ISO corner drain holes, and paint. Lack of these items did not affect the outcome of the certification tests.

6. Small steel accelerometer mounting blocks and threaded steel lifting bosses were attached to the outside surface of the CTU. Also, six swivel hoist rings and mounting bases, weighing a total of 120 kg, were attached to the CTU. These items were not involved with any test damage, and their weight was insignificant, so they did not affect test results.
7. The debris shield seal holder on the closure lid was fabricated using ASTM A240/A479 TYPE 304/304L material in a welded configuration rather than the specified UNS S31803 duplex stainless steel in a non–welded configuration. Use of a lower strength material and welded construction on the CTU is conservative.
8. The guide bars which are located on the inside walls of the payload cavity were located approximately 13 mm below the location shown on the SAR drawings. In spite of this, the square tube bumpers on the SLB2 properly interfaced with the guide bars during the test.
9. The bolting bosses in the body flange included 35 mm diameter × 40 mm deep holes on the back side (towards the inside of the flange). These holes had no effect on test results.
10. Several nonconformances were encountered during fabrication of the CTU. All are recorded in the data package for the CTU, and were dispositioned according to the Quality Assurance program and approved by AFS. The nonconformances were very minor in nature and did not have a significant effect on the performance of the CTU during testing. The most significant nonconformances are noted in the following list.
    - The CSA body face flange thickness for the CTU ranged from 27 – 31 mm, compared to the specified thickness of 20 – 30 mm. This difference is negligible.
    - The 28.5 mm thick lifting plate on each ISO corner was to be welded to the 8 mm thick side plate using an 8 mm groove weld from the outside only. The actual components featured an additional 6 mm fillet backing weld on the inside of the ISO corner weldment. This had a negligible effect on the strength of the ISO corner component.
    - Due to welding-related distortion, the outside surface of the CSA top, bottom, and side surfaces were out–of–flat by 8 mm, which required the addition of small pieces of 8–mm plate to bridge the gap between the square frame containing the overpack cover bolt bosses on the front end to the CSA body.
    - The 3–piece polyurethane glued foam assembly in the right front cheek broke at the glue line, and was installed without repair of the joint. This had no effect on the test results, since the right cheek was not deformed by any of the tests.
    - To prevent out-gassing from behind the debris shield receptacle (which would lead to a high background reading in the payload cavity and interfere with the ability to perform the metallic containment boundary leakage rate testing), epoxy material was applied at various places to the receptacle attachment welds and inside the receptacle opening where the receptacle component was thinned or locally penetrated during machining of the opening. This localized use of epoxy had no effect on debris shield performance or on any other test results.
    - The bars from which the debris shield receptacle were machined did not match up properly at the four corners. The resulting gaps were filled using epoxy.

- Due to welding-related distortion, the width between the front cheeks on the CTU where they weld to the CSA measured 2105 mm on the top versus the specified width of 2120 ± 10 mm (which applies at the attachment of the cheeks to the CSA). To permit assembly of the overpack cover between the cheeks, the width of the overpack cover was locally reduced by a total of approximately 10 mm. This change was made only to the lips of the overpack cover (a region 272 mm long, measured from the bolting flange). The resulting lateral fit up gaps between the overpack cover and the cheek inside dimension were measured and are recorded in Table 2.12.6-4.

Prior to any certification testing, the CTU was subject to acceptance testing, including a lifting load test, an internal pressure (1.5 times MNOP) test, and leakage rate tests of the containment boundary.

The test payload included a prototypic roller floor, pallet, and SLB2, shown in Figure 2.12.6-3. The SLB2 was loaded with a quantity of square-ended, two-inch and four-inch diameter aluminum bars. Approximately one quart of debris was added to the payload cavity of the CTU (outside the SLB2). The debris was composed of crushed concrete and fine grinding grit found in the fabrication shop, and was poured into the cavity just before the final installation of the closure lid. It was placed primarily in the gap between the lower front debris shield receptacle bar and the roller floor, and between the two side walls and the roller floor nearest the opening. The debris is shown on white paper in Figure 2.12.6-9 and shown in the CTU cavity in Figure 2.12.6-10. Weights are detailed in Table 2.12.6-1. The gross weight of CTU-2 was 25,154 kg, slightly more than the maximum gross weight of the TRUPACT–III package of 25,000 kg.

2.12.6.4 Instrumentation

2.12.6.4.1 Accelerometers

Four single axis piezoresistive accelerometers were utilized to record the free drop impact. Accelerometers were not used for the puncture drop tests. The accelerometers were attached to solid stainless steel blocks that were attached by screws and epoxy to the outer sheet on the body at the locations shown in Figure 2.12.6-1. Data was recorded and conditioned by a calibrated stand-alone Spectral Dynamics data acquisition system. A Fast Fourier Transform (FFT) of the raw data was performed to determine the appropriate cutoff, or filtering frequency. The accelerometer data was filtered using a six-pole Butterworth filter with the cutoff set at 200 Hz.

2.12.6.4.2 Thermocouples

Type K thermocouples were installed as shown in Figure 2.12.6-2 to measure the temperature of the polyurethane foam in the critical region near the impact event on the lower left corner of the CTU. The data was monitored during the chilling period, and continued until impact.

2.12.6.5 Initial Test Conditions

2.12.6.5.1 Internal Pressure

Since internal pressure has the effect of increasing the stress on the containment boundary, the CTU was pressurized to an internal pressure of 170 kPa at a temperature of -4 °C, which conservatively exceeded the design pressure of 172 kPa at 21 °C. Since resistance to puncture is not significantly affected by internal pressure, the CTU was not pressurized for the puncture tests. Since the pressure is only an initial condition, monitoring the pressure was not performed.

2.12.6.5.2 Temperature

As discussed in Section 2.7.1.1.3, *Free Drop Test on CTU-2*, the maximum damage from the c.g.-over-corner free drop will occur at the minimum regulatory temperature condition of -29 °C. The actual temperature of the energy-absorbing material in free drop test LD91 is recorded in Section 2.12.6.7.1, *Free Drop, CG-Over-Corner, Overpack Cover Down, HAC (LD91).* Prevailing temperature was used for all puncture drop tests.

2.12.6.6 Certification Tests Performed

The evaluation and selection of tests to be performed for certification testing is discussed in Section 2.7.1, *Free Drop*, and Section 2.7.3, *Puncture*. One HAC free drop and two puncture drops were performed, as summarized in Table 2.12.6-2. The free drop is designated LD91 and is shown schematically in Figure 2.12.6-4. The punctures are designated LP91 and LP92, and shown schematically in Figure 2.12.6-5 and Figure 2.12.6-6, respectively.

2.12.6.7 Test Results

After each of the tests, a vacuum was placed between the closure lid seals as an approximate confirmation of the sealing integrity of the containment seal, using the special test port on the CTU side. The vacuum achieved in each case is recorded in the sections below. For the puncture tests, the internal pressure was bled off to a value nominally equal to atmospheric.

Prior to performing any tests, helium leakage rate tests were performed on the containment metallic boundary, the main O-ring seal, and the sampling/vent port plug O-ring seal according to an approved procedure. Photos of certification testing are provided in Figure 2.12.6-7 to Figure 2.12.6-20.

2.12.6.7.1 Free Drop, CG-Over-Corner, Overpack Cover Down, HAC (Test LD91)

Test LD91 was a free drop from a conservative height of 9.2 m, with the CTU axis oriented approximately 47° to the ground, striking the lower left corner of the package as shown in Figure 2.12.6-4. The center of gravity of the package was over the point of initial impact. The average temperature of thermocouples T1, T2, and T7 was -33.6 °C. These temperatures represent both shallow and deep readings in the corner of the package. The ambient temperature was 5.6 °C. Accelerations were obtained from gages A1 through A4. The raw signals were filtered at 200 Hz, and the resulting acceleration plots are shown in Section 2.12.6.9, *Acceleration Time History Plots.* The shapes of the accelerometer curves were not consistent with each other, nor (with one

exception) were the recorded peaks as high as expected. The resulting curve which best fit the expectation based on the high speed video and on the results obtained from CTU-1 was accelerometer A1. This was also the highest acceleration. The impact was therefore considered to be best characterized by the A1 result, and the results of A2 – A4 were not used. The accelerometers were mounted with their measuring axis parallel to the package axis; the resulting acceleration perpendicular to the ground was found using:

$$A1_{\perp} = \frac{A1}{\cos(43)} = 80.8g$$

where A1 is the filtered accelerometer peak value from the table below, and the axial direction is oriented at an angle of 90° – 47° = 43° to the vertical as defined in Figure 2.12.6-4.

A1	A2	A3	A4	$A1_{\perp}$
59.1	(25.8)	(37.1)	(33.7)	**80.8**

The impact caused a triangular flat region having dimensions of 737 mm along the overpack cover, 864 mm along the bottom, and 787 mm along the left side of the CTU. The damage to the overpack cover included a gap of up to 70 mm at the center between the cheek and the overpack cover left edge, see Figure 2.12.6-12. The gap exposed some foam, but narrowed to nearly zero a short distance from the surface. No significant weld seam failures were noted from this test. A hard vacuum of below 200 millitorr was obtained between the closure lid seals as a preliminary confirmation of leak tightness. Photos of the damage are shown in Figure 2.12.6-11 and Figure 2.12.6-12.

2.12.6.7.2 Puncture Drop On CG-over-Corner Damage (Test LP91)

The drop height for this test was one meter. The ambient temperature for this test was 15 °C and the package surface temperature was 19 °C. The CTU was rigged as shown in Figure 2.12.6-5. The bar was 762 mm long (above the baseplate). The puncture bar struck on the overpack cover portion of the prior c.g.-over-corner free drop (LD91) damage. The depth of puncture, measured to the center of the damage hole in an axial direction from the undeformed surface of the overpack cover, was 146 mm. The damage loosened the entire lower quadrant of the overpack cover outer sheet and a significant portion of the low density (0.16 kg/dm^3) foam fell out. The bar corner partially sheared into the 6-mm thick puncture resistant plate located between the low density and high density (0.48 kg/dm^3) foam by an amount of 38 mm. However, little of the high density foam was exposed and essentially none was lost. A hard vacuum of 224 millitorr was obtained between the closure lid seals as a preliminary confirmation of leak tightness. The puncture bar remained intact after the impact. A photograph of the damage is shown in Figure 2.12.6-13.

2.12.6.7.3 Puncture Drop On CTU Bottom (Test LP92)

The drop height for this test was one meter. The ambient temperature for this test was 12 °C, and the package surface temperature was 15 °C. The bar was 965 mm long (above the baseplate). The puncture bar struck as shown in Figure 2.12.6-6, with the edge of the bar placed approximately 476 mm from the closed outer end of the package, with the package inclined 40° from the horizontal. The bar penetrated the outer skin and impacted the CSA outer structural sheet, creating a crack in the weld between the structural sheet and the rear diagonal corner stiffener of the CSA, and in some of the adjacent plug welds which connect the outer structural

sheet to the V-stiffener nearest the impact. This condition required weld repairs in order to support helium leakage rate testing of the containment boundary structure. (The CSA outer wall structure must be capable of retaining the helium test gas for the containment boundary leakage rate test to be performed.) However, there was no evidence of any dent or bulge in the CSA inner (containment) sheet at the puncture site. In addition, the containment boundary was leaktight as discussed in Section 2.12.6.8.1, *Leakage Rate Tests*. A hard vacuum of below 250 millitorr was obtained between the closure lid seals as a preliminary confirmation of leak tightness. The puncture bar remained intact after the impact. The damage is shown in Figure 2.12.6-14 and Figure 2.12.6-15. Figure 2.12.6-15 shows the cracked outer structural sheet weld.

2.12.6.8 Leakage Rate Tests and Post-Test Measurements

2.12.6.8.1 Leakage Rate Tests

Post-test leakage rate testing of the containment boundary was performed using helium tracer gas and a mass spectrometer leak detector (MSLD). The leaktight criterion was 2.2×10^{-8} Pa-m^3/s, He. All tests were successful. Testing result details are provided in Table 2.12.6-3. The testing consisted of three elements:

- Closure lid containment O-ring seal
- Vent port containment O-ring seal
- Metallic portion of the containment boundary

2.12.6.8.1.1 Closure Lid and Vent Port Containment O-ring Seals

The closure lid and vent/test port containment seals were both tested by connecting a MSLD to the space between the containment seal and the test seal and then filling the payload cavity with helium. Testing was performed at the prevailing ambient temperature of the fabrication shop. This test was equivalent to a test at the minimum regulatory temperature of -20 °F due to the intentionally low O-ring compression used in the CTU. As shown in Section 2.12.6.3, *Test Unit Configuration*, the room-temperature compression of the closure lid containment O-ring in the CTU was 25.8%, and the minimum room-temperature compression in a prototypic unit is 27.8%. The reduction in compression in the seal at a temperature of -29 °C (caused by thermal contraction of the rubber) may be inferred to be approximately 1%, based on the calculation performed in Section 2.12.2.6, *Test Results*, for a temperature of -40 °C. Therefore, a prototypic unit at a temperature of -29 °C would have a minimum compression of 27.8 – 1 = 26.8%, which is 1% greater than the compression in the CTU at the test temperature. Therefore testing the CTU at room temperature was conservative. The leakage rate of both containment seals was acceptable as shown in Table 2.12.6-3.

2.12.6.8.1.2 Metallic Containment Boundary

The metallic portion of the containment boundary was tested by connecting a MSLD to the payload (interior) cavity and then replacing the air in the annulus between the containment and structural sheets of the CSA with helium. Helium could then pass through any openings in the containment boundary to the inside of the package, and register on the MSLD connected to the

cavity. In order to achieve the required vacuum in the payload cavity to support the leakage rate test and to ensure there were no obstructions to any potential leak paths, the closure lid was removed, the contents were removed, and the payload cavity was thoroughly cleaned. The lid was then reinstalled and the bolts tightened to approximately 400 N-m, which was conservatively much less than the measured minimum residual torque for any bolt (see Section 2.12.6.8.2.1, *Overpack Cover and Closure Lid Observations*). Since the leakage rate tests of the closure lid O-ring and vent port seals had already been completed, removal of the closure lid had no effect on any test. Further, a leak in the metallic boundary, had one existed, would not be affected by the removal of the closure lid, of the contents, or by the cleaning. The leakage rate was acceptable as shown in Table 2.12.6-3.

2.12.6.8.2 CTU Measurements

Besides measurement of the damage reported above, various measurements were taken of the CTU during disassembly as discussed below.

2.12.6.8.2.1 Overpack Cover and Closure Lid Observations

The gaps between the overpack cover and the cheeks were measured in several locations before and after the test, and reported in Table 2.12.6-4. The results show that the cover moved away from the impact, and the total gap width decreased, as expected. It is concluded that the cover did not move very far as a result of the tests.

The lid moved slightly relative to the body as demonstrated by the scribe line offsets. On assembly, four scribe lines were made between the lid and body. After the test, the scribe lines were offset by 1.3 mm top left; 1.8 mm top right; 0.25 – 0.50 mm lower left; and 0 – 0.13 mm lower right. The lid appeared to have moved to the left, i.e, toward the c.g.-over-corner impact (test LD91).

It was noted that a 0.102 mm thick feeler gauge could not be inserted between the lid and body flanges (with one very limited exception) along the top and bottom flanges. The sides were not checked due to the presence of the cheeks. It is thus concluded that the closure lid flange was in clamped contact with the body flange. As noted in Section 2.12.6.8.2.2, *Observations with the Closure Lid Removed*, some galling of the flanges near the bolt holes testified to a high clamping force during the test.

None of the bolt heads had rotated, based on the location of the rotational index marks, and based on the residual torques. Residual torques were checked in the clockwise direction by applying a torque of 1,356 N-m to each bolt. No bolts rotated as a result of this torque application. Residual loosening torque was recorded as the largest counter-clockwise torque value obtained during removal of the bolts. Of note, all bolts were tested for loosening torque without significantly reducing the preload of any. Only after checking the residual loosening torque of all bolts were any bolts significantly loosened and removed. The residual loosening torques varied between a minimum of 1,112 N-m and a value greater than 1,356 N-m (which was the maximum capacity of the torque wrench used for this test). The average was 1,260 N-m, which is equal to 1,260/1,600×100 = 79% of the original tightening torque value of 1,600 N-m. Residual torques are given in Table 2.12.6-5.

There was some interference between the overpack cover cups and the closure bolt washers on about 61% of the bolts, from bolt no. 13 on the right side, down the right side, across the bottom,

and up the left side as far as bolt no. 40[6]. Washer nos. 41 on the left side, up through no. 12 on the top, had no interference with the cups. The struck location was uniformly between 6:30 O'clock and 7:00 O'clock, which indicates that the overpack cover slid primarily upward and slightly to the right, away from the free drop impact. The washers showed no evidence of denting or imprinting from the bolt head or lid hole, and no out-of-flat deformation. Only a little scuffing/galling from use was evident. The greatest displacement of washers relative to the lid surface occurred centered on the lower left corner impact zone. For bolt no. 33 (lower left corner, adjacent to the impact), the washer displaced approximately 0.5 mm toward the upper right. However, none of the bolts were bent. Bolt nos. 31 through 35 showed no runout when checked using a V-block and dial indicator. None of the bolt heads were struck by the cups, only some washers as stated. Typical evidence of interference between an overpack cover cup and a washer is shown in Figure 2.12.6-16.

2.12.6.8.2.2 Observations with the Closure Lid Removed

The debris shield was in good condition and protected the containment O-ring seal from contact with any of the debris which had been introduced into the payload cavity before testing. The only anomaly was that on the top side, the foam rubber component appeared to have caught an edge – apparently the edge of the receptacle – during lid assembly or removal and pulled away from the holder on the outside (nearest the flange). However, most of the silicone foam rubber in the affected sections was still compressed in the receptacle as designed, and the shield function was unaffected. There was a small pile of debris on the inside of the shield on the lid as shown in Figure 2.12.6-17, which functioned properly in preventing access of the debris to the containment seal.

The metallic portion of the containment boundary was in good condition. There was no evidence of any bulge in the inner containment wall at the site of puncture LP92. There was a little galling between the lid and body appearing next to some of the bolt holes, indicating good clamping force local to the bolts, as shown in Figure 2.12.6-18. There was also a narrow line of scuffing across the top flange. There were no deformations on the closure lid or in the body cavity due to contact with the SLB2 except for a dent in the debris shield receptacle on the left side at the elevation of the SLB2 lid as shown in Figure 2.12.6-19. This condition did not affect the function of the debris shield, since it locally increased the compression of the foam rubber shield.

Measurements of the payload cavity, shown in Table 2.12.6-6, demonstrate essentially no change to the cavity due to the test impacts. The small differences which were noted (up to two millimeters) are considered to be measurement anomalies, rather than evidence of permanent deformation. A view of the cavity with all of the contents removed is shown in Figure 2.12.6-20.

The SLB2, roller floor, and pallet were in very good condition after the test. The payload bars caused the panel walls of the SLB2 to bulge outward from the impact, and the lower of the three square tube bumpers were flattened on the front face and left side. (The level of the payload bars did not reach the middle or upper bumpers, and thus, they were not deformed.) One bar poked through the front panel of the SLB2 at the bottom. The roller floor and pallet were fully functional during removal of the SLB2 from the CTU.

[6] Bolt no. 1 is the leftmost bolt on the top side, and numbered clockwise.

Table 2.12.6-1 – CTU-2 Weight

Component	Weight, kg
Empty CTU, without closure lid or overpack cover	14,506
Closure lid and (44) closure bolts	1,796
Overpack cover and 10 attachment bolts	2,758
Empty Package Sum	19,060
Roller floor	235
Pallet	196
Loaded SLB2 (must weigh 4,763 kg minimum)	5,543
Contents Sum	5,974
Large swivel hoist rings (6)	120
Total CTU-2 Weight (must weigh 25,000 kg minimum)	25,154

Table 2.12.6-2 – CTU-2 Test Summary

Test	Description[1]	Orientation	Temperature[2]	Accelerometers & Direction	Temperature Monitors
LD91	CG-over-corner, overpack cover down, HAC	CTU axis inclined 47° from horizontal, impacting on lower left corner. See Figure 2.12.6-4.	Cold	A1 thru A4	T1, T2 & T7
LP91	On c.g.-over-corner damage	Impact on crushed corner at same orientation as test LD91, through CG. See Figure 2.12.6-5.	Prevailing	NA	NA
LP92	On bottom wall	Impact on bottom wall, aiming at puncture-resistant plate gap. CTU axis at 40° to horizontal. See Figure 2.12.6-6.	Prevailing	NA	NA

Notes:
1. HAC free drop height 9.2 m.
2. Recorded temperatures of the energy absorbing material are reported in Section 2.12.6.7.

Table 2.12.6-3 – Leakage Rate Test Results

Test Date	Test Performed	Adjusted Leak Rate ($Pa\text{-}m^3/s$, He)[1]	Pass/Fail
12/10/09	Metallic containment boundary	1.7×10^{-9}	Pass
12/2/09	Closure lid containment seal	Zero[2]	Pass
12/2/09	Vent port containment seal	Zero[2]	Pass

Notes:
1. Pass criterion equals 2.2×10^{-8} $Pa\text{-}m^3/s$, He.
2. Zero leakage rate means no detectable leakage on the range tested (10^{-9} $Pa\text{-}m^3/s$, He).

Table 2.12.6-4 – Overpack Cover Gap Measurements, mm

	Pre-test		Post-test	
	Left Cheek	Right Cheek	Left Cheek	Right Cheek
Top: rear	5	5	3	2
Top: front	20	20	14	18
Front: top	20	23	13	17
Front: bot	24	15	Not Accessible	13
Front: max	27	22	30	18
Front: min	13	13	13	13
Bot: rear	3	2	10[2]	0[2]
Bot: front	10[1]	9[1]	Not Accessible	Not Accessible
Cover surface to cheek surface (axial)	+8[3]	+15	+17	+12

Notes:
1. Measured approximately 305 mm from front face.
2. At back corner.
3. A positive sign indicates protrusion beyond the cheek ends.

Table 2.12.6-5 – Closure Lid Bolt Residual Torques (Loosening), N-m

Bolt No.	Residual Torque, Top Flange	Bolt No.	Residual Torque, Right Flange	Bolt No.	Residual Torque, Bot. Flange	Bolt No.	Residual Torque, Left Flange
1	1,248	12	1,187	23	1,268	34	1,248
2	1,288	13	1,227	24	1,295	35	1,112
3	1,281	14	>1,356	25	>1,356	36	1,193
4	>1,356	15	1,248	26	1,220	37	1,207
5	1,200	16	1,254	27	1,248	38	1,220
6	1,302	17	1,315	28	1,193	39	1,295
7	1,200	18	1,302	29	1,173	40	1,268
8	1,261	19	>1,356	30	1,295	41	>1,356
9	1,248	20	1,153	31	>1,356	42	1,302
10	1,220	21	1,302	32	1,153	43	1,288
11	>1,356	22	1,193	33	1,302	44	1,220

Note: Note: All closure bolts were tested for residual tightening (clockwise) torque up to a value of 1,356 N-m (1,000 ft-lb). When 1,356 N-m was applied to the bolts clockwise, none of the bolts rotated. The values in this table are the residual loosening (counter-clockwise) torque. See Section 2.12.6.8.2.1 for a definition of these quantities.

Table 2.12.6-6 – Payload Cavity Measurements, mm

Measurement	Pre-test	Post-test
Width, 100 mm from Top	1,840	1,840
Width, 100 mm from Bottom	1,840	1,840
Height, 100 mm from Left	2,000	2,001
Height, 100 mm from Right	2,000	2,002
Diagonal, LL to UR	2,701	2,701
Diagonal, UL to LR	2,703	2,703
Depth, center left wall, 100 mm from wall	2,791	2,791
Depth, center top wall, 100 mm from wall	2,794	2,794
Depth, center right wall, 100 mm from wall	2,793	2,791
Depth, center bottom wall, 100 mm from wall	2,789	2,790

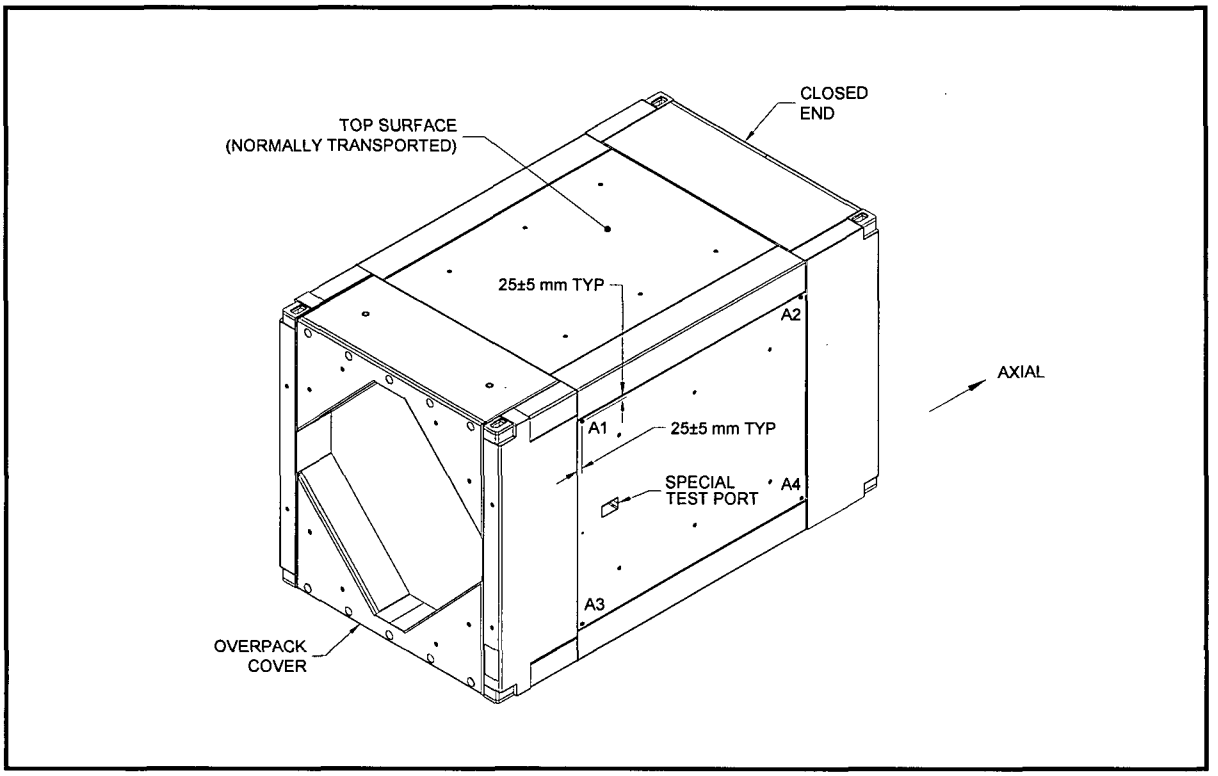

Figure 2.12.6-1 – Accelerometer Locations

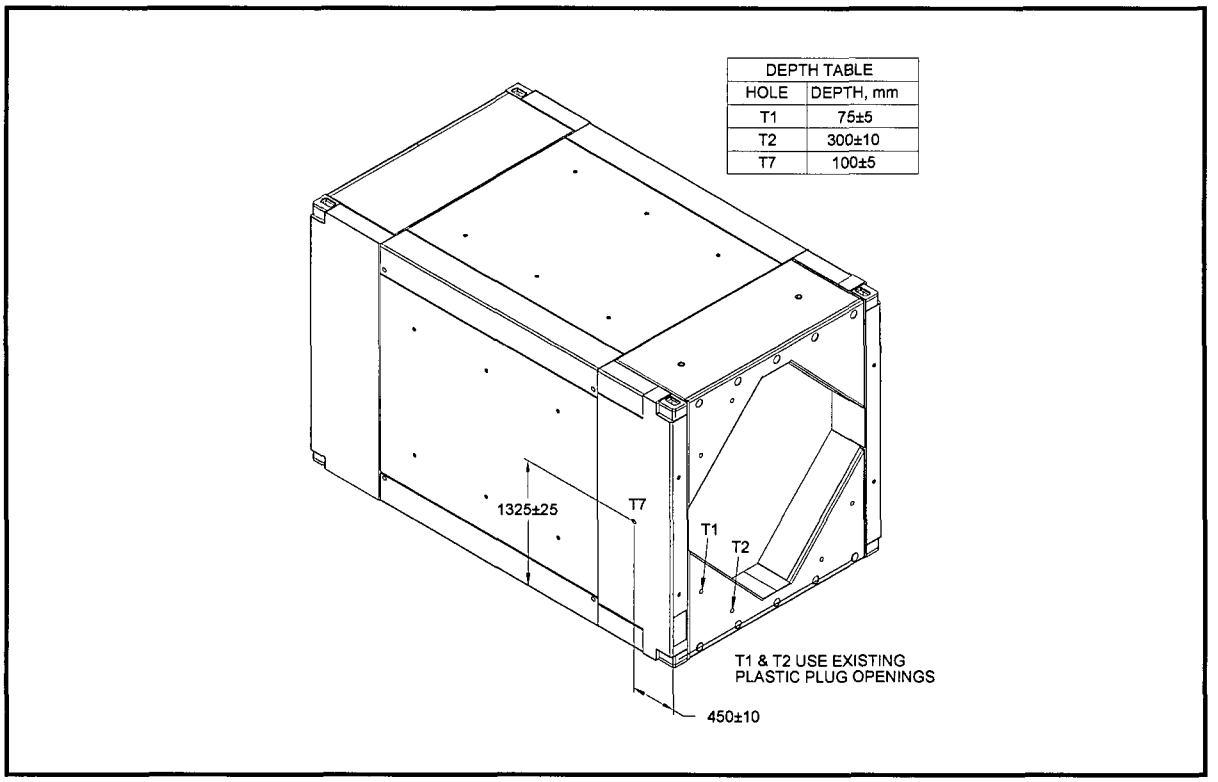

Figure 2.12.6-2 – Thermocouple Locations

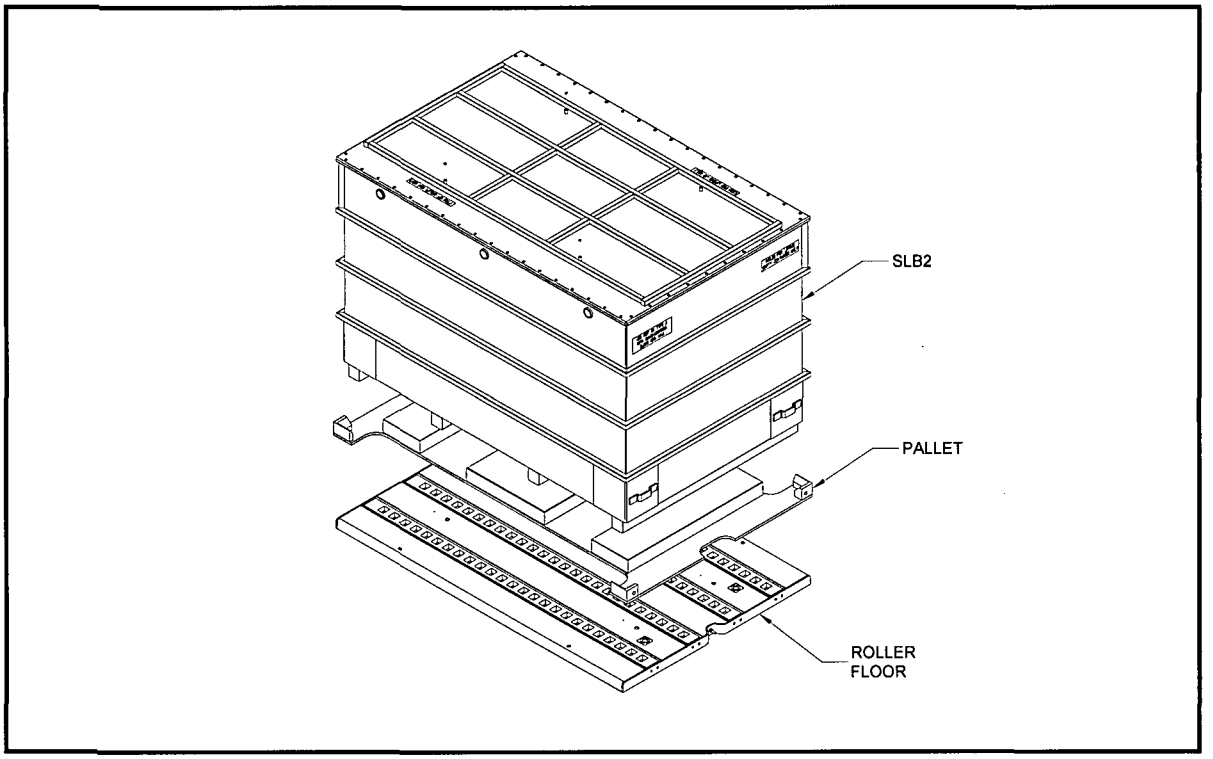

Figure 2.12.6-3 – CTU-2 Contents

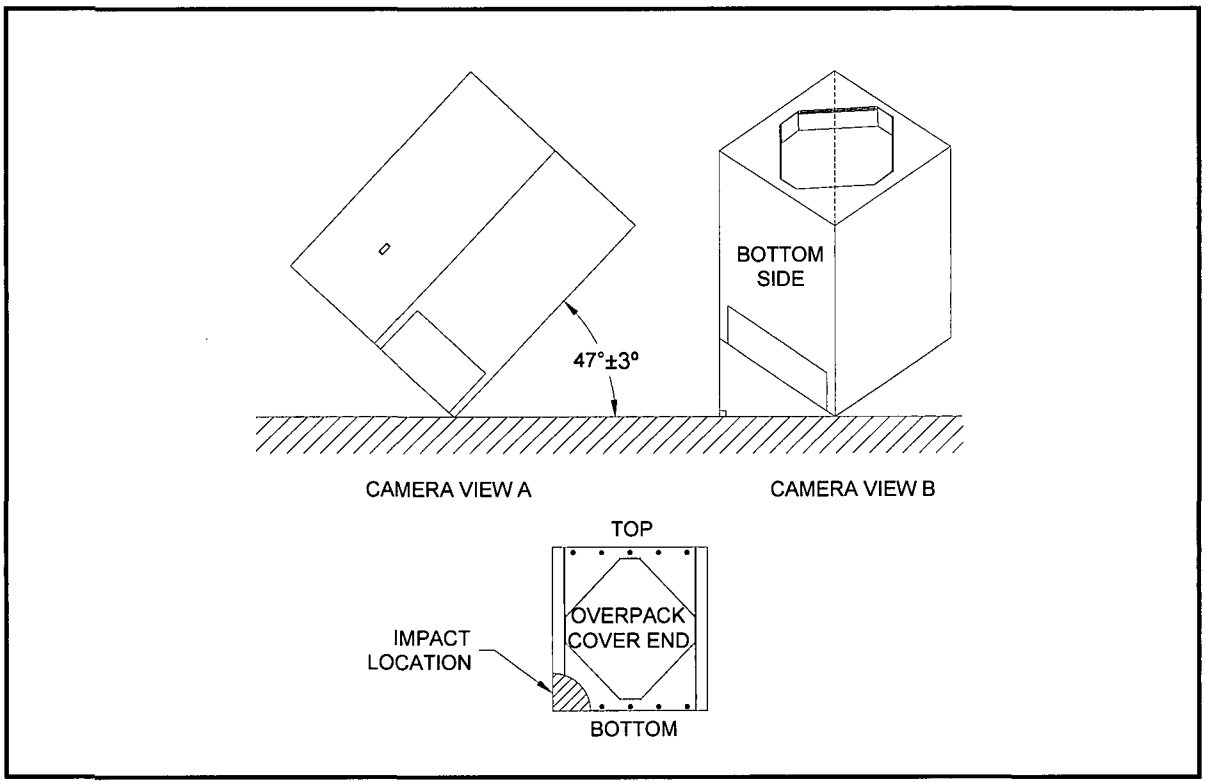

Figure 2.12.6-4 – CG-Over-Corner Free Drop Orientation, Test LD91

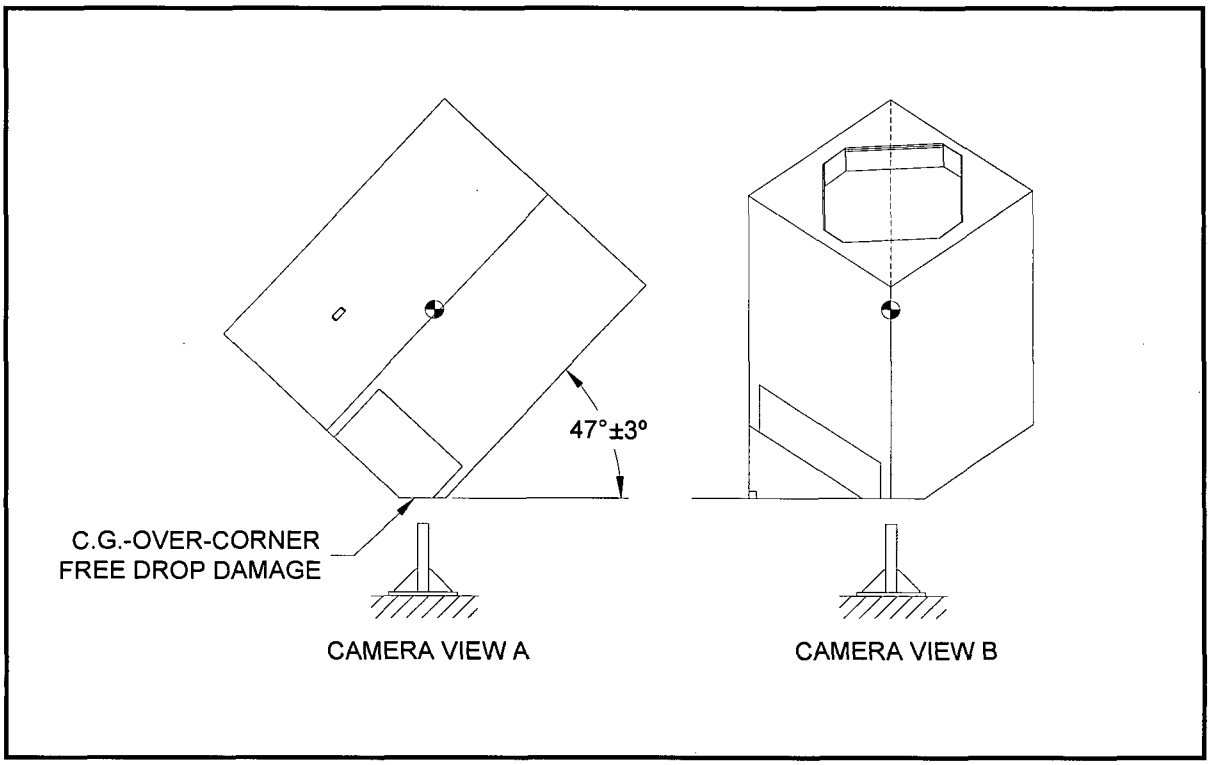

Figure 2.12.6-5 – Puncture on Prior CG-Over-Corner Damage, Test LP91

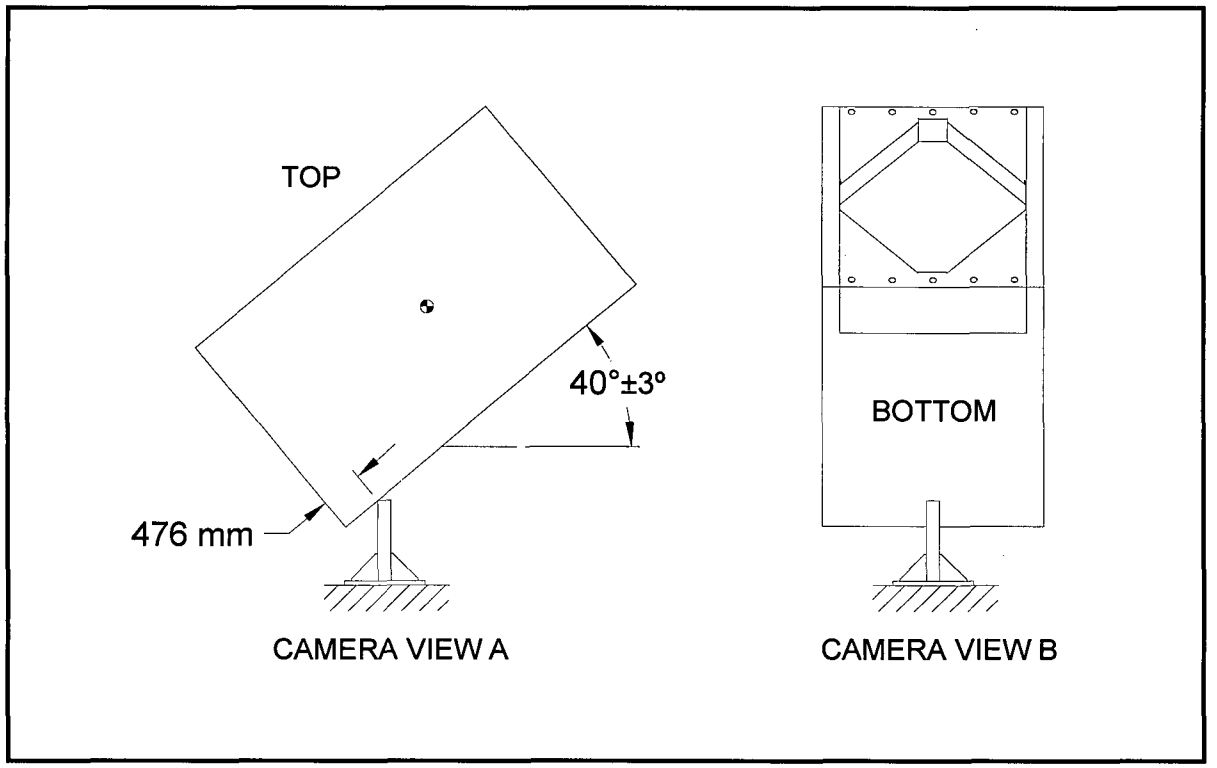

Figure 2.12.6-6 – Puncture on Bottom, Test LP92

Figure 2.12.6-7 – Aluminum Bars Inside the SLB2

Figure 2.12.6-8 – SLB2 and Pallet Installed in the Payload Cavity

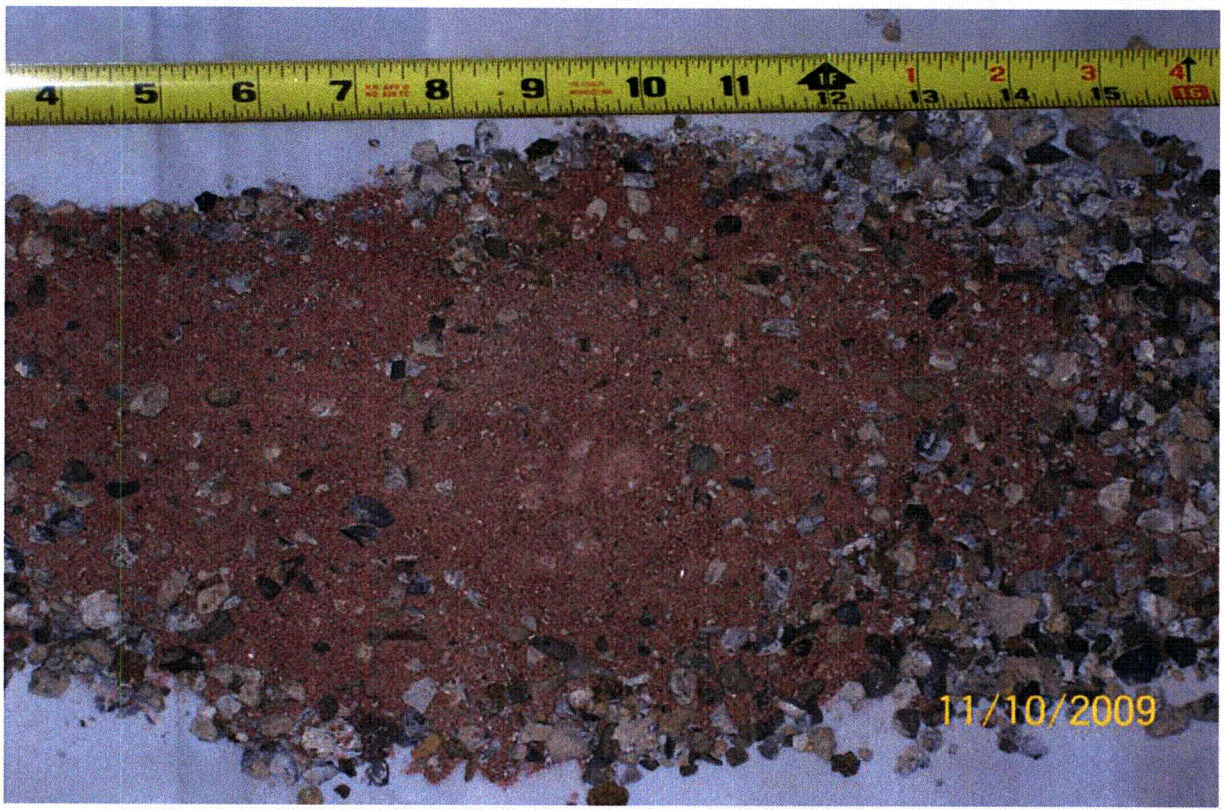

Figure 2.12.6-9 – Test Debris Used in CTU-2

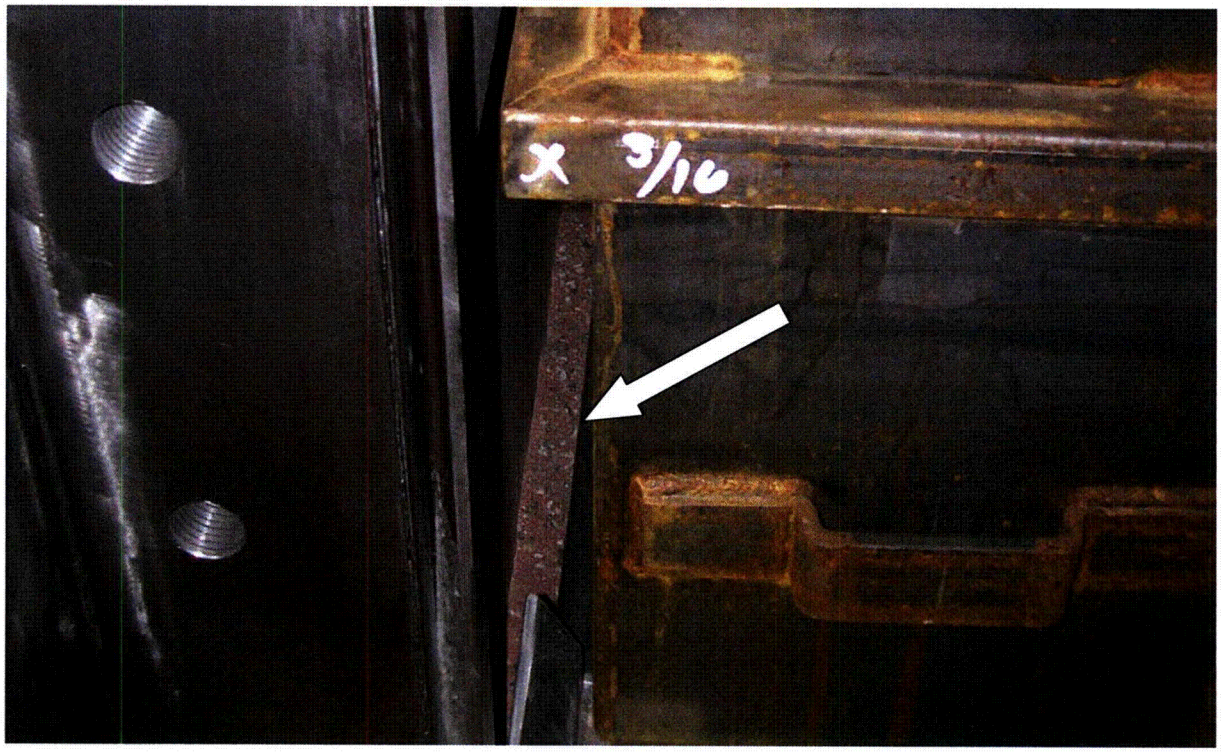

Figure 2.12.6-10 – Part of the Debris Between Roller Floor and Sidewall

Figure 2.12.6-11 – Test LD91, CG-Over-Corner Free Drop Damage

Figure 2.12.6-12 – Test LD91, CG-Over-Corner Free Drop Damage, Detail

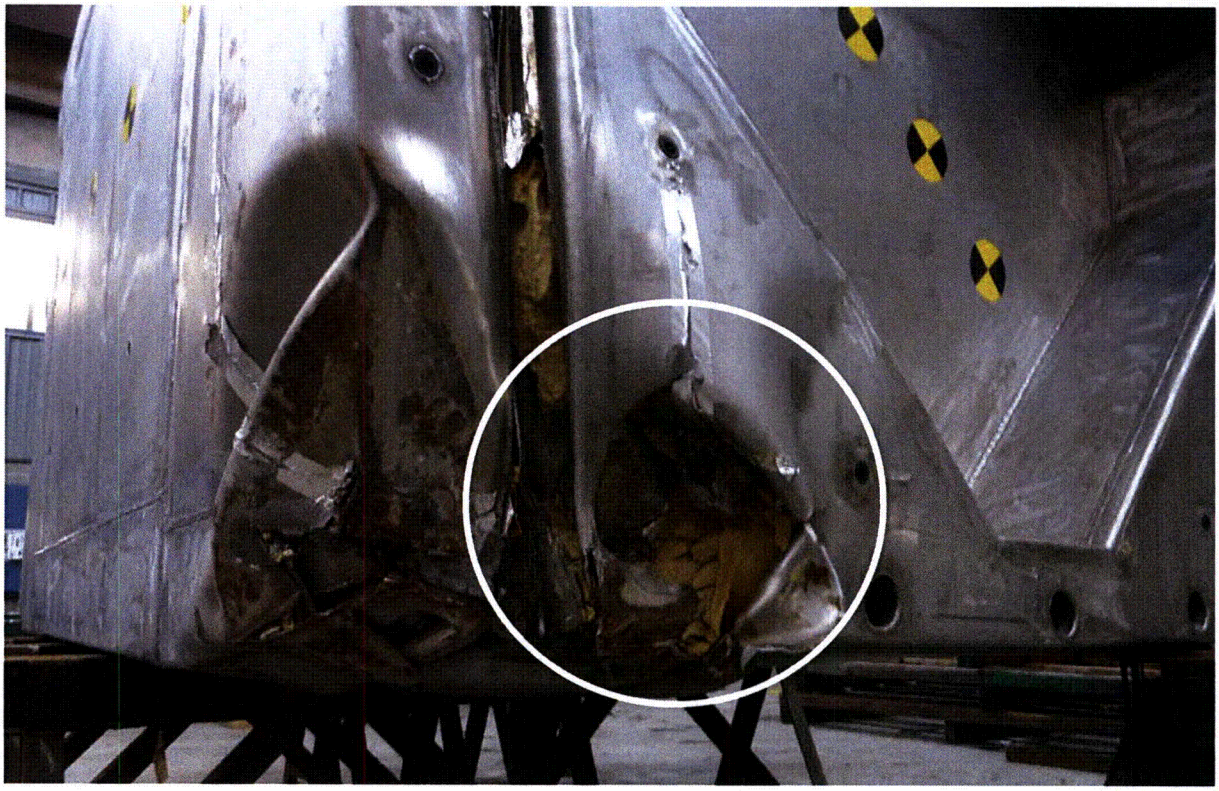

Figure 2.12.6-13 – Test LP91, CG-Over-Corner Puncture Damage

Figure 2.12.6-14 – Test LP92, Puncture on Bottom Wall Damage

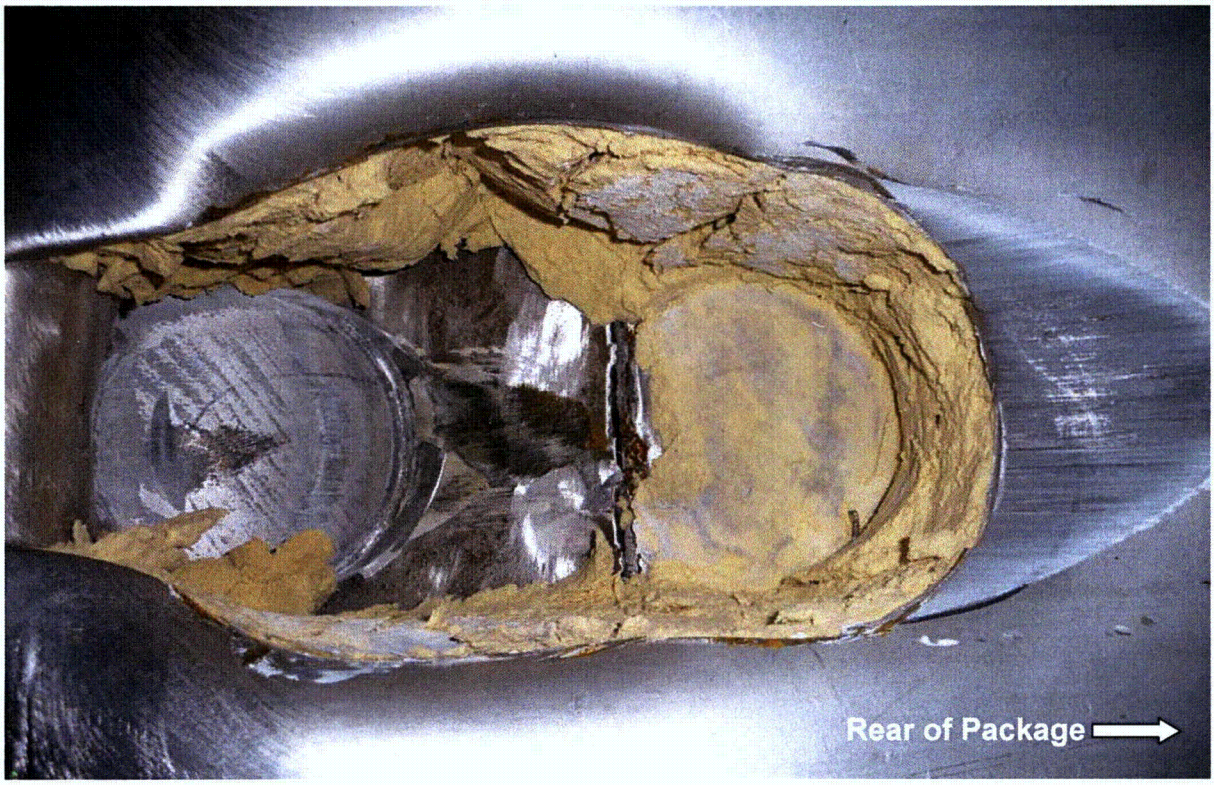

Figure 2.12.6-15 – Test LP92, Puncture on Bottom Wall Damage, Detail

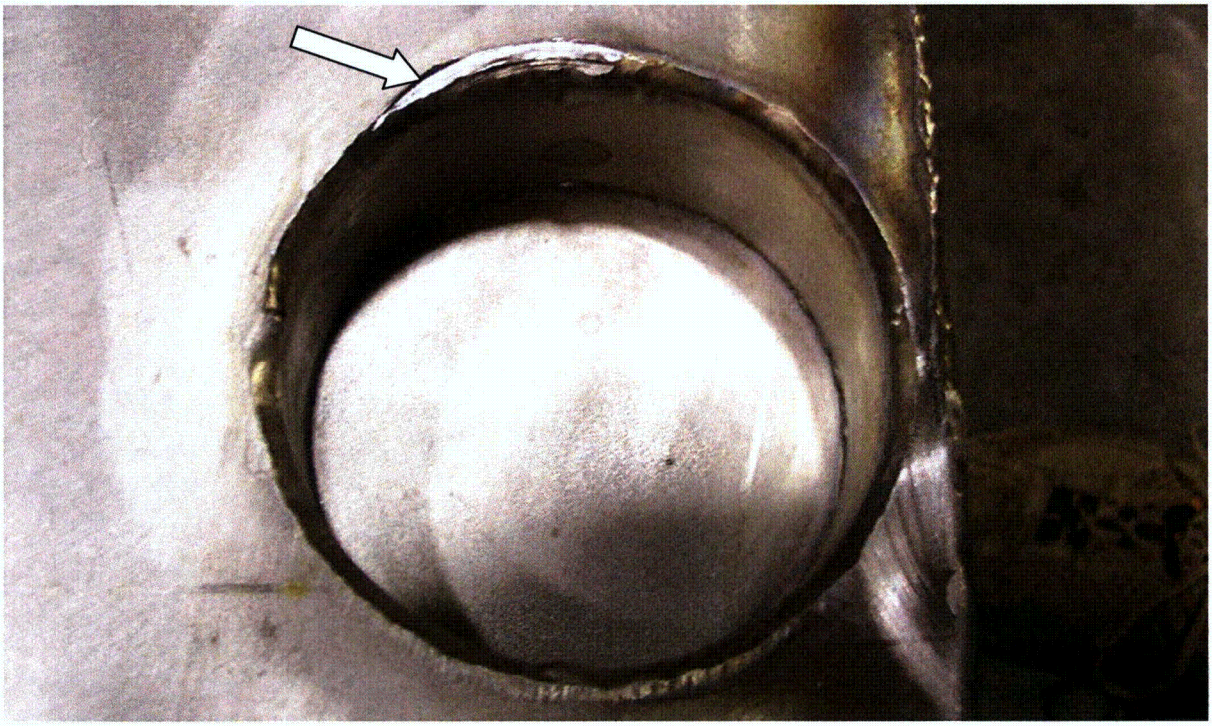

Figure 2.12.6-16 – Typical Damage to Overpack Cover due to Interference with Closure Bolt Washers

Figure 2.12.6-17 – Debris and Debris Shield (red) Upon Closure Lid Removal

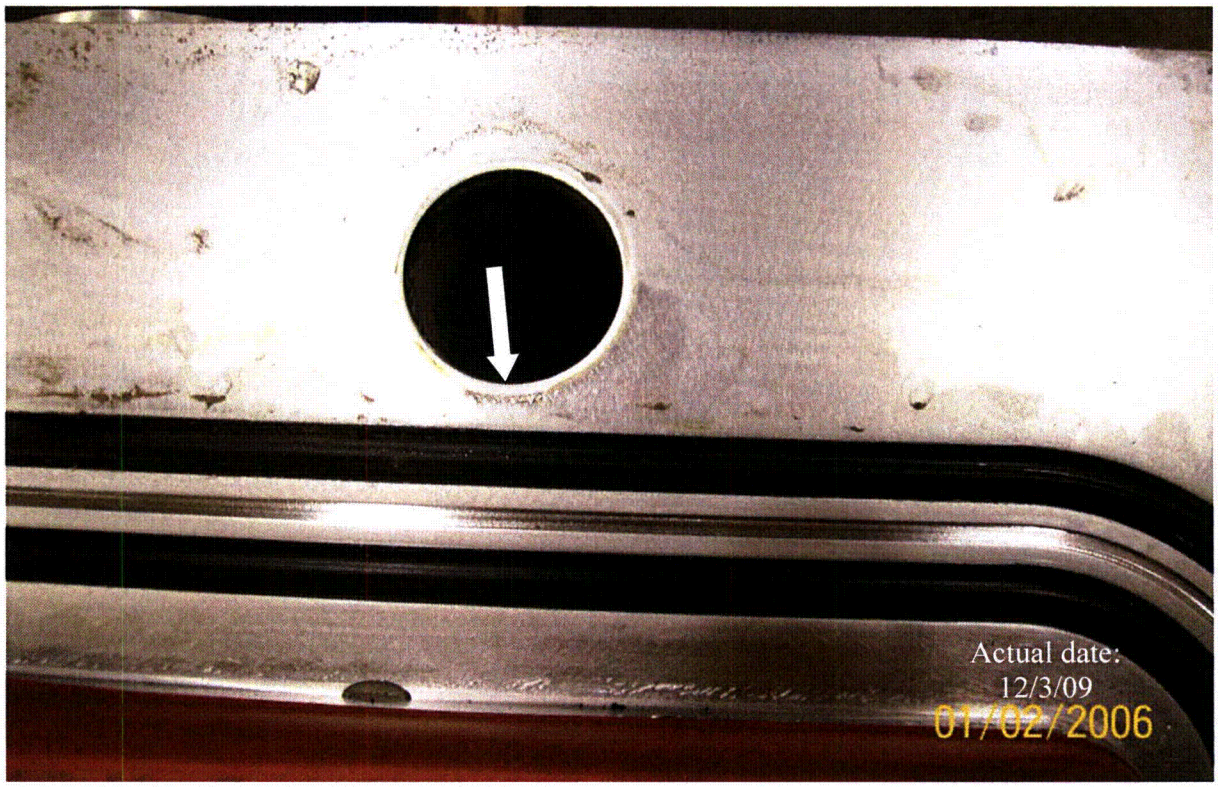

Figure 2.12.6-18 – Galling on Flange Around Closure Bolt Holes

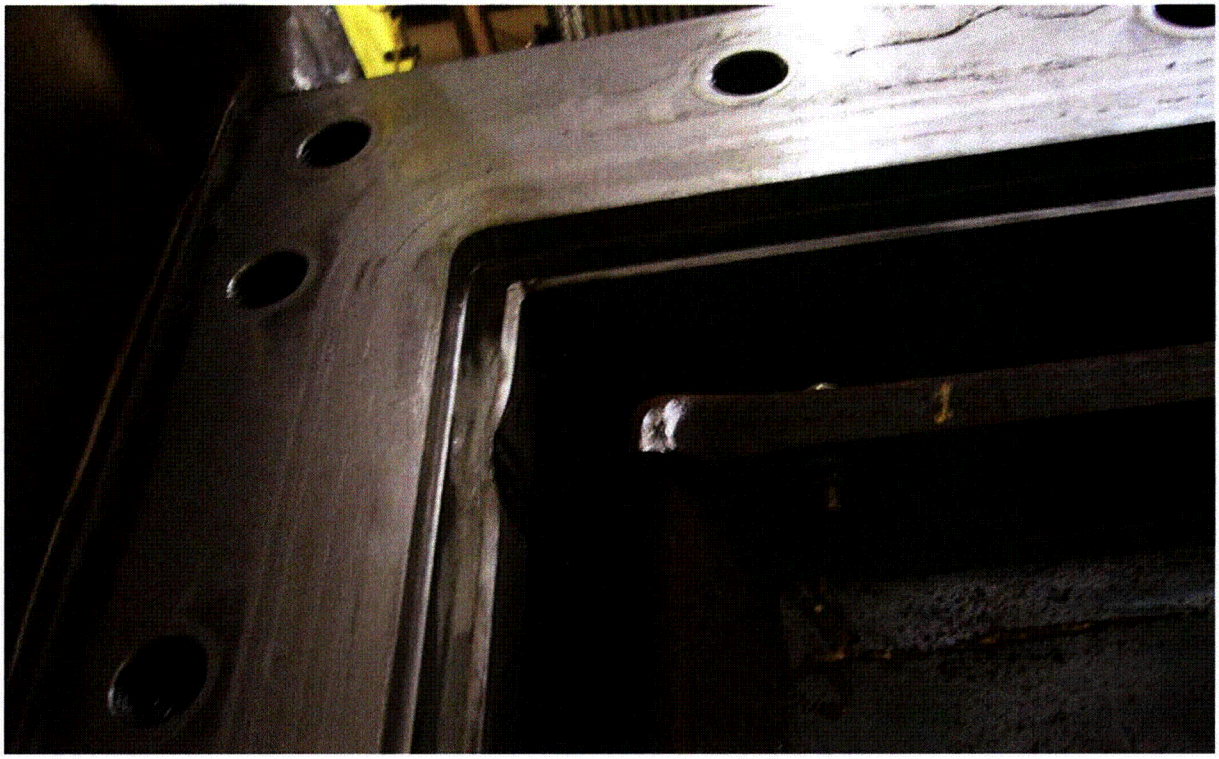

Figure 2.12.6-19 – Dent in Debris Shield Receptacle Caused by SLB2

Figure 2.12.6-20 – Payload Cavity with All Contents Removed

2.12.6.9 Acceleration Time History Plots (Free Drop Test LD91)

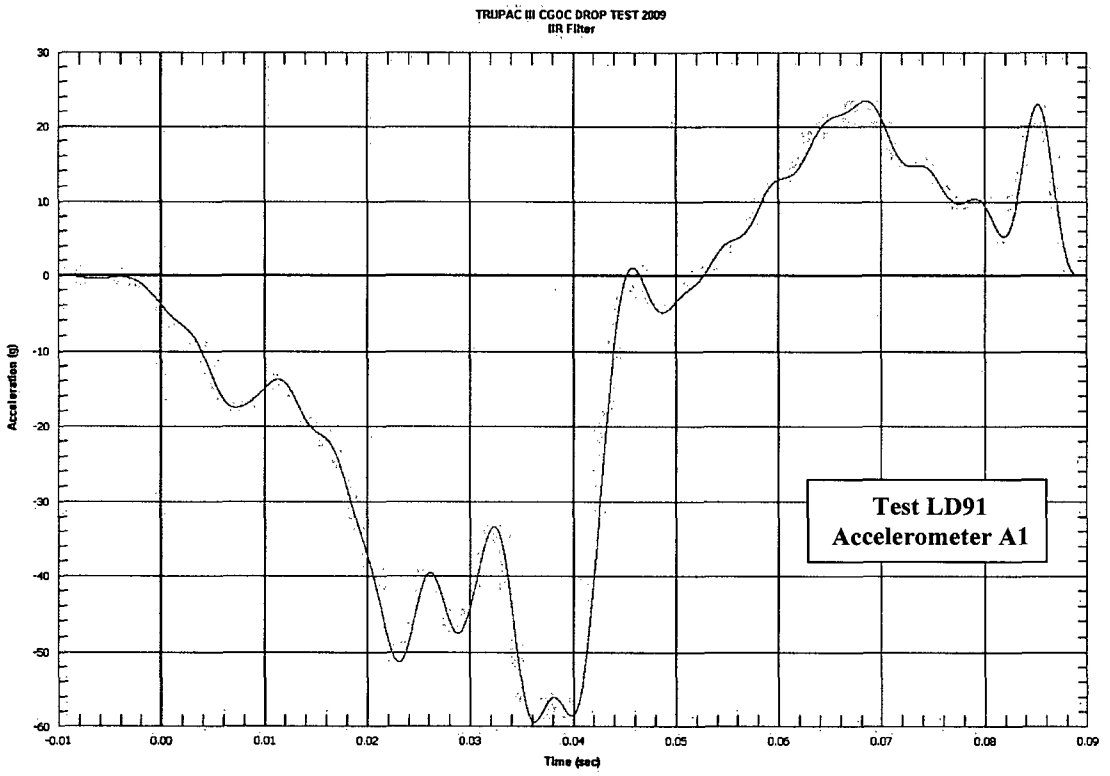

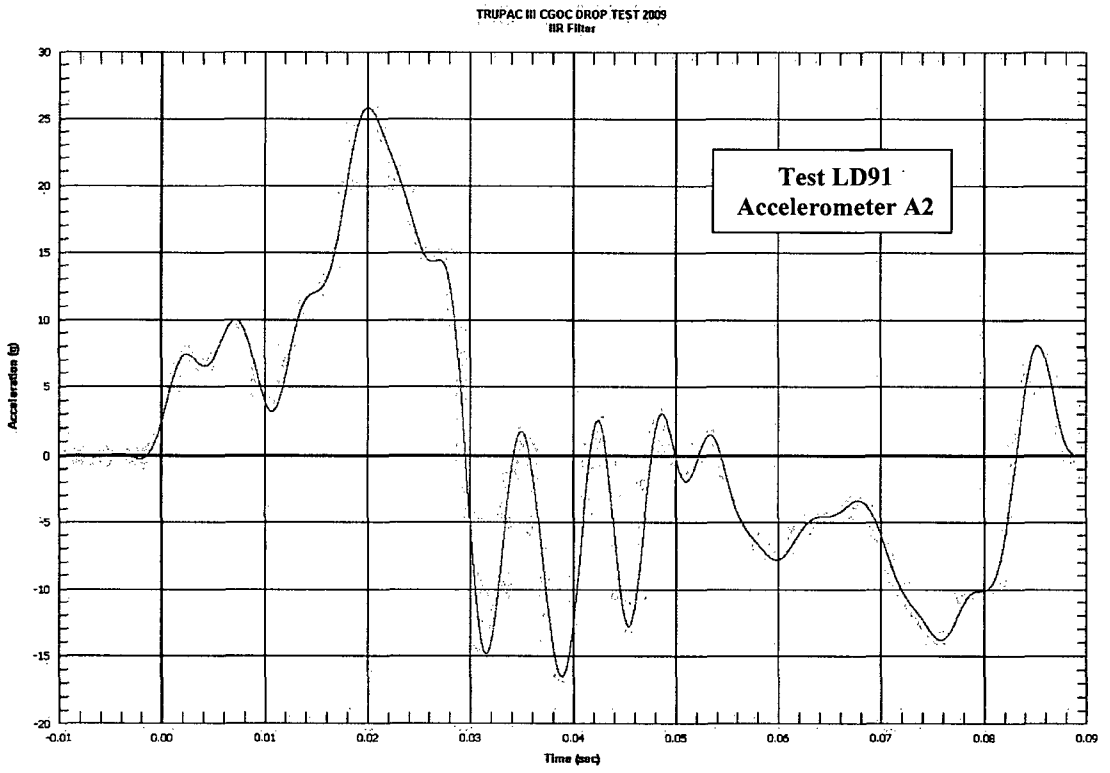

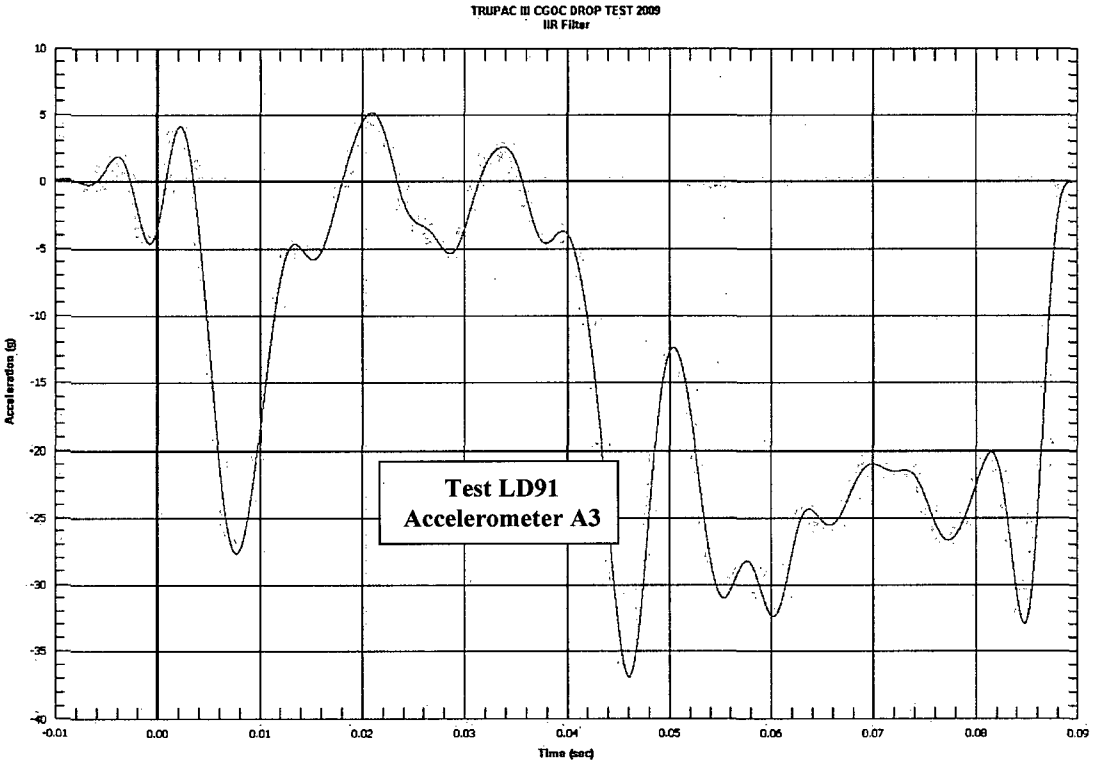
TRUPAC III CGOC DROP TEST 2009
IIR Filter
Acceleration (g)
Time (sec)
Test LD91
Accelerometer A3

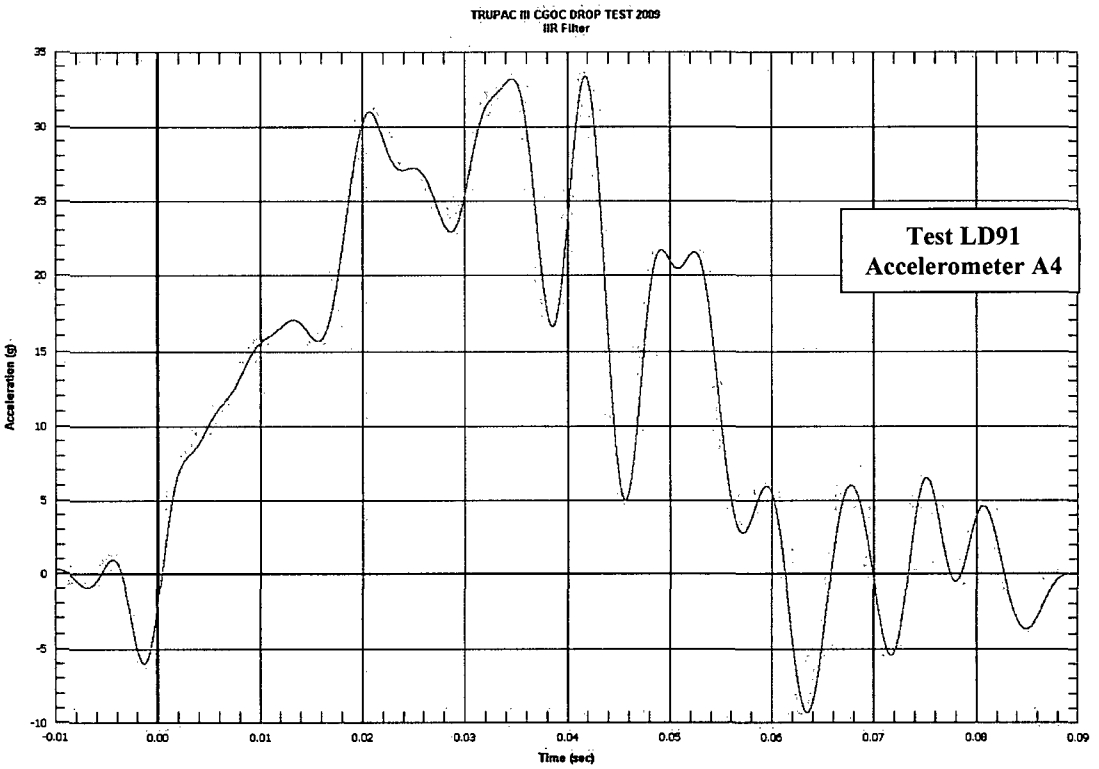
TRUPAC III CGOC DROP TEST 2009
IIR Filter
Acceleration (g)
Time (sec)
Test LD91
Accelerometer A4

2.12.7 Closure Lid, Bolt, and Washer Interaction

2.12.7.1 Introduction

This appendix demonstrates that the TRUPACT–III lid closure bolt washer is not the weakest link in the closure joint, i.e., not the first component to yield under HAC loadings. The other components in the joint include the lid, bolt, and body flange. For the purposes of this analysis, the body flange is assumed to be rigid. The purpose of this analysis is to show that:

- With increasing load on the closure joint, the first component to incur permanent deformation is the bolt, not the washer.
- If an initially preloaded closure joint were to be loaded up to the yield load of the bolt, and then released, the residual preload on the joint is over 90% of the initial preload force.

The closure joint, including representations of the lid, bolt, and washer, is analyzed using a Finite Element Analysis (FEA) model. The model is evaluated using the FEA program ANSYS® Version 11.0. This analysis assumes the lid moves parallel to the bolt axis, without flange rotation. While some rotation will occur under circumstances of lid loading in an impact, this analysis is intended only to demonstrate the general robustness of the closure joint, and that the washer is not the weakest component in the joint. The actual performance of the closure under HAC free drop impacts is discussed in detail in Section 2.7.1, *Free Drop.*

Dimensions of the components are taken from Appendix 1.3.1, *Packaging General Arrangement Drawings*. The lid is a machined weldment comprised of duplex stainless steel Type UNS S31803. The portion of the lid represented in the FEA model is primarily the lid bolt tube, as discussed below. The closure lid bolts are socket head cap screws with M36 x 4 threads and a 30 mm shank diameter. The bolt material is ASTM A320 Grade L43. The washers are M36 x 6 mm thick with a 64 mm outer diameter. The washer material is age-hardened stainless steel, ASTM A564 Grade 630 Condition H1025. The bolt installation torque is 1,600 N-m. The bolt preload is calculated in Section 2.6.1.6, *Closure Bolts*, to be 222.2 kN.

Material properties are evaluated at the NCT hot condition of 71 °C. Material properties for the lid are taken from Table 2.2-1 and Table 2.2-2. The material properties for the bolt and washer are taken from Table 2.2-4 and Table 2.2-8, respectively. The temperature-interpolated values are shown Table 2.12.7-1.

2.12.7.2 Finite Element Analysis Methodology

The FEA model consists of a 2-D axisymmetric representation of the bolt, washer, and lid. The bolt and lid are only modeled in sufficient length such that stresses surrounding the washer contact region are not influenced by the model boundary constraints. Similarly, the lid bolt tube is modeled with a larger outer diameter. A value of 102 mm instead of 64 mm was used in order to include a reasonable representation of the 20 mm thick top plate of the lid that is adjacent to the washer bearing area. This prevents a discontinuity in the model at the outer edge of the washer bearing area with the lid. The increased stiffness of the lid bolt tube due to the larger outer diameter is reasonable with respect to the stiffness of the boxed outer section of the lid and conservative with respect to determining if the washer will yield.

Three parts are defined in the model as described in Table 2.12.7-2, and each part is meshed with PLANE82 2-D 8-Node structural solid elements. The interaction between the bolt and washer, and washer and lid, are modeled with contact elements. CONTA172 2D 3-Node surface-to-surface contact elements are used in conjunction with TARGE169 2-D target segments. Friction is conservatively neglected. The element mesh is sized such that the region of interest around the washer is very refined and slowly transitions to coarser density away from the washer. The 2-D axisymmetric model has 4,693 nodes, 1,444 structural elements and 100 contact elements. The bolt is constrained in the x-direction (radial) along its axis for the axisymmetric condition. The bolt and lid have y-direction (vertical) displacement constraints along their bottom nodes. The lid is also constrained in the x-direction along its bottom nodes. The washer is only restrained by the bolt and lid contact forces. The FEA model is shown Figure 2.12.7-1 and Figure 2.12.7-2.

To analyze the bolt joint and washer capability, the model is solved in a series of steps to represent a generic hypothetical drop condition. First, the bolt is preloaded such that the tensile force is approximately 222.2 kN, which corresponds to the nominal preload torque of 1,600 N-m. The lid is then displaced into the preloaded bolt such that the tensile force in the bolt is approximately 491.9 kN, which is the force necessary for the bolt shank to reach the material yield strength. The lid is then released to its original position and the bolt is left with residual preload. Finally, the bolt is released to its original position and only parts that exceeded their yield strength show residual stresses. The arbitrary displacements necessary to induce the preload and yield load in the bolt are determined iteratively until the model reaction forces match the desired values. To represent this series of conditions the model is solved in four sequential load steps:

1. Lid is constrained and the lower end of the bolt shank is displaced downward to apply the initial preload force.

2. The lid is displaced upward parallel to the bolt axis while the bolt is constrained in the initial preload location, to apply a tensile force in the bolt such that the shank approximately reaches the bolt material yield strength.

3. The lid is returned to its originally constrained preload location, which leaves the bolt with a residual preload.

4. The bolt is returned to its original location, thus releasing the residual preload.

Since the bolt shank is loaded up to the material yield strength, the model uses nonlinear material properties. For the lid, the UNS S31803 stress-strain data shown in Table 2.2-2 is in the form of true stress and strain. The multilinear kinematic hardening (KINH) material type is used. The bolt and washer material properties are defined using the bilinear kinematic hardening (BKIN) material type. The bolt and washer material properties in Table 2.12.7-1 are used to develop the true material yield strength and tangent modulus required for the BKIN material type.

Bolt Material A320 Gr. L43:

True Yield Strength: $S_{yt} = S_y\left(1+\left(\frac{S_y}{E}+0.002\right)\right) = 696\left(1+\left(\frac{696}{18.8(10^4)}+0.002\right)\right) = 700 \text{ MPa}$

True Ultimate Strength: $S_{ut} = S_u(1+e_u) = 862(1+0.16) = 999.9 \text{ MPa}$

True Yield Strain: $\varepsilon_{yt} = \ln(1+e_y) = \ln\left(1+\left(\frac{696}{18.8(10^4)}+0.002\right)\right) = 0.00569$

True Ultimate Strain: $\varepsilon_{ut} = \ln(1+e_u) = \ln(1+0.16) = 0.148$

Tangent Modulus: $E_{tan} = \frac{S_{ut}-S_{yt}}{\varepsilon_{ut}-\varepsilon_{yt}} = \frac{999.9-700}{0.148-0.00569} = 2{,}107.4 \text{ MPa}$

Washer Material A564 Gr. 630 Condition H1025:

True Yield Strength: $S_{yt} = S_y\left(1+\left(\frac{S_y}{E}+0.002\right)\right) = 948\left(1+\left(\frac{948}{19.3(10^4)}+0.002\right)\right) = 954.6 \text{ MPa}$

True Ultimate Strength: $S_{ut} = S_u(1+e_u) = 1{,}069(1+0.12) = 1{,}197.3 \text{ MPa}$

True Yield Strain: $\varepsilon_{yt} = \ln(1+e_y) = \ln\left(1+\left(\frac{948}{19.3(10^4)}+0.002\right)\right) = 0.00689$

True Ultimate Strain: $\varepsilon_{ut} = \ln(1+e_u) = \ln(1+0.12) = 0.113$

Tangent Modulus: $E_{tan} = \frac{S_{ut}-S_{yt}}{\varepsilon_{ut}-\varepsilon_{yt}} = \frac{1{,}197.3-954.6}{0.113-0.00689} = 2{,}287.2 \text{ MPa}$

2.12.7.3 Finite Element Analysis Results

The stress intensities for each part at each load step are listed in Table 2.12.7-3 and shown in Figure 2.12.7-3 through Figure 2.12.7-10. The stress intensities show the washer does not yield for a hypothetical condition where the bolt is loaded to its yield strength. The washer maximum stress is 758.9 MPa, which is less than the engineering yield strength of 948 MPa at 71 °C. The bolt shank measured 691.6 MPa, which is approximately the bolt engineering yield stress of 696 MPa. The discontinuity between the bolt head and shank exceed the yield strength as expected. The lid tube also shows minor yielding with a residual stress of 100.9 MPa after the bolt is unloaded.

The bolt reaction loads are listed in Table 2.12.7-4. The reduction in bolt preload force is less than 10% of the initial preload force after being loaded up to its yield strength.

$$\text{Reduction of Preload} = \frac{222.6-201.4}{222.6} \times 100 = 9.5\,\%$$

2.12.7.4 Closure Lid, Bolt, and Washer Interaction Summary

The FEA results show that none of the TRUPACT–III closure lid components experiences significant permanent deformation when a load equal to the bolt shank yield load is applied to the joint. Local yielding in the sharp corner under the bolt head and at the outer sharp edge of the bolt head does occur, but yield of the washer does not occur. Very limited yielding in the lid surface

also occurs. The insignificance of these deformations is demonstrated by the fact that, after the full loading sequence has been applied, the initial preload force applied to the bolt has been reduced by only 9.5%. Therefore, the components of the lid closure joint are adequately designed. Adequacy of the joint to maintain closure in the worst-case HAC free drop is demonstrated by test.

Table 2.12.7-1 – Bolt and Washer Material Properties at 71 °C

Bolt Material A320 Gr. L43[1]	
Yield Strength, MPa	696
Ultimate Strength, MPa	862
Elastic Modulus, MPa	18.8×10^4
Elongation[3] (%)	16
Washer Material A564 Gr. 630 H1025[2]	
Yield Strength, MPa	948
Ultimate Strength, MPa	1,069
Elastic Modulus, MPa	19.3×10^4
Elongation[3] (%)	12

Notes:

1. Material properties interpolated using data from Table 2.2-4.
2. Material properties interpolated using data from Table 2.2-8.
3. The total elongation is from ASME B&PV Code, Section II, Part A.

Table 2.12.7-2 – Model Parts

Part #	Description	Material Size (mm)	Material Type
1	Washer	M36 x 6 THK	ASTM A564 Gr. 630 H1025
2	Lid, Tube	44 ID	ASTM A240/A479 UNS S31803
3	Bolt, SHCS	M36 x 4, 30 OD Shank	ASTM A320 Gr. L43

Table 2.12.7-3 – Maximum Stress Intensity Results Summary, MPa

Load Step	Washer	Lid	Bolt Head	Bolt Shank
1, Bolt preload	389.3	393.2	709.6	314.4
2, Bolt yield load	758.9	540.3	835.1	691.6
3, Bolt residual preload	353.6	248.2	420.8	284.5
4, Bolt unloaded	0	100.9	599.9	0

Table 2.12.7-4 – Reaction Load Summary

Load Step	Bolt Force, kN
1, Bolt preload	222.6①
2, Bolt yield load	489.7②
3, Bolt residual preload	201.4
4, Bolt unloaded	0

Notes:

1. Adequately close to the target preload of 222.2 kN.
2. Adequately close to the target yield load of 491.9 kN.

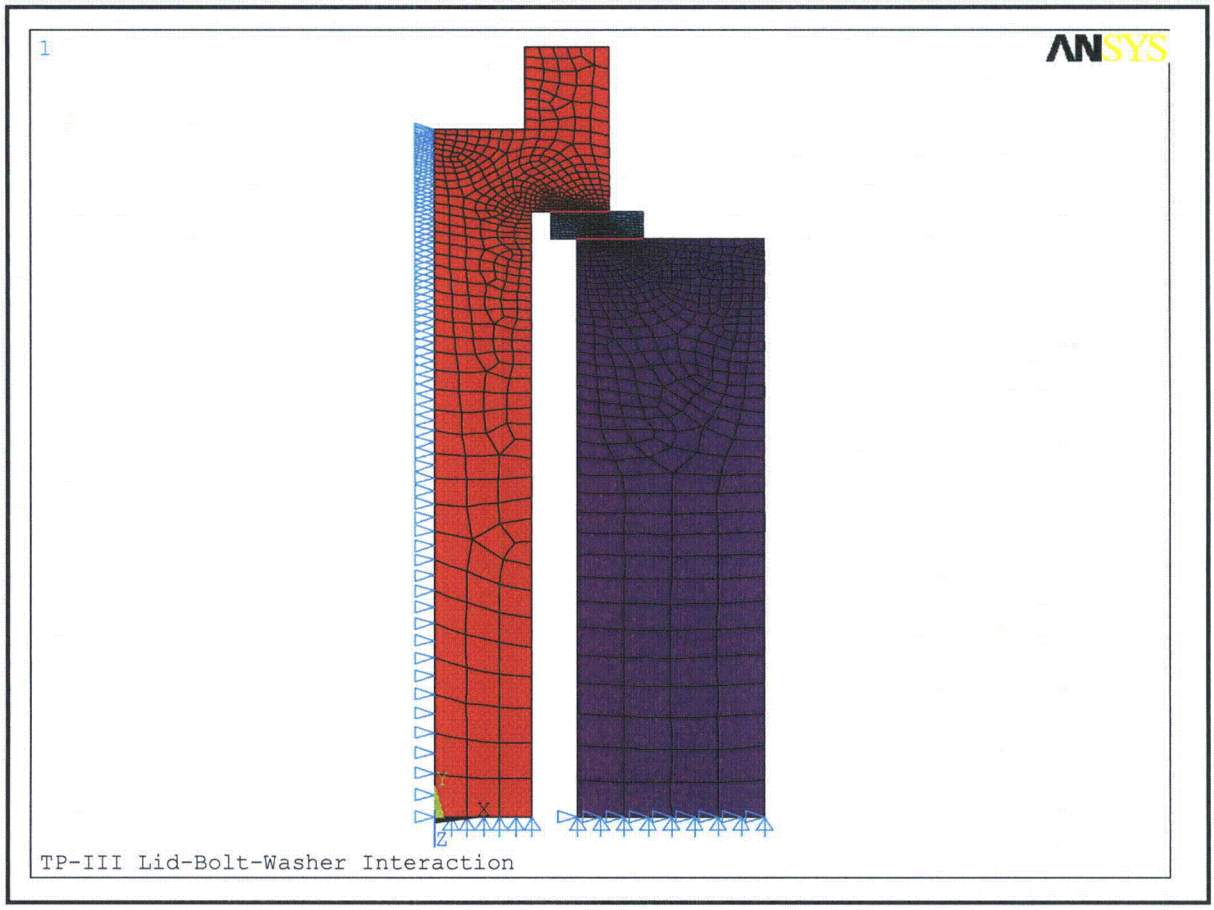

Figure 2.12.7-1 – ANSYS® Model Element Plot with Boundary Constraints

Figure 2.12.7-2 – ANSYS® Model with Washer Detail Element Plot

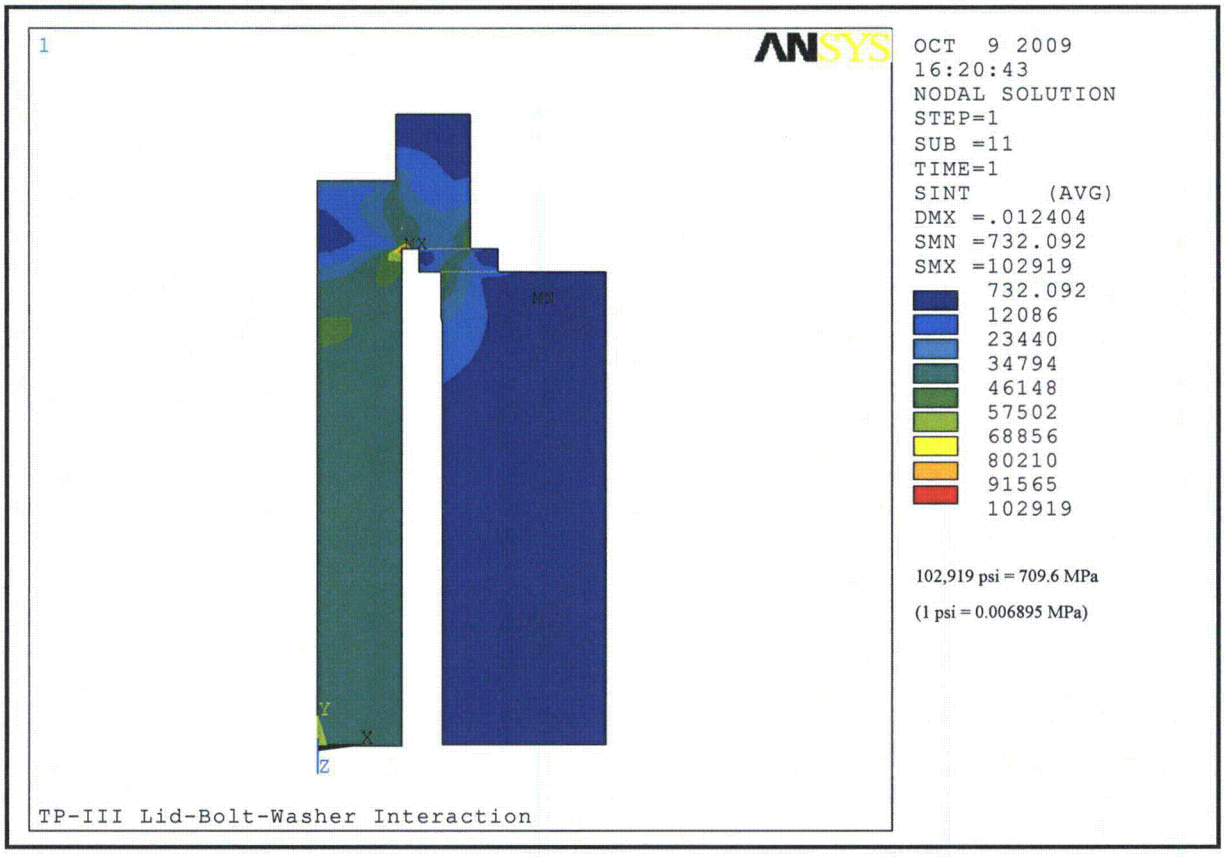

Figure 2.12.7-3 – Preload Stress Intensity Model View

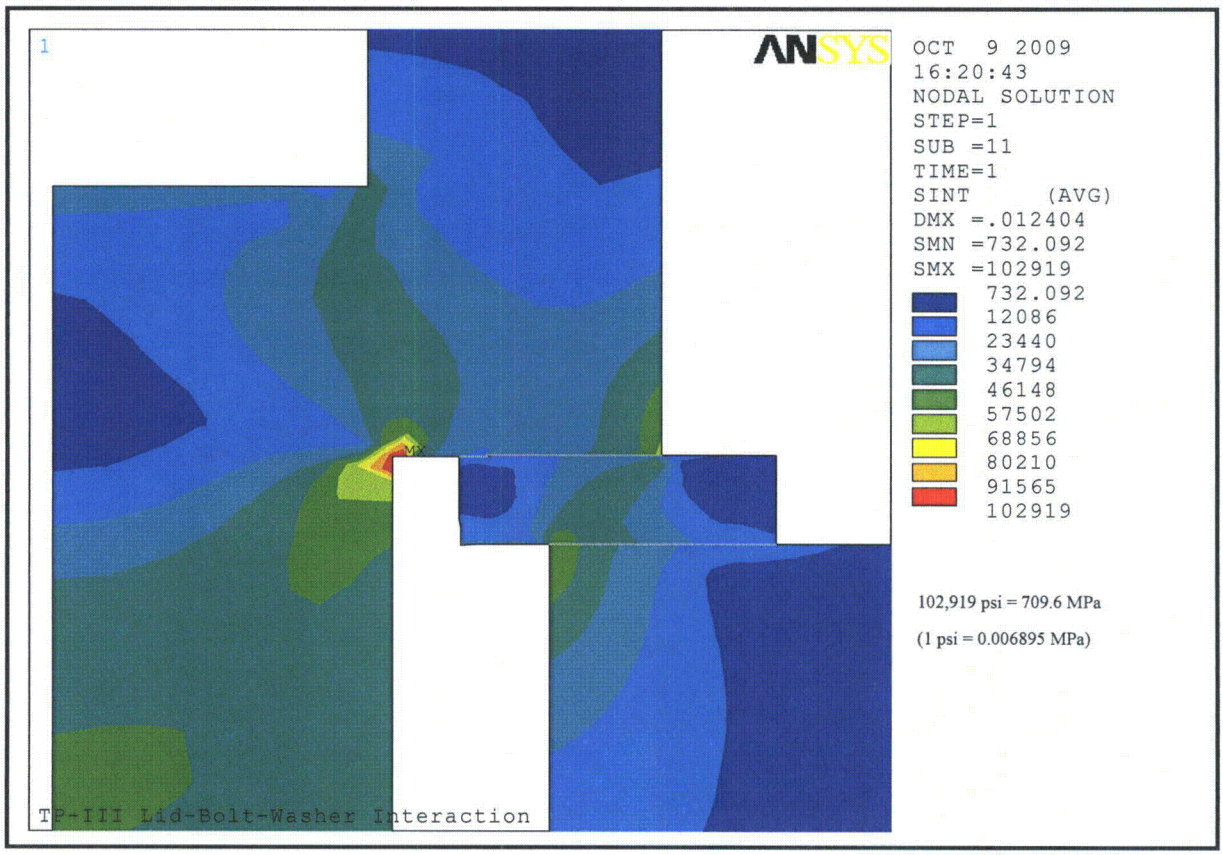

Figure 2.12.7-4 – Preload Stress Intensity Detail View

Figure 2.12.7-5 – Yield Load Stress Intensity Model View

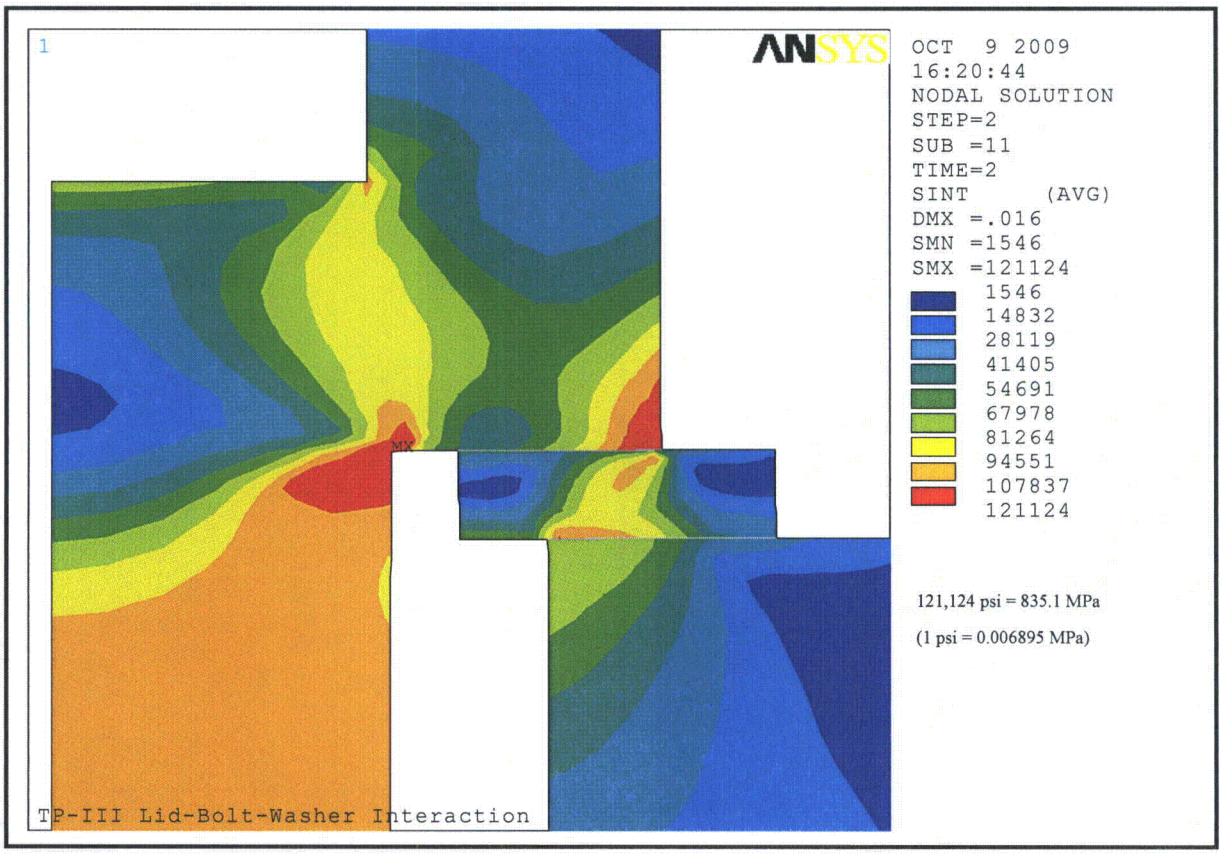

Figure 2.12.7-6 – Yield Load Stress Intensity Detail View

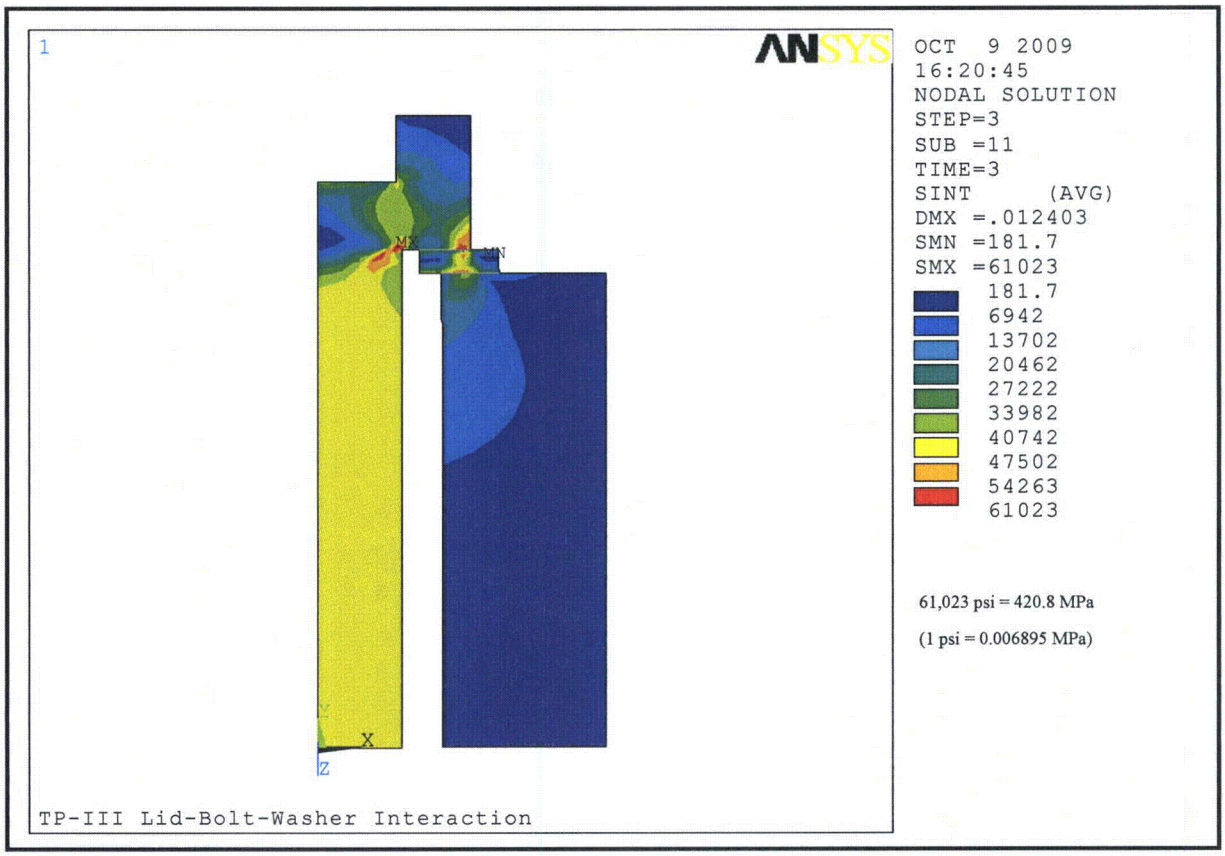

Figure 2.12.7-7 – Residual Preload Load Stress Intensity Model View

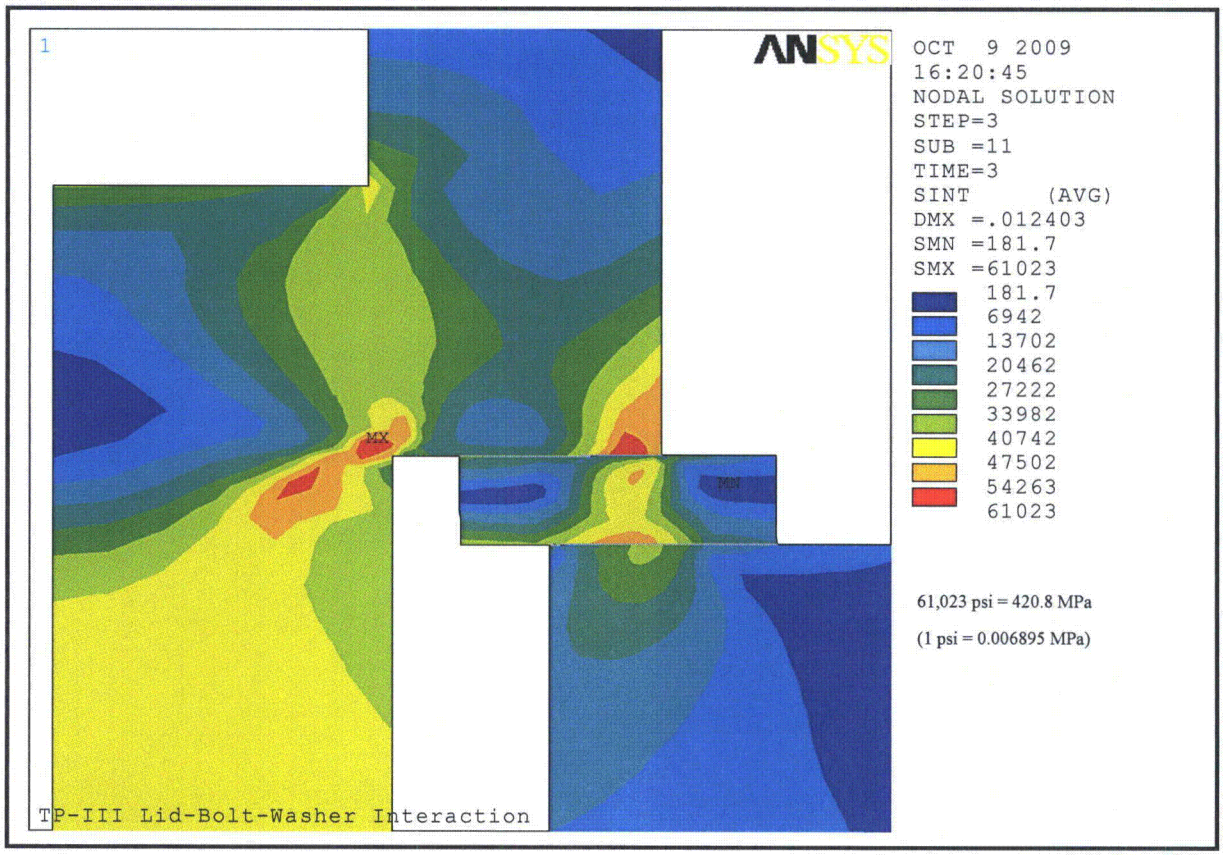

Figure 2.12.7-8 – Residual Preload Load Stress Intensity Detail View

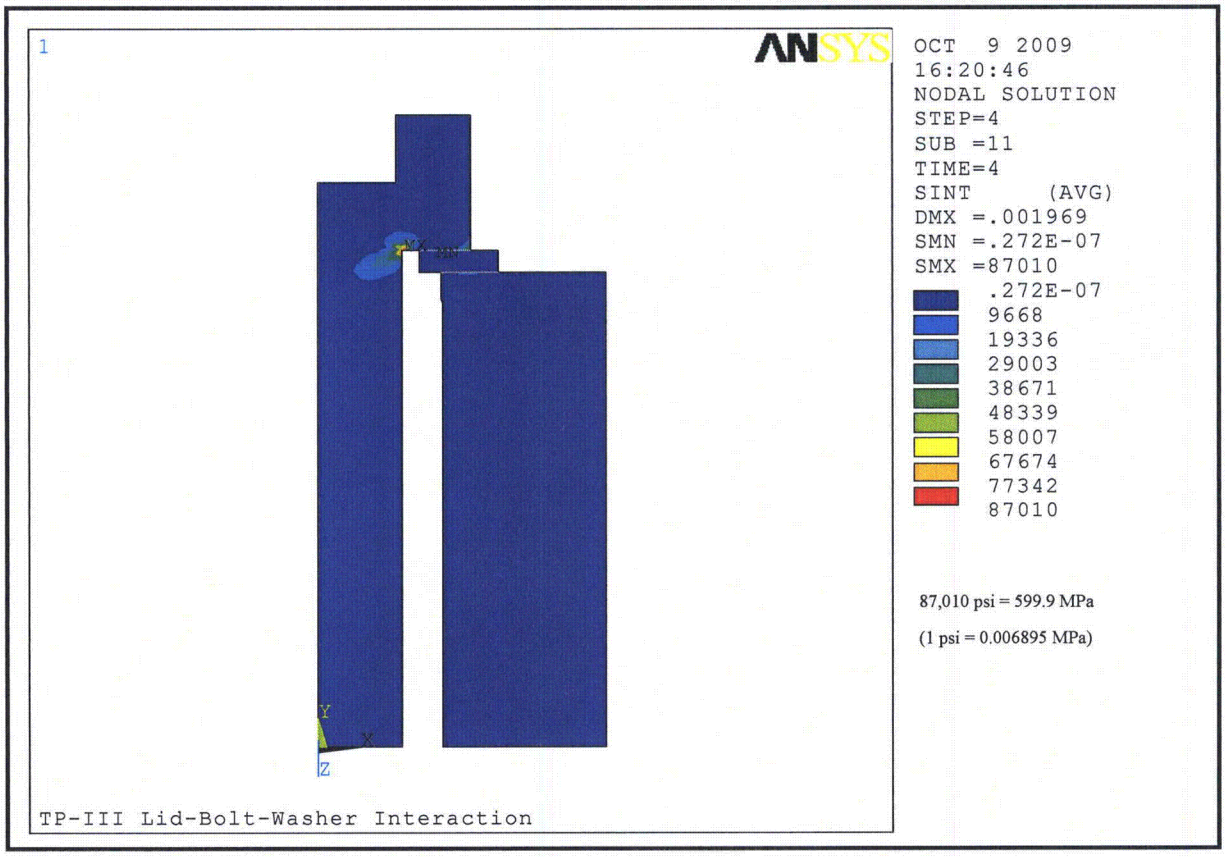

Figure 2.12.7-9 – Unloaded Residual Stress Intensity Model View

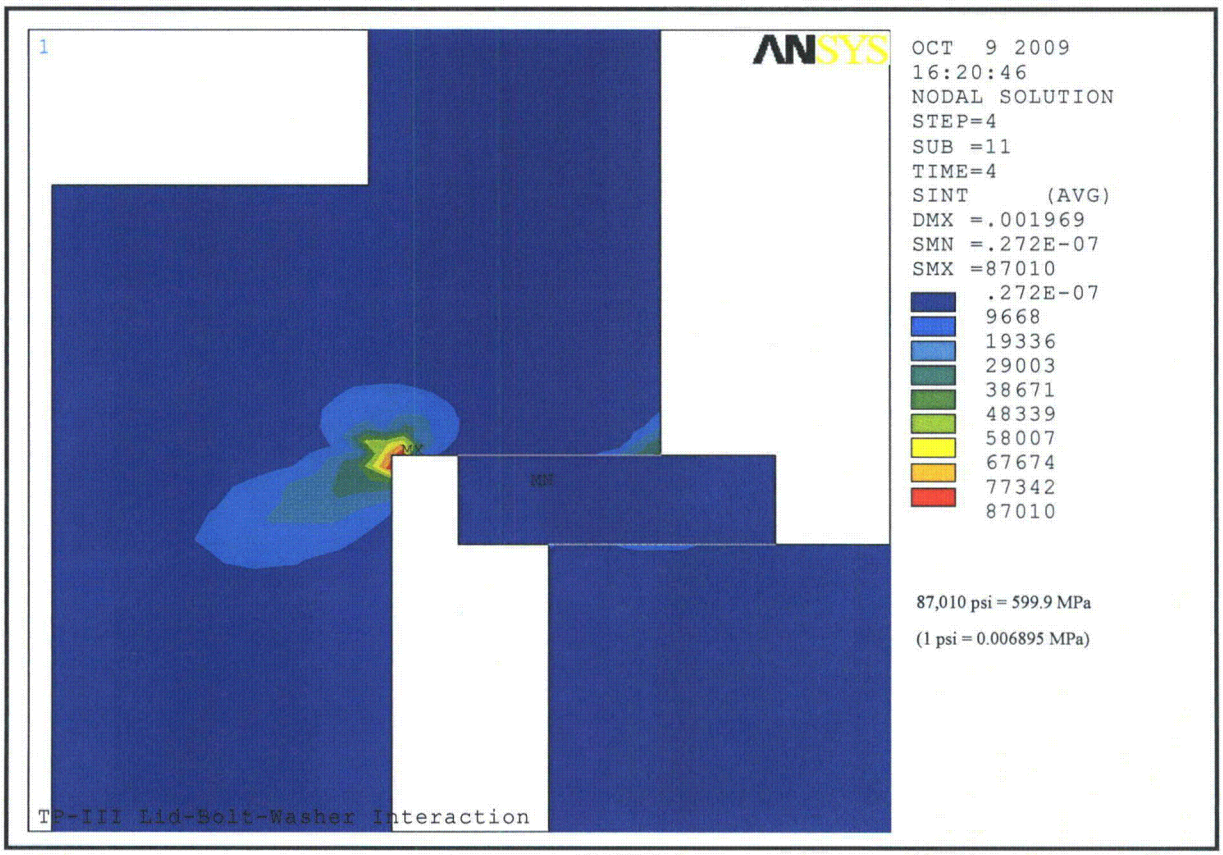

Figure 2.12.7-10 – Unloaded Residual Stress Intensity Detail View

This page intentionally left blank.